Identification and functional characterization of CNS pericytes and the role they play in neurovascular coupling in physiological and pathological conditions

Clare Reynell

A thesis submitted to University College London for the degree of Doctor of Philosophy

Department of Neuroscience, Physiology and Pharmacology

University College London

September 2013

Abstract

Brain blood flow increases, evoked by neuronal activity, power neural computation and are the basis of BOLD functional imaging. However, it is controversial whether blood flow is controlled solely by arteriole smooth muscle, or also by capillary pericytes. The experimental work within this thesis examines capillary pericytes, and the role they play in neurovascular coupling in physiological and pathological conditions.

I show that pericytes can be identified using several protein markers and that, using the same technique, pericytes can be distinguished from other perivascular cell types.

I demonstrate that pericytes respond to the neurotransmitters noradrenaline and glutamate. Noradrenaline depolarizes pericytes and constricts capillaries, and this constriction reflects pericyte contraction while glutamate, mimicking neuronal activity, hyperpolarizes pericytes and dilates capillaries, and this dilation reflects pericyte relaxation. Glutamate-evoked dilation is mediated by prostaglandin E_2 or a related compound acting at EP_4 receptors, but requires nitric oxide release to suppress synthesis of the vasoconstrictor 20-HETE.

In pathology, I show that pericytes die when exposed to ischaemia. This may lead to pericytes irreversibly constricting capillaries and to damage of the blood-brain barrier. Pericyte death increases on reperfusion after ischaemia, and is reduced by block of glutamate receptors or Ca^{2+} removal, but not by scavenging reactive oxygen species.

These data establish pericytes as active regulators of capillary tone and thus as potential regulators of brain blood flow. My data also suggest prevention of pericyte death as a strategy to reduce the long-lasting blood flow decrease which contributes to neuronal death after stroke.

This thesis also contains a discussion of how energy supply to the brain alters with age, and how this may affect the BOLD signal.

Statement of the candidate's contribution to this thesis

All of the data analysis, figure production and writing in this thesis was done by Clare Reynell. The work in the 5 results chapters of this thesis was performed primarily by Clare Reynell (with normal supervisorial input from David Attwell), with her contribution to each project as described below.

(1) Immunohistochemistry
Immunohistochemical experiments in Chapter 3 were planned, carried out and analysed entirely by Clare Reynell (with initial guidance from Catherine Hall).

(2) Imaging capillaries in the cerebellum
The imaging experiments in Chapter 4 were done in collaboration with Catherine Hall. Clare did 60% of the planning, execution and analysis of these experiments.

(3) Patch-clamp recording of pericytes in the cortex and cerebellum
The patch-clamp experiments in Chapter 5 were planned, carried out and analysed entirely by Clare Reynell (with initial guidance from Nicola Hamilton-Whitaker).

(4) Pericyte death in oxygen-glucose deprivation
The oxygen-glucose deprivation experiments in Chapter 6 were planned, carried out and analysed entirely by Clare Reynell (with initial guidance from Catherine Hall and Nicola Hamilton-Whitaker).

(5) The physiology of developmental changes in the BOLD signal
The paper that was the basis of Chapter 7 was researched and written in collaboration with joint first author, Julia Harris, with Clare and Julia each contributing 50% to the final article.

Signed (candidate)
Clare Reynell Date

Signed (supervisor)
David Attwell Date

Acknowledgments

My greatest thanks go to my supervisor, Professor David Attwell, for his guidance, support and patience throughout my PhD. I feel very grateful to have had such an experienced and inspiring supervisor.

I would also like to thank all members of the Attwell lab, past and present, who have taught me so much and kept me consistently entertained: Catherine Hall, Nicola Hamilton-Whitaker, Julia Harris, Laura Clarke, Christian Madry, Elisabeth Engl, Lorena Arancibia-Carcamo, Fergus O'Farrell, Renaud Jolivet, Anusha Mishra, Yamina Bakiri, Karolina Kolodziejczyk, Valeria Burzamato, Johanne Egge Rinholm, and Kaylene Young.

I'm particularly grateful for Catherine Hall's limitless help and advice over the years that we have worked together. I'm also lucky enough to have had the opportunity to work closely with Nicola Hamilton-Whitaker and Julia Harris. Working with you guys has made me feel very optimistic about the future of women in science!

Finally I could never thank my family and friends enough for their love and encouragement. I may never fully comprehend the impact that my Mother's unconditional pride has had on me, but I appreciate it more than anything.

Contents

List of figures

List of tables

Chapter 1: Introduction

1.1 Overview

This thesis is concerned with pericytes, a type of perivascular cell located on capillaries. In this thesis I will report on the identification and classification of these cells and investigate the role they play in regulating capillary function under physiological and pathophysiological conditions. In this introduction, I will provide the general background needed to understand the experiments described in the Results chapters. More specific background relevant to each set of experiments is presented in the Introduction to each Results chapter.

1.2 Energy supply to the brain

The brain comprises 2% of the body's weight but uses 20% of the body's resting energy production (Clark and Sokoloff, 1999). This high energetic demand is due to the large amount of ion pumping activity, mainly within neurons, mediated by the Na^+/K^+–ATPase (Attwell and Laughlin, 2001), which is needed to pump out ions whose entry generates synaptic and action potentials. Because of this large energy consumption, the blood flow to the brain needs to be highly controlled. Increases in neural activity, and thus increases in energy demand, are associated with a compensatory local increase in cerebral blood flow.

Neurovascular coupling is the mechanism by which neuronal activity produces an increase of local blood flow (also termed functional hyperaemia). Roy and Sherrington (1890) postulated that chemical products of metabolism affected the vessel wall, altering the vessel calibre, and it is often assumed that functional hyperaemia serves to adjust the blood flow to meet energy needs. Accumulation of the metabolic products adenosine and lactate do contribute to activity-induced blood flow increases (Gordon et al., 2008; Ko et al., 1990), and metabolic CO_2 generation may promote blood flow after conversion to H^+ by carbonic anhydrase (Colonnese et al., 2008). However, the idea that a metabolic need signal, such as a fall of oxygen or glucose concentration, is the main trigger of increased blood flow in response to neuronal activity has been superseded with the discovery that neurotransmitter mediated pathways alter blood flow (Akgören et al., 1994; Li & Iadecola, 1994; Zonta et al., 2003; reviewed by Attwell et al., 2010), and that block of these pathways greatly reduces functional hyperaemia without affecting energy use by the tissue (Leithner et al., 2010; Offenhauser et al., 2005; St Lawrence et al., 2003).

The supply of oxygen and glucose to neurons occurs mainly across the walls of capillaries in the brain parenchyma (but with some oxygen passing across arteriolar walls: Yaseen et al., 2011; Kasischke et al., 2011). The amount of blood flow providing these nutrients is thought to be determined by the contractile tone of smooth muscle cells around arterioles, which controls the diameter of the vessels and hence the resistance

to blood flow. Although the basal tone setting the resting blood flow is, in part, set by mediators released from endothelial cells lining the blood vessels, changes in blood flow in response to neuronal activity are evoked by events in neurons and astrocytes situated in close proximity to the vasculature. In brief, the release of neurotransmitters from active neurons generates neuron- and astrocyte-derived messengers (Fig. 1.1) which either modulate ion channel activity in the smooth muscle, leading to a change of calcium concentration, or change the calcium-sensitivity of the contractile apparatus, both of which lead to altered contraction (reviewed by Attwell et al., 2010; Iadecola, 2004; Koehler et al., 2009).

1.2.1 Neurovascular coupling via neuronal nitric oxide

Neuronal activity can dilate blood vessels as a result of synaptically released glutamate binding to NMDA (*N*-methyl-*D*-aspartate) receptors on neurons, causing a calcium influx, which activates neuronal nitric oxide synthase (nNOS) (Garthwaite et al., 1988). Nitric oxide then diffuses to the vasculature where it produces vessel dilation, in part via the activation of guanylate cyclase and generation of cGMP (Fig. 1.1; Busija et al., 2007), which promotes relaxation (see section 1.4). Nitric oxide is reported to act as a direct mediator of neuronally evoked blood flow responses in the cerebellum (Akgören et al., 1996) whereas in the cerebral cortex, although it is necessary for NO to be present in order for neural activity induced dilation to occur, changes of the level of NO are not the primary mediator of vasodilation (Lindauer et al., 1999). In Chapter 4 I will demonstrate a similar phenomenon for capillary pericytes in the cerebellum. In the cortex nNOS is often found in GABAergic inhibitory interneurons near blood vessels (for reviews see Estrada and DeFelipe, 1998; Hamel, 2006), which can also express other vasoconstrictive mediators such as neuropeptide Y and somatostatin (Cauli et al., 2004). Other interneurons, which lack nNOS (Estrada and DeFelipe, 1998), may release vasoactive intestinal peptide which mediates dilation. In human cortex, in addition to being present in interneurons, nNOS is also expressed by a subpopulation of excitatory pyramidal cells (Judas et al., 1999; Wallace et al., 1995), and it has also been reported in excitatory pyramidal cells of the rat hippocampus (Burette et al., 2002).

1.2.2 Neurovascular coupling via astrocytes

Astrocytes are large glial cells, which extend many processes that envelope surrounding synapses. In humans, an individual astrocyte may be able to sense the activity at ~2 million synapses (Oberheim et al., 2006). Astrocytes also form perivascular endfeet on blood vessels (Simard et al., 2003), and so have an anatomy suitable for signalling from neurons to arterioles to control blood flow.

Astrocytes show a rise of intracellular calcium concentration in response to synaptic activity, partly as a result of metabotropic glutamate receptors being activated by synaptic glutamate release (Porter and McCarthy, 1996). There is some evidence, however, that the metabotropic receptor thought to be responsible for the activity-induced calcium concentration increase (mGluR5), is only expressed by astrocytes during development (Sun et al., 2013). Other mGluRs (mGluR2/3) may raise $[Ca^{2+}]_i$ through activation of L-type voltage-gated calcium channels (Haak et al., 1997), or via their G-protein subunit coupling to PLC (Zeng et al., 2003), and ATP released during neuronal activity also contributes to astrocyte $[Ca^{2+}]_i$ rises (Newman, 2001). Calcium concentration rises in astrocytes can lead to arteriole dilation (Gordon et al., 2008; Takano et al., 2006; Zonta et al., 2003). This occurs mainly as a result of calcium activating the enzyme phospholipase A_2 (Fig. 1.1) to generate arachidonic acid and its vasoactive metabolites, which include prostaglandins, epoxyeicosatrienoic acids (EETs) and 20-hydroxyeicosatetraenoic acid (20-HETE).

Prostaglandins are produced from arachidonic acid by cyclooxygenase (COX) enzymes, both forms of which (COX1 in astrocytes and COX2 in astrocytes and neurons) are involved in blood flow control (Niwa et al., 2000; Takano et al., 2006). COX initially produces prostaglandin H_2 which is then converted to the vasodilator prostaglandin E_2 by PGE synthase. PGE_2 relaxes smooth muscle by acting through EP_4 receptors to activate cyclic AMP production (Davis et al., 2004), promoting relaxation (see section 1.4). Prostaglandins also hyperpolarize arteriolar smooth muscle cells by activating calcium-dependent potassium channels (Serebryakov et al., 1994), reducing voltage-gated Ca^{2+} entry and thus decreasing contraction. The actions of prostaglandins are terminated by re-uptake into cells expressing the prostaglandin transporter. Experiments in Chapter 4 test the role of prostaglandins in causing dilation of capillaries by pericytes.

EETs are produced in astrocytes from arachidonic acid by epoxygenases, a class of cytochrome P450 enzyme (Alkayed et al., 1996; Amruthesh et al., 1993). EETs can hyperpolarize and thus relax smooth muscle by activating a Ca^{2+} influx through TRPV4 channels, which in turn activates large conductance (BK_{Ca}) Ca^{2+}-activated K^+ channels (Campbell et al., 1996; Earley et al., 2005). EETs may also cause relaxation by inhibiting vasoconstricting thromboxane A_2 receptors (Behm et al., 2009). EETs are inactivated by soluble epoxide hydrolase which converts epoxides to their corresponding dihydroxyeicosatrienoic acids (Fang et al., 2001; Iliff et al., 2010; Spector et al., 2004), although EETs can also be inactivated by COX activity or by slow insertion into phospholipid stores (Bernstrom et al., 1992; Ellis et al., 1990). In Chapter 4, I test the role of EET release in generating dilation of capillaries by pericytes.

Arachidonic acid formed in astrocytes can also diffuse to arteriolar smooth muscle and be converted

into 20-HETE by the ω-hydroxylase enzyme, CYP4A (Gebremedhin et al., 1998; Metea and Newman, 2006; Mulligan and MacVicar, 2004). 20-HETE constricts smooth muscle by activating protein kinase C, inhibiting potassium channels, depolarizing the cells and thus increasing voltage-gated Ca^{2+} influx (Lange et al., 1997). NO released by neural activity inhibits CYP4A and thus reduces 20-HETE mediated constriction (Roman, 2002), an effect which will be crucial for the interpretation of my data in Chapter 4.

Activity-evoked $[Ca^{2+}]_i$ rises can also increase blood flow by opening calcium-activated potassium channels in astrocytes. This leads to an increase in extracellular potassium concentration that enhances the conductance of inward-rectifying K^+ channels in smooth muscle, causing hyperpolarization and vessel dilation (Filosa et al., 2006).

1.3 Vasoconstriction by noradrenaline, dopamine and 5-HT

For the activity-evoked dilation of arteriolar smooth muscle described above to occur, there has to be a tonic constriction of the arterioles, which is partly produced by aminergic input to the vessels. We will see in Chapter 4 that similar events occur in capillary pericytes. Within the brain parenchyma, blood vessels are close to noradrenergic terminals of neurons from the locus coeruleus, which appear to release their transmitter close to astrocyte endfeet (Cohen et al., 1997; Paspalas and Papadopoulos, 1996). Noradrenaline constricts brain blood vessels (Raichle et al., 1975). In part this may be because it increases astrocytic $[Ca^{2+}]_i$ by acting on α_1 receptors (Bekar et al., 2008; Duffy and MacVicar, 1995) leading to vessel constriction, presumably via the 20-HETE pathway described above (Mulligan & MacVicar, 2004). Noradrenergic innervation can also directly affect vascular smooth muscle. Smooth muscle cells express both G_q coupled α_1 and G_i coupled α_2 receptors (Drew and Whiting, 1979) and activation of these receptors increases $[Ca^{2+}]_i$ leading to vessel constriction (Vanhoutte and Rimele, 1982). α_1 adrenergic receptors are thought to be responsible for neuron-mediated vasoconstriction as these receptors are located close to locus coeuruleus nerve terminals, whereas $\alpha_{2\ receptors}$ are located away from the nerve terminals (McGrath, 1983; McGrath and Wilson, 1988). Smooth muscle cells also express G_s coupled β adrenergic receptors (Lowe and Gilboe, 1971). Activation of which leads to dilation through increased cAMP production, although noradrenaline has a higher affinity for α adrenoceptors (Molinoff, 1984). Dopaminergic fibres from the ventral tegmental area and 5-HT-releasing axons from the raphe nucleus may also contribute to vasoconstriction (Cohen et al., 1996; Krimer et al., 1998). The arteriole tone set by aminergic input may affect how much blood flow increase is produced by the mainly glutamate-mediated signalling pathways which dilate vessels in response to neuronal activity. For example dilations evoked by raised extracellular $[K^+]$ or by raising astrocyte $[Ca^{2+}]_i$ pharmacologically are

larger when the vessels are more preconstricted by a thromboxane agonist (Blanco et al., 2008).

1.4 Regulation of smooth muscle tone

As mentioned in section 1.2, blood flow is regulated by the diameter of blood vessels, which is determined by the tone of the smooth muscle cells that line these vessels. Vasoactive agents released from astrocytes and neurons control the tone of the smooth muscle cells by altering the membrane potential, and thus the intracellular calcium concentration, as well as by altering the sensitivity to Ca^{2+} of the contractile proteins involved in contraction via changes in cyclic nucleotide levels and phosphorylation. Smooth muscle contraction, like all muscle contraction, is controlled by cross bridge cycling of actin and myosin. Unlike in striated (skeletal and cardiac) muscle, the actin and myosin in smooth muscle is not organized into well-defined sarcomere structures. The intracellular calcium concentration increase triggering contraction is produced by calcium entry as well as release from intracellular stores, and the actin binding proteins regulating contraction are different from those in skeletal and cardiac muscle.

Smooth muscle contraction is regulated by cross-bridge cycling of myosin light chain (MLC) and α smooth muscle actin (αSMA; Webb, 2003). The interaction between these proteins is controlled by changes of intracellular calcium concentration (Hathaway et al., 1991), which alters the activity of myosin light chain kinase (MLCK), as shown in Figure 1.2.

Vasoconstrictive substances bind to receptors on the cell surface and lead to entry of extracellular calcium (in the case of ligand-gated ion channels) or the release of calcium from intracellular stores (in the case of G protein-coupled receptors). Calcium entry from the extracellular space is required for smooth muscle contraction as the sarcoplasmic reticulum is not as complex as in skeletal muscle and does not contain enough calcium to produce sustained contraction on its own. Calcium combines with calmodulin and, once four calcium ions have bound, the complex activates MLCK, which phosphorylates MLC. MLC phosphorylation increases the affinity of myosin for αSMA, so the filaments interact and contraction occurs (Sanders, 2008). Smooth muscle contraction is tonic and the muscle will remain contracted as long as calcium is bound to calmodulin and MLC remains phosphorylated. When the intracellular calcium concentration drops below the affinity of calmodulin for Ca^{2+}, the calcium-calmodulin complex disassembles and the phosphate is removed from the MLC via MLCP. This decreases the affinity of myosin for αSMA, which inhibits interaction and results in relaxation.

Smooth muscle tone is also regulated by the cyclic nucleotides, cAMP and cGMP and their downstream protein kinases, PKA and PKG. Vasodilatory substances increase the concentration of cyclic

nucleotides, which leads to a reduction in the $[Ca^{2+}]_i$ by decreasing IP_3-mediated calcium release from the sarcoplasmic reticulum, by phosphorylating the IP_3R or by decreasing PLC activity (via cGMP-dependent protein kinases) and therefore reducing IP_3 production (Fritsch et al., 2004; Rapoport, 1986). Cyclic GMP also reduces the $[Ca^{2+}]_i$ by enhancing Ca^{2+} uptake into the sarcoplasmic reticulum (Cornwell et al., 1991). Cyclic nucleotides also reduce calcium influx into smooth muscle cells, by inhibiting VGCCs (voltage gated calcium channels), and increase calcium efflux, by activating the plasma membrane Ca^{2+}-ATPase (Xiong and Sperelakis, 1995; Rashatwar et al., 1987). Another method through which cyclic nucleotides promote relaxation is through activation of potassium channels, leading to potassium efflux (Aiello et al., 1995; Natarajan et al., 2010; Standen and Quayle, 1998). As well as promoting membrane hyperpolarization and thus reducing the $[Ca^{2+}]_i$, cyclic nucleotides can alter the relationship between calcium concentration and MLC phosphorylation and thus the Ca^{2+} sensitivity of the contractile myofilaments. Cyclic AMP-dependent protein kinase can inhibit MLC kinase by phosphorylating the calmodulin-binding domain thus decreasing the affinity for binding (Conti and Adelstein, 1981), while PKG increases MLC phosphatase activity by phosphorylating its regulatory subunit (Nakamura et al., 2007). Finally, cyclic nucleotide-dependent protein kinases are thought to phosphorylate the heat shock-related protein, HSP20, which leads to dissociation of contractile force from MLC phosphorylation. This may occur through dissociation of the contractile apparatus from specific focal contacts, such as dense bodies and dense plaques, which provide a framework for the attachment of contractile structures to the cytoskeleton (Woodrum et al., 1999).

1.5 An overview of pericytes

Capillaries are not surrounded by a continuous layer of smooth muscle but instead have spatially separated contractile cells called pericytes at intervals along their length (see Figure 1.3). Here I will introduce pericytes, the main focus of this thesis.

1.5.1 Pericyte morphology

Pericytes are vascular mural cells. These cells can be identified by their rounded cell body and their position on capillaries, and have been described as having a “bump on a log” morphology (see Figure 1.3). Less visible are the processes that extend along vessels, and may even extend to contact multiple vessels (Williamson et al., 1980). On a single vessel, primary processes run parallel to the long axis of the vessel. These processes then branch into secondary processes that wrap circumferentially around the capillary (Figure 1.3; Forbes et al., 1977). Pericytes are present on pre-capillary arterioles, capillaries and post-capillary

venuoles. The morphology of pericytes on these different vessel types varies. Pericytes on larger vessels appear similar to smooth muscle cells. Vascular smooth muscle cells are orientated in a circular manner around arteries and show very little variation in morphology (Figure 1.3; Walmsley and Canham, 1979; Peters et al., 1983) but their morphology becomes more varied at the level of arterioles (Ushiwata and Ushiki, 1990). Here smooth muscle cells have rounded cell bodies and numerous processes (Ushiwata and Ushiki, 1990) and thus distinguishing between smooth muscle cells and pericytes at this level can be difficult. At true capillaries, pericytes are thought to have less complex processes (Zimmermann, 1923).

In this thesis I report experiments studying capillary pericytes. I identify these cells using the morphology described above. I ensure that I am studying capillaries by identifying vessels that are under 10 μm in diameter and lack a continuous smooth muscle lining. Capillaries consist of a layer of thin, elongated endothelial cells making up the tunica intima. These cells are in very close contact with the mural cells, pericytes, which form the tunica media. Both endothelial cells and pericytes are completely covered by basement membrane (Sims, 1986). The perivascular space beyond the basement membrane (referred to as the Virchow-Robin space at the arteriole level) has been found to contain meningeal cells and immune cells (Bechmann et al., 2007). This perivascular space is less evident at the level of capillaries. Beyond the perivascular space is the juxtavascular space where astrocyte endfeet lie (astrocyte foot processes lie 20 nm from the capillary endothelium) and further immune cells, such as microglia, are observed. Distinguishing between pericytes and other perivascular cells becomes difficult at the capillary level because of the absence of the Virchow-Robin space and the term pericyte is frequently used in the literature to demote any microvascular periendothelial mesenchymal cell (Armulik et al., 2011). In Chapter 3 I will report experiments that define better the cell types in this perivascular location on capillaries.

Pericytes cover 22%-37% of the cerebral capillary surface (Frank et al., 1987; Mathiisen et al., 2010). The average distance between pericyte cell bodies in the CNS is 50 μm (de Oliveira, 1966) and each cell's processes usually span several endothelial cells along the capillary (Armulik et al., 2011). The ratio of the number of endothelial cells to the number of pericytes is between 1:1 and 3:1 in the CNS (Mathiisen et al., 2010; Sims, 1986; Pardridge et al., 1999).

Electron microscopy has revealed details about the relationship of the contacts between pericytes and endothelial cells. These cells are connected through several kinds of specialized contacts. 'Peg and socket' contacts are interdigitating attachments where pericyte cytoplasmic fingers insert into endothelial invaginations, while adhesion plaques are points at which microfilament bundles in pericytes are located close

to electron-dense material in endothelial cells (Courtoy and Boyles, 1983). Pericytes and endothelial cells also make tight junctions with each other (Tilton et al., 1979; Larson et al., 1987; Díaz-Florez et al., 2009).

1.5.2 Pericyte surface markers

There is no single, entirely specific pericyte marker. This may be because pericytes are a heterogeneous population (Sims, 1991; Allt and Lawrenson, 2001; Dore-Duffy, 2006). Table There are however many markers which can be specific to pericytes depending on tissue type, species, vessel size, differentiation, and which are up and down regulated in conjunction with developmental stage. Table 1 shows a list of known pericyte markers. Here I will discuss some of the problems encountered when using these markers.

The pericyte marker I mainly used in this thesis is NG2 (neural glial protein 2, or high-molecular-weight melanoma-associated antigen, HMW MAA; Ozerdem et al., 2001). NG2 is a chondroitin sulfate proteoglycan involved in vasculogenesis and angiogenesis (Stallcup, 2002; Fukushi et al., 2004). It is known that NG2 is not only expressed by pericytes, but is also expressed by multiple cell types, including oligodendrocyte precursor cells (Nishiyama et al., 1991; 1996; see Table 1) which can be distinguished by their non-vascular location, and expression of olig2 and PDGFRα. There are also some claims that endothelial cells express NG2 (Schrappe et al., 1991; Grako and Stallcup, 1995; Corselli et al., 2010; but see below). Another commonly used pericyte marker, PDGFRβ (Lindahl et al., 1997), a tyrosine-kinase receptor involved in angiogenesis and blood brain barrier formation and maintenance, is also expressed by multiple cell types including fibroblasts, astrocytes, certain tumour cells and neurons (Lindahl et al., 1997; Smits et al., 1991; Beazely et al., 2006). Using a marker that also labels other cell types may lead to confusion when identifying pericytes.

Early studies found that pericytes express α-smooth muscle actin (αSMA; Herman and D'Amore, 1985; Skalli et al., 1989), a contractile protein involved in smooth muscle contraction, and this is still often used as a pericyte marker (Yemisci et al., 2009; Fernández-Klett, 2010). There has been some controversy, however, about whether this protein is expressed by all pericytes or, rather, just by pericytes on larger vessels, which appear more morphologically similar to smooth muscle cells (Nehls and Drenckhahn, 1991). Pericyte expression of αSMA has also been shown to vary greatly between *in vitro* and *in vivo* experiments, since 60-80% of pericytes are labelled by αSMA antibody *in vitro*, whereas *in vivo* αSMA antibody only labels 1-10% of pericytes (Nehls and Drenckhahn, 1991). There is also controversy over pericyte expression of another contractile protein, desmin (Fujimoto and Singer, 1987; Nehls et al, 1992), which is an intermediate

filament expressed near the Z line in sarcomeres in striated muscle and associated with dense bodies in smooth muscle cells (Kargacin et al., 1989). It has been suggested that desmin is not expressed by CNS pericytes (Díaz-Flores et al., 1991). It is important to investigate contractile protein expressed by pericytes as expression of these proteins supports their role in control of capillary diameter, and thus of blood flow (see section 1.6.5 and Chapter 3).

NG2 positive perivascular cells have been suggested to express the immune cell markers ED2 (Graeber et al., 1989; Balabanov et al., 1996) and Iba1 (Yokoyama et al., 2006; Matsumoto et al., 2008). A study examining *ex vivo* human CNS cell preparations claimed that the majority of NG2 positive cells belong to the microglial lineage (i.e. they expressed CD68 and CD11c; Pouly et al. 1999). The expression of these markers by pericytes suggests that they may have a role as an immune cell. This is further discussed in section 1.6.4, but my data in Chapter 3 contradict this idea.

1.6 The many roles of pericytes

As described above, pericytes show structural heterogeneity, it is also thought that these cells show functional heterogeneity. Here, I discuss the multiple roles that pericytes have been suggested to play in the CNS.

1.6.1 Angiogenesis

Pericytes are thought to play a key role in angiogenesis. Pericytes are early recruits to newly vascularized tissue during embryogenesis (endothelial cells begin angiogenesis at E12 and pericytes appear at E19). They appear at the tip of sprouting vessels and appear to guide newly formed vessels (Nehls et al., 1992). The balance between the number of endothelial cells and pericytes appears to be highly controlled (Frank et al., 1987). Paracrine interactions between pericytes and endothelial cells are involved in initiation of vessel growth as well as vessel stabilization. These cells release soluble factors that act in a paracrine manner, including platelet derived growth factor B (PDGF-B), transforming growth factor β (TGFβ), vascular endothelial growth factor (VEGF) and angiopoietins (Angs).

Endothelial cells release PDGFB, which is thought to recruit pericytes to growing vessels (Hellström et al., 1999; Hirschi et al., 1999; Betsholtz, 2004). Mice deficient in the PDGFβ receptor, which is expressed in pericytes, show attenuation of pericyte recruitment to sprouting capillaries, and these vessels are found to be unstable (Lindblom et al., 2003). Pericytes also release several factors that contribute to vessel development and stabilization. TGFβ is activated by pericyte-endothelial cell interaction and inhibits endothelial cell

proliferation and migration (Orlidge and D'Amore, 1987; Sato and Rifkin, 1989). TGFβ also promotes differentiation of pericytes (via the Wnt/beta-catenin pathway: Darland and D'Amore, 2001; Stenman et al, 2008) and reduces VEGF receptor expression (Bergers and Song, 2005). Vascular endothelial growth factor (VEGF) is also released by pericytes (Yamagishi et al., 1999; Darland et al, 2003) and has been found to promote transformation of endothelial cells on sprouting vessels into pericytes. The notch receptor, which is highly expressed in pericytes (Wang et al., 2008) downregulates endothelial VEGF receptor expression to stop vessel growth (Siekmann and Lawson, 2007). Angiopoietins (Ang1) released from pericytes acts on tyrosine kinase receptor (Tie-2) on endothelial cells and promote vascular stabilization (Uemura et al., 2002; Thurston, 2003). Deficiencies in either Ang1 or Tie2 lead to poor vessel growth (Jones et al., 2001) and reduced pericyte expression (Patan, 1998). Another angiopoietin, Ang2, has the converse effect and appears to be pro-angiogenic. Overexpression of Ang2 leads to dense vascular networks with poor pericyte coverage (Feng et al., 2007). Other factors involved in angiogenesis include NG2, which is expressed on pericytes and promotes endothelial cell motility and angiogenesis (Fukushi et al., 2004). NG2 has been shown to be a co-receptor for PDGF (Grako et al., 1999; Grako and Stallcup, 1995). Receptors for ephrins are expressed on endothelial cells and activation of these receptors has been proposed to promote pericyte migration and vessel formation (Foo et al., 2006; Salvucci et al., 2009).

1.6.2 Blood brain barrier maintenance

The blood brain barrier (BBB) is a key feature of the CNS. It serves to restrict exchange of substances between the circulation and the parenchymal tissue (Betz and Goldstein, 1986), thus protecting the brain from injury and disease. A functioning BBB is characterized by tight junctions (restricting paracellular transport), low rates of trancytosis, and the expression of specific transporters and enzymes (Ballabh et al., 2004). The BBB is made up of endothelial cells, pericytes and basal lamina, and more recently a role of astrocytes in BBB control has been reported (Mathiisen et al., 2010).

The role of pericytes in blood brain barrier maintenance was first considered due to the increased ratio of pericytes to endothelial cells observed in the CNS compared to other organs (Frank et al., 1987; Shepro and Morel, 1993; Díaz-Flores et al., 2009; Zlokovic, 2008). It is also of note that there are tight junctions between endothelial cells and pericytes (Tilton et al., 1979) and that pericytes induce synthesis of the molecules that make up the tight junction via Ang1 (Hori et al., 2004). Pericytes also produce extracellular matrix that contributes to the BBB (Hartmann et al., 2007).

Using transgenic mice with PDGFRβ expressed at half the normal level to downregulate pericyte generation, it has been shown that pericytes are necessary for the formation of the BBB (Daneman et al., 2010) and that the pericyte coverage of a capillary determines its vascular permeability (Armulik et al., 2010; Daneman et al., 2010). Pericyte-deficient mice do not show a reduction in endothelial expression of BBB-specific genes, but instead they fail to down regulate genes which increase vascular permeability (Daneman et al., 2010). Pericytes are not only involved in BBB development, but also play a crucial role in maintenance of the BBB in adulthood and ageing (Armulik et al., 2010; Bell et al., 2010). As the number of pericytes decreases in ageing vascular permeability increases (Bell et al., 2010).

Formation of the BBB has also been suggested to rely on astrocytes (Janzer and Raff, 1987; Sobue et al., 1999) but there is some controversy regarding the timing of astrocyte development and BBB formation (Bauer et al., 1993; Kniesel et al., 1996; Daneman et el., 2010), suggesting that pericytes play a more important role at this stage. It is likely, however, that astrocytes are involved in maintenance of the BBB.

1.6.3 Glial scar formation

A subtype of pericyte (approximately 10% of the total population) has been seen to give rise to a scar-forming stromal cell in injured spinal cord (Göritz et al., 2011). These cells migrate from their perivascular location, are recruited to the site of injury, and become positive for fibroblast markers. They function to 'seal' the injured tissue by producing extensive networks of extracellular matrix proteins, which will eventually form connective tissue and make up the stromal component of scar tissue. This structure is formed in order to prevent further damage. Previously it had been thought that astrocytes were the only cells that played this role, and thus it was referred to as the glial-scar (Sofroniew, 2009). Astrocytes do comprise part of the glial scar, and this astrocytic component surrounds the stromal cells. Pericytes have also been found to form dermal scars, and kidney and liver fibrosis (Humphreys et al., 2010; Sundberg et al., 1996; Wirz et al., 2008).

1.6.4 Pluripotent cell

Pericytes are considered to be multipotent precursors for several different cell types (Dore-Duffy et al., 2006, 2008). Several researchers have identified pericytes as potential progenitors of mesenchymal stem cells (Zimmerlin et al., 2011; Crisan et al., 2008; Corselli et al., 2010). Much like pericytes, mesenchymal stem cells are a cell type that is not clearly defined in the literature. There is no specific marker for mesenchymal stem cells and their characteristics differ throughout the literature (Javazon et al., 2004). Mesenchymal stem cells are said to be 'captured' by developing vessels and become pericytes, but to retain nascent stem cell

properties (Bautch, 2011). Pericytes show mesenchymal stem cell marker expression (Corselli et al., 2010; Crisan et al., 2008)

Evidence has also been found for pericytes transforming into many other cell types including smooth muscle cells (Meyrick and Reid, 1978; Sims, 1986; Rhodin and Fujita, 1989), adipocytes (Cinti et al., 1984), chondrocytes (Reilly et al., 1998) and neurons (Dore-Duffy et al., 2006). It has also been speculated that pericytes are resting microglial cells (Baron and Gallego, 1972; Hager et al., 1975) or a precursor cell for macrophages (Maxwell and Kruger, 1965; More and Leblond, 1969). Following irradiation, pericytes are suggested to become mobile and penetrate the parenchyma to become microglia (Maxwell and Kruger, 1965), and a phagocytic potential of pericytes has been demonstrated multiple times (Cancilla et al., 1972; Balabanov et al., 1996; Thomas, 1999). In Chapter 3 of this thesis I will combine transgenic labelling of pericytes with antibody labelling of immune cell markers to assess whether pericytes and perivascular immune cells share cell markers.

1.6.5 Contractility

Pericytes have long been suspected to be contractile cells (Rouget, 1874; Vimtrup, 1922; Zimmermann, 1923). This was originally put forward due to the position and structure of these cells. As described in section 1.4.1, pericytes have processes that encircled capillaries and contain bands of microfilaments and dense bodies similar to smooth muscle cells (Vimtrup, 1922; Zimmermann, 1923). With the advent of immunocytochemistry, pericytes were found to express many of the contractile proteins expressed in smooth muscle cells. Pericytes express cyclic GMP-dependent protein kinase, and several classes of myosin (Joyce et al., 1984; Joyce et al., 1985a; Joyce et al., 1985b). These are essential components needed for smooth muscle contraction. It has also been observed that pericytes express microfilaments resembling actin and myosin (Le Beux and Wilemot, 1978; Ho, 1985) and that actin microfilaments of pericytes can activate myosin ATPase (Chan et al., 1986). Expression of αSMA and desmin have been observed (Herman and D'Amore, 1985; Fujimoto & Singer, 1987; Skalli et al., 1989), although there is controversy about the proportion, and type, of pericytes that express these proteins (Joyce et al., 1985; Nehls and Drenkhahn, 1991; Bandopadhyay et al., 2001, see section 1.5.2). However, the contractile nature of pericytes has also come into question as these cells do not express functional markers of smooth muscle cells such as calponin and caldesmon (Hughes and Chan-Ling, 2004). While actin and myosin are expressed in non-contractile cells, as they play a role in structural support, the calcium-binding proteins calponin and caldesmon regulate tone and are only found in contractile cells (Frid et al., 1992).

Functional evidence for pericyte contractility has been found in culture. Retinal pericytes, cultured on a collagen lattice, respond to application of multiple vasoconstricting substances by reducing the surface area of the lattice. This change was attributed to contraction of the pericyte (Schor and Schor, 1986; Kelley et al., 1987, 1988). Constrictions were seen in response to histamine, serotonin, ATP, ET-1, thromboxane and angiotensin II (Kelley et al., 1988; Das et al., 1988; Dodge et al., 1991; Matsugi et al., 1997a), whereas dilations were observed on application of prostacyclin and adenosine (Dodge et al., 1991; Matsugi et al., 1997b). Contractility in retinal pericytes *in situ* has also been observed in response to several substances (Schonfelder et al., 1998; Peppiatt et al., 2006).

Like smooth muscle, pericytes express receptors for vasoactive substances such as noradrenaline (Elfont et al., 1989) and the majority (65%) of the noradrenergic innervation of CNS vasculature ends near capillaries rather than arterioles (Cohen et al., 1997). Noradrenaline has been found to produce membrane depolarization of pericytes (Helbig et al., 1992 – attributed to α_1 receptors) via a rise of cAMP concentration (Kelley et el., 1988; Markhotina et al., 2007). Other neuronal terminals are located close to capillaries and pericytes, including those containing dopamine (Favard et al., 1990; Krimer et al., 1998), GABA (Gragera et al., 1993), VIP (vasoactive intestinal peptide; Benagiano et al., 1996), acetylcholine (Arneric et al., 1988) and NO (Roufail et al., 1995), which might therefore all be candidates for regulating pericyte tone and capillary diameter.

In retinal pericytes, much like in smooth muscle cells, constrictions appear to be evoked by rises of intracellular calcium concentration (Sakagami et al., 1999, 2001; Kamouchi et al., 2004; Sugiyama et al., 2005; Peppiatt et al., 2006). Calcium responses in ureter pericytes, however, appear to be slower and less oscillatory than those seen in smooth muscle cells (Borysova et al., 2013). Pericyte dilations could be produced by potassium channel activation leading to hyperpolarization, which decreases Ca^{2+} influx, or by NO directly inhibiting voltage-gated Ca^{2+} channels (Li & Puro, 2001; Sakagami et al., 2001). Secondary messengers that are thought to be involved in regulating pericyte tone include cGMP, which decreases calcium and chloride currents in retinal pericytes and reduces contractile tone (Haefliger et al., 1994; Sakagami et al., 2001), and cAMP, which is involved in potassium channel activation in response to PGI_2 (Burnette and White, 2006). Though a great deal of this work has been carried out in retinal pericytes, evidence has also been found for pericyte control of capillary diameter in cerebellar slices, where noradrenaline causes a constriction of capillaries and glutamate produces a dilation (Peppiatt et al., 2006).

Evidence supporting pericyte mediated changes in capillary diameter *in vitro* suggest that they may play a role in blood flow control *in vivo*. Capillaries are located closer to neurons than to arterioles (8-23 μm away compared to 70-160 μm in hippocampus; Lovick et al., 1999), and nerve terminals releasing multiple transmitters are located close to capillaries (see above). It therefore appears that these cells are well placed to respond rapidly to signals indicating changes in energy demand due to neuronal activity. It is possible that these cells receive a signal to which they not only respond but which they also propagate back to larger vessels as pericytes and smooth muscle cells may be electrically coupled (Berg et al., 1997; Borysova et al., 2013). If this were the case, capillaries may be actively involved in the initiation of blood flow changes. However some studies have found current and calcium concentration changes in local capillary endothelial cells in response to skeletal muscle stimulation, leading to a dilation of upstream arterioles without any dilation at the local capillary (Sarelius et al., 2000; Murrant et al., 2004).

Some evidence for capillary level blood flow control has been found *in vivo*. In the olfactory bulb, tentative evidence for active capillary responses was reported by two-photon imaging (Chaigneau et al., 2003), and dilations and constrictions of cerebral capillaries have been seen in rat somatosensory cortex on forepaw stimulation (Stefanovic et al., 2008) and in rat cortex on hypercapnia (Hutchinson et al., 2006). Attenuation of *in vivo* blood flow responses to whisker stimulation was observed in pericyte-deficient mice that have fewer pericytes (Bell et al., 2010). However, Fernández-Klett et al. (2010) have claimed that pericytes do not mediate active changes in blood flow, although their illustrations of vessels that did respond, which were identified as arterioles, may in fact show capillaries with pericytes on them, implying that pericytes are mediating the observed responses.

1.7 Pathology of ischaemia

In Chapter 6 of this thesis, I examine the response of pericytes to a common CNS pathology, ischaemia. Brain ischaemia is a critical reduction in cerebral blood flow that leads to irreversible brain damage in conditions such as stroke. Stroke is one of the leading causes of death and disability in developed countries. In this thesis I use incubation in solution lacking oxygen and glucose (in brain slices) and middle cerebral artery occlusion (MCAO) as animal models of stroke. The reduced supply of oxygen and glucose occurring in ischaemia, during stroke or MCAO, results in various extracellular and intracellular changes that finally lead to impaired neuronal function and cell death. In this overview I will highlight the main changes in cellular physiology evoked by ischaemia.

1.7.1 Energy failure

One of the most profound features of ischaemia is the energy failure due to inhibition of oxidative phosphorylation. The lack of oxygen supply initially results in glycolysis becoming the major source of ATP production but as this process is much less efficient than oxidative phosphorylation (producing 2 as opposed to 28 ATP molecules per molecule of glucose), and because local stores of glycolytic intermediates and of astrocyte glycogen are no longer being replenished by glucose arriving in the blood, the cell is soon deprived of sufficient ATP (Lipton, 1999). That leads to an inhibition of cellular kinases and ATP-dependent pumps, notably the Na^+/K^+-ATPase, on which 75% of the brain energy is used (Attwell and Laughlin, 2001). This causes a severe run down of transmembrane ionic gradients, which results in membrane depolarization.

1.7.2 Ionic imbalance

Impaired energy supply is the direct cause of the ion homeostasis disruption in ischaemia. As mentioned above, the Na^+/K^+-ATPase fails during ischaemia due to ATP depletion. Under normal conditions the Na^+/K^+ pump results in potassium influx, returning K^+ that exits the cell under resting conditions, because cell resting potentials are more positive than the Nernst potential for K^+. In ischaemia, this pump does not function, so the extracellular potassium concentration ($[K^+]_o$) rises. Increased extracellular $[K^+]$ causes depolarization of neurons and glia, and initially some action potential firing and an excessive synaptic vesicle release triggered by a $[Ca^{2+}]_i$ rise that is action potential independent (Katchman and Hershkowitz, 1993). After several minutes a regenerative increase of $[K^+]_o$ occurs, resulting in $[K^+]_o$ rising to 40 mM in anoxia and approximately 55mM in ischaemia (Hansen, 1985). This is observed alongside a reduction of extracellular sodium concentration ($[Na^+]_o$) by a similar amount due to a sodium flux into the cell. These changes depolarize cells to about -20mV; an event termed the anoxic depolarization.

1.7.3 Glutamate release and excitotoxicity

The initial depolarization, and increase in intracellular calcium concentration, causes excessive synaptic release of neurotransmitters, including glutamate. Glutamate release in ischaemia also occurs through reversal of glutamate transporters, and indeed this is the main release route for glutamate during severe ischaemia (Szatkowski and Attwell, 1994; Rossi et al., 2000; Hamann et al., 2005; See Figure 1.4).

Under physiological conditions, glutamate transporters are responsible for glutamate uptake, which is very important in maintaining the extracellular glutamate concentration at a value that does not activate glutamate receptors. Glutamate transport is Na^+-dependent and electrogenic: for each glutamate anion

entering the cell, three Na^+ ions and one proton enter, and one K^+ ion moves out of the cell. However in ischaemia, the ionic gradient rundown, and associated depolarization, cause the transporter to reverse and pump glutamate out of the cell (Rossi et al., 2000). This process generates a massive increase in the extracellular glutamate concentration, reaching up to approximately 100 µM (Globus et al., 1991; Phillis et al., 1996), and leads to the overactivation of glutamate receptors. The resulting activation of NMDA receptors in particular permits an excessive calcium influx, the effect of which is described below.

1.7.4 Calcium influx

A massive calcium influx from the extracellular space during ischaemia is triggered by multiple factors (Figure 1.4). Predominantly, as mentioned above, it is caused by activation of AMPA and NMDA receptors when the extracellular glutamate level increases (Rossi et al., 2000; Hamann et al., 2005; for a review see Seisjö, 1988, and Lipton, 1999). However, activation of other channels and receptors may also contribute to the Ca^{2+} influx: acid sensing ion channels (Xiong et al., 2004), transient receptor potential channels (Aarts et al., 2003; Lipski et al., 2006) and ATP receptors ($P2X_7$: Domercq et al., 2010) are all Ca^{2+}-permeable and open during ischaemia. In addition, membrane depolarization opens voltage-gated calcium channels, and the rise of $[Na^+]_i$ produced by glutamate-gated Na^+ entry reverses the action of the Na^+/Ca^{2+} exchanger, both of which result in a further increase in the intracellular calcium concentration (Hertz, 2008). At the same time, calcium extrusion from the cell by the ATP-dependent calcium pump is blocked because of ATP depletion (Nestler et al., 2008).

The calcium concentration rise in the cell cytoplasm can also have an intracellular source. Calcium-induced calcium release (CICR) occurs at the endoplasmic reticulum through activation of ryanodine receptors (Lipton, 1999; Nestler et al., 2008). Additionally, activation of G_q-coupled metabotropic glutamate receptors leads to the production of inositol trisphosphate, which also causes calcium release from the endoplasmic reticulum (Nestler et al., 2008). During ischaemia, the sequestration of calcium into the endoplasmic reticulum is blocked, as this process is dependent on ATP. As intracellular $[Ca^{2+}]$ increases, Ca^{2+} is taken up into the mitochondria (Sciamanna et al., 1992; Schinder et al., 1996). This leads to mitochondrial depolarization and opening of the mitochondrial permeability transition pore (MPTP; Halestrap, 2006), which causes the release of apoptogenic proteins and generates reactive oxygen species (ROS; Piantadosi and Zhang, 1996; Starkov et al., 2004).

All of these factors contribute to an increase in intracellular calcium concentration from approximately 50 nM under normal conditions to approximately 2.5 µM during ischaemia (Lipton, 1999). This causes

overstimulation of normally well-controlled Ca^{2+} dependent processes. The increased activation of proteases, such as calpain, leads to cleavage of the Na^{+}-Ca^{2+} exchanger and the plasma membrane Ca^{2+} -ATPase, which prevents calcium efflux (Bano and Nicotera, 2007). Elevated $[Ca^{2+}]_i$ also leads to an increased activation of lipases, such as phospholipases A (PLA) and C (PLC) (Raichle, 1983), whose action causes breakdown of membrane phospholipids and may result in decreased membrane integrity. Activation of lipases also leads to the production of free fatty acids, including arachidonic acid (AA), which in turn stimulates the production of eicosanoids, such as 20-HETE (Tegtmeier et al., 1990). Eicosanoids can exacerbate the ischaemic insult by promoting vasoconstriction and platelet aggregation and in this way further block the supply of oxygen and glucose to the affected area (Raichle, 1983).

The promotion of reactive radical formation by Ca^{2+} is not restricted to the production of eicosanoids. Binding of nitric oxide (NO) synthase to the Ca^{2+}-calmodulin complex, when $[Ca^{2+}]_i$ rises, initiates the production of NO from arginine (Lipton, 1999), which may result in the formation of highly increased levels of reactive nitrogen species, the downstream effects of which are described below.

1.7.5 Formation of reactive radicals

Excitotoxicity is frequently associated with the formation of reactive radicals (also known as free radicals or reactive oxygen and nitrogen species; ROS and RNS respectively). Free radicals are molecules with an unpaired electron in an outer shell; this unpaired electron causes the molecule to be unstable and highly reactive, targeting membrane fatty acids with double bonds and protein sulphydryl groups, which greatly destabilises their structures and leads to changes in their properties (Nester et al., 2008).

The production of ROS and RNS requires the presence of some oxygen, and greatly increases in the penumbra of an ischaemic area where some oxygen is still provided by unblocked vessels nearby, and during reperfusion, when blood flow is restored after ischaemia. Due to their high activity, free radicals (which may normally serve as second messengers in various signalling pathways) become pathological, causing DNA damage, lipid peroxidation and severe protein oxidation, which can lead to increased membrane permeability, prolonged inhibition of protein synthesis and promotion of DNA cleavage, including cleavage via the activation of pro-apoptotic signalling systems such as mitogen-activated protein kinases (MAPKs; Matsuzawa and Ichijo, 2005), which eventually cause extensive apoptotic cell death (Raichle, 1983; Siesjö, 1988; Lipton, 1999).

The formation of superoxide anion, which may be initiated by phospholipase activation, is a prerequisite for the formation of other ROS, and it is involved in the RNS pathway. Superoxide anions transformed by superoxide dismutase (SOD) react with nitric oxide to form peroxynitrite (Saran et al., 1990).

Peroxynitrite causes lipid peroxidation and protein oxidation, which leads to membrane disruption and enzyme inactivation (Halliwell, 1992). Peroxynitrite is also a precursor of other RNS radicals (e.g. nitrosoperoxycarbonate).

In ischaemia, therefore, the greatly increased Ca^{2+} flux into the cell may lead to excessive ROS formation (through the activation of phospholipases; Raichle, 1983) and RNS formation (by NO synthase stimulation; Lipton, 1999). Most of the free radicals, however, are formed during reperfusion after ischaemia. Upon a sudden increase in oxygen level, mitochondria drastically raise their level of superoxide production due to side reactions of electron carriers along the respiratory chain (mostly complexes I and III: Sugawara and Chan, 2003; Sugawara et al., 2004). Additionally, radicals are formed during the autooxidation of many compounds (e.g. catecholamines) and in the xanthine oxidase reaction (Lipton, 1999).

1.7.6 Vascular response to ischaemia

Ischaemia is associated with obstruction of the downstream microvasculature even after reperfusion of the occluded supply arteries occurs (as a result of endogenous clot removal mechanisms or clot removal surgically or with tissue plasminogen activator). This phenomenon of vascular no-reflow was first observed by Ames and colleagues (1968). In their study, a period of global ischaemia was followed by injection of colloidal carbon into the intracerebral vasculature. Following ischaemia, large regions of brains showed no dye filled vessels, signifying a failure of reperfusion. Subsequent experiments that have investigated blood flow after ischaemia and reperfusion found that, upon reperfusion, a brief period of hyperperfusion ('reactive hyperaemia') was followed by a long lasting decrease in blood flow (Hauck et al., 2004). The flow in capillaries was also noticeably more heterogeneous and 6.4% of capillaries showed no flow at all. Capillary diameter was also reduced, suggesting that ischaemia and reperfusion caused capillary constriction. The responsivity of vessels following ischaemia is also affected (Leffler et al., 1989).

These data suggest that, even when circulation is restored following ischaemia, blood flow may not be restored enough to adequately fuel neuronal processes. A chronic decrease in blood flow following ischaemia may exacerbate neuronal death by limiting oxygen and glucose delivery to, and removal of CO_2 from, the tissue that is struggling to recover from metabolic disruption. Microcirculatory failure despite successful opening of the occluded artery may thus be one of the factors accounting for the low success rate of reperfusion therapies (Juttler et al., 2006).

Blood flow regulation by pericytes is thought to have a pathological role in the brain. Ischaemia leads to a constriction of retinal capillaries near pericytes (Peppiatt et al., 2006). The contractility of pericytes is

regulated by the intracellular calcium concentration (Peppiatt et al., 2006; Kamouchi et al., 2004). In pathological conditions such as ischaemia, when ATP is depleted, there is expected to be a failure in calcium removal from pericytes leading to an uncontrolled rise in intracellular calcium concentration. Reactive oxygen species have been shown to increase the calcium concentration in cultured human pericytes (Kamouchi et al., 2007) and to induce constriction of capillaries following MCAO, despite successful reperfusion of the artery, indicating a contribution to the no-reflow phenomenon (Yemisci et al., 2009). In the latter study, capillaries were found to be 'pinched off' at localised points, trapping erythrocytes, and these constrictions were attributed to pericyte contractions. Previous studies have attributed capillary constriction following ischaemia and reperfusion to aggregation of polymorphonuclear leukocytes (del Zoppo et al., 1991; Mori et al., 1992), activated platelet and fibrin deposition (del Zoppo, 2008), or swelling of glia and endothelial cells (Ames et al., 1968; Ito et al., 2011).

There is also evidence that pericytes are vulnerable to death following exposure to reactive oxygen species and hypoxia in culture (Shojaee et al., 1999; Yu et al., 2012), and following MCAO and reperfusion *in vivo* (Fernández-Klett et al., 2013). Pericyte death may, therefore, contribute to the long lasting constriction and reduced blood flow seen following ischaemia.

Modelling studies have found that even small perturbations in capillary geometry and flow produced by ischaemia can lead to increased heterogeneity of capillary blood flow, which reduces tissue oxygen extraction, compounding the effects of the ischaemia (Jespersen and Østergaard, 2012). Consequently, even sparse pericyte constriction may contribute to no-reflow, not only by reducing blood flow, but also by increasing heterogeneity of blood flow, and thus impairing oxygenation. In Chapter 6 I investigate the pericyte response to ischaemia.

1.8 The structure and role of the cerebellum

In chapter 4, I report experiments on capillary diameter in the molecular layer of the cerebellum. This brain region was chosen as it is well described in the literature, the microcircuits have been examined in depth, and it had been used previously to study pericyte properties by other workers in our lab, so my results could be directly compared with those previously obtained. In this section I will give the background information on the cerebellum that is needed to understand the experiments that I performed. The anatomy and function of the cerebellar cortex can be summarised as follows.

The main function of the cerebellum is to store motor programmes and use them to provide fine motor control. The cerebellum does not initiate movement *per se*, but it is important for the regulation of precise

motor output to confer proper balance, posture and smooth motor movements. The cerebellum is located behind the cerebral cortex and has a highly organised and uniform structure. It can be divided into three lobes, denoted flocculondular, anterior and posterior, of which the last two can be further divided into the central vermis and the two lateral cerebellar hemispheres. My experiments were carried out in the vermis, which is composed of multiple folia, each of which is characterised by the same layered structure. Each folium comprises grey matter surrounding centrally located white matter. The grey matter can be divided into three layers: the granule cell, Purkinje cell and molecular layers. My experiments were carried out on capillaries in the molecular layer. This was due to the structure of the cerebellar vasculature, and the sparcity of cell bodies to obscure the capillaries of this layer (Kandel et al., 2000).

The innermost granule cell layer is composed of a high number of densely packed granule cells and a smaller number of interneurons (Golgi cells), astrocytes and NG2 positive oligodendrocyte precursor cells. Granule cells are distinguished by their small cell body and 4-5 dendrites which receive excitatory synaptic input from the mossy fibres and inhibitory input from the Golgi cells (which also receive input from the mossy fibres). The mossy fibres are myelinated axons which provide information to the cerebellar cortex on the sensory environment (information derived from peripheral receptors) and on the desired motor output (information from the cortex and other brain areas). In the granule cell layer this input information is recoded into the firing of the granule cells. Each granule cell projects its axon (which is unmyelinated in rodents) vertically through the molecular layer where it splits into two branches which travel horizontally in opposite directions to form a so-called parallel fibre, which is approximately 4mm long in the adult rat. The parallel fibre sends excitatory synapses onto the dendritic tree of approximately 130 Purkinje cells as well as onto the dendrites of interneurons, the basket and stellate cells, which inhibit the Purkinje cells. The Purkinje cells have their somata arranged in a thin layer – the Purkinje cell layer, which also contains the somata of radial glial cells (the Bergmann glia) which send long processes through the molecular layer. The elaborate Purkinje cell dendritic tree is flattened in a plane perpendicular to the cerebellar folds, so that the molecular layer mainly consists of an array of these dendritic trees, with the parallel fibres running perpendicular to them, like telephone wires on a pole. In addition to receiving excitatory synaptic input from the parallel fibres, the Purkinje cell also receives excitation from (myelinated) climbing fibres which arise in the inferior olive. This input may provide a teaching input to induce plasticity at the parallel fibres and thus correct erroneous motor outputs. After integration of the information arriving on the approximately 100,000 synapses impinging on the Purkinje cell dendritic tree, the final output from the cerebellum passes via the Purkinje cell output axon

through the white matter to the deep cerebellar nuclei, whose cells are inhibited by Purkinje cells. The deep cerebellar nuclear neurons then send axons to the premotor cortex, primary motor area and red nucleus to modulate the motor output of the body. For the cerebellar cortex to process motor information rapidly, information has to arrive on the mossy and climbing fibres and leave on the Purkinje cell axons at high speed. This is achieved by these long distance axons in the white matter of the cerebellum being myelinated. In addition to the myelinated axons, the white matter consists of oligodendrocytes, astrocytes, microglia and blood vessels.

My experiments were carried out in the molecular layer of the P12 rat vermis, at which age the cerebellum is as described above, although synaptic connections and myelin are still developing.

1.8.1 Vascular supply of the cerebellum

The cerebellum receives blood supply from three arteries, which are the superior cerebellar artery (SCA), the anterior inferior cerebellar artery (AICA) and the posterior inferior cerebellar artery (PICA). Both the SCA and the AICA branch from the basilar artery whereas the PICA branches from the vertebral artery. The SCA supplies blood to the superior portion of the cerebellum as well as the superior pons and pontomedullary junction. The AICA supplies blood to the anterior portion of the inferior cerebellum and part of the caudal pons. The PICA supplies blood to the inferior portion of the cerebellum as well as the choroid plexus and much of the lateral medulla (Martin, 2012).

The vascular system within the cerebellar cortex can further be divided into three layers. These are the superficial, middle and deep intracortical vascular layers. The superficial layer supplies the molecular layer of the cerebellum. The blood vessels in this layer enter the cortex perpendicular to the surface and appear to form hairpin loops (Hoddle and Sercombe, 1996). These are the vessels that I have studied. The middle intracortical vascular layer terminates in the Purkinje cell layer, where these vessels divide into branches extending parallel to the surface connecting with capillaries from the molecular layer and the granule cell layer. The deep intravascular vascular layer supplies the granule cell layer. This layer is one of the most vascularised regions of the brain (Duvernoy et al., 1983; Akima et al., 1987; Hoddle and Sercombe, 1996).

1.9 The structure and role of the forebrain

In chapter 6, I report experiments on pericyte death in the forebrain, in both the striatum and cortex. This brain region was chosen because it is dependent on the middle cerebral artery, which is the most common vessel to become occluded in stroke (Stephens and Stilwell, 1969).

The cerebral hemispheres are the mostly highly developed portions of the central nervous system. The cerebral cortex is responsible for higher order functions such as thought, language and memory. It is made up of six layers that each have a distinct structure and composition. These are the molecular layer (layer 1), the external granular layer (layer 2), the external pyramidal layer (layer 3), the internal granular layer (layer 4), the internal pyramidal layer (layer 5) and the polymorphic layer (layer 6).

The striatum is part of the basal ganglia. This region receives inputs from the sensory-motor and association cortex as well as from the rest of the basal ganglia system, and is separated into compartments dependent on these inputs. The compartments of the striatum include the sensorimotor compartment, which receives input from the sensory cortex and contains the caudate nucleus and the putamen, the associative compartment, which receives input from the association cortex and contains the internal capsule, and the limbic compartment, which receives input from other parts of the basal ganglia and contains the nucleus accumbens. The striatum is responsible for eye movement control and cognition, control of limb and trunk movements and control of emotions (Martin, 2012).

1.9.1 The vascular supply of the forebrain

The forebrain receives blood supply through two main pairs of arteries: the anterior circulation, which is made up of the internal carotid arteries, and the posterior circulation which is made up of the vertebral arteries. The frontal hemispheres are supplied by the anterior circulation. The internal carotid arteries divide into the anterior cerebral artery and the middle cerebral artery. Each of these arteries is comprised of deep and cortical branches. The deep branches are proximal and supply deep brain grey matter and white matter whilst the cortical branches are distal and supply various neuronal laminae of the cerebral cortex.

There are two sites at which the anterior and posterior circulation communicate. This makes it possible for a decreased flow in one system to be compensated for by an increased flow in the other. The internal carotid artery and the basilar artery are joined through the circle of Willis (see Figure 1.5). This complete anastomotic ring is made up of the anterior cerebral arteries, the posterior communicating arteries, and, in rats, the internal carotid arteries. The terminal ends of the cerebral arteries anastomose on the dorsal convexity of the cerebral hemisphere (Martin, 2012).

The middle cerebral artery is the largest branch of the internal carotid artery and supplies blood to the lateral convexity of the cortex. It passes through the lateral sulcus and the surface of the insular cortex as well as over the inner opercular surfaces of the frontal, temporal and parietal lobes. The MCA is the most common artery to become occluded in stroke (Stephens and Stilwell, 1969).

Pial vessels, which arise from arteries, line the surface of the cortex. In humans, these large vessels (260-280 μm diameter) then branch perpendicularly, giving rise to penetrating arterioles. Penetrating arterioles can be divided into six different groups according to their morphology, the depth of the cortex that they penetrate and their branching pattern (Duvernoy et al., 1981). Group 1 arterioles and venuoles have a small diameter (approximately 10 μm) and only penetrate into the molecular layer (layer 1), and possibly the external granule layer (layer 2), of the cortex. Group 2 vessels, also known as intermediate vessels have a slightly larger diameter (15-25 μm) and reach the external pyramidal layer (layer 3). The third group of vessels are a similar diameter to group 2 and reach the internal granule cell layer (layer 4). The vessels that make up groups 4-6 all penetrate through the grey matter of the cortex to reach the sub cortical white matter but they show different branching properties. Group 6 in particular shows no branching throughout the grey matter and only branches in the white matter. This group are known as the medullary vessels.

Penetrating arterioles and venules have been found to form a regular pattern, with a single venuole being surrounded by a hexagonal array of arterioles (Duvernoy et al., 1981), although more recent studies found the ratio of venules to the arterioles to be 1:1.6 (rather than 1:6; Weber et al., 2008). Capillaries form dense patterns between these larger vessels and show variation in density throughout the cortical layers. The lowest capillary density is found in layer 1 while the highest density is found in layer 4 (Duvernoy et al., 1981; Weber et al., 2008). The vascular density in different layers correlates with the synapse number in each layer as well as with the average metabolic demand in the layers (Rissle et al., 1993; Woolsey et al., 1996; Tieman et al., 2004).

The vascular supply to the striatum comes from the MCA, via the lenticulostriate artery, and from the ACA, via the recurrent artery of Heubner. The sensorimotor compartment is supplied by the lateral lenticulostriate artery, the associative compartment is supplied by the medial lenticulostriate artery, and the limbic compartment of the striatum is supplied by the recurrent artery of Heubner. These vessels have similar branching patterns; penetrating vessels give rise to two to four secondary branches, these vessels then branch again, and the tertiary branches form small pre-capillary arteriole envelopes (Feekes et al., 2005).

1.10 Relevance to functional brain imaging

Because of the high energy use of neurons, the energy supply to the brain must be allocated flexibly to brain regions according to neuronal demand. Consequently, blood flow is increased to active areas (Roy and Sherrington, 1890), as explained above neural activity leads to ATP expenditure, largely on the pumping out from neurons of ions which enter to generate synaptic and action potentials (Attwell and Iadecola, 2002).

This evokes an increase in oxygen consumption to regenerate ATP which, within a few seconds, is followed by a disproportionate increase of blood flow to the active area. Associated with these local changes in oxygen consumption and blood supply, there are changes in the local oxygen concentration, which initially falls due to consumption, and then rises above its baseline value when the increased blood flow brings in more oxygen (Offenhauser et al., 2005; Enager et al., 2009). Concomitantly, there are changes in the levels of oxygenated and deoxygenated haemoglobin. This increase in blood flow, and thus in the level of oxygen and of oxygenated haemoglobin, is exploited by blood oxygen level dependent (BOLD) functional imaging, which detect the mismatch between energy use and supply in small brain regions. A local increase in signal (which is produced by blood flow increasing more than oxygen consumption in the targeted region) is assumed to reflect an increase in neuronal activity. This technique works as follows.

When an object is exposed to a magnetic field, all the protons within the object align themselves with (parallel to) or against (antiparallel to) the direction of the imposed magnetic field, B_0 (Figure 1.5A-C). Protons aligned parallel to B_0 have a lower energy than those aligned antiparallel and at any given time there is a tendency for a greater number of protons to be aligned parallel to the field. However, for quantum mechanical reasons, the magnetic dipole moments of the nuclei are not perfectly aligned with the field, but precess around its direction. Pulses of electromagnetic energy (radiofrequency (RF) pulses, B_1) which are perpendicular to the main field, are then applied to 'flip' the protons out of alignment with B_0 (Figure 1.5D). The net magnetization is now aligned more perpendicular to B_0 and continues to precess around the direction of B_0 (Figure 1.5D, E) The small, oscillating, magnetic field induces a current in the receiver coil and hence produces a magnetic resonance signal. When B_1 is no longer applied two relaxation processes occur, which result in the loss of signal, in two ways:

(1) Longitudinal relaxation (described by the time constant T1): the protons relax back to their original orientation aligned with B_0 as energy is dispersed from the protons to neighbouring nuclei (Figure 1.5F,G);

(2) Transverse relaxation (also known as 'spin-spin relaxation', described by time constant T2): the protons go out of phase with the precession of neighbouring protons due to tiny differences in the local magnetic field, caused by other magnetic nuclei and atoms moving nearby (Figure 1.5H)

BOLD contrast depends on the level of deoxyhaemoglobin in the blood. The iron in deoxyhaemoglobin is paramagnetic (Pauling & Coryell, 1936) and so creates local inhomogeneties in the magnetic field which result in the precessing nuclei no longer moving in phase. During the initial increase in oxygen consumption, oxygen

is taken from diamagnetic oxyhaemoglobin, leaving behind paramagnetic deoxyhaemoglobin, which makes the magnetic field experienced by protons in surrounding water molecules less homogenous and thus decreases the magnetic resonance signal from these protons. However, during the subsequent increase of blood flow (which in fact partly overlaps with the increase of O_2 consumption), the initial tendency to an increase in deoxyhaemoglobin level is converted to a decrease, by the delivery of fresh oxygenated blood with a low deoxyhaemoglobin concentration (Fox and Raichle, 1986; Malonek et al., 1997). It is this decrease in deoxyhaemoglobin level which increases the signal from the protons and which is thus detected as a BOLD signal, because when deoxyhaemoglobin levels decrease there are fewer magnetic field inhomogeneities and so transverse relaxation occurs more slowly and the BOLD signal increases (Ogawa et al., 1990). Thus, the size of the BOLD fMRI signal is determined by the difference between the amount of blood flow increase, which increases the signal, and the use of O_2 by neurons, which reduces the signal.

It is important to note that the BOLD signal cannot be viewed as a direct read-out of the metabolic demand associated with activity in the tissue (indeed, as noted above, O_2 consumption *decreases* the BOLD signal). In particular, BOLD signals need not directly report spiking activity in the imaged area, but instead reflect the many factors associated with neural activity, which lead to an increase in blood flow. Most importantly, neurotransmitters released during synaptic activation are now known to directly influence local blood flow and it is thought that the BOLD signal may most closely reflect the excitatory synaptic component, rather than the action potential component, of neural activity (reviewed by Attwell & Iadecola, 2002; Logothetis, 2008; Attwell et al., 2010).

Several aspects of the work in this thesis are relevant to understanding functional imaging signals such as BOLD fMRI. First, understanding the increase in blood flow which occurs following an increase in neuronal activity is necessary to explain where positive BOLD signals will be produced. The signals involved in increasing blood flow in response to activity are addressed in Chapters 4 and 5. Secondly, in Chapter 7 I consider the problems that may arise from using this indirect measurement of neuronal activity to infer meaning from imaging studies that are performed on participants over different stages in development.

1.11 Aim of this thesis

The main aim of the work described in this thesis was to learn more about pericytes, including the role that they play in neurovascular coupling and, therefore, energy supply to the brain, in physiological and pathological conditions. In Chapter 3, I investigate the expression of multiple pericyte markers and markers for other perivascular cell types that have been suggested to overlap with pericytes. In Chapter 4, I study the

signalling pathways involved in glutamate-evoked capillary dilation in cerebellar slices. In Chapter 5, I investigate the pericyte membrane currents that underlie the constriction and relaxation of pericytes in response to vasoactive agents. In Chapter 6, I quantify pericyte death in response to oxygen-glucose deprivation and reoxygenation. Using pharmacological agents, I identify some of the signalling pathways involved in pericyte death in these conditions. In Chapter 7, I discuss the changes in neurovascular coupling and energy use that may occur throughout development, and how these changes would impair evaluation of neurological changes in functional imaging studies.

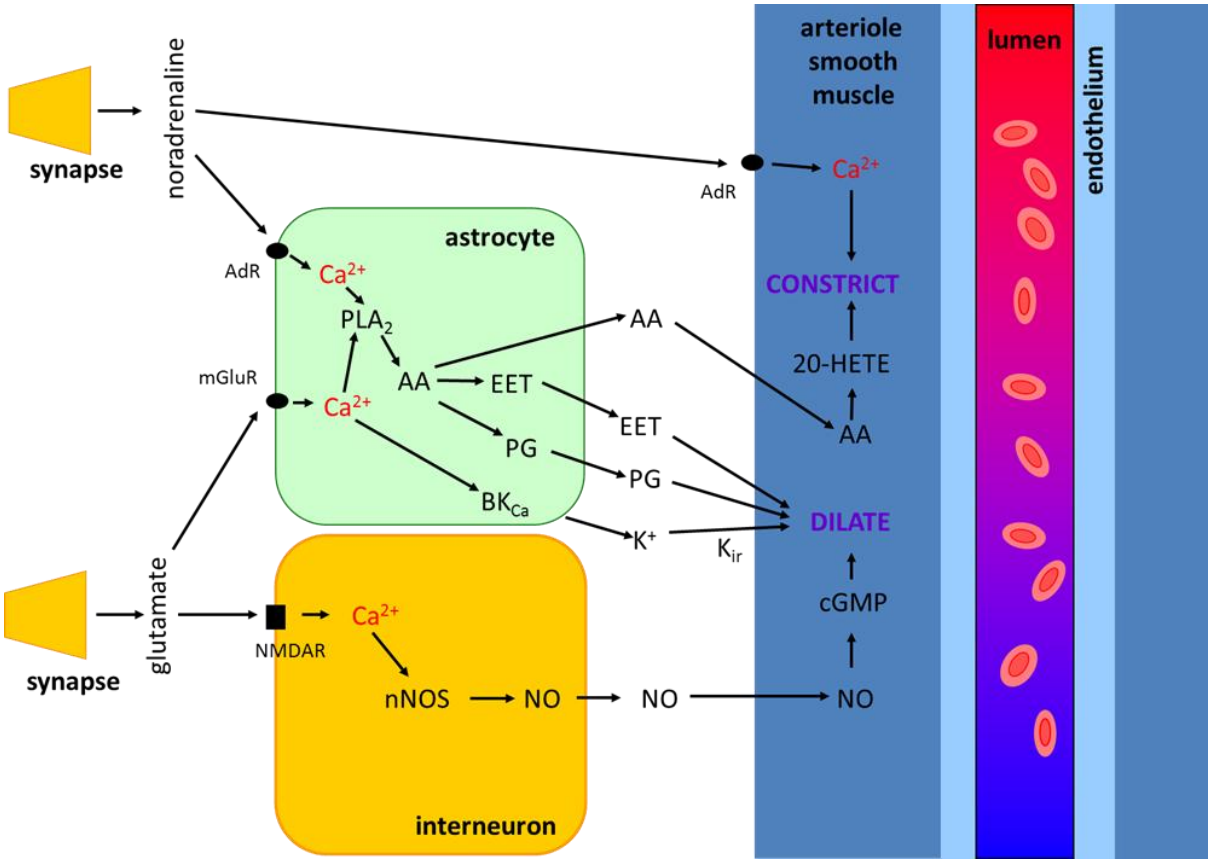

Figure 1.1: Signalling pathways mediating neurovascular coupling. When neurons are active they release glutamate which generates action potentials in interneurons containing NOS and activates metabotropic glutamate receptors (mGluR) in astrocytes. As a result, $[Ca^{2+}]_i$ rises in both cell types, releasing NO and derivatives of arachidonic acid (EETs and prostaglandins) to dilate local arterioles and increase blood flow. In addition, arachidonic acid diffuses to arterioles and is converted into 20-HETE which constricts the vessels. K^+ release from astrocytes via large conductance Ca^{2+}-activated K^+ channels (BK_{Ca} channels) may also dilate vessels by promoting K^+ efflux through smooth muscle inward rectifier K^+ channels (K_{ir} channels) and thus generating hyperpolarization of the smooth muscle. Blood flow changes evoked by release of adenosine, lactate and interneuron peptide transmitters are not shown on this diagram. Vasodilation occurs in the context of the constriction of arterioles produced by the amine transmitters, noradrenaline, dopamine and 5-HT. Noradrenaline evokes constriction by acting on α-adrenergic receptors on arteriole smooth muscle and on astrocytes. For more details see sections 1.2 and 1.3.

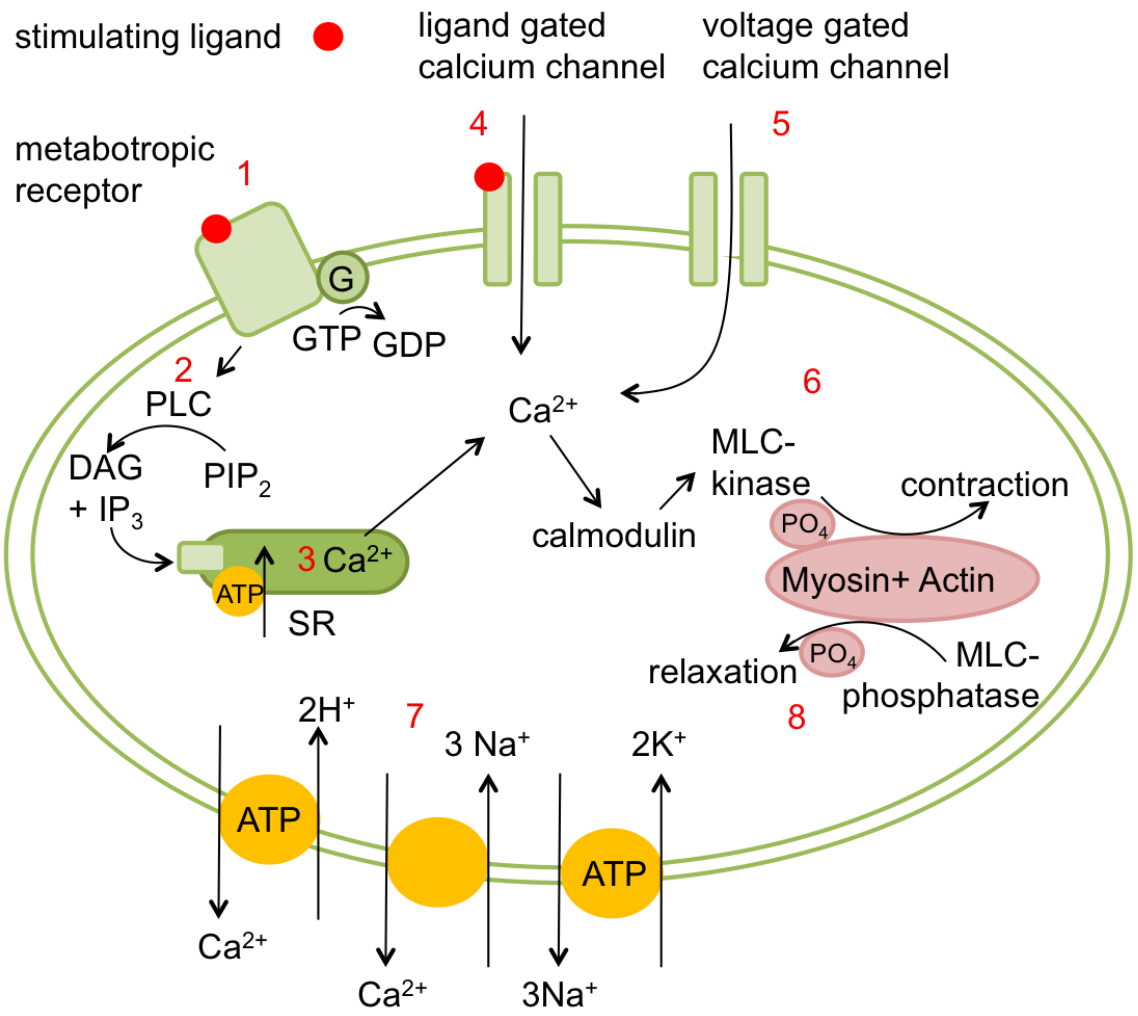

Figure 1.2: Regulation of smooth muscle tone. Stimulating ligand can bind to G protein-coupled metabotropic receptors on the smooth muscle cell (1). This leads to activation of phospholipase C (PLC) that hydrolyses phosphatidyl inositol diphosphate (PIP_2) into inositol trisphosphate (IP_3) and diacylglycerol (DAG; 2). IP_3 binds to a receptor on the sarcoplasmic reticulum (SR) and this elicits a controlled release of calcium (3). Stimulating ligand may also bind to ligand-gated calcium channels (LGCC) on the surface of smooth muscle cells causing calcium entry (4). Membrane depolarization allows further calcium entry through voltage-gated calcium channels (VGCC; 5). Crossbridge cycling is regulated by a myosin light chain (MLC) kinase and is dependent on both calcium and calmodulin. The phosphorylation of myosin is triggered by the binding of calmodulin (with 4 Ca^{2+} bound) to MLC kinase forming a complex. The phosphorylated light chain of myosin reacts with actin, and triggers smooth muscle contraction (6). The intracellular calcium concentration is regulated by calcium pumps on the sarcoplasmic reticulum, mitochondria and the plasma membrane, as well as by sodium-calcium exchangers on the plasma membrane (7). Below the affinity of calmodulin for calcium, the MLC are dephosphorylated by MLC phosphatase and muscle relaxes (8). For more detail see section 1.4.

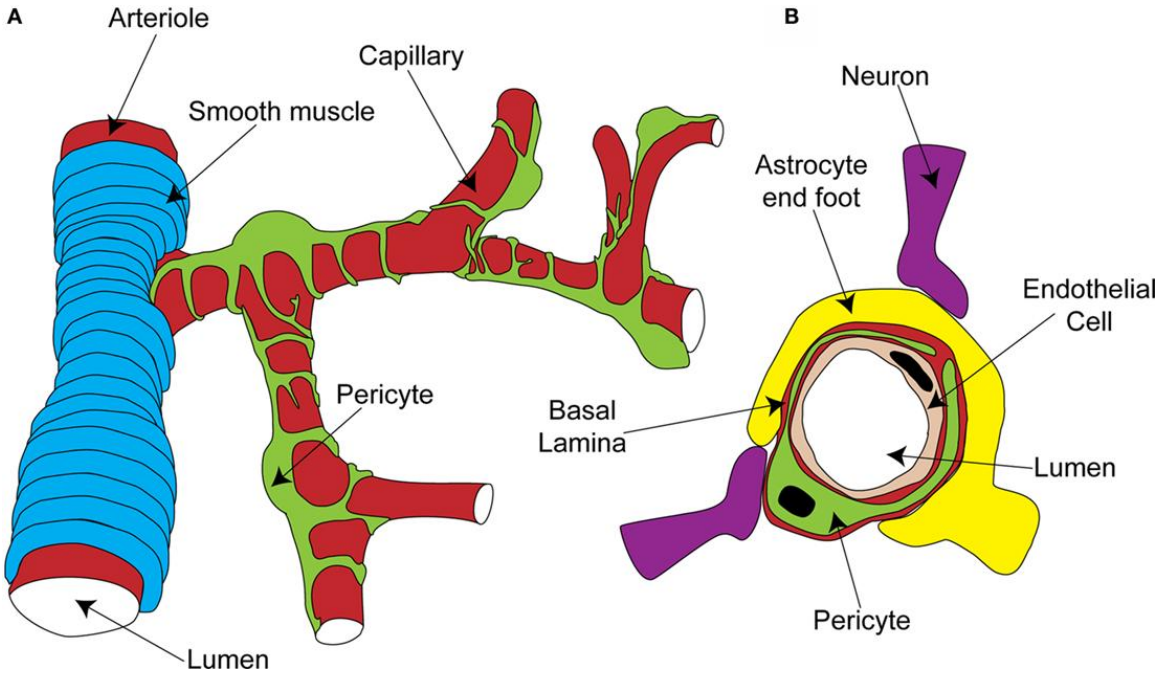

Figure 1.3: Organisation of the capillary neurovascular unit. A Rings of smooth muscle encircle arterioles, while pericytes send processes along and around capillaries, without fully covering the vessel. **B** Pericytes are located outside the endothelial cells and are separated from them and from the parenchyma by a layer of basal lamina. In the parenchyma, astrocyte end-feet and neuronal terminals are closely associated with the capillary. From Hamilton et al. (2010).

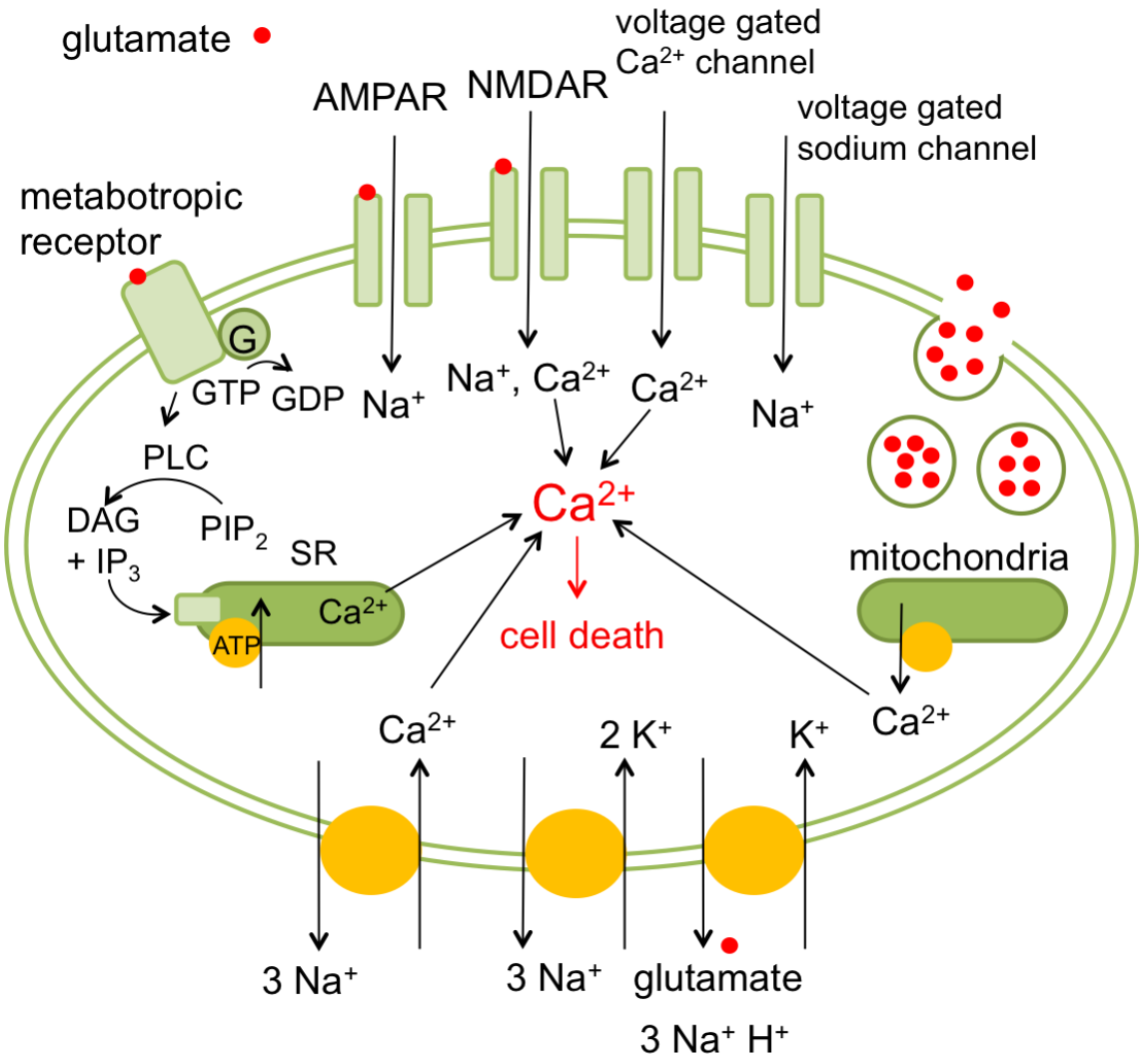

Figure 1.4: Mechanisms of intracellular calcium rise during ischaemia. During ischaemia the extracellular concentration of glutamate increases as depolarization triggers synaptic vesicle release, and ATP depletion leads to the reversal of glutamate transporters. Glutamate binds to postsynaptic receptors, triggering further depolarization and a rise of intracellular calcium concentration through ionotropic glutamate receptors (AMPARs and NMDARs) and metabotropic glutamate receptors. The depolarization and Na^+ entry through ionotropic glutamate receptors leads to further entry of calcium through voltage-gated calcium channels (VGCC) and reversal of the sodium-calcium exchanger, as well as IP_3 mediated calcium release from the endoplasmic reticulum (ER). Calcium cannot be removed from the cell or sequestered into organelles as there is no ATP to fuel the pumps. The increased intracellular calcium concentration leads to cell death through several mechanisms, which are described in section 1.6.

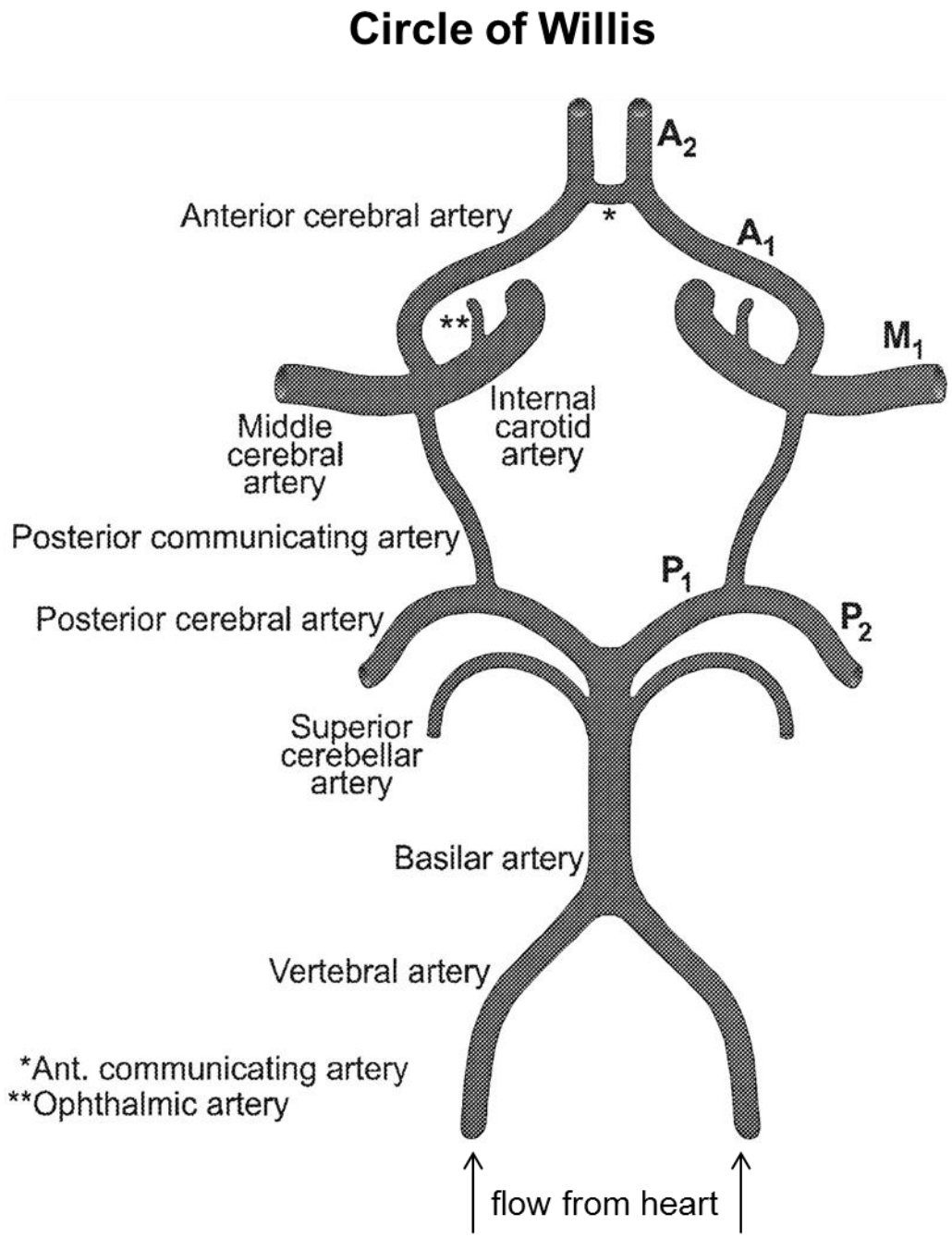

Figure 1.5: Typical normal polygon configuration of the circle of Willis. In humans, the circle of Willis is made up of the anterior communicating arteries and the posterior communicating arteries (in the rat the interior carotid arteries also contribute to the circle of Willis; see Figure 2.4). This structure creates collaterals in the cerebral circulation and allows compensatory flow during partial occlusion. M1 indicates main trunk of the middle cerebral artery; A1, pre-communicating part of the anterior cerebral artery; A2, posterior communicating part of the anterior cerebral artery; P1, pre-communicating part of the posterior cerebral artery P2, posterior communicating part of the posterior cerebral artery; and Ant., anterior. From Hoksbergen et al. (2000).

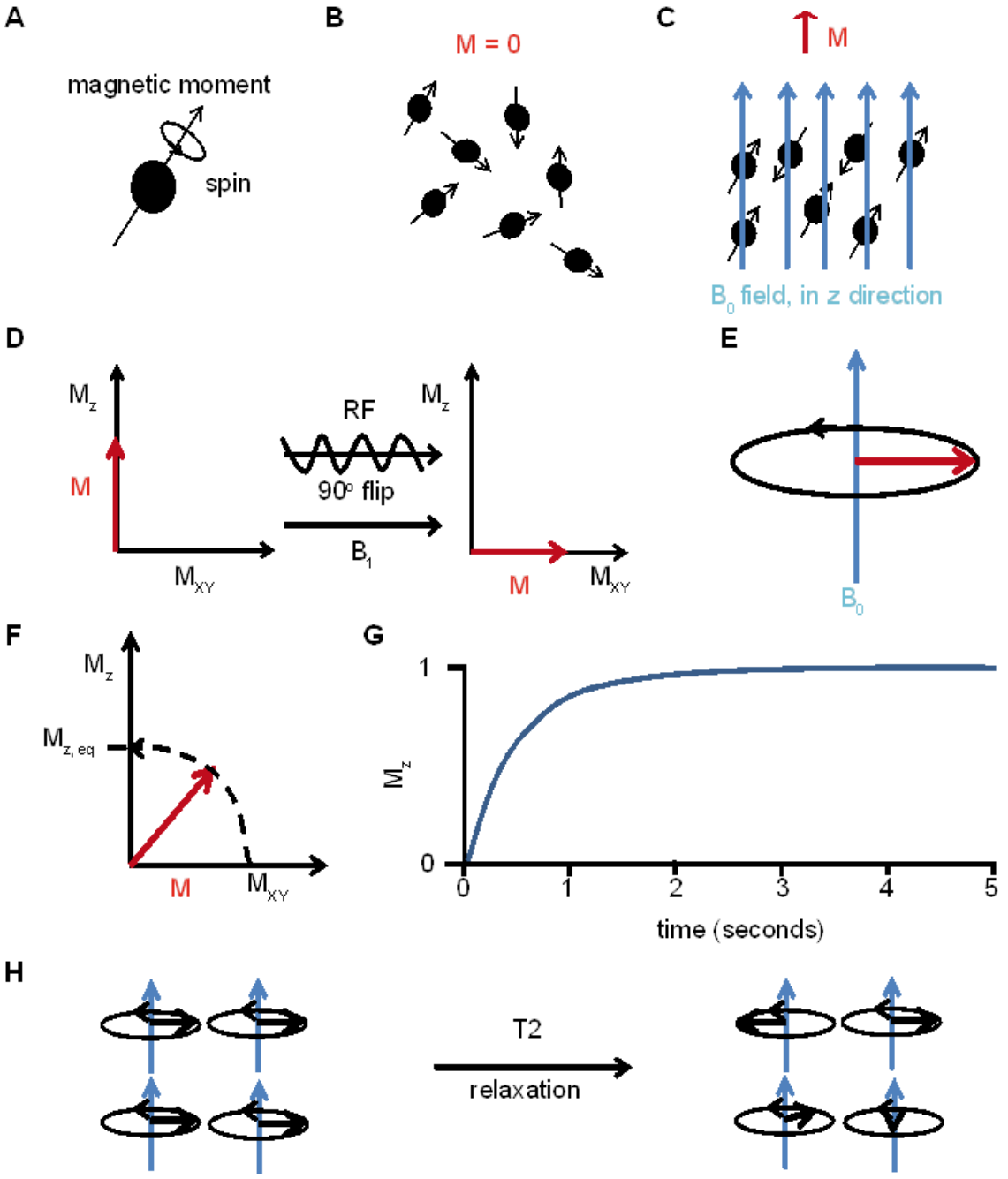

Figure 1.6: Basics of MRI. A Each proton (mainly present in water) has a "spin" or magnetic moment. **B** In the absence of an externally applied magnetic field (M=0), the spins of the protons are randomly orientated. **C** In the presence of a magnetic field, B_0, protons are aligned roughly parallel or antiparallel to B_0, producing a net magnetization, M. Each nucleus precesses around the direction of B_0. **D** Following a radiofrequency pulse at 90^O to B_0, the spins are flipped out of alignment with B_0. **E** M continues to precess around the direction of B_0, producing the MR signal, and initially all proton spins precess in phase with each other. **F** Gradually the spins re-align with B_0 – this is called longitudinal relaxation and occurs with a time constant called T1. **G** Recovery of magnetization over time following an RF pulse, grey matter, T1 = 920 ms. **H** In addition the phase alignment of the precessing displaced protons is lost. This transverse relaxation is produced by local inhomogeneities in magnetic field produced, e.g. by paramagnetic deoxyhaemoglobin molecules, and occurs with a time constant called T2.

Pericyte marker	Gene symbol	Other cell types that express marker	References
NG2 (chondroitin sulphate proteoglycan 4)	Cspg4	Developing cartilage, bone, muscle; early postnatal skin; adult skin stem cells; adipocytes; vSMCs; neuronal precursor cells; oligodendrocyte precursor cells; endothelial cells; microglia; mesenchymal stem cells	Ozerdem et al., 2001; Ruiter et al., 1993; Huang et al., 2010
PDGFRβ (Platelet derived growth factor receptor beta)	Pdgfrb	Interstitial mesenchymal cells during development; smooth muscle; neurons, neuronal precursor cells; myofibroblasts; mesenchymal stem cells	Lindahl et al., 1997; Winkler et al., 2010
CD13 (alanyl (membrane) aminopeptidase)	Anpep	vSMCs, inflamed and tumour endothelial cells; myeloid cells; epithelial cells	Dermietzel and Krause, 1991; Kunz et al., 1994
αSMA (alpha-smooth muscle actin)	Acta2	vSMCs; myofibroblasts; myoepithelium	Nehls and Drenckhahn, 1993
Desmin	Des	Skeletal, cardiac, smooth muscle	Nehls et al., 1992
Vimentin	Vim	Neuronal precursor cell	Díaz-Flores et al., 2001
RGS5	Rgs5	vSMCs; cardiomyocytes?	Bondjers et al., 2003; Cho et al., 2003
SUR2	Abcc9	Skeletal, cardiac, smooth muscle; renal tubular epithelium	Bondjers et al., 2006
Kir6.1	Kcnj	vSMCs	Bondjers et al., 2006
Endosialin	Cd248	vSMCs, myofibroblasts; fibroblasts; T cells	Christian et al., 2008
DLK1 (delta-like 1 homolog)	Dlk1	vSMCs; hepatoblasts; adipocyte progenitors	Bondjers et al., 2006

Table 1.1: Known pericyte markers. Adapted from Armulik et al. (2011).

Chapter 2: Methods

In this chapter I will describe the general methods used for the experimental studies carried out in this thesis. Details of the specific methods used for each study are given in the Methods section of each Results chapter.

2.1 Solutions

2.1.1 Extracellular solution

Brain slices were incubated in or perfused with extracellular solution mimicking cerebrospinal fluid (artificial cerebrospinal fluid, aCSF) which contained (in mM): 124 NaCl, 2.5 KCl, 26 $NaHCO_3$, 1 $MgCl_2$, 1 NaH_2PO_4, 10 D-glucose, 2 $CaCl_2$, pH 7.4, osmolarity 295-315 mOsm. This solution was gassed with 20% O_2/5% CO_2/75% N_2 or 95% O_2/5% CO_2. For the experiments in Chapter 4 and 5, this solution was perfused through the recording chamber by a peristaltic pump at a flow rate of 2-4ml/min. The solution was heated to 32-35^{0}C (by manually adjusting the current flow through a series of resistors attached to a heating block, according to the thermometer reading in the recording chamber). For experiments in Chapter 6, slices were incubated in this solution at 37^{0}C.

The neurotransmitters and other drugs that were added to the extracellular solution are listed in Table 2.1. To prevent oxidation when using noradrenaline, 100 μM ascorbic acid was added to the extracellular solution (Maxwell et al., 1983).

2.1.2 Ischaemic solution

For the experiments in Chapter 6, brain ischaemia was mimicked *in vitro*. Glycolytic and mitochondrial ATP production was blocked by removing glucose and O_2. To do this I used a bicarbonate-based solution as described in section 2.1.1, but with 7 mM sucrose (substituted for 10 mM D-glucose) and equilibrated with 95% N_2/5% CO_2 (substituted for 95% O_2/5% CO_2). Solution was heated to 37^{0}C in a water bath.

2.1.3 Pipette solution

The whole-cell patch clamping experiments in Chapter 5 were performed using a potassium-gluconate based solution containing (in mM):130 K-gluconate, 4 NaCl, 0.5 $CaCl_2$, 10 HEPES, 10 BAPTA, 2 Na_2ATP, 2 $MgCl_2$, 0.5 Na_2GTP, 0.05 Alexa Fluor 488, pH set to 7.3 with KOH, 280-300 mOsm.

2.2 Transgenic mice expressing fluorescent constructs

NG2-DsRedC57BL/6J mice were a kind gift from Akiko Nishiyama (Department of Physiology and

Neurobiology, University of Conneticut, Storrs, CT, USA). These transgenic mice provided a means to identify NG2-glia in living brain slices, before patch-clamping them. These mice were generated using the bacterial artificial chromosome (BAC) modification technique (Figure 2.1 describes the generation of NG2DsRedBAC transgene; Zhu et al., 2008). The NG2-DsRedC57BL/6J mouse line was maintained as a heterozygous breeding colony to prevent genetic drift, because the C57BL/6J strain of mice is inbred.

2.3 Slice and tissue preparation

2.3.1 Cerebellar slice preparation

Twelve-day-old Sprague-Dawley rats or 10-15 day old NG2-DsRedC57BL/6J mice were used for the preparation of the cerebellar slices for the experiments in Chapter 4 (Sprague-Dawley rats) or in Chapters 3 and 5 (NG2-DsRedC57BL/6J mice). All animals were killed humanely by cervical dislocation in accordance with the Animals (Scientific Procedures) Act (1986). Animals were decapitated following cervical dislocation, and the head was immersed in ice-cold oxygenated slicing medium, containing (in mM): 124 NaCl, 2.5 KCl, 26 $NaHCO_3$, 1 $MgCl_2$, 1 NaH_2PO_4, 10 D-glucose, 2 $CaCl_2$, pH 7.4, osmolarity 295-315 mOsm (gassed with 95% O_2/5% CO_2). Kynurenic acid (1 mM) was included in the slicing medium to block glutamate receptors, and thus reduce potential excitotoxic damage. The scalp was removed and the skull was opened by making lateral cuts on either side of the head from posterior to anterior. The skull was removed using forceps and the brain was placed in ice-cold oxygenated slicing medium. The cerebellum was separated from the rest of the brain by making cuts through the inferior colliculus and the spinal cord, and the cerebellar hemispheres were removed. The cerebellar vermis was glued to the cutting stage of a Vibratome (Leica VT1000s) and stabilised with an agar block. The tissue was immersed in ice-cold oxygenated slicing medium throughout the slicing process. Sagittal slices of the vermis (200 µm thick) were cut and placed oxygenated slicing medium at room temperature until used for imaging or recording. All slices were allowed to recover from slicing for at least 30 minutes prior to use.

2.3.2 Forebrain slice preparation

Sprague-Dawley rats (21 days old) and adult Wistar rats, or 10-15 day old NG2-DsRedC57BL/6J mice, were used for the preparation of the forebrain slices for the experiments in Chapter 6 (Sprague-Dawley and Wistar rats) and chapters 3 and 5 (NG2-DsRedC57BL/6J mice). Adult Wistar rats were killed by anaesthetic overdose while Sprague-Dawley rats and NG2-DsRedC57BL/6J mice were killed as in section 2.3.1. Brains were removed as described in section 2.3.1. Each hemisphere was isolated using a cut down the

midline, glued to the stage of a vibratome (Leica VT1000S or Campden Instruments MA752), and stabilised with an agar block. The tissue was immersed in ice-cold oxygenated slicing medium throughout the slicing process. Coronal slices of the forebrain (200 µm thick) were cut and placed oxygenated slicing medium at room temperature until used for recording. All slices were allowed to recover from slicing for at least 30 minutes prior to use.

2.4 Immunocytochemistry

2.4.1 Live labelling

For the experiments in Chapter 3 and 6, slices were incubated with isolectin B_4-FITC conjugate (IB_4, 10 µg/ml) for 30 minutes to 1 hour, to label blood vessels. For the experiments in Chapter 6, slices were incubated with propidium iodide (PI, 37 µM) for 1 to 2 hours, to label dead cells.

2.4.2 Antibody labelling

In order to label with antibodies, slices were fixed in 4% paraformaldehyde in 0.1 M phosphate-buffered saline (PBS) for 20 minutes at room temperature. Fixed slices were then washed three times for 15 minutes in 0.1 M PBS and in order to block generalised secondary antibody staining and permeabilise the tissue, slices were treated with solution containing 10% goat serum, 0.05% Triton X-100 and 0.1 M PBS, for 4-6 hours at room temperature. This was followed by incubation with the primary antibodies listed in table 2.2 for 12-16 hours. Slices were then washed three times for 20 minutes with 0.1 M PBS, before being incubated with goat anti-rabbit secondary antibody (conjugated to AlexaFluor; see Table 2.3). Slices were then washed another 3 times and labelled with DAPI (4',6-diamidino-2-phenylindole at 82 µg/L; Molecular Probes) to label cell nuclei. Slices were mounted on a microscope slide with Citifluor (glycerol/PBS, Citifluor), covered with a 0.17 mm thick glass cover slip, and sealed with nail varnish. A control experiment to check for non-specific binding of the secondary antibody was performed for each antibody by omitting the primary antibody when labelling one slice during the staining procedure.

2.4.3 Confocal imaging

Fixed slices were imaged with a confocal laser scanning microscope (LSM). The confocal microscope used was either a Zeiss LSM 510, 700 or 710. Images were obtained using x20 water-immersion or x40 oil immersion objectives.

Imaging with multiple wavelengths was performed as sequential scans at each wavelength, to

minimise “bleed through” of emitted fluorescence between imaging channels. The argon laser 488 nm line was used to excite FITC and Alexa 488 fluorophores, and the 458 nm laser line of the argon laser was used for DsRed, propidium iodide and Alexa fluor 546 fluorophores. The ultraviolet laser 364 nm laser line was used for the detection of DAPI. Scanning of areas of interest in slices was done in the x-y and then z directions, and averaged 2-6 times depending on the signal. The gain and offset settings were initially chosen for each set of images in an experiment depending on the signal intensity being detected. For the experiments in Chapter 6, the settings for propidium iodide were kept constant for all slices within an experiment in order to compare the cell death between slices. The settings for other fluorophores were adjusted throughout experiments to optimise detection of the labelling.

2.5 Imaging of capillaries

For bright-field recording of capillary diameter (Chapter 4), capillaries were imaged at 20-50 μm depths within the molecular layer of cerebellar slices, using a x40 water immersion objective. Images were acquired with a Coolsnap HQ2 CCD camera, and Metafluor software (Molecular Devices). Images were acquired every 2-5 sec, with an exposure time of 5 msec. The pixel size was 300 nm. Capillaries were classified as vessels lacking a continuous layer of smooth muscle (which is seen around arterioles) and <10 μm in diameter. Pericytes were identified by their position on the outer walls of capillaries and their characteristic ‘bump on a log’ morphology (Kuwabara and Cogan, 1960), but pericyte identification is imprecise using bright field illumination (Krueger and Bechmann, 2010). Nevertheless, the distance between pericyte cell bodies is only 50 μm in the brain (Hirschi and D’Amore, 1996), so a pericyte soma is expected to be present on any given 50 μm length of capillary, even if it is not easily visible (e.g. because it is underneath the capillary). Thus, spatially localised capillary constrictions and dilations were attributed to pericytes even when the pericyte soma was not clearly visible. The lengths of vessel imaged ranged from approximately 30-70μm. Vessel internal diameters were measured by manually placing a measurement line (perpendicular to the vessel) on the image (at locations which constricted when noradrenaline was applied), using Metamorph software. I was blinded as to the timing of drug applications during the measurement process. Drugs were superfused for at least 5 minutes. For statistical analysis of the effects of drugs on capillary diameter, the diameter measurement for each drug was taken from the last 5 recorded images in that drug. Data in the presence of blockers of signalling pathways were compared with interleaved data obtained without the blockers.

2.6 Patch-clamp set-up

For patch-clamp recording of pericytes (Chapter 5), both coronal slices of cortex and sagittal slices of cerebellum were prepared from P10-15 NG2-DsRed C57BL/6J mice. Pericytes were identified as DsRed-expressing cells located on capillaries (oligodendrocyte precursor cells also express NG2-DsRed but these can be distinguished from pericytes morphologically and by their position in the parenchyma). Pericytes were whole cell clamped with ~7-9 MΩ electrodes containing the intracellular solution described in section 2.1.3. This solution contained AlexaFluor 488 (1mg/ml), to allow identification of the patch-clamped cell.

2.6.1 Whole-cell configuration

As the patch pipette was lowered into the bath, a 200 msec, -5 mV voltage step was delivered at 5 Hz to monitor the pipette resistance before and after contacting the cell membrane. Positive pressure was applied to the pipette (through a 1 ml syringe connected to the pipette via tubing) while it was lowered towards the cell, to prevent the pipette tip becoming blocked by debris. Upon approaching the cell soma, gentle suction was applied to form a high resistance seal (over 1 GΩ) between the cell membrane and the tip of the patch pipette, thus achieving cell-attached mode. At this point, the holding potential was set to between -55 and -75mV (close to the cell's resting membrane potential) and the pipette capacitance was compensated (using the fast and slow electrode compensation controls). Finally, the transition from cell-attached to whole-cell configuration was made by applying further suction to break through the piece of membrane at the tip of the pipette, thus gaining diffusive and electrical access to the cell's interior.

2.6.2 Liquid junction potential and its compensation

Because of the different composition of the pipette solution and the bath solution, a potential difference (the junction potential) exists at the end of the electrode when it is in the bath, but is not present in whole-cell configuration when the pipette solution has diffused into the cell (Fenwick et al., 1982). The junction potential depends on the diffusion coefficients of the anions and cations present in each solution, which are determined by each ions molecular weight and charge (which affect ion mobility). For the solutions used, the principal ions responsible for generating the junction potential were K^+, Na^+, $Cl^-$and gluconate. K^+ ions diffuse out of the patch pipette more quickly (D_k = 1.99 x 10^{-9} m^2s^{-1}) than Na^+ ions diffuse in (D_{Na} = 1.36 x 10^{-9} m^2s^{-1}), and gluconate ions diffuse out more slowly ($D_{gluconate}$ = 1.06 x 10^{-9} m^2s^{-1}) than Cl^- ions diffuse in (D_{Cl} = 1.99 x 10^{-9} m^2s^{-1}) (Robinson and Stokes, 1965), so the patch pipette potential becomes more negative than the bath potential (Figure 2.2).

The junction potential can be measured experimentally using an agar bridge (containing 4M NaCl) to connect the bath solution to a reference electrode. This avoids changes in the reference electrode potential following a change in the external solution. When zero current is applied, the junction potential is the difference between the voltage value obtained when both the patch electrode and the bath contained the same solution (both internal solution, so there is no junction potential) and the value obtained when the bath solution was used for experiments (external solution described in 2.1.1). For my experimental solutions, the junction potential was measured to be -14mV, and all voltage data have been adjusted accordingly (1.e. -14mV was added to all voltages measured with patch-clamp).

2.6.3 The electrical circuit for whole-cell patch-clamp recordings in voltage clamp

The cell membrane, which is composed of a lipid bilayer and embedded proteins, is an electrical insulator. In contrast, the extracellular and intracellular components are filled with salt solutions, which are excellent conductors of current. This combination of the cell membrane (an insulator) and the surrounding intra- and extracellular solutions (conductors) forms a capacitor, which can store charge. The charge stored (Q) is proportional to the applied voltage (V) and the capacitance, (C), which is a measure of the membrane's capacity for storing charge:

$$Q = CV \qquad 2.1$$

The physical dimensions of the membrane are important for determining the capacitance: the more membrane, the more charge can accumulate. Thus, capacitance is proportional to the membrane surface area. Importantly, capacitors prevent instantaneous changes in voltage, which affect both the conduction of electrical signals in biology and electrophysiological recordings. For example, in excitable cells, local changes in membrane potential, such as an action potential travelling along an axon, are subject to a delay in propagation due to the time needed for charging the cell membrane, therefore limiting the speed of the action potential propagation. Similarly, during whole-cell voltage-clamp recordings, a step change in desired membrane potential can only be produced after the charging time of the membrane capacitance. The current flowing through a capacitor (C) is proportional to the rate of voltage change (ΔV) with time (Δt):

$$I = C \frac{\Delta V}{\Delta t} \qquad 2.2$$

In addition to being a capacitor, the cell membrane is a conductor due to the presence of ion channels which allow the passage of charged ions. Current flowing through these ion channels can charge or discharge the membrane capacitance and therefore cause changes in the membrane potential. The electrical circuit equivalent of a spatially compact cell in the whole-cell configuration is represented by a capacitor (the membrane capacitance, C_m) and a resistor (the membrane resistor, R_m) connected in parallel, both connected in series to a patch electrode (with electrode series resistance, R_s) (Figure 2.3).

The current flow (I) through this circuit in response to a voltage step (V_s) (Figure 2.3) can be predicted by (Tessier-Lavigne et al., 1988):

$$I(t) = \left(\frac{Vs}{Rm+Rs}\right).\left(1 + \frac{Rm \cdot e^{-t/\tau}}{Rs}\right) \qquad 2.3$$

Where t is the time after onset of the voltage step, and τ, the decay time constant of the current transient, is:

$$\tau = C_m \left(\frac{R_s \cdot R_m}{R_s+R_m}\right) \qquad 2.4$$

At the onset of the voltage step (t=0), the cell capacitance is uncharged and the voltage across it is zero. Consequently, just as the voltage step is applied, the voltage across the series resistance is the applied voltage step, and the initial current flowing allows calculation of the series resistance (from equation 2.3 at t=0) as:

$$R_s = \frac{V_s}{I\,(t=\infty)} \qquad 2.5$$

When the current reaches a steady state (t=∞), the cell capacitance is fully charged and no current flows through it. The membrane resistance can then be calculated from the voltage step and the current at t=∞ (by rearranging equation 2.3):

$$R_m = \frac{V_s}{I\,(t=\infty)} - R_s \qquad 2.6$$

Substituting R_s from equation 2.5 gives:

$$R_m = V_s \left(\frac{I\,(t=0) - I\,(t=\infty)}{I\,(t=\infty).\ I\,(t=0)}\right) \qquad 2.7$$

The membrane conductance (G_m) is the inverse of this:

$$G_m = \frac{1}{R_m} \qquad 2.8$$

The membrane capacitance can be calculated by rearranging equation 2.4 to give:

$$C_m = \tau \left(\frac{R_s + R_m}{R_s \cdot R_m} \right) \qquad 2.9$$

For an electrically compact cell which can be represented by a single-compartment model (Figure 2.3), the time constant, τ, can be obtained by fitting the current transient in response to a voltage step with a single exponential.

2.6.4 Series resistance and its compensation

In whole-cell patch-clamp experiments, the electrode resistance leads to voltage errors because it is in series with the membrane resistance. Because voltage sums across resistors in series, this means that, when current flows through the circuit (Figure 2.3), there will be a voltage drop across the electrode's resistance. This means that (a) the cell will not be clamped at the voltage applied to the top of the patch electrode, and (b) synaptic currents will be recorded with an error of magnitude. The higher the series resistance or the larger the current, the larger the voltage drop. The exact voltage drop for a given series resistance and current flow can be calculated using Ohm's law (V = IR). For example, for a series resistance of 10 MΩ and a current flow of 1 nA, the voltage drop would be 10 mV. It is therefore ideal to minimize the physical series resistance by using appropriately sized pipette tips and aiming for complete removal of the patch of cell membrane at the pipette tip when entering the whole-cell configuration (section 2.6.1).

The combination of the series resistance with the capacitance of the cell or pipette also creates a filtering problem, where any voltage change introduced to the cell will be slowed and distorted. The time course of a change in the membrane potential (V_m) as a result of a step voltage command (V_s) is described by:

$$V_m = V_s \left(\frac{R_m}{R_s + R_m} \right) \left(1 - e^{\frac{-t}{\tau}} \right) \qquad 2.10$$

In voltage-clamp mode, the series resistance that cannot be physically eliminated can be compensated for electronically. A positive feedback circuit is used to add to the command potential a voltage

that is proportional to the current flowing. This increases the pipette voltage when current flow and the voltage error is greatest, driving extra current through the electrode, which is exactly what would happen if the electrode had a lower resistance. In practice, because the positive feedback circuit can lead to oscillation and cell death, series resistance can only be compensated by 60-70%. In my experiments, the series resistance after compensation was 20-40 MΩ.

2.7 Cell death experiments

2.7.1 Oxygen-glucose deprivation

Coronal forebrain slices were prepared from P21 Sprague-Dawley rats and incubated in aCSF in which glucose was replaced with 7 mM sucrose and oxygen was removed by equilibrating solutions with 5% CO_2 and 95% N_2. Control slices were incubated in aCSF, gassed as usual with 95% O_2/5% CO_2. After 60 min, some slices were immediately fixed in 4% paraformaldehyde, while others were placed in control aCSF, to be exposed to glucose and oxygen again for a further 60 min. All solutions also contained 37 µM propidium iodide (PI) and FITC-conjugated 10 µg/ml isolectin B_4 to label dead cells and blood vessels. Slices were swiftly washed in aCSF prior to fixation and mounted as described in section 2.3.2. PI-positive dead IB_4 labelled cells were counted using ImageJ software. When assessing cell death, I was blind to the condition that each tissue slice had undergone (image identities were recoded using a custom-written macro). Cells in the 20 µm closest to the slice surface were excluded from analysis to prevent confounds from slicing-induced damage, as described in Chapter 6. Dead or alive pericytes were identified by their “bump on a log” morphology on vessels surrounded by isolectin B_4 labelling.

2.7.2 Middle cerebral artery occlusion (MCAO)

The surgery for MCAO was carried out by my colleague Brad Sutherland. All procedures conformed to the Animal (Scientific Procedures) Act 1986 (UK), and were approved by the University of Oxford Animal Ethics Committee and the Home Office (UK). Male Wistar rats (Harlan, UK) weighing 253-312g, housed on a 12h light/dark cycle with *ad libitum* access to food and water, underwent transient middle cerebral artery occlusion (MCAO). In brief, animals were anaesthetised with 4% isoflurane and maintained in 1.5-2% isoflurane carried in 70% N_2O and 30% O_2. A midline incision was made in the neck, the right external carotid artery was cauterised and cut, and the right common carotid and internal carotid arteries were temporarily ligated. Through a small arteriotomy in the external carotid artery stump, a 4-0 nylon filament coated with silicone at the tip was advanced up the internal carotid artery to occlude the right middle cerebral artery at its

origin. A diagram of the cerebral artery and filament position is included in Figure 2.2A, B. For sham animals, the entire procedure was followed except the filament was only advanced up the beginning of the internal carotid artery before being withdrawn (see Figure 2.2C). During the sham protocol, blood flow is reduced (as the common and internal carotid arteries are ligated) but there still blood entering the anterior cerebral artery through the circle of Willis. Following 90 minutes of MCAO, the filament was retracted, and the common carotid artery ligation was released to allow maximal reperfusion. Core temperature was maintained at 37°C by a rectal thermister probe attached to a heating pad. Cerebral blood flow changes and behavioural changes induced by the MCAO were monitored as described in Chapter 6. Animals (including an additional 3 naïve control animals) were then anaesthetised, decapitated, and 200 µm forebrain slices were prepared on a vibratome (as described in section 2.3.2) and labelled with PI and FITC-isolectin B_4 in aCSF for 60 min, then washed, fixed, and mounted so that cortical and striatal images could be captured. Live and dead pericytes were counted in both regions as described in section 2.7.1 except that dead endothelial cells were also counted (identified by their elongated nuclei). The total number of endothelial cells present, and therefore the percentage of dead endothelial cells, was estimated from the total number of pericytes, assuming a 1:3 ratio of pericytes to endothelial cells (Pardridge, 1999).

2. 8 Data analysis and statistics

Data are presented as mean ± s.e.m. Statistical significance was assessed with 2-tailed Student's t-tests samples when samples had a normal distribution. Normality of data was assessed using Kolmogorov–Smirnov tests. When the distribution was not normal, non-parametric tests were used (Mann-Whitney U or Wilcoxon signed-rank test for independent and paired samples respectively). A correction procedure equivalent to the Holm-Bonferroni method was used when making multiple comparisons (for N comparisons in a given experiment, the most significant p value is multiplied by N, the 2^{nd} most significant by N-1, the 3^{rd} most significant by N-2, etc.; the resulting corrected p values are significant at the 5% level when p is less than 0.05).

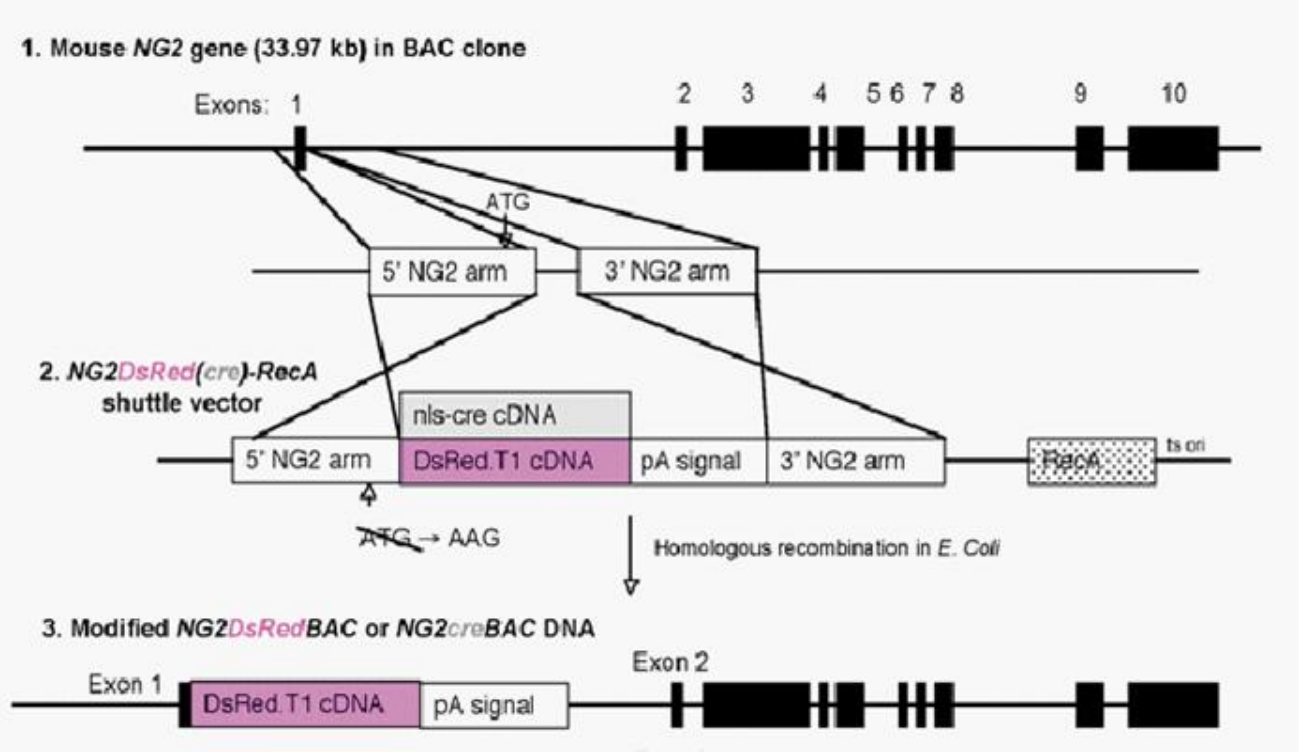

Figure 2.1: Generation of NG2-DsRed BAC transgene. Diagram 1 shows the structure of the mouse NG2 gene (not to scale). Exons are indicated as black blocks. The regions used for 5′ and 3′ homology arms are indicated. Diagram 2 shows the structure of the NG2-DsRedBAC-RecA shuttle vector that was used to modify the BAC DNA in order to insert the DsRed cDNA and polyadenylation sequence into the BAC clone that contained the NG2 gene in the centre. Diagram 3 shows the structure of the modified BAC DNA that was used for microinjection into fertilized oocytes (pA signal means polyadenylation signal; ATG, translation initiation codon of the NG2 gene; ts ori, temperature-sensitive origin of replication). From Zhu et al. (2008).

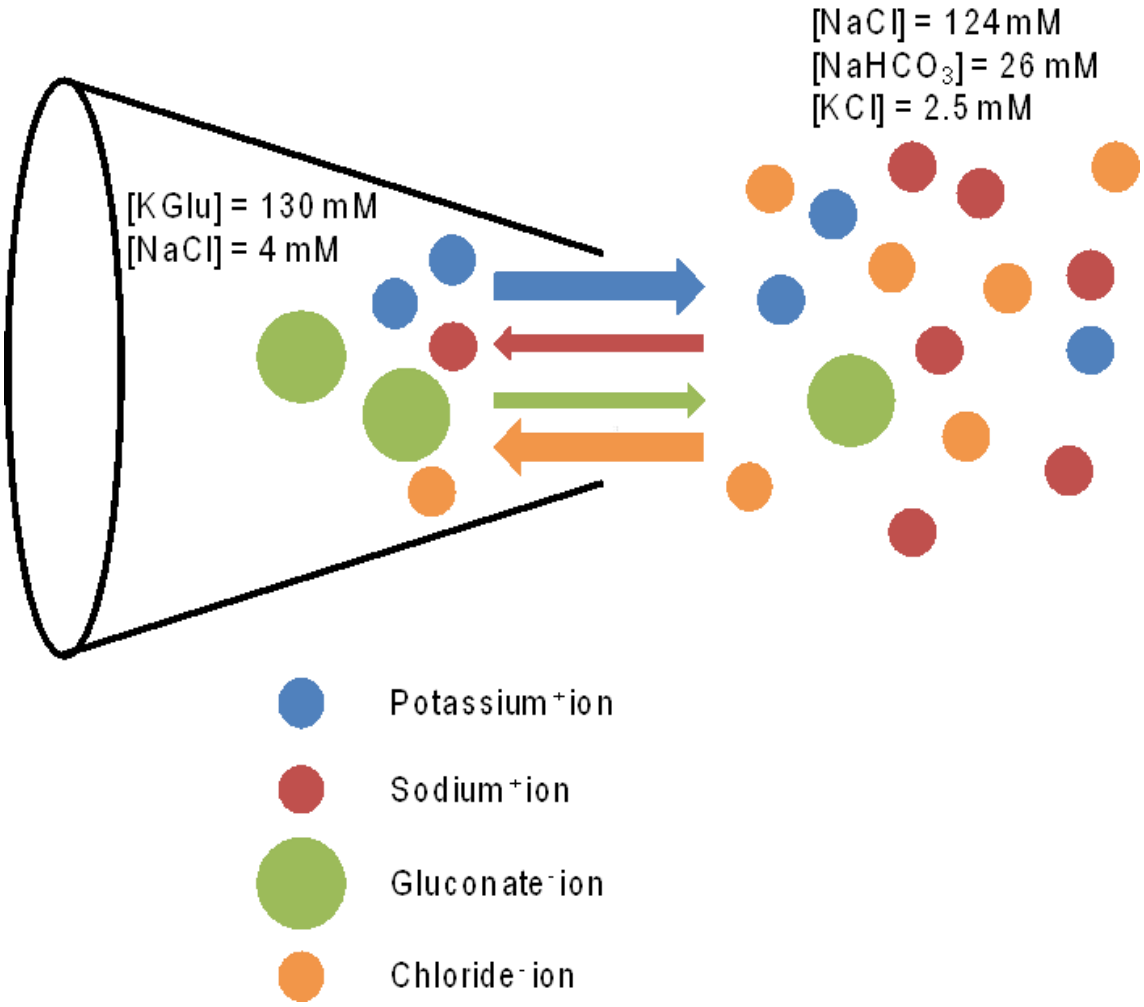

Figure 2.2: Liquid Junction potential. A potential difference (the junction potential) exists at the interface between two solutions with different compositions. When the patch electrode is placed in the bath a junction potential exists at the tip of the electrode because the ionic composition of the internal solution inside the electrode differs from the external solution in the bath. This junction potential does not exist in the whole-cell mode because the electrode solution diffuses into the cell. The junction potential present with the electrode in the extracellular solution depends on the diffusion coefficients of the anions and cations present in each solution (which depends on their molecular weight and charge, which affects the mobility of ions). For my solutions the principal ions responsible for generating the junction potential are K^+, Na^+, Cl^-, and gluconate$^-$, all of which are represented here. Bicarbonate ions (HCO_3^-) are not depicted due to their small contribution to the junction potential. Thicker arrows indicate more movement, due to more free diffusion of the ion.

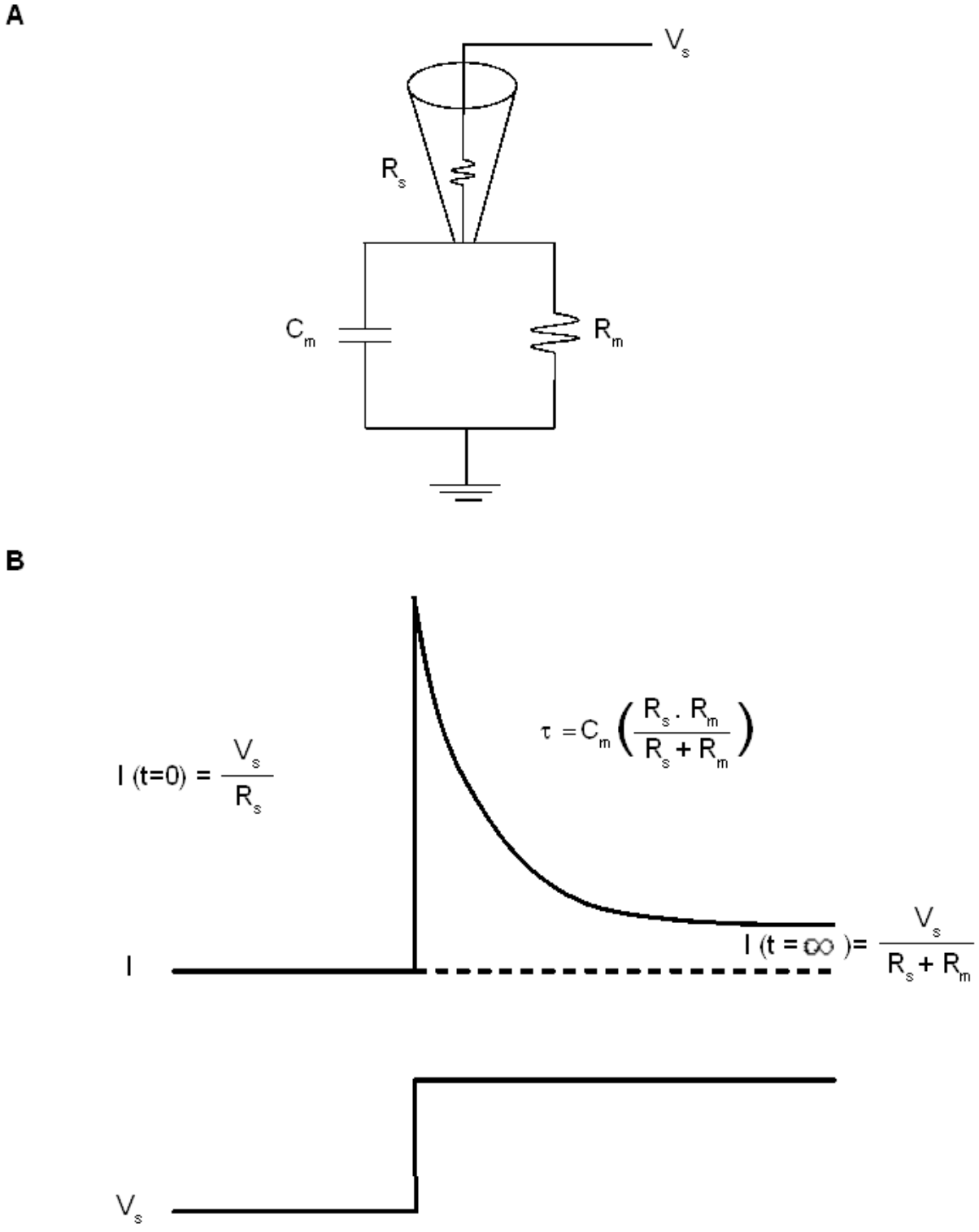

Figure 2.3: Electrical circuit and current measurement in voltage clamp mode. A Electrical circuit model for spatially compact cells in whole-cell configuration. **B** The current response (top trace, *I*) of a whole-cell patch clamped cell to a voltage step (bottom trace, V_s) injected through the patch pipette. The series resistance (R_s) is calculated from the peak current recorded at the onset of the voltage pulse (*I*(t=0)), the membrane resistance is calculated from the steady state current, when the membrane is fully charged (I(t=∞)). The cell capacitance (C_m) can be calculated by measuring the decay constant of the current (τ).

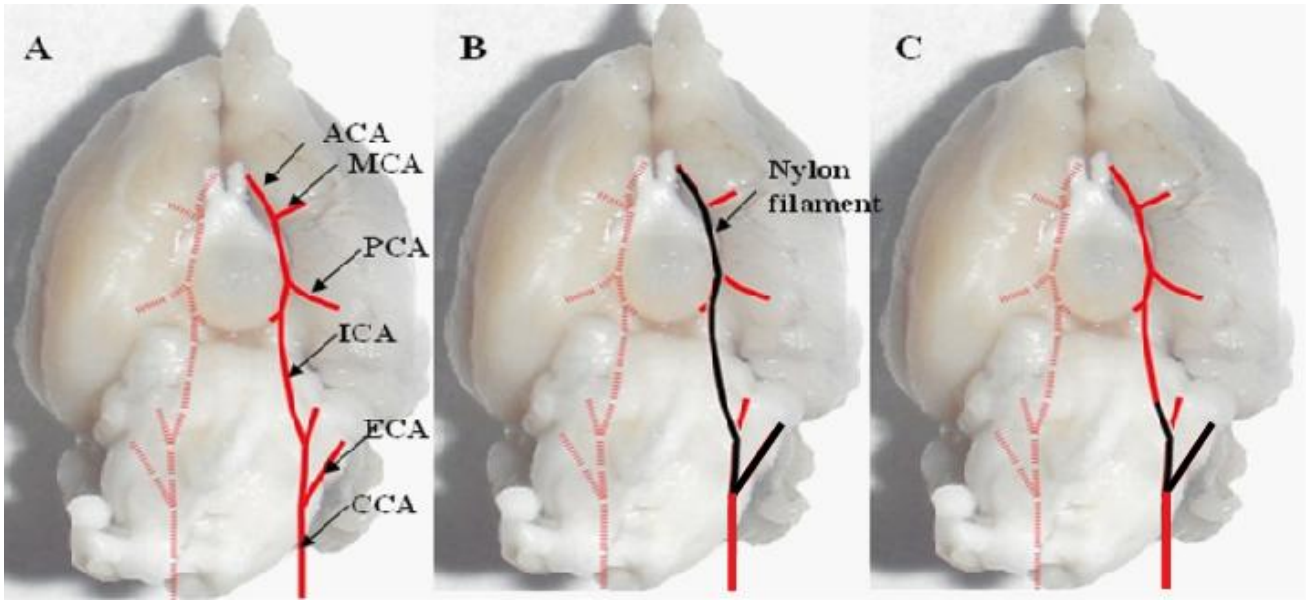

Figure 2.4: A diagram of the cerebral arteries in rats. Labels denote the: anterior cerebral artery (ACA), middle cerebral artery (MCA), posterior cerebral artery (PCA), internal carotid artery (ICA), external carotid artery (ECA), common carotid artery (CCA). **B** Diagram of the MCAO protocol. The CCA and ICA are ligated and a filament is inserted into the ECA and advanced to block the MCA, thus there will be no blood flow to the brain regions supplied by the MCA during the procedure. **C** Diagram of the sham protocol. The CCA is ligated and a filament is inserted into the ECA, as in **B**, but not advanced to block the MCA. The blood flow to the brain will be reduced due to the CCA ligation and the filament occluding vessels. There will, however, be blood flow to the MCA through the circle of Willis. Images have been adapted from Zuo et al. (2012).

Table 2.1: Source and concentration of compounds used in this thesis

Drug	**Supplier**	**Concentration used (μM)**
Noradrenaline (**NA**)	Sigma-Aldrich	2
Glutamate (**Glut**)	Sigma-Aldrich	500
Tetrodotoxin (**TTX**)	Alomone labs	1
L-N^G-Nitroarginine (**L-NNA**)	Sigma-Aldrich	100
1H-(1,2,4)oxadiazolo(4,3-a)quinoxalin-1-one (**ODQ**)	Tocris Bioscience	10
N-hydroxy-N′-(4-butyl-2-methylphenyl)-formamidine (**HET0016**)	Cayman Chemical	1
N-(methylsulfonyl)-2-(2-propynyloxy)-benzene-hexanamide (**MS-PPOH**)	Cayman Chemical	20
N-((4'-((3-butyl-1,5-dihydro-5-oxo-1-(2-(trifluoromethyl)phenyl)-4H-1,2,4-triazol-4-yl)methyl)(1,1'-biphenyl)-2-yl)sulfonyl)-3-methyl-2-thiophenecarboxamide (**L161,982**)	Cayman Chemical	1
D-(-)-2-amino-5-phosphonopentanoic acid (**D-AP5**)	Tocris Bioscience	50
7-Chlorokynurenic acid (**7-CK**)	Tocris Bioscience	100
2,3-Dioxo-6-nitro-1,2,3,4-tetrahydrobenzo[*f*]quinoxaline-7-sulfonamide (**NBQX**)	Tocris Bioscience	25
(*RS*)-α-methyl-4-carboxyphenylglycine (**MCPG**)	Sigma-Aldrich	500
Ru360	Merck Chemicals	50
Mn(III)tetrakis(4-benzoic acid)porphyrin chloride (**MnTBAP**)	Santa Cruz	150
N-T-butyl-alpha-phenylnitrone (**PBN**)	Sigma-Aldrich	100

Table 2. 2: Source and dilution of primary antibodies used in this thesis

Primary Antibody	Supplier	Dilution
Rabbit anti-NG2	Millipore	1:200
Rabbit anti-PDGFRβ	Santa Cruz	1:200
Rabbit anti-vWF	AbCam	1:200
Rabbit anti-Iba1	Synaptic Systems	1:1000
Rabbit anti-desmin	Millipore	1:500
Rabbit anti-αSMA	AbCam	1:200

Table 2. 3: Source and dilution of secondary antibodies used in this thesis

Secondary Antibody	Supplier	Dilution
Goat anti-rabbit 488	Molecular Probes	1:1000
Goat anti-rabbit 546	Molecular Probes	1:1000

Chapter 3: Distinguishing pericytes from other perivascular cell classes

3.1 Introduction

Identification of pericytes is critical for studying their function. Pericytes can be identified visually using certain morphological traits, such as a more rounded nucleus than that of the endothelial cells making up the capillary wall. This trait is often described as a 'bump on a log' morphology (Kuwabara and Cogan, 1960). Identifying pericytes by their morphology and likely location is subjective and may, therefore, not be completely accurate. To aid identification of pericytes several markers are commonly used, including neural glial proteoglycan 2 (NG2) and platelet-derived growth factor receptor β (PDGFRβ; Armulik et al., 2011). Neither of these markers, nor any other known marker, are specific for pericytes. This may be because of the heterogeneity of their developmental origins or it may reflect developmental changes that these cells undergo (Sims et al., 2000; Allt and Lawrenson, 2001).

As described in Chapter 1, pericytes are suggested to have several roles including contractility, angiogenesis, blood brain barrier maintenance and glial scar formation. It has also been suggested that pericytes are pluripotent and have the ability to differentiate into multiple cell types (Dore-Duffy, 2008). Although there may be subtypes of pericyte, poorly defined identification methods for pericytes may also lead to incorrect identification as pericytes of other, similarly poorly defined, perivascular cells, such as endothelial cells, mesenchymal stem cells and perivascular immune cells (Balabanov & Dore Duffy, 1998; Krueger & Bechmann, 2009).

Amongst their many suggested roles, pericytes have been implicated in blood flow regulation at the capillary level (Peppiatt et al., 2006; also see Chapter 4). A role for pericytes in blood flow control is supported by evidence that they express numerous proteins necessary for generation and regulation of contractility, such as cGMP-dependent protein kinase, tropomyosin, smooth muscle isomyosin, desmin and α-smooth muscle actin (Joyce, 1984, 1985a, 1985b; Herman & D'Amore, 1985; Fujimoto & Singer, 1987). There has, however, been controversy over the heterogeneity of expression of several of these proteins, especially expression of α-smooth muscle actin (Skalli, 1986; Nehls and Drenkhahn, 1991; Toribatake et al., 1997) and desmin (Fujimoto & Singer, 1987). Some studies suggest that capillaries which branch directly from arterioles and venuoles contain contractile protein, whereas pericytes on 'true' capillaries, defined as those in the middle of the capillary bed, do not express contractile proteins (Nehls and Drenkhahn, 1991), although other studies find that α-smooth muscle actin is expressed in some of these 'true' capillary cells (Bandopadhyay et al., 2001). This distinction is further complicated by controversy over the definition of a capillary (see section 1.5.1).

Another suggested role of pericytes is that of a perivascular immune cell (Balabanov et al., 1995) or a cell with the ability to transform into a microglial cell (Barón and Gallego, 1972). Evidence put forward for an overlap in the population of pericytes and immune cells is the shared expression of pericyte markers and markers for immune cells (ED2: Esiri, 1986; Graeber et al., 1989; Balabanov et al., 1995; Thomas, et al., 1999; Iba1: Yokoyama et al., 2006). It has, however, also been acknowledged that these perivascular immune cells may just be 'pericyte-like' (Kida et al., 1993; Thomas et al., 1999) and the apparent overlap in markers for these cells may be caused by the lack of an accurate marker for either cell type.

In this chapter I will compare the pericyte populations defined by several commonly used pericyte markers, I will explore the expression of contractile proteins in NG2-labelled pericytes, and I will try to distinguish NG2-labelled pericytes from endothelial cells and perivascular immune cells. The approach used in this Chapter was labelling of brain slices with multiple fluorescent markers and antibodies.

3.2 Methods

3.2.1 Preparations

Experiments were performed on 200 µm sagittal slices of cerebellum and coronal slices of cortex from P12 or P21 Sprague-Dawley rats and P12-14 NG2-DsRed transgenic mice. Tissue preparation and solutions used are described in Chapter 2, section 2.3. Immunocytochemistry was carried out as listed in Chapter 2, section 2.4.

3.2.2 Imaging

Slices were imaged with a confocal laser scanning microscope (LSM), either a Zeiss LSM 510, 700 or 710. Images were obtained using a x40 oil immersion or x20 water immersion DIC objective. Images were 300 microns by 300 microns. Z-stacks were acquired between 20 and 80 microns in depth.

3.2.3 Analysis and statistics

Images were analysed in ImageJ using the cell counter plugin. Where possible, the total number of cells expressing each marker was quantified along with the overlap of expression between markers. Data are presented as mean ± s.e.m of counts from each image.

3.3 Results

3.3.1 NG2 as a pericyte label

NG2 (previously called HMW-MAA (high molecular weight-melanoma associated antigen) and chrondroitin sulfate proteoglycan 4 (CSPG4)) is a surface proteoglycan, and is commonly used as a pericyte marker (Schlingemann et al., 1990; Ozerdem et al., 2001). I first confirmed that pericytes in both rats and mice expressed NG2.

In rat cortex and cerebellum, I found that rabbit anti-NG2 antibody (Millipore) clearly labelled perivascular cells that had the classic 'bump on a log' appearance of pericytes (Kuwabara and Cogan, 1960). The antibody also outlined the shape of the vessels, which is to be expected, as pericyte processes cover 22 to 37% of cortical capillaries in the rat (Frank et al., 1987; Mathiisen et al., 2010). Example images of pericytes labelled with NG2 antibody can be seen in Figure 3.1A. Because NG2 is a surface membrane proteoglycan, the antibody binds to the cell membrane and the resulting fluorescence outlines the pericyte cell bodies as well as the processes lining the vessels.

In transgenic mouse cortex and cerebellum, where DsRed is expressed under the control of the NG2 promoter (NG2-DsRed; for a description of the transgenic mouse see Chapter 2, section 2.2; Zhu et al., 2008), fluorescence is seen within perivascular cells that fit the description of pericytes as well as in processes lining the capillaries. In this case the fluorescence is seen within the cell, because the DsRed is a cytoplasmic protein produced under the control of the NG2 promoter.

NG2 is also expressed in other cell types (see table 1) including OPCs (Nishiyama et al., 1991, 1996) but we can easily distinguish these cells from pericytes because of the distinct morphology of each cell type. OPCs tend to have a slightly larger cell body than pericytes (10-15 μm rather than ~10 μm) and they have multiple branched processes that are decorated with filopodia and lamellopodia. These processes have a different orientation depending on the brain region, projecting radially in the grey matter and longitudinally in the white matter (Levine et al., 2001). Figure 3.1C shows an example of a fluorescent OPC in NG2-DsRed tissue.

These results confirm that expression of NG2 defines pericytes in the cortex and the cerebellum, in both rat and mouse. In this thesis, therefore, whenever possible I used NG2 as a pericyte marker.

3.3.2 The population of NG2 positive pericytes overlaps with PDGFRβ labelled cells

PDGFRβ is often used as a pericyte marker (Krueger and Bechmann, 2010). Data from labs that define pericytes by different markers are often compared. Because of this, I tested whether the population of pericytes that were labelled in NG2-DsRed mice showed overlap with pericytes labelled with an antibody against PDGFRβ (1:200 Santa Cruz).

Using antibody labelling in transgenic mice expressing DsRed under the NG2 promoter, I found that NG2 positive pericytes, in both the cortex and cerebellum, also express PDGFRβ (Figure 3.2A and 3.2B respectively). I counted cells in 13 Z-stack images from 6 cortical and 7 cerebellar slices from 4 NG2-DsRed animals. I identified 144 NG2-DsRed and 148 PDGFRβ labelled perivascular cells in cortical slices and 274 NG2-DsRed and 280 PDGFRβ labelled perivascular cells in the cerebellar slices. Pooling data from the cerebellum and the cortex, 95.0±2.2% of the cells identified by NG2 labelling also expressed PDGFRβ (Figure 3.2C) while 96.4±0.9% of cells that are identified by PDGFRβ labelling also expressed NG2 (Figure 3.2D).

These findings suggest that the vast majority of NG2 positive pericytes also express PDGFRβ. The expression of these markers, however, does not show complete overlap and neither marker labels all perivascular cells that fit the morphology of pericytes (an example of a cell labelled with NG2 but not PDGFRβ can be seen in Figure 3.2A (yellow arrow). It is, therefore, possible that the cells that express NG2 but not PDGFRβ (or vice versa) are slightly different populations of pericytes with different functions to those that express both markers.

3.3.3 The population of NG2 positive pericytes overlaps with isolectin-B_4 labelled cells

Isolectin-B_4 is a known microglial marker (Streit et al., 1987), but it also labels galactosyl epitopes of the basement membrane (Peters and Goldstein, 1979). It is, therefore, possible that isolectin-B_4 labelling reveals pericytes, which are encased by basement membrane. I investigated whether isolectin-B_4 conjugated to fluorescein isothiocyanate (FITC) could be used to identify pericytes in the cortex and the cerebellum of rats and mice.

In NG2-DsRed mice I found that incubation with isolectin-B_4 (10 µg/ml) labelled capillaries in the cortex and the cerebellum and that, with this labelling, pericytes could easily be identified by their ‘bump on a log’ morphology (see Figure 3.3A and 3.3B respectively). The vast majority of cells identified in this way were also positive for NG2 (96.1±2.5% averaged over 5 z-stack images; 67/73 cells from 3 cortical and 2 cerebellar brain slices from 2 animals Figure 3.3C). Similarly in rat, isolectin-B_4 labelling also allowed identification of

pericytes (see Figure 3.3D) with the great majority of pericytes identified using isolectin-B_4 labelling also being labelled for NG2 (92.6±1.0% or 667/718 cells assessed in 13 z-stack images from 6 cortical slices and 7 cerebellar slices from 2 animals; Figure 3.3E). All perivascular cells positive for NG2 in both species were encased in IB_4 labelled basement membrane.

These results suggest that isolectin-B_4 conjugated to FITC, along with morphological assessment of cells, is sufficient for identifying the vast majority of pericytes (defined by NG2 labelling) in the cortex and the cerebellum of mice and rats. However, much like the finding with PDGFRβ, the overlap in labelling was not absolutely complete, perhaps reflecting the existence of a small population of cells with a different function. It would be of interest for further study to investigate whether the cells that are encased in basement membrane and have the morphology of pericytes but do not express NG2, would be labelled by an antibody for PDGFRβ.

Using isolectin-B_4 conjugated to a fluorescent protein is a favourable method for labelling pericytes, compared to using antibody to NG2 or PDGFRβ as it is more time efficient than antibody labelling and it penetrates into tissue well. Although in most of this thesis identification of pericytes was carried out using antibody to NG2 or DsRed expression from the NG2 promoter, the method was used for the majority of experiments in Chapter 6.

3.3.4 The population of NG2 positive pericytes shows heterogeneous expression of desmin and αSMA

It is not only necessary to identify pericytes, but also to learn more about the proteins that they express in relation to their purported functions. One of the roles that pericytes are thought to play is in regulation in blood flow. As mentioned above, this role is supported by observations that pericytes can control capillary diameter (Peppiatt et al., 2006) as well as several studies showing pericytes express proteins necessary for contractility (Joyce 1984, 1985a, b; Herman & D'Amore, 1985; Fujimoto & Singer 1987). It has, however, been suggested that not all pericytes express contractile proteins (Skalli, 1986; Nehls and Drenkhahn, 1991; Balabanov and Dore-Duffy, 1998; Bandopadhyay et al., 2001). I investigated the proportion of NG2-DsRed labelled pericytes that may have contractile properties by labelling brain slices from these mice with antibodies for the contractile proteins α-smooth muscle actin (αSMA; 1:200 AbCam) and desmin (an intermediate filament found in contractile cells, 1:500 Millipore).

In the cerebellum, some perivascular NG2 positive cells did express αSMA (Figure 3.4A), but expression was rarely seen on smaller vessels (demonstrated by yellow arrows in Figure 3.4A and 3.4B). There was little parenchymal αSMA labelling. Similarly, desmin expression was seen on vessels in both the cortex (3.5A) and the cerebellum (3.5B) but the labelling appeared stronger in larger vessels (Figure 3.5B). As

the desmin labelling did not cover the cell body of perivascular cells, it was not possible to quantify the overlap between desmin and NG2 positive cells. NG2 positive pericyte processes cannot be attributed to a particular cell body as processes from different pericyte somata appear to overlap on the vessel surface.

The labelling of NG2-DsRed mice with antibodies to αSMA and desmin suggests that contractile proteins are present at the capillary level, however expression of these proteins was not seen in all pericytes defined by NG2 expression, and the expression of αSMA appears to be more common in larger vessels. These findings agree with previous studies that have suggested that only a small population of pericytes express contractile proteins *in vivo* (Nehls and Drenkhahn, 1991; Nehls 1992; Boado and Pardridge, 1994; Ozerdem et al., 2001). However, there are generic problems with this kind of analysis which may lead to false positive or false negative assessment of the presence of these proteins in pericyte processes. It is hard to resolve whether the αSMA and desmin labelling seen along and around vessels (where it needs to be to constrict the capillaries) is in pericyte processes or in endothelial cells, which may lead to endothelial cell expression being attributed to pericytes. Alternatively, if the expression of αSMA and desmin is low in pericytes, it may fall below the level needed for detection by immunocytochemistry.

3.3.5 The population of NG2 positive pericytes does not overlap with vWF labelled cells

The vascular wall of capillaries is composed of endothelial cells, forming the inner lining, along with pericytes (Rhodin, 1968). It is generally thought that pericytes can be distinguished from endothelial cells through morphology. However, since I was using NG2 as a pericyte marker, I was aware that it has been reported that NG2 also labels endothelial cells (Schrappe et al., 1991; Grako and Stallcup, 1995; Pouly et al., 2001). It is therefore possible that the small population (<5%) of NG2 positive perivascular cells that do not label for PDGFRβ are endothelial cells. To investigate this, I used the NG2-DsRed mice and looked for the possible presence of NG2-DsRed labelled endothelial cells, by labelling brain slices from these mice with an antibody to the known endothelial cell marker, von Willebrand factor (vWF; 1:200 AbCam), a glycoprotein involved in clotting.

Using antibody labelling in NG2-DsRed mice, I counted cells in 9 z-stack images from 4 cortical and 5 cerebellar slices from 4 NG2-DsRed animals (counting 111 and 175 NG2-DsRed labelled perivascular cells, and 244 and 336 vWF positive cells, in the cortex and cerebellum respectively). I found that NG2 positive pericytes, in both the cortex and the cerebellum, did not express vWF (Figure 3.6A and 3.6B respectively). This implies that pericytes defined by perivascular location and NG2 expression differ from endothelial cells.

The ratio of pericytes to endothelial cells that I counted (1:2.2 and 1:1.9 in the cortex and the cerebellum respectively) did not fit the ratio that has previously been reported (1:3; Pardridge et al., 1999). This may be due to the reliance of my endothelial cell counts on DAPI (nuclear) labelling. Endothelial cells are flat cells lining blood vessels and it is, therefore, very difficult to distinguish neighbouring cells, unless their cell nuclei are labelled. When the DAPI labelling was weaker I may have underestimated the number of endothelial cells, thus giving an apparently increased ratio of pericytes to endothelial cells. On the other hand, previous estimates of the pericyte to endothelial cell ratio were made from isolated brain capillaries (Pardridge et al., 1999), so the difference in estimates may be due to pericyte damage or removal during isolation.

This finding contradicts the previous reports that NG2 labels endothelial cells. It has been suggested that the previous claims were made due to a reliance on αSMA labelling of pericytes (Ozerdem et al., 2001). In those studies, perivascular cells that did not express αSMA were identified as endothelial cells. This classification method has been superseded by the belief that αSMA only labels a subset of pericytes (see section 3.3.4; Nehls & Drenckhahn, 1991; Verbeek et al., 1994; Bandopadhyay et al., 2001)

3.3.6 NG2 positive pericytes do not express the immune cell marker Iba-1

It has been speculated that some cells that are identified as pericytes are in fact perivascular immune cells (Graeber et al., 1989; Balabanov 1995; Thomas, 1999). As with the expression of contractile proteins, if NG2 positive pericytes label for a marker of immune cells, it may help us to learn more about the function of pericytes. Indeed, it has been suggested that these cells express macrophage-like activity (Thomas et al., 1999; see Chapter 1 section 1.6.4).

I used an antibody to Iba-1 (ionized calcium-binding adaptor molecule 1; 1:1000, Synaptic systems), which is an immune cell marker that labels both ramified and perivascular microglia as well as other monocytic cell lines (Ito et al., 1998), and has been found to label perivascular cells encased within the basement membrane (Bechmann et al., 2001). I investigated whether NG2 positive pericytes also express Iba-1. I counted cells in 15 Z-stack images from 7 cortical and 8 cerebellar slices from 5 NG2-DsRed animals, and found that none of 135 (cortex) and 212 (cerebellum) NG2-DsRed labelled perivascular cells co-labelled for Iba1 (although Iba1 labelled 110 cells in the cortical slices and 136 cells in the cerebellar slices; Figure 3.7A and 3.7B).

These data strongly suggest that pericytes identified by NG2 are not immune cells. I can, therefore, be confident that the cells that I class as pericytes, defined by NG2 expression, are a population separate from perivascular immune cells.

3.4 Discussion

I have investigated the expression of several markers that have been suggested to label pericytes. The results indicate that, firstly, pericytes can be identified by labelling for NG2, PDGFRβ or isolectin-B_4. Secondly, some pericytes appear to express the contractile proteins desmin and αSMA, however further work is needed to clarify what proportion of pericytes express these proteins. I also found that based on expression of markers, pericytes (defined by NG2 expression) can be distinguished from endothelial cells (defined by vWF expression) or perivascular immune cells (defined by Iba-1 expression).

3.4.1 Pericytes can be identified by NG2, PDGFRβ or isolectin-B_4 labelling

The absence of a specific marker to label pericytes has exacerbated the confusion surrounding the many possible roles of these cells. It is now widely accepted that both NG2 and PDGFRβ can be used to label pericytes (Armulik et al., 2011). However, there is some doubt about whether NG2 is consistently expressed throughout development (Miller et al., 1995). My labelling was performed on relatively young rats and mice, to match the ages of the animals used for functional studies elsewhere in the thesis. The importance of both NG2 and PDGFRβ expression in pericytes is supported by the absence of pericytes in animals where these proteins have been knocked out or knocked down (Daneman et al., 2010; Winkler et al., 2010; You et al., 2013). The finding that the cell populations labelled by these two markers are not 100% identical leads to the possibility that a small percentage of the cells (<5%) in studies using each of these markers may have different properties. The vast majority of the cells are, however, labelled by both markers, suggesting that either can be used as reliable markers for pericytes.

The finding that isolectin-B_4 conjugated to a fluorescent protein can be used to identify pericytes is very convenient. Unlike the production, or purchase, of a transgenic mouse or the procedures for antibody labelling, isolectin-B_4 labelling is cost and time efficient.

3.4.2 Not all pericytes express contractile proteins

The first role suggested for pericytes on their discovery was of a contractile nature (Rouget, 1874; Zimmermann, 1923). Supporting that, the first studies looking at protein expression in pericytes, using cultured cells, found that pericytes express contractile proteins, including αSMA (Herman and D'Amore, 1985). From later studies looking at pericytes *in situ* or *in vivo*, however, it appeared that contractile protein expression was not universal in this cell type, but that pericytes on larger vessels expressed contractile proteins whereas pericytes on 'true' capillaries, many branch points away from the arteriole, did not (Nehls and Drenckhahn,

1991; Boado and Pardridge, 1994). Nevertheless, studies looking at the function of pericytes have found that they are involved in controlling capillary diameter (Peppiatt et al., 2006; Fernández-Klett et al., 2013), so it is possible that contractile proteins are expressed even in small capillaries. The finding that capillaries were positive for labelling with both αSMA and desmin supports a contractile role for pericytes. However, my study is far from thorough enough to make any kind of estimate or assumption about the subtypes of pericytes that have this function, and ideally immunocytochemistry at the electron microscopic level would be required to determine with certainty which cell types express αSMA and desmin.

3.4.3 The population of pericytes identified by NG2 is distinct from endothelial cells

The heterogeneous expression of contractile proteins may be responsible for the belief that NG2 is expressed by endothelial cells as well as pericytes. Early studies used αSMA as a pericyte marker, so that any αSMA negative perivascular cell was classed as an endothelial cell (Ozerdem et al., 2001). I found there was no expression of NG2 on vWF positive endothelial cells. This finding allows me to continue using NG2 as a pericyte marker without worrying about a contamination from endothelial cells within the population of cells that I am studying.

3.4.4 The population of pericytes identified by NG2 is distinct from perivascular immune cells

It has been suggested that pericytes are perivascular immune cells (Balabanov et al., 1995), or that they are confused with a ‘pericyte-like’ perivascular immune cell (Kida et al., 1993; Thomas et al., 1999). I found that there was no overlap between the expression of NG2 and Iba-1 in perivascular cells. This finding implies that the pericytes identified with NG2 labelling are not immune cells.

3.4.5 Conclusion

Overall, my data suggest that there are several potential pericyte markers, but that investigators must be aware that the population of pericytes that they identify with a specific marker may not include absolutely all pericytes that are identified by other pericyte markers, although the percentage not identified by any particular marker is small (<5%).

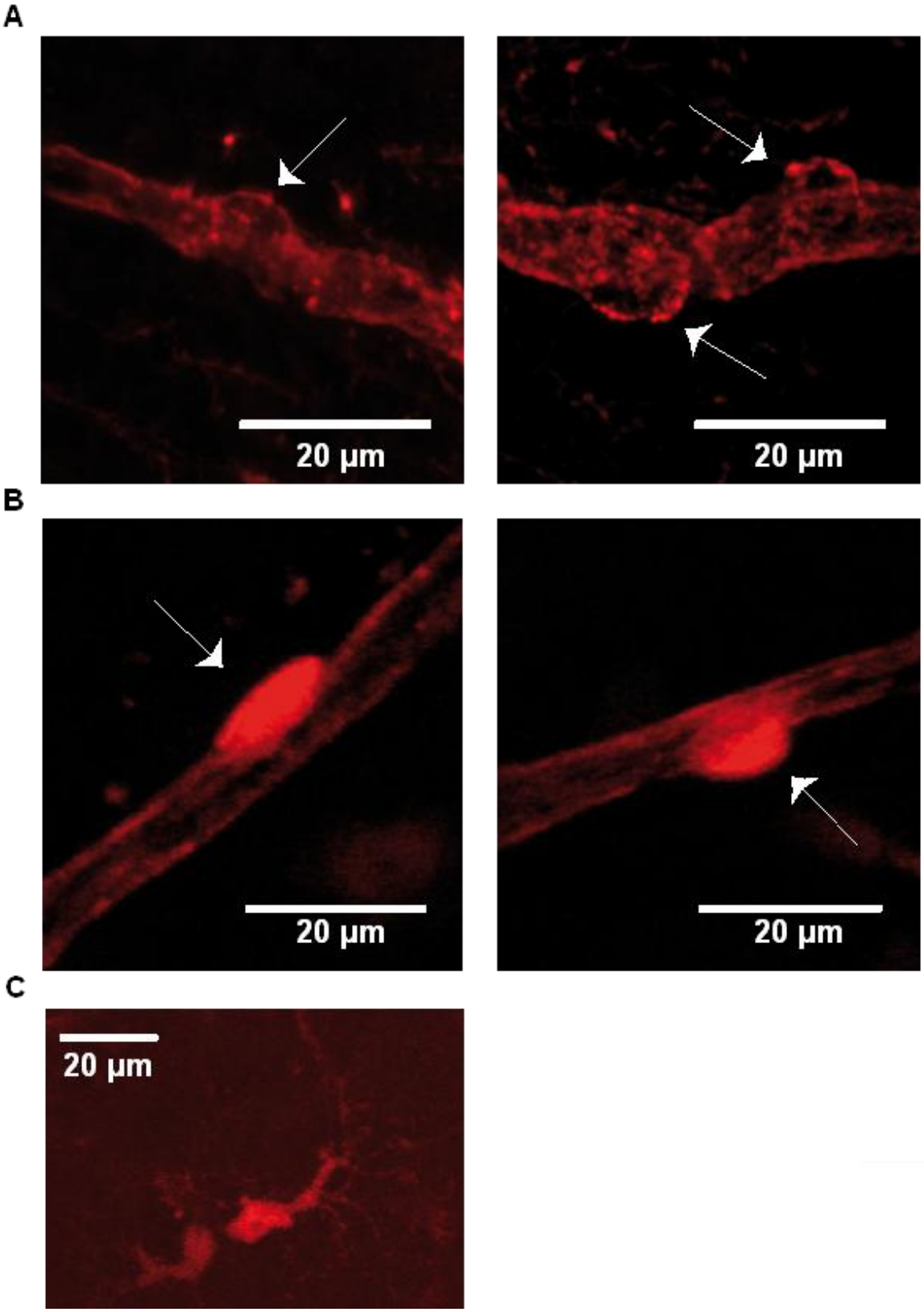

Figure 3. 1: Labelling of NG2 positive cells. A Cortical slices from rat labelled with an antibody to NG2 (red) **B, C** Cortical slices from NG2-DsRed transgenic mice showing NG2 positive pericytes (**B**) and oligodendrocyte precursor cells (OPCs; **C**).

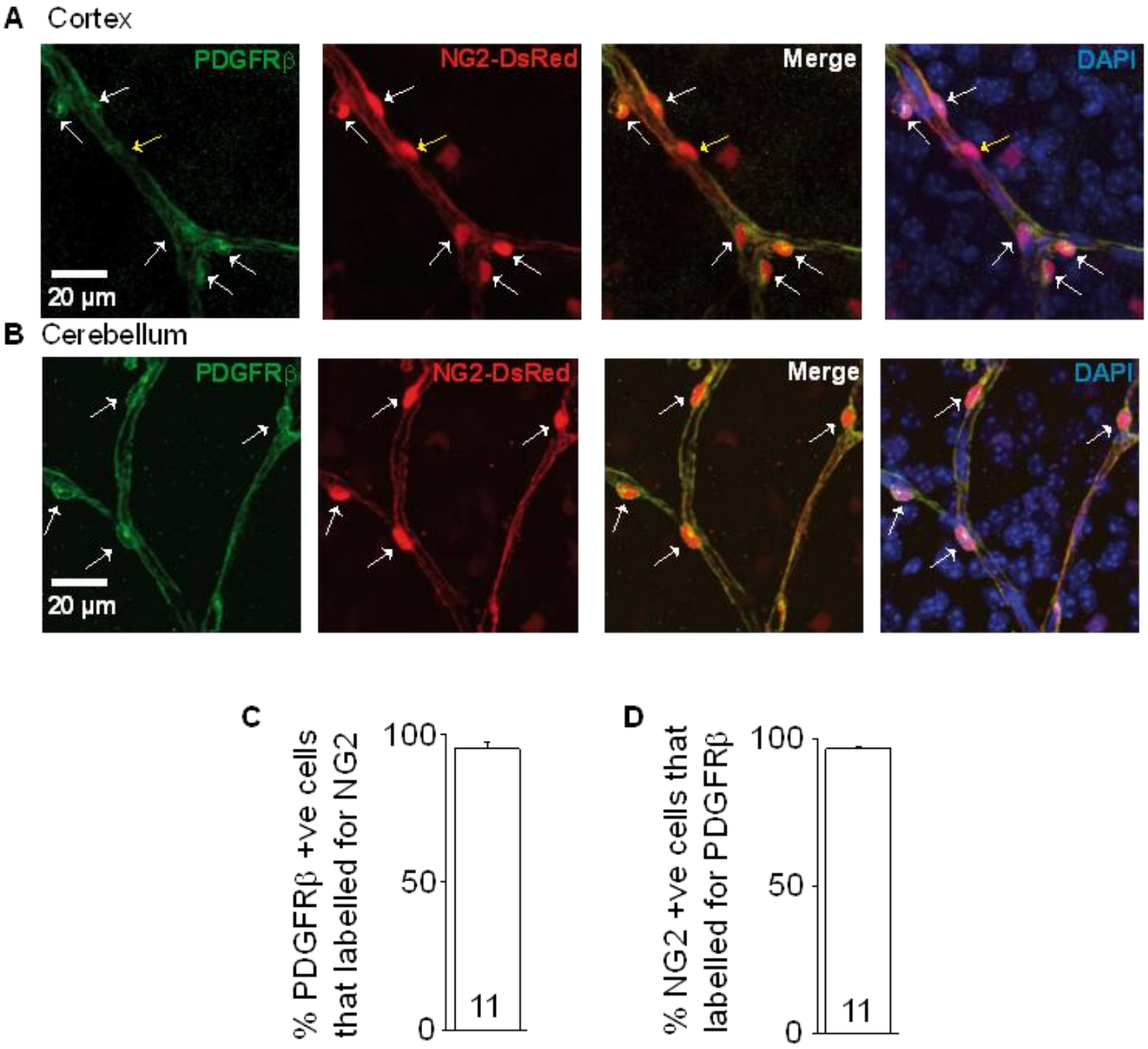

Figure 3. 2: PDGFRβ labelling in NG2-DsRed mice. Cortical (**A**) and cerebellar **(B)** slices from NG2-DsRed transgenic mice labelled with PDGFRβ (green). Pericytes that are labelled for NG2 (red) and PDGFRβ are indicated by white arrows. Yellow arrows indicate perivascular cells that are labelled for NG2 but not PDGFRβ **C** Plot of the percentage of pericytes defined by PDGFRβ labelling which were also NG2 positive. **D** Plot of the percentage of pericytes defined by NG2 labelling which were also PDGFRβ positive.

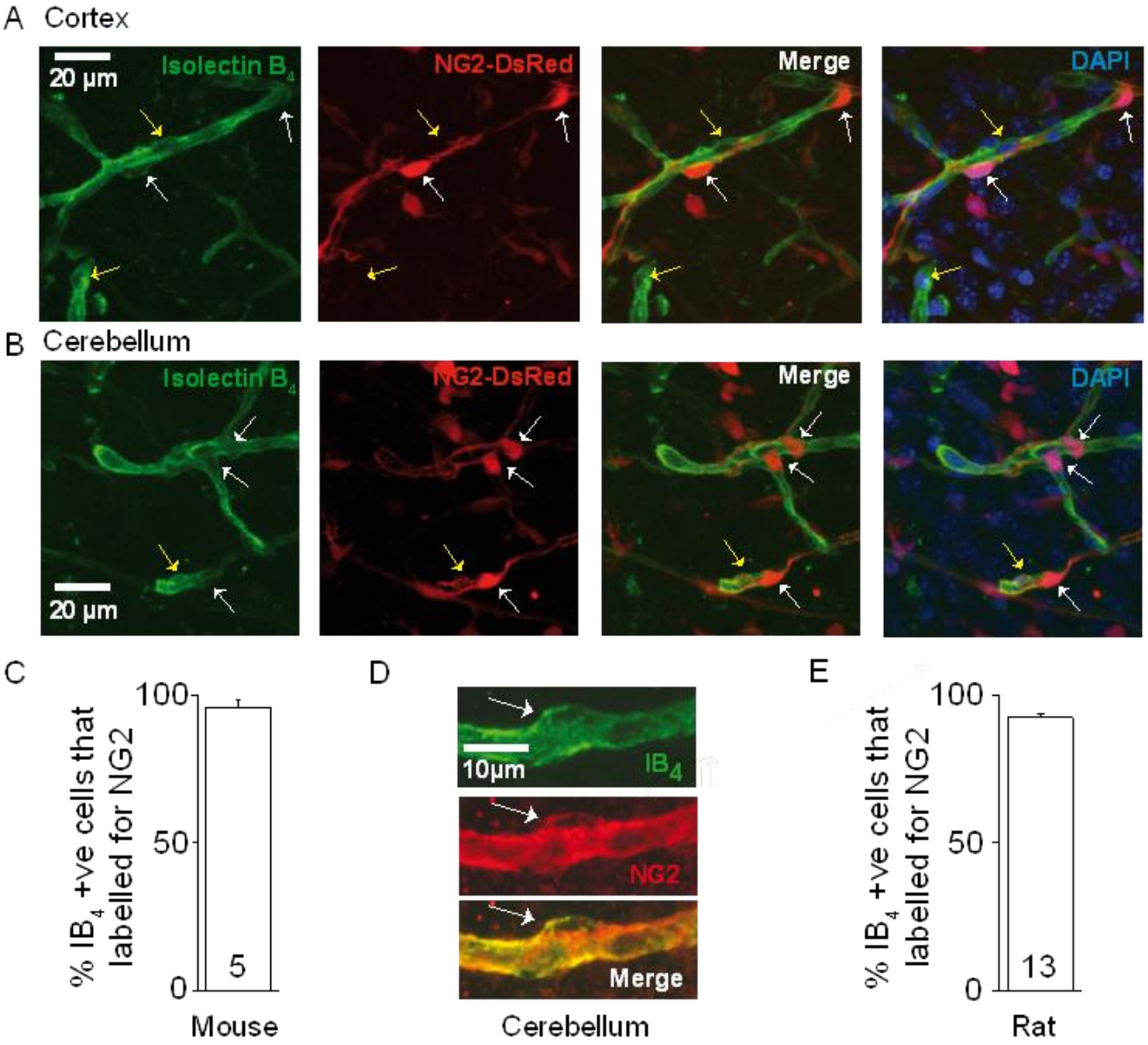

Figure 3. 3: Isolectin-B4 as a pericyte marker. Cortical (**A**) and cerebellar (**B**) slices from NG2-DsRed transgenic mice labelled with isolectin B_4-FITC conjugate (IB_4; green). Pericytes that express NG2 (red) and IB_4 are indicated by white arrows. Yellow arrows indicate perivascular cells that are labelled with IB_4 but not NG2. **C** Plot of the percentage of pericytes in mouse (pooled from cerebellum and cortex) defined by IB_4 labelling which were also NG2-DsRed positive. **D** Cerebellar slice from rat labelled with IB_4 (green) and a rabbit anti-NG2 antibody (red). A pericyte labelled with both markers is indicated by white arrow. **E** Plot of the percentage of pericytes in rat (pooled from cerebellum and cortex) defined by IB_4 labelling which were also NG2 positive.

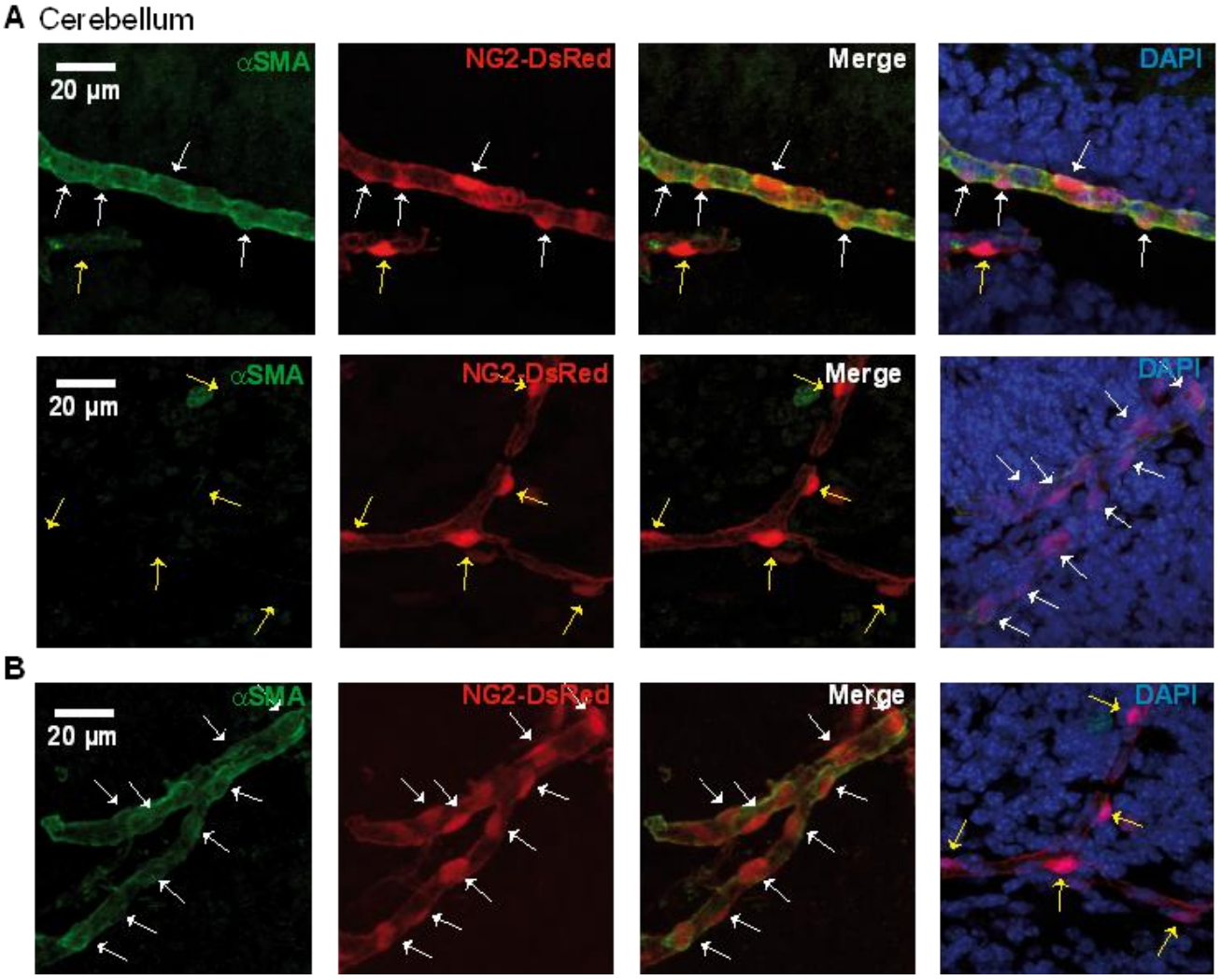

Figure 3. 4: αSMA labelling in DsRed NG2 mice. A Cerebellar slices from NG2-DsRed transgenic mice labelled with an antibody to αSMA. Pericytes labelled for αSMA (green) and NG2-DsRed (red) are indicated by white arrows. Pericytes labelled with NG2 but not αSMA are indicated by yellow arrows. **B** Cerebellar slice from NG2-DsRed transgenic mice labelled with an antibody to αSMA showing a vessel with no αSMA labelling. Pericytes labelled for NG2 but not αSMA are indicated by yellow arrows.

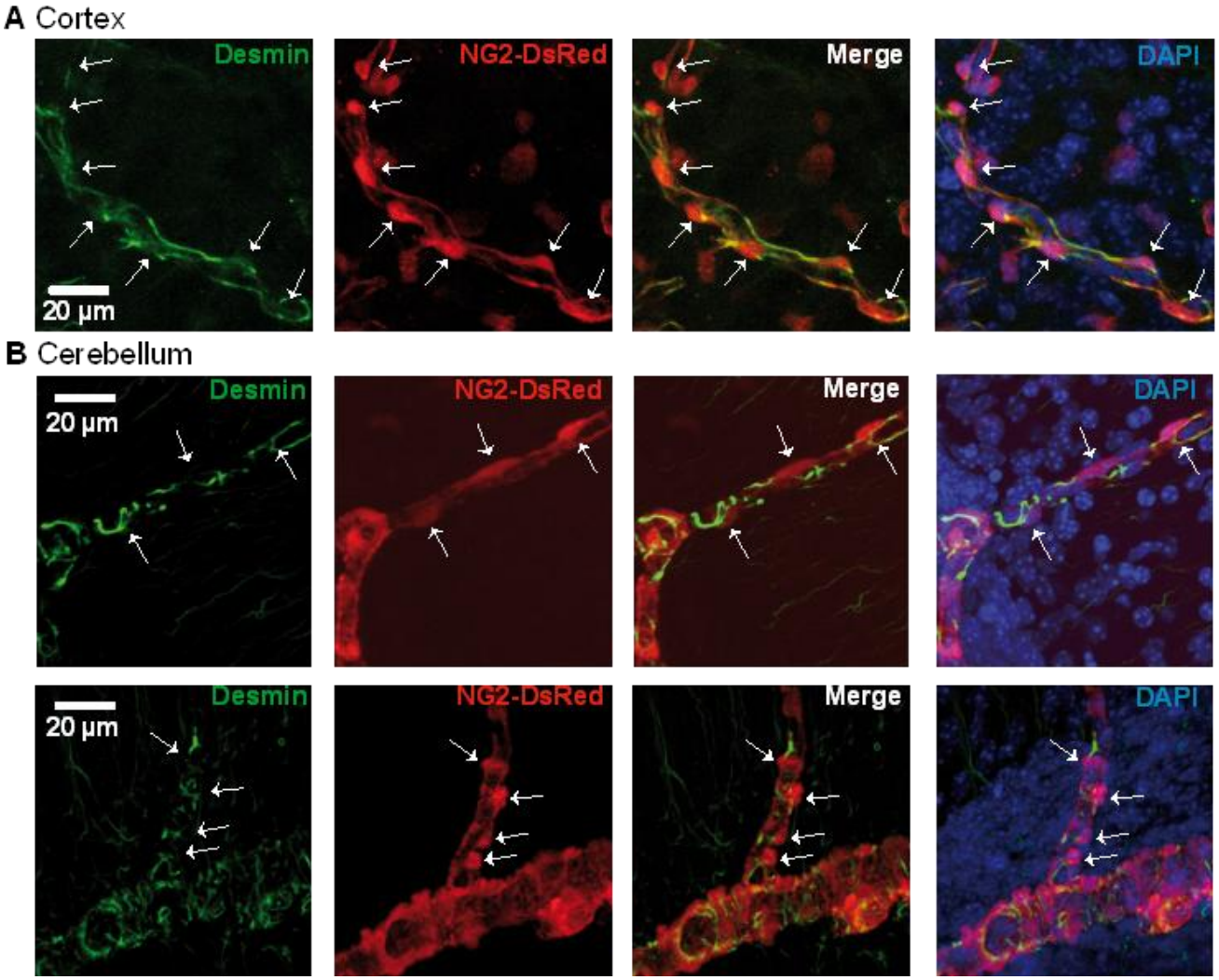

Figure 3. 5: Desmin labelling in DsRed NG2 mice. Cortical (**A**) and Cerebellar (**B**) slices from NG2-DsRed transgenic mice labelled with an antibody to desmin (green). Pericytes labelled for NG2 (red) are indicated by white arrows.

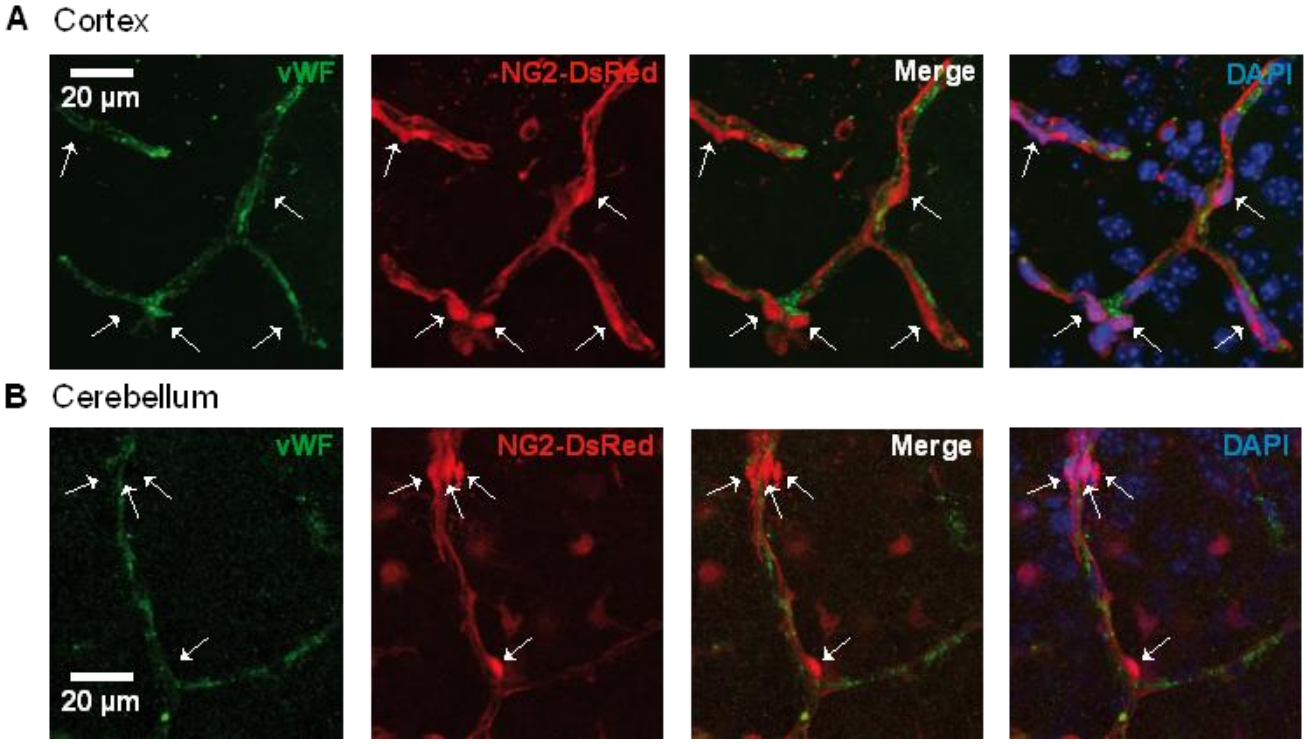

Figure 3. 6: vWF labelling in DsRed NG2 mice. Cortical (**A**) and cerebellar (**B**) slices from NG2-DsRed transgenic mice labelled with an antibody to vWF (green). Pericytes that express NG2 (red) are indicated by white arrows.

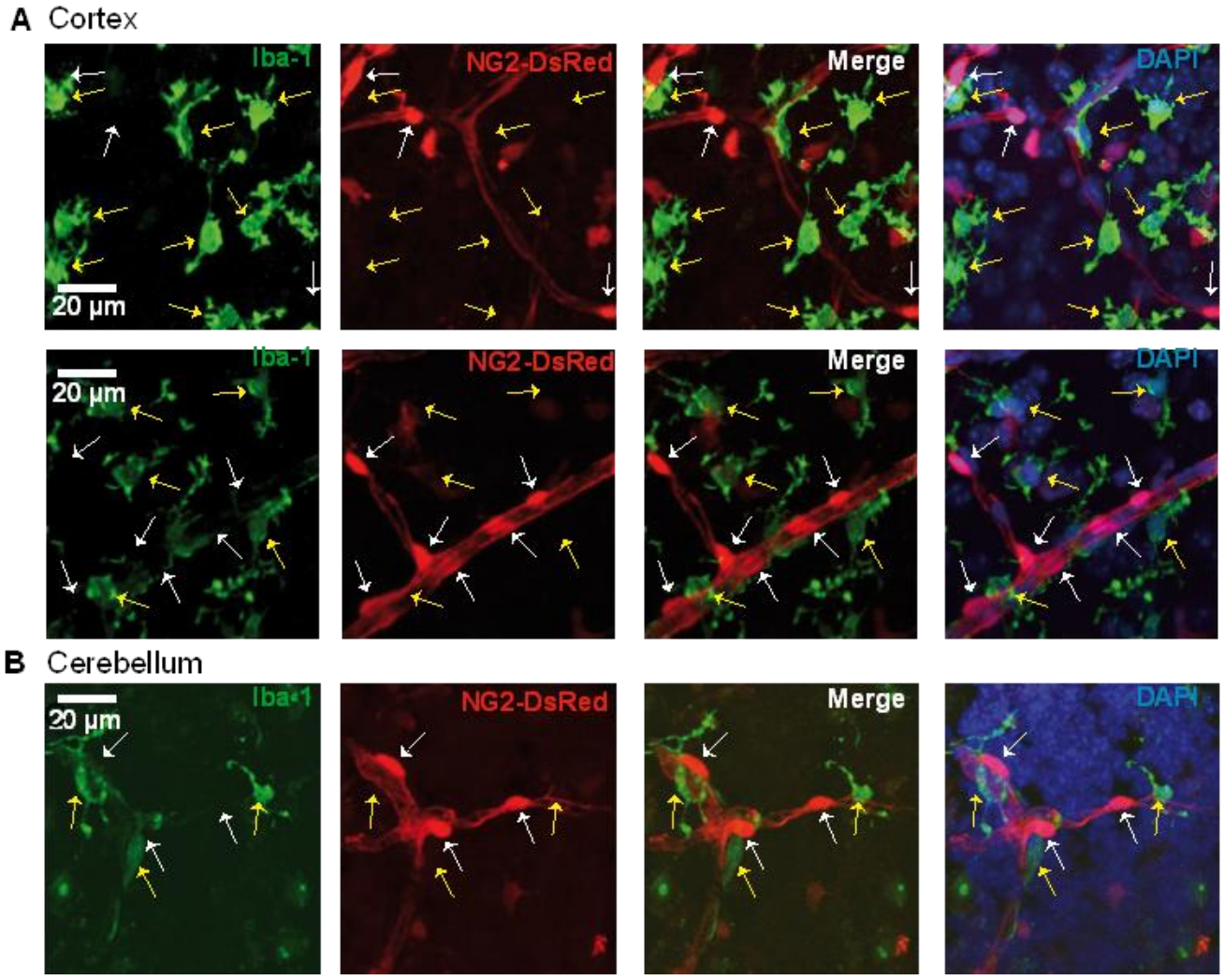

Figure 3. 7: Iba-1 labelling in DsRed NG2 mice. Cortical (**A**) and cerebellar (**B**) slices from NG2-DsRed transgenic mice labelled for Iba-1 (green). Pericytes, labelled with DsRed (red), are indicated by the white arrows. Immune cells, labelled for Iba-1 (green), are indicated by the yellow arrows.

Chapter 4: Signalling pathways underlying pericyte dilation of CNS capillaries in response to glutamate

4.1 Introduction

As reviewed in Chapter 1, cerebral blood flow is normally thought to be regulated at the arteriole level, but may also be regulated by pericytes, at the capillary level. For arterioles, synaptically released glutamate regulates blood flow by sending messengers to influence the smooth muscle around the arterioles. In neurons, particularly interneurons (see Chapter 1 section 1.2.1), glutamate acts on N-methyl-D-aspartate receptors (NMDARs) to raise $[Ca^{2+}]_i$, causing neuronal nitric oxide synthase (nNOS) to produce NO, which evokes smooth muscle relaxation and vessel dilation (Faraci and Breese, 1993). Glutamate can also raise $[Ca^{2+}]_i$ in astrocytes by activating metabotropic glutamate receptors (mGluRs; Porter and McCarthy, 1996), which leads to arteriole dilation (Zonta et al., 2003; Takano et al., 2006; Gordon et al., 2008). The dilation evoked by increases in astrocytic calcium is thought to occur through increased production of arachidonic acid and its vasoactive metabolites, which include the vasodilatory prostaglandins (Niwa et al., 2000) and EETs (Peng et al., 2002), as well as the vasoconstrictor 20-HETE (Harder et al., 1994). A rise of $[Ca^{2+}]_i$ in astrocyte endfeet may also activate Ca^{2+}-gated K^+ channels ($BK_{(Ca)}$), releasing K^+, which also dilates vessels (Filosa et al., 2006). (See Chapter 1 section 1.2.2 for a more thorough description of these pathways). It is unknown whether these same pathways mediate signaling from neurons to pericytes.

Control of blood flow at the level of capillaries has been little studied, although these vessels do have spatially separated contractile cells called pericytes at intervals along their length. Contractility has been observed in cultured retinal pericytes (Kelley et al., 1987, 1988; Das et al., 1988), pericytes in whole retinal mounts (Schonfelder et al., 1998) and in cerebellar slices (Peppiatt et al., 2006). There has also been some evidence of pericyte contractility *in vivo* (Fernández-Klett et al., 2010). See Chapter 1.6.5 for a full description of current knowledge of pericyte contractility.

Here, I examine pharmacologically the pathways by which glutamate dilates capillaries imaged in cerebellar slices. The approach used was to preconstrict vessels with noradrenaline (mimicking its release from the locus coeruleus *in vivo*, as well as tone generated by blood flow and pressure *in vivo*) and then to apply glutamate (mimicking neuronal activity) to dilate vessels, while applying blockers of mediators thought to be involved in the signalling pathways. As a framework for assessing the data, Figure 4.1 shows the signaling pathways that control arteriole dilation (from Figure 1.1) transposed to the pericyte situation.

4.2 Methods

4.2.1 Preparations

Experiments were performed on 200μm sagittal slices of cerebellum from P12 rats. Solutions and tissue preparation are described in Chapter 2, sections 2.1.1 and 2.3.1.

4.2.2 Imaging

Capillaries, lacking the continuous smooth muscle seen around arterioles and <10μm in diameter, in the molecular layer of the cerebellum, were visualised using a CCD video microscopy system, and images were captured with Metafluor software (Molecular Devices). Superfusion with each drug (or combination of drugs) was maintained for approximately 5 minutes (except when prolonged incubation was needed for drugs to act). For drugs manipulating signalling pathways, before testing the effect of the drug on responses to noradrenaline and glutamate, each drug was applied to the preparation on its own in order to establish the effect of the drug on the baseline capillary diameter (except in the case of MS-PPOH which required 30 minutes incubation so a pre-drug baseline diameter was not measured). Noradrenaline was then applied and the noradrenaline-evoked constriction in the drug was measured. Glutamate was then added in the presence of the noradrenaline in order to establish the dilation it produced after preconstriction with noradrenaline.

4.2.3 Analysis and statistics

Images were analysed in Metamorph software (Molecular Devices) and Image-Pro software (MediaCybernetics). The inner diameter of the capillary lumen was measured at 5-10 second intervals, wherever possible at locations where pericyte somata were visible. For statistical analysis of the effects of drugs on capillary diameter, the diameter measurement for each drug was taken from the last 1-5 recorded images in that drug. The diameter or diameter change in each condition was measured as shown in Figure 4.2A. Capillary diameter in the absence of any agents is represented by the letter A. The vessel diameter in noradrenaline is represented by the letter B. The change in vessel diameter on glutamate application is represented by the letter C. For analysis, these values are expressed as a percentage of the diameter A. Thus, on application of noradrenaline the constriction is measured as the diameter in noradrenaline as a percentage of the diameter in the absence of any agents, B/A. On application of glutamate the dilation is measured as the change in diameter as a percentage of the diameter in the absence of any agents, C/A (see Figure 4.2A).

Data are presented as mean ± s.e.m. Results in each condition are compared to results in interleaved controls. Statistical methods are given in Chapter 2, section 2.8. All statistical analysis was conducted using IBM SPSS21 statistics software or Microsoft Excel.

4.3 Results

4.3.1 Influence of oxygen concentration on vessel diameter

The oxygen concentration in the tissue is of concern in *in vitro* studies. Most brain slice work is carried out at high oxygen concentrations, using solution gassed with 95-100% oxygen, leading to concentrations of ~150-400μM O_2 at varying depths in the tissue, whereas using a lower oxygen concentration in the solution (20% oxygen) leads to concentrations of 2-130μM in the tissue (Hall et al., 2012). Thus data obtained at 20% are more comparable to the physiological range of O_2 *in vivo,* 20-60 μM (Dings et al., 1998), and tissue superfused with 95-100% O_2 has supra-physiological O_2 levels. It has been found that this difference of oxygen concentration can change arteriole responses, for example dilation is seen in response to uncaging calcium in astrocytes at 20% O_2 while constriction is seen at 95% O_2 (Gordon et al., 2008).

This change in capillary response at different oxygen concentrations may in part be due to an effect on the enzymes that produce the regulators of vascular tone. Oxygen is required for the synthesis of nitric oxide and of arachidonic acid derivatives, but the O_2 -dependence of the relevant synthesis reactions varies between the different reactions (see Figure 4.1, which shows K_m values for messenger synthesis in the order NO>20-HETE>PGs=EETs). This suggests that the relationship between the different signaling pathways will be altered as the oxygen concentration is changed. At *in vivo* oxygen levels, NO and 20-HETE synthesis would be expected to be significantly limited by oxygen availability. For this reason I carried out experiments at both 20% and 95% O_2 to explore whether the responses at physiological and supra-physiological oxygen concentrations differ.

The baseline vessel diameter was slightly but significantly lower in the vessels that were held (for at least an hour) and studied in 95% O_2 conditions than those held and studied in 20% O_2 conditions ($p=1x10^{-3}$ by independent samples t-test; Figure 4.2B). Nevertheless the baseline diameter of capillaries was not altered significantly in the short term (10 minutes) when the superfusion solution was changed from solution bubbled with 95% O_2 to solution bubbled with 20% O_2 (104.2±2.3% of initial diameter at 95% O_2; p=0.08), perhaps because it takes time for vessel diameter to adapt to the change of O_2 level.

In the remainder of this chapter, experimental results are presented for most manipulations at both 20% and 95% O_2.

4.3.2 Capillary constriction by noradrenaline

It has previously been shown that noradrenaline constricts capillaries in rat cerebellar slices (Peppiatt et al., 2006). As the first step in this study, I tested whether I could reproduce this result in solution containing either 20% or 95% O_2 solution, and also investigated whether this response was maintained over the experimental time period I would use later for experiments investigating the effects of glutamate and signalling pathway blockers.

I observed that 2 μM noradrenaline significantly constricted capillaries at spatially restricted locations of cerebellar capillaries in solution containing 95% oxygen (bright field images and a specimen time course are shown in Figure 4.3A and B). In the 7 capillaries studied the diameter was reduced to 51.8±11.2% of the diameter in the absence of drugs after 5 minutes of exposure ($p=0.01$ compared to no response) and there was no significant difference in the capillary diameter after 5 and 10 minutes of noradrenaline superfusion ($p=0.94$; Figure 4.3C). Thus, noradrenaline constricts cerebellar capillaries and this constriction is sustained over 10 minutes. This provides sufficient time to superimpose glutamate (in the presence or absence of signalling pathway blockers) on top of the noradrenaline and investigate the response in the presence of a constant vessel tone.

A specimen response to noradrenaline at 20% O_2 is shown in Figure 4.3D. This response appears less dramatic than that seen at 95% O_2 in Figure 4.3B, and in fact the 13 capillaries studied at 20% O_2 with long durations of noradrenaline application (Figure 4.3F) showed a larger constriction than the 7 capillaries studied at 95% O_2 (Figure 4.3F). Nevertheless when all 59 capillaries studied at 20% O_2 (i.e. mainly capillaries studied with only 5 minute applications of noradrenaline) were compared with all 155 capillaries at 95% O_2 then the constriction produced after 5 minutes noradrenaline superfusion was not significantly different (in noradrenaline the diameter was 79.4±3.6% and 81.1±1.9% of the diameter in the absence of drugs respectively; Figure 4.3E).

In the sample of 13 capillaries measured for 10 minutes superfusion with noradrenaline at 20% O_2, the noradrenaline-evoked constriction did not reach significance when p values were corrected for multiple comparisons ($p=0.06$ and 0.28 after 5 minutes and 10 minutes superfusion of noradrenaline; Figure 4.3F), however there was no significant decrease of the constriction on extending the superfusion to 10 mins ($p=0.56$; Figure 4.3F).

4.3.3 Capillary dilation by glutamate application

Glutamate has been shown to dilate capillaries in cerebellar slices (Peppiatt et al., 2006). Having established that noradrenaline can be used as a means of constricting capillaries over the experimental time period I was interested in, I next replicated the glutamate-evoked dilation of preconstricted capillaries, as a prelude to assessing the signalling systems mediating these dilations. Bright field images of an example capillary before drug application, in 2 μM noradrenaline, as well as with 500 μM glutamate superimposed are shown in Figure 4.4A. Specimen time courses for the diameter changes of capillaries during application of noradrenaline followed by glutamate are shown for both 20% and 95% oxygen in Figure 4.4B and 4.4C respectively. The diameter decreased on application of 2 μM noradrenaline (as in earlier Figures), but increased on application of 500 μM glutamate (in the maintained presence of the noradrenaline).

The glutamate-evoked dilation (as a percentage of the diameter in the absence of drugs) in both O_2 conditions is shown in Figure 4.4D. On application of 500 μM glutamate a dilation of 18.2±3.2% and 10.2±1.6% occurred at 20% and 95% oxygen, respectively, both of which were significant dilations ($p=3.7x10^{-7}$ and $p=3.2x10^{-9}$ respectively). The glutamate-evoked dilation was significantly larger at 20% O_2 when compared to the dilation at 95% O_2 ($p=0.01$). This difference in dilation size at the two oxygen concentrations may be due to a difference in the production of vasoactive mediators at the different O_2 levels, as the synthesis of each mediator has a different dependence on O_2. For example, since 20-HETE synthesis requires a higher concentration of O_2, one would expect the influence of the 20-HETE pathway to be less significant at 20% O_2 (see Figure 4.1), allowing glutamate to evoke a larger dilation.

4.3.4 The effect of TTX on capillary diameter and responses to noradrenaline and glutamate

When noradrenaline or glutamate are applied to brain slices there may be changes of action potential firing that contribute to the capillary responses by releasing vasoactive agents. I therefore examined the effect of blocking action potentials (and downstream neurotransmitter release) on the baseline capillary diameter, the noradrenaline-evoked capillary constriction and the glutamate-evoked capillary dilation.

When slices were superfused with the sodium channel blocker, TTX (1 μM), at 95% O_2 there was no significant change in the capillary diameter (100.1±2.5% of the diameter in the absence of drugs; $p=0.99$; Figure 4.5B). Capillaries exposed to TTX still showed a significant noradrenaline-evoked constriction (to 65.3±9.3% of the diameter in the absence of drugs; $p=2x10^{-3}$; Figure 4.5A, C), which was not significantly different to that seen in the absence of TTX ($p=0.1$).

Capillaries exposed to TTX showed a significant glutamate-evoked dilation (dilating by 30.6±10.9% of the diameter in the absence of drugs; p=0.05; Figure 4.5A, D). The glutamate-evoked dilation in the presence of TTX showed a trend towards being larger than in the absence of TTX (p=0.09). This could reflect the capillaries chosen for these recent experiments being healthier than some of those studied early in my PhD and included in the global average of data in the absence of TTX. These results, showing that the glutamate-evoked dilation in TTX is not smaller than that in the absence of TTX, argue against the idea that the dilation evoked by glutamate is partly mediated by glutamate evoking action potentials.

4.3.5 The effect of NOS inhibition on capillary diameter and responses to noradrenaline and glutamate

Arteriole dilation is often mediated by glutamate activating neuronal production of nitric oxide (Figure 4.1 and see section 1.2.1). To examine the effect of nitric oxide production on capillary diameter, on noradrenaline-evoked capillary constriction and on glutamate-evoked capillary dilation, capillaries were treated with the general nitric oxide synthase inhibitor, L-N^G-nitroarginine (L-NNA; 100 μM). The IC_{50} for L-NNA inhibiting cerebellar NO production evoked by NMDA application has been found to be $\leq$600 nM (East & Garthwaite, 1990; Arima et al., 1997).

Application of 100 μM L-NNA significantly decreased the capillary diameter at 20% O_2 (to 94.9±2.2% of the diameter in the absence of drugs; p=0.03; Figure 4.6A, B) and at 95% O_2 (to 86.6±3.3% of the diameter in the absence of drugs; $p=4x10^{-4}$; Figure 4.6B). Thus, there is tonic production of vasodilating NO in the slice. The constricting effect of L-NNA on the capillaries was not significantly different between 20% and 95% O_2 (p=0.1; Figure 4.6B).

Capillaries exposed to L-NNA showed a further significant noradrenaline-evoked constriction at 20% O_2, to 80.7±4.9% of the diameter in the absence of drugs ($p=4x10^{-3}$; Figure 4.6A, C). Similarly at 95% O_2, noradrenaline constricted capillaries to 84.4±5.9% of the diameter in the absence of drugs (p=0.01; Figure 4.6C). The noradrenaline-evoked constriction was not significantly different in the absence or presence of L-NNA (p=0.94 and p=0.82, at 20% and 95% O_2 respectively).

However, unlike in the absence of L-NNA, capillaries exposed to L-NNA did not show a significant glutamate-evoked dilation at 20% O_2. The capillaries dilated by only 5.0±2.9% of the diameter in the absence of drugs (p=0.22; Figure 4.6A, D). Similarly at 95% O_2, capillaries actually constricted by 2.0±4.5% of the diameter in the absence of drugs (p=0.66; Figure 4.6D). These responses to glutamate in the presence of L-NNA were significantly different to the glutamate responses in control capillaries at 20% and 95% O_2 (p=0.02 and p=0.04 respectively).

Thus, inhibition of nitric oxide synthase with L-NNA slightly decreases the diameter of cerebellar capillaries and greatly inhibits the glutamate-evoked dilation. However L-NNA does not alter the noradrenaline-evoked constriction in capillaries.

4.3.6 The effect of ODQ on capillary diameter and responses to noradrenaline and glutamate

To examine whether nitric oxide mediates its effects on the glutamate-evoked dilation via cGMP production, slices were treated with ODQ (1H-[1,2,4]oxadiazolo[4,3-a]quinoxalin-1-one; 10 μM). ODQ is a selective guanylyl cyclase inhibitor with an IC_{50} of approximately 20 nM (Garthwaite et al., 1995). At the concentration used ODQ has a rapid onset time, inhibiting approximately 90% of the guanylyl cyclase activity after a five second incubation (Bellamy and Garthwaite, 2002). ODQ application did not have a significant effect on the baseline capillary diameter at 20% or 95% O_2 (100.0±3.9% and 101.0±3.1% of the diameter in the absence of the drug respectively; p=0.96 and p=0.74; Figure 4.7B).

Capillaries exposed to 10 μM ODQ showed a significant noradrenaline-evoked constriction in both 20% and 95% O_2, to 74.3±5.4% and 69.4±6.4% of the diameter in the absence of drug respectively ($p=1.4x10^{-4}$ and $p=1.1x10^{-4}$; Figure 4.7A, C). The noradrenaline-evoked constriction was not significantly different in the absence or presence of ODQ at 20% O_2 (p=0.31) but was significantly increased in the presence of ODQ at 95% O_2 (p=0.04).

Capillaries exposed to ODQ showed a significant glutamate-evoked dilation at 20% O_2 (dilating by 13.0±4.7% of the diameter in the absence of drugs; p=0.02; Figure 4.7A, D) but the glutamate-evoked dilation did not quite reach significance at 95% O_2 (dilating by 10.9±6.2% of the diameter in the absence of drugs; p=0.09; Figure 4.7D). The glutamate-evoked dilations seen at both 20% and 95% O_2 were, however, not significantly different in the absence or presence of ODQ (p=0.55 and 0.56 respectively). This suggests that the glutamate-evoked dilation is still present when cGMP production is inhibited, and thus, that NO may be involved in the glutamate-evoked dilation via a signalling pathway separate from that mediated by ODQ-sensitive guanylyl cyclase.

4.3.7 The effect of blocking 20-HETE production on how NOS block affects responses to noradrenaline and glutamate

As shown above, blocking NOS inhibits the glutamate-evoked dilation, but not by raising the level of cyclic GMP. However as mentioned in Chapter 1, nitric oxide may also mediate glutamate-evoked dilation by inhibiting 20-HETE production. The vasoconstricting arachidonic acid derivative 20-hydroxy-5,8,11,14-

eicosatetraenoic acid (20-HETE) is thought to be produced from astrocyte arachidonic acid when neurons are active (Figure 4.1). To examine the effect of 20-HETE production on how NOS block affects noradrenaline-evoked capillary constriction and glutamate-evoked capillary dilation, capillaries were treated with the cytochrome P-450 enzyme inhibitor, N-hydroxy-N′-(4-butyl-2-methylphenyl)-formamidine (HET0016; 1 μM) in combination with L-NNA (100 μM). HET0016 selectively inhibits the cytochrome P450 ω-hydroxylase enzymes, CYP4A and CYP4F, that produce 20-HETE, with an IC_{50} of 8.9±2.7 nM (Miyata et al., 2001). In the presence of both HET0016 and L-NNA the capillary diameter was not significantly altered at 20% or 95% O_2 (107.3±3.1% and 93.1±3.6% of the diameter in the absence of drugs respectively; both p=0.09; Figure 4.8B). HET0016 application significantly reduced the constricting effect of L-NNA at 20% O_2 ($p=4x10^{-3}$; Figure 4.8A, B) but this effect of HET0016 was not significant at 95% O_2 (p=0.38; Figure 4.8B).

Capillaries exposed to 1 μM HET0016 and 100 μM L-NNA showed a significant noradrenaline-evoked constriction at 95% O_2 (to 66.1±8.8% of the diameter in the absence of drug; p=0.01; Figure 4.8A, C) but the constriction was not quite significant at 20% O_2 (82.6±8.6% of the diameter in the absence of drugs; p=0.06; Figure 4.8C). The level of noradrenaline-evoked constriction in the presence of 100 μM L-NNA was, however, not significantly different in the absence and presence of 1 μM HET0016 at either oxygen level (p=0.84 and p=0.12 at 20% and 95% O_2, respectively).

In the presence of HET0016 and L-NNA, capillaries showed a significant glutamate-evoked dilation at 20% O_2 (dilating by 15.8±3.3% of the diameter in the absence of drugs; $p=1x10^{-3}$; Figure 4.8A, D) and a trend towards a dilation at 95% O_2 (dilating by 24.0±8.8% of the diameter in the absence of drugs; p=0.06; Figure 4.8D). The glutamate-evoked dilation in the presence of HET0016 and L-NNA was significantly larger than the response to glutamate in L-NNA alone at both 20% and 95% O_2 (both p=0.02), and indeed was not significantly different from the normal glutamate-evoked dilation seen in Figure 4.4D in the absence of L-NNA (p=0.79 and p=0.18 at 20% and 95% O_2 respectively).

These results indicate that inhibition of nitric oxide synthesis with L-NNA no longer decreases vessel diameter or glutamate-evoked dilation in cerebellar capillaries in the presence of HET0016, i.e. with 20-HETE synthesis inhibited. This suggests, firstly, that the tonic dilation produced by the level of NO release occurring in the slice is mainly mediated by a reduction of 20-HETE synthesis and, secondly, that suppression of 20-HETE formation by NO is necessary for glutamate to evoke a significant dilation. The existence of a glutamate-evoked dilation in the presence of blockers of production of NO and 20-HETE suggests that the dilation is not primarily produced by NO (although NO needs to be present to suppress 20-HETE formation).

4.3.8 The effect of blocking 20-HETE production alone on capillary diameter and responses to noradrenaline and glutamate

Since I saw an effect of HET0016 in the presence of L-NNA, I wanted to check whether it had an effect on capillary responses without L-NNA present. HET0016 application had no significant effect on the baseline capillary diameter at either 20% or 95% O_2 (99.6±1.6% and 97.5±3.6% of the diameter in the absence of drugs respectively; p=0.79 and 0.49; Figure 4.9A, B). This suggests that there is no resting 20-HETE production.

Capillaries exposed to 1 μM HET0016 showed a significant noradrenaline-evoked constriction at 20% O_2 (to 82±6.5% of the diameter in the absence of drugs; p=0.04; Figure 4.9A, C), but the constriction did not reach significance at 95% O_2 (constriction to 87.8±7.1% of the diameter in the absence of drugs; p=0.11; Figure 4.9C). The noradrenaline-evoked constriction was, however, not significantly different in the absence and presence of HET0016 at either 20% or 95% O_2 (p=0.93 and p=0.74 respectively), suggesting that this constriction is not mediated by noradrenaline acting on its receptors on astrocytes to increase 20-HETE production as has been suggested (Mulligan and MacVicar, 2004).

Capillaries exposed to HET0016 showed a significant glutamate-evoked dilation both at 20% O_2 (dilating by 14.6±4.7% of the diameter in the absence of drugs; p=0.02; Figure 4.9A, D) and at 95% O_2 (dilating by 18.9±8.2% of the diameter in the absence of drugs; p=0.04; Figure 4.9D). The glutamate-evoked dilation was not significantly different in the absence or presence of HET0016 at 20% or 95% O_2 (p=0.79 and p=0.18).

Thus, in the absence of L-NNA, inhibition of 20-HETE production with HET0016 does not have an effect on the capillary diameter, nor on the noradrenaline-evoked capillary constriction or the glutamate-evoked capillary dilation. The lack of effect on the glutamate-evoked dilation implies that NO release evoked by glutamate is normally sufficient to block 20-HETE production.

4.3.9 The effect of the EET synthesis blocker MS-PPOH on responses to noradrenaline and glutamate

To test for an effect of EET production on noradrenaline-evoked capillary constriction and glutamate-evoked capillary dilation, slices were treated with the cytochrome P-450 enzyme inhibitor, MS-PPOH (N-(methylsulfonyl)-2-(2-propynyloxy)-benzene-hexanamide; 20 μM). MS-PPOH selectively inhibits the cytochrome P450 epoxygenase enzymes, CYP4A2 and CYP4A3, that synthesise EETs, with an IC_{50} of 13 μM

in renal microsomes (Wang et al., 1998). MS-PPOH requires 30 minutes incubation to act, so it was not possible to measure the capillary diameter in the absence of MS-PPOH in the same vessels.

Capillaries exposed to 20 μM MS-PPOH showed a significant noradrenaline-evoked constriction at 20% O_2 (to 77.2±5.5% of the diameter in the absence of drugs; $p=2x10^{-3}$; Figure 4.10A, B), and 95% O_2 (53.6±5.8% of the diameter in the absence of drugs; $p=2.6 \times 10^{-6}$; Figure 4.10B). The noradrenaline-evoked constriction was not significantly different in the absence or presence of MS-PPOH, both at 20% or 95% O_2 (p=0.84 and p=0.94 respectively).

In the presence of MS-PPOH capillaries showed a significant glutamate-evoked dilation both at 20% O_2 (dilating by 15.3±3.3% of the diameter in the absence of drugs; $p=7.2x10^{-4}$; Figure 4.10A, C) and at 95% O_2 (dilating by 30.8±6.8% of the diameter in the absence of drugs; $p=7.6x10^{-4}$; Figure 4.10C). The glutamate-evoked dilation was not significantly different in the absence or presence of MS-PPOH at 20% or 95% O_2 (p=0.32 and p=0.66 respectively).

These results show that inhibition of EET synthesis with MS-PPOH does not have an effect on the noradrenaline-evoked constriction or the glutamate-evoked dilation in cerebellar capillaries.

4.3.10 The effect of the EP4 receptor blocker L161,982 on capillary diameter and responses to noradrenaline and glutamate

To examine the role of PGE_2 action in controlling baseline capillary diameter, noradrenaline-evoked capillary constriction and glutamate-evoked capillary dilation, slices were treated with the EP_4 receptor blocker, L161,982 (N-[[4'-[[3-butyl-1,5-dihydro-5-oxo-1-[2-(trifluoromethyl)phenyl]-4H-1,2,4-triazol-4-yl]methyl][1,1'-biphenyl]-2-yl]sulfonyl]-3-methyl-2-thiophenecarboxamide; 1 μM). L161,982 is 200-fold more selective for EP_4 than for the EP_{1-3} subtypes, with a K_i of 32nM (Machwate et al., 2001). L161,982 application had no significant effect on the baseline capillary diameter at 20% O_2 (98.0±5.0% of the diameter in the absence of drugs; p=0.7; Figure 4.11A, B) or at 95% O_2 (100.2±3.9% of the diameter in the absence of drugs; p=0.96; Figure 4.11B). Thus, there is no tonic activation of EP_4 receptors in cerebellar slices.

Capillaries exposed to 1 μM L161,982 showed a significant noradrenaline-evoked constriction at 20% O_2 (to 73.6±7.1% of the diameter in the absence of drugs; $p=7x10^{-3}$; Figure 4.11A, C), and 95% O_2 (to 57.5±5.2% of the diameter in the absence of drugs; $p=1.8x10^{-8}$; Figure 4.11C). The noradrenaline-evoked constriction was not significantly different in the absence or presence of L161,982 at either 20% or 95% O_2 (p=0.87 and p=0.62 respectively).

Despite the lack of effect of EP_4 receptor block on the capillary diameter and on the noradrenaline-evoked constriction, capillaries exposed to L161,982 showed greatly reduced responses to glutamate. Capillaries did not show a significant glutamate-evoked dilation at 20% O_2 (dilating by 2.9±6.3% of the diameter in the absence of drugs; p=0.65; Figure 4.11 A, D). There was a significant dilation at 95% O_2 (dilating by 10.5±4.4% of the diameter in the absence of drugs; p=0.04; Figure 4.11D), but this was only 37.9% of the dilation seen in the absence of L161,982. The response to glutamate was significantly reduced in the presence of L161,982, compared to the response in the absence of drugs, at both 20% and 95% O_2 (p=0.05 and p=0.01 respectively; Figure 4.11A, D).

These results indicate that EP_4 receptor activation contributes to the glutamate-evoked dilation in cerebellar capillaries (but not to the noradrenaline-evoked constriction). Although I have not identified the molecule activating the EP_4 receptor, studies on arterioles suggest it is likely to be prostaglandin E_2 (Davis et al., 2004).

4.4 Discussion

I have investigated the mechanisms by which glutamate dilates capillaries in the cerebellar slice preparation, by evoking constriction and dilation with noradrenaline and glutamate respectively, and then blocking action potentials (with TTX), nitric oxide synthase (with L-N^G-nitroarginine), guanylyl cyclase (with ODQ) CYP enzymes that make 20-HETE (with HET0016) and EETs (with MS-PPOH), and inhibiting EP_4 receptors (with L161,982). The results from this study indicate that, firstly, glutamate-mediated dilation does not involve glutamate evoking action potentials (although normally it will be action potentials that evoke the glutamate release that causes dilation). Secondly, nitric oxide release is necessary for glutamate-evoked capillary dilation to occur. Thirdly, the mechanism by which nitric oxide exerts this effect does not involve guanylyl cyclase activation but, instead, involves an inhibition of 20-HETE production. Fourthly, EET production does not appear to be involved in glutamate-evoked capillary dilation. Finally, activation of EP_4 receptors is needed for glutamate-evoked capillary dilation.

4.4.1 Glutamate-evoked capillary dilation requires nitric oxide to inhibit 20-HETE production

My data suggest a similarity in the mechanisms of dilation at the capillary and arteriole level. Several studies have found an involvement of nitric oxide in glutamate-evoked dilation at the arteriole level *in vivo* (Dirnagl et al., 1993; Akgören et al., 1996; Lindauer et al., 1999). These studies showed a decrease in stimulation-evoked blood flow increase when nitric oxide synthase was inhibited (using L-N-nitroarginine or 7-

nitroindazole). Liu et al (2008) suggested that, in response to stimulation *in vivo*, nitric oxide may be exerting its effect through 20-HETE inhibition, as I find. They found that, although a nitric oxide synthase inhibitor abolished stimulation-evoked dilations, application of HET0016, to inhibit 20-HETE production, restored the stimulation-evoked blood flow responses (Liu et al., 2008). Several studies have, however, unlike my work, found support for nitric oxide exerting its dilatory effects through cGMP production, which activates protein kinase G. Sobey and Faraci (1997) found that blocking cGMP production with ODQ inhibited nitric oxide-mediated dilation in cortical pial arterioles by 82%. A further mechanism of nitric oxide-mediated dilation has been suggested by Bolotina et al. (1994). They suggest that nitric oxide may directly activate K^+ channels, however it is possible that 20-HETE may be involved in this mechanism (Sun et al., 2000; Yu et al., 2002).

The role of nitric oxide in neurovascular coupling at the arteriole level has been found to be different in different brain regions. In the cerebellum, nitric oxide has been reported to act as a direct mediator of neuronally evoked blood flow responses (Akgören et al., 1996) whereas in the cerebral cortex, although it is necessary for nitric oxide to be present in order for neural activity to induce dilation, changes in the level of nitric oxide are not the primary mediator of vasodilation since the tonic presence of nitric oxide is sufficient to allow activity to evoke a dilation (Lindauer et al., 1999). Although my study was on the vasculature of the cerebellum it was carried out at the capillary level rather than the arterioles (as studied by Akgören et al., 1996). I found that nitric oxide was not directly responsible for the glutamate-evoked dilation of cerebellar capillaries but that its presence was required to inhibit a constriction generated by the release of 20-HETE. This suggests that there may be different mechanisms of glutamate-evoked dilation at arterioles and capillaries within the cerebellum.

4.4.2 Glutamate-evoked capillary dilation requires EP_4 receptor activation, presumably by prostaglandin E_2

Prostaglandin E_2 has been found to be involved in neurovascular coupling at the level of arterioles. Application of prostaglandin E_2 causes dilation of cerebral arterioles in slices and *in vivo* (Zonta et al., 2003; Takano et al., 2006), and in brain slices the COX inhibitor aspirin reduces the number of responses seen to t-ACPD application and to electrical stimulation of either astrocytes or neuronal afferents (Zonta et al., 2003). Furthermore, *in vivo* non-specific COX inhibition, as well as inhibition of COX-1 and COX-2 separately, blocks functional hyperaemia (Niwa et al., 2000; Takano et al., 2006).

Unlike in my study, there is evidence that EETs are involved in glutamate-evoked dilation at the arteriole level, at least outside the cerebellum. Inhibition of cytochrome *P*-450 epoxygenase activity, using

either miconazole or MS-PPOH, attenuated the cortical flow response to subdural glutamate or NMDA superfusion (Alkayed et al., 1997; Bhardwaj et al., 2000) as well as whisker stimulation (Peng et al., 2002), and reduced dilations evoked by light in retinal arterioles (Metea and Newman, 2007). This suggests that there may be differences in the mechanisms of glutamate-evoked dilation either between arterioles and capillaries, or for cortex and retina versus cerebellum.

4.4.3 Methodological issues

Brain slice preparations offer the advantage of being able to control the composition of the fluid around capillaries better than *in vivo* studies, which allows better pharmacological studies, but there are several potential problems with studying neurovascular coupling in the slice preparation. These include the lack of blood flow and pressure in the preparation, which will alter the tone of the capillary. This may affect the timing of onset of capillary responses: indeed vessel responses are faster in *in vivo* studies (Zonta et al., 2003; Takano et al., 2006).

In this study I have attempted to overcome the problem of loss of tone by preconstricting capillaries with noradrenaline. Pharmacological preconstriction is commonly used in slice studies (often using the thromboxane analog U46619). It is not clear, however, whether preconstriction will alter the signalling pathways that I am interested in. It is sometimes assumed that noradrenaline causes constriction by increasing astrocytic $[Ca^{2+}]_i$, by acting on α_1 receptors (Duffy and MacVicar, 1995; Bekar et al., 2008), perhaps causing capillary constriction via the 20-HETE mediated pathway described in Chapter 1 and Figure 4.1. It is also possible that noradrenaline acts directly on pericytes as they express α_2 receptors (Elfont et al., 1989). Activation of α_2 receptors decreases cAMP production which ultimately increases phosphorylation of the myosin light chain, leading to contraction (Webb, 2003; see Chapter 1 section 1.4).

Another point to note for my study is the young age of the animals used (P12). There are many neurological changes during development that may affect neurovascular coupling (for more detail see Chapter 7). Developmental changes include a down-regulation of the metabotropic glutamate receptors, mGluR5, on astrocytes (Sun et al., 2013). One may, therefore, speculate that astrocyte-mediated signalling would become less significant in adulthood, as mGluR5 expression in astrocytes decreases. This means that the data presented in this study cannot be used to make assumptions about the signalling pathways involved in capillary-level neurovascular coupling at later stages of development.

4.4.4 Conclusion

My data suggest that pericytes are involved in neurovascular coupling at the capillary level and that the signalling pathways involved are broadly similar to those found at the arteriole level, but with some differences. I have identified the messenger that dilates cerebellar capillaries in response to glutamate as prostaglandin E_2 (or a related species active at EP_4 receptors), but also found that this dilation requires NO release to suppress 20-HETE formation. This finding suggests that blood flow control occurs not only at the level of larger cerebral vessels but also involves capillaries.

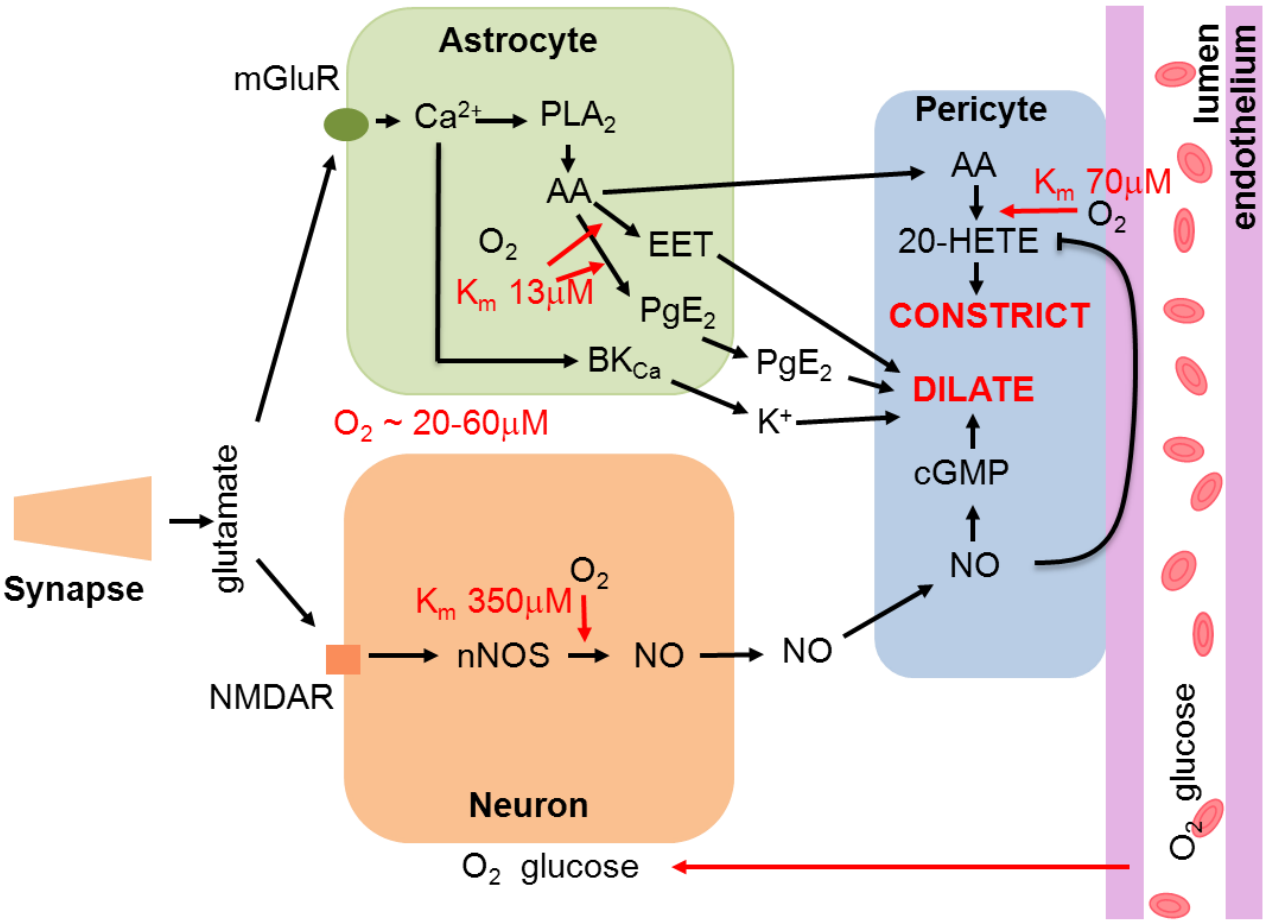

Figure 4.1: Hypothesised mechanisms by which glutamate regulates cerebral blood flow at the capillary level. Major pathways from astrocytes and neurons (left) that may regulate blood flow by sending messengers (arrows) to influence pericytes on the capillaries that supply oxygen and glucose to the tissue (right, shown as the capillary lumen surrounded by endothelial cells and pericyte soma). This diagram is based on pathways known to regulate arteriole tone (Attwell et al., 2010) as shown in figure 1.1. In neurons, synaptically-released glutamate acts on *N*-methyl-D-aspartate receptors (NMDAR) to raise $[Ca^{2+}]_i$. In some neurons (mainly interneurons) this causes neuronal nitric oxide synthase (nNOS) to release NO, which activates smooth muscle guanylate cyclase. This generates cGMP to dilate vessels. Glutamate raises $[Ca^{2+}]_i$ in astrocytes by activating metabotropic glutamate receptors (mGluR; but see Sun et al., 2013), generating arachidonic acid and thus three types of metabolite: prostaglandins (by COX-1 and possibly COX-3, and COX-2 in pathological situations) and EETs (by P450 epoxygenase) in astrocytes, which dilate vessels, and 20-HETE (by P450 ω-hydroxylase) in the pericyte, which constricts vessels. (There is also some prostaglandin production in neurons: not shown). A rise of $[Ca^{2+}]_i$ in astrocyte endfeet may also activate Ca^{2+}-gated K^+ channels ($B_{K(Ca)}$), releasing K^+, which also dilates vessels. The concentration of O_2 in the extracellular space is 20–60µM. This is significantly higher than the effective K_m for O_2 activating the enzymes synthesizing EETs and prostaglandins, but is in a range in which changes in O_2 concentration may modulate the production of NO and 20-HETE.

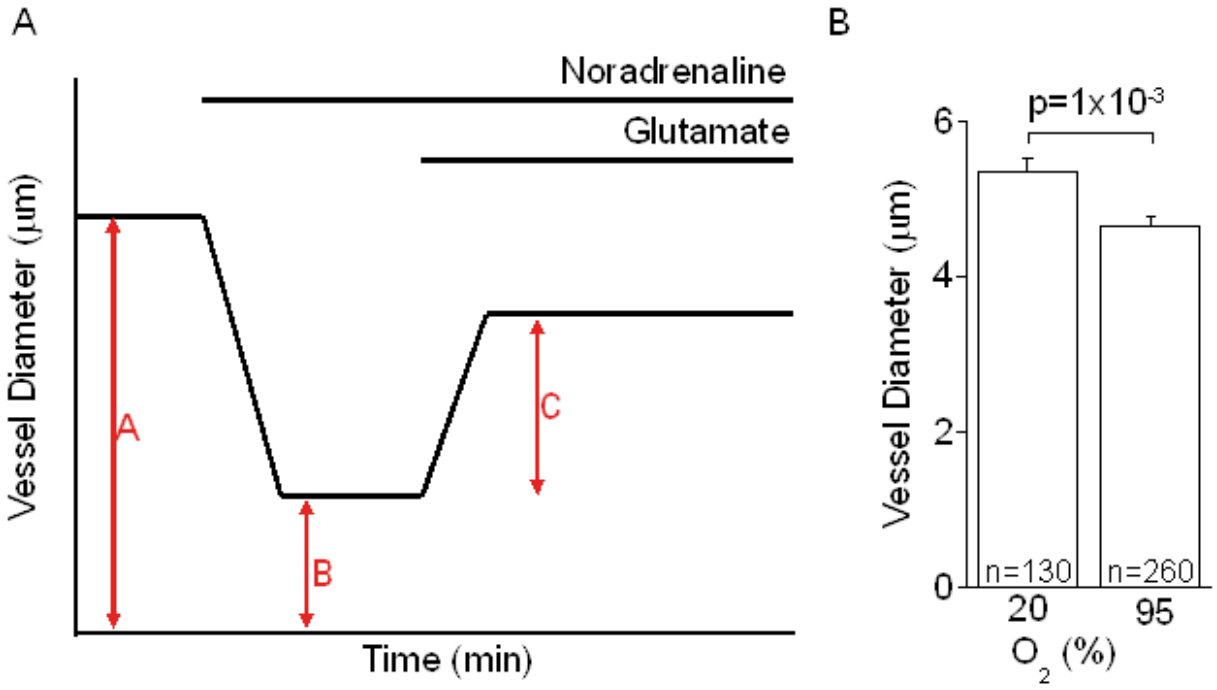

Figure 4.2: **Methodology. A** Schematic displaying how capillary responses to noradrenaline and glutamate were measured. Diameter in the absence of drugs is represented by A. Diameter in noradrenaline is represented by B. Change in diameter on glutamate application is represented by C. **B** Mean (±s.e.m) capillary diameter in the absence of drugs at 20% and 95% O_2. P value above the bars assesses the significance of the difference between the diameters in 20% and 95% O_2 using an independent samples t-test.

Figure 4.3: Localised constriction of capillary in cerebellar molecular layer by noradrenaline. A Image of a capillary in the molecular layer before and during 2 μM noradrenaline superfusion (in solution containing 95% O_2). Red blood cells can be seen within the lumen of the capillary. In the presence of noradrenaline the capillary constricts at a spatially localised point near a pericyte soma (indicated by yellow arrows). **B** Plot of diameter of the capillary in A at the region constricted by a pericyte during 2 μM noradrenaline superfusion. Arrows indicate points at which the capillary diameter was measured for statistical analysis: the first arrow indicates the diameter in the absence of drugs, the second arrow indicates the diameter in 2 μM noradrenaline after 5 minutes exposure, and the third arrow indicates the diameter in noradrenaline after 10 minutes exposure. **C** Mean (±s.e.m) capillary diameter after 5 and 10 minutes superfusion of 2 μM noradrenaline, as a percentage of the diameter in the absence of drugs, at 95% O_2. P values on the bars assess the significance of the noradrenaline-evoked constriction compared to 100% using a one-sample t-test. P value above the bars assesses the significance of the difference between the noradrenaline-evoked constriction at the two time points using an independent samples t-test. **D** Plot of capillary diameter at a region constricted by a pericyte during application of 2 μM noradrenaline in solution containing 20% O_2. Arrows indicate points at which the diameter was measured for statistical analysis: the first arrow indicates the diameter in the absence of drugs, the second arrow indicates the diameter in 2 μM noradrenaline after 5 minutes exposure, and the third arrow indicates the diameter in noradrenaline after 10 minutes exposure. **E** Mean (±s.e.m) capillary diameter following 5 minutes of exposure to 2 μM noradrenaline as a percentage of the diameter in the absence of drugs, in solution containing 20% and 95% O_2. P values on the bars assess the significance of the noradrenaline-evoked constriction compared to 100% by one-sample t-test. P value above the bars assesses the significance of the difference in the noradrenaline-evoked constriction between 20% and 95% O_2 using an independent samples t-test. **F** Mean (±s.e.m) capillary diameter after 5 and 10 minutes superfusion of 2 μM noradrenaline, as a percentage of the diameter in the absence of drugs, in solution containing 20% O_2. P values on the bars assess the significance of the noradrenaline-evoked constriction compared to 100%, using a one-sample t-test. P value above the bars assesses the significance of the difference between the noradrenaline-evoked constriction at the different time points using an independent samples t-test.

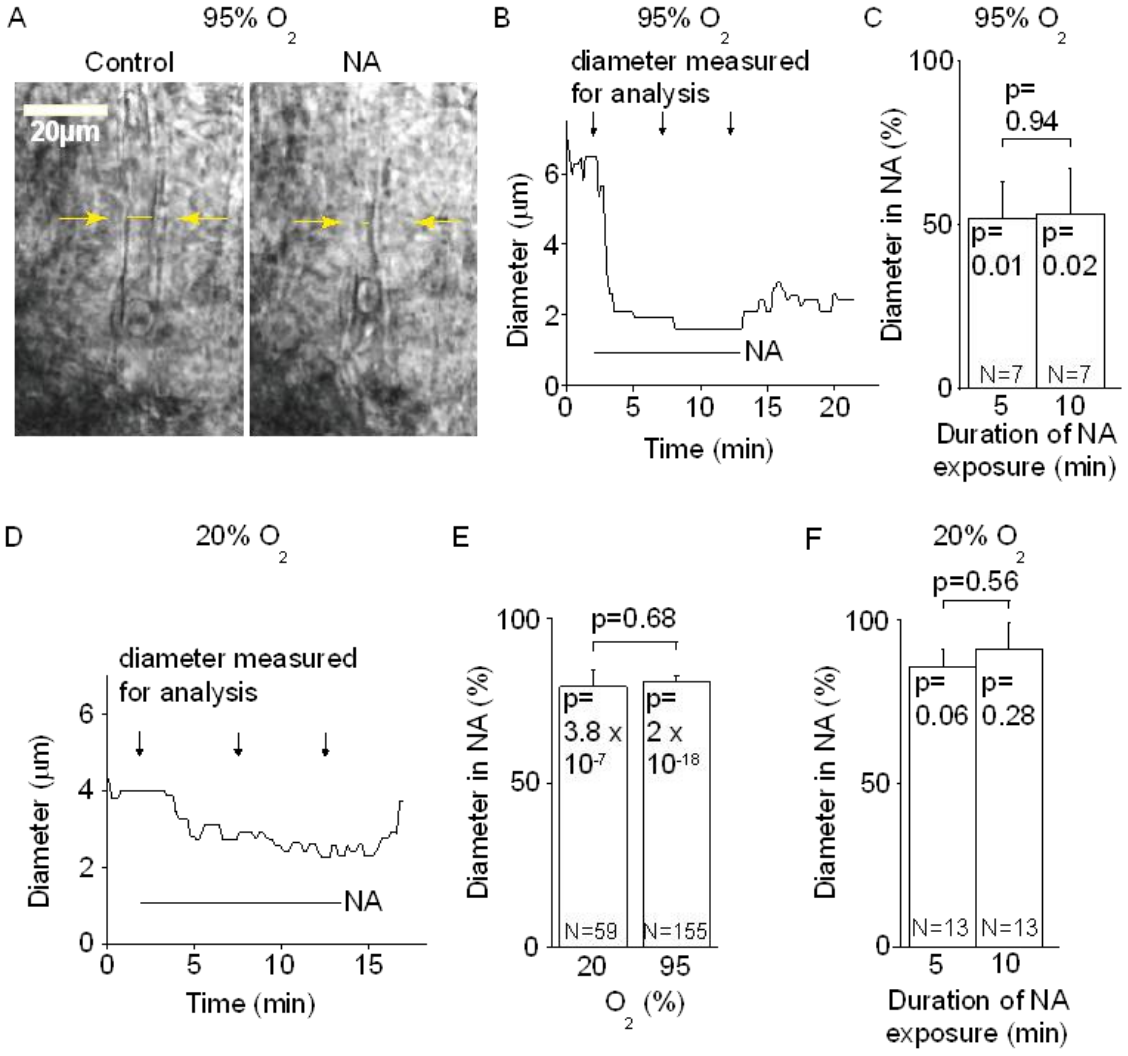
A
95% O2
Control
NA
20µm
B
95% O2
diameter measured
for analysis
Diameter (µm)
NA
Time (min)
C
95% O2
Diameter in NA (%)
p=
0.94
p=
0.01
p=
0.02
N=7
N=7
Duration of NA
exposure (min)
D
20% O2
diameter measured
for analysis
Diameter (µm)
NA
Time (min)
E
p=0.68
Diameter in NA (%)
p=
3.8 x
10-7
p=
2 x
10-18
N=59
N=155
O2 (%)
F
20% O2
p=0.56
Diameter in NA (%)
p=
0.06
p=
0.28
N=13
N=13
Duration of NA
exposure (min)

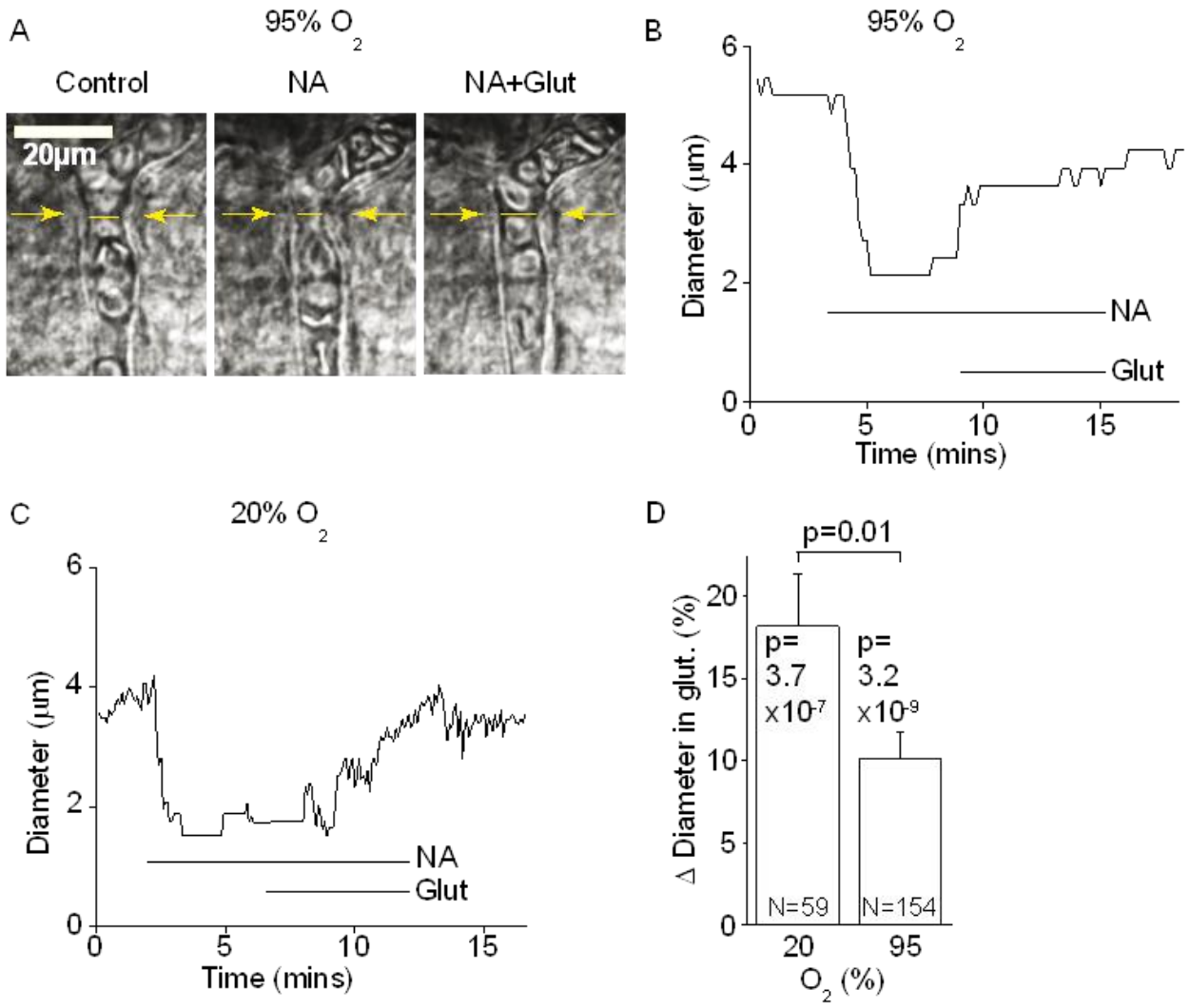

Figure 4.4: Capillaries preconstricted with noradrenaline dilate on application of glutamate. **A** Image of a capillary in the molecular layer before drug application, during 2 µM noradrenaline application, and during 2 µM noradrenaline and 500 µM glutamate application (in solution containing 95% O_2). Red blood cells can be seen within the lumen of the capillary. In the presence of noradrenaline the capillary constricts at a spatially localised point in the capillary near a pericyte (visible to the right of the capillary). In the presence of glutamate the capillary dilates. **B** Plot of diameter of the capillary in A at the region constricted by a pericyte. **C** Plot of capillary diameter at a region constricted by a pericyte in solution containing 20% O_2. **D** Mean (±s.e.m) increase of capillary diameter evoked by 500 µM glutamate in solution containing 20% and 95% O_2 at regions constricted by pericytes when noradrenaline was applied (as a percentage of the diameter in the absence of drugs). P values on the bars assess the significance of the glutamate-evoked dilation (compared to no response) using the Wilcoxon signed-rank test at 20% O_2 and a one-sample t-test at 95% O_2. P value above bars assesses the significance of the difference in response between the two oxygen levels using a Mann-Whitney U-test.

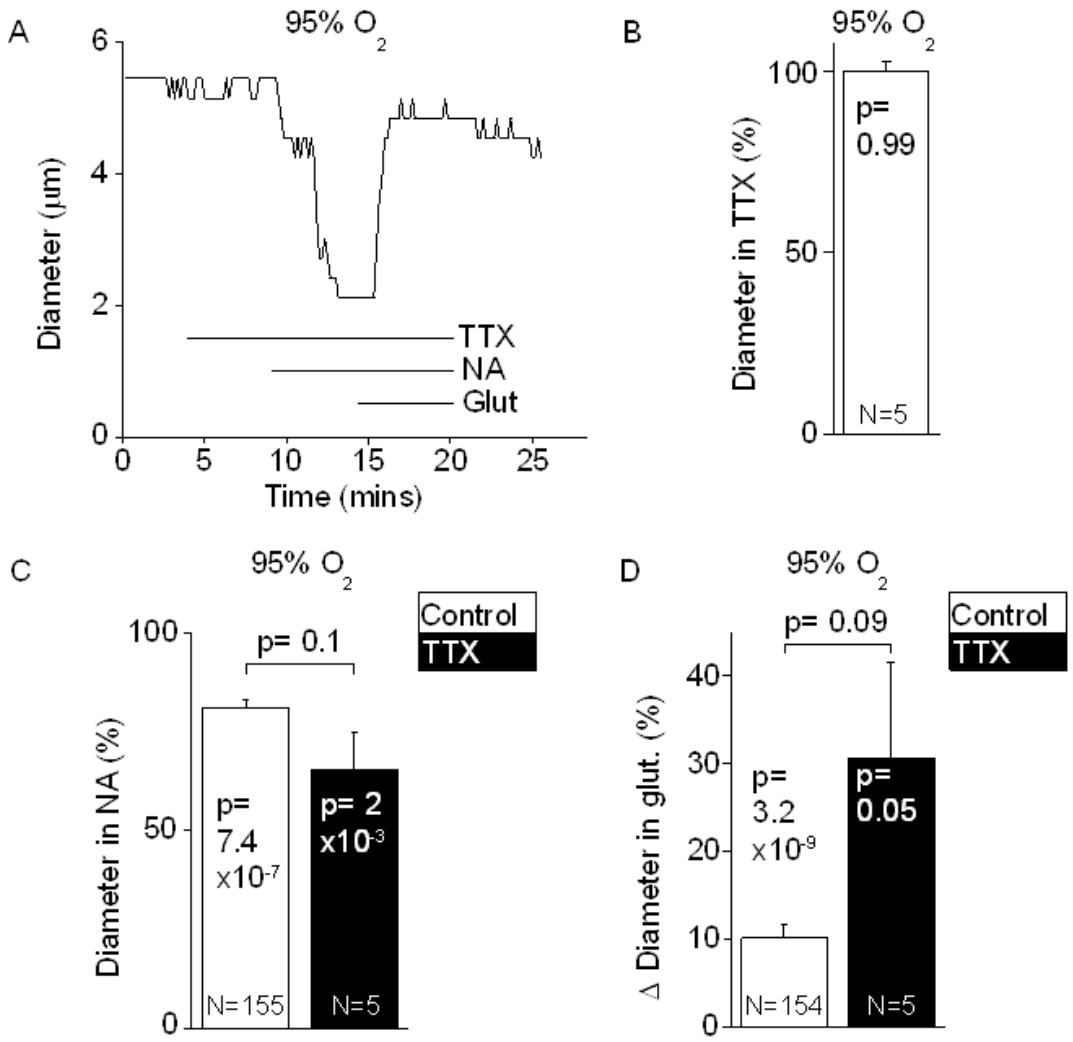

Figure 4.5: Effect of TTX on capillary diameter and responses to noradrenaline and glutamate. A Plot of the capillary diameter (at a region constricted by a pericyte when noradrenaline was applied), in solution containing 95% O_2. **B** Mean (±s.e.m) capillary diameter in 1 µM TTX (as a percentage of the diameter in the absence of drugs) at a region constricted by a pericyte when noradrenaline was applied, in solution containing 95% O_2. P value assesses the significance of the TTX-evoked diameter change compared to 100% using a one-sample t-test. **C** Mean (±s.e.m) capillary diameter in 2 µM noradrenaline (as a percentage of the diameter in the absence of drugs) in the absence (control) and in the presence of 1 µM TTX. P values on bars assess the significance of the constriction compared to 100% using a one-sample t-test. P value above bars assesses the significance of the difference between the noradrenaline-evoked constriction in the absence and presence of TTX using an independent samples t-test. **D** Mean (±s.e.m) increase in diameter (as a percentage of the diameter in the absence of drugs) in 500 µM glutamate, in the absence and presence of 1 µM TTX. P values on bars assess the significance of the diameter increase (compared to no response) using a one-sample t-test. P value above the bars assesses the significance of the difference between the glutamate-evoked dilation in the absence and presence of TTX using an independent samples t-test. All data in this figure were obtained in solution containing 95% O_2.

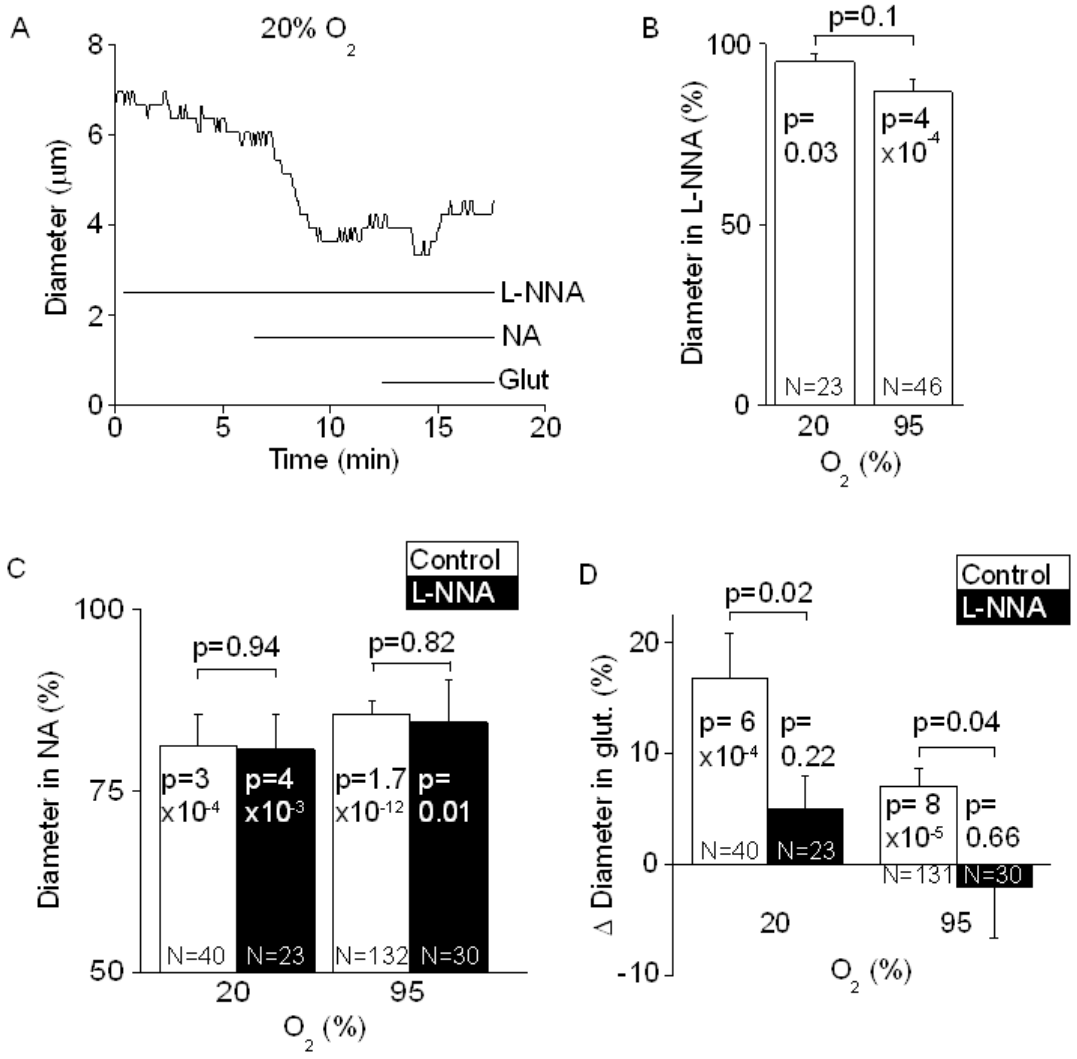

Figure 4.6: Effect of the NOS blocker L-NG-nitroarginine on capillary diameter and responses to noradrenaline and glutamate. A Plot of capillary diameter (at a region constricted by a pericyte when noradrenaline was applied) in solution containing 20% O_2. **B** Mean (±s.e.m) capillary diameter (as a percentage of the diameter in the absence of drugs) in 100 µM L-N^G-nitroarginine in solution containing 20% and 95% O_2. P values on bars assess the significance of any diameter change evoked by L-N^G-nitroarginine compared to 100% using one-sample t-tests. P value above the bars assesses the significance of the L-N^G-nitroarginine-evoked diameter change between 20% and 95% O_2 using an independent samples t-test. **C** Mean (±s.e.m) capillary diameter (as a percentage of the diameter in the absence of drugs) in 2 µM noradrenaline in the absence and presence of 100 µM L-N^G-nitroarginine. P values on the bars assess the significance of the noradrenaline-evoked constriction compared to 100% using one-sample t-tests. P value above the bars assesses the significance of the difference between noradrenaline-evoked constriction in the presence and absence of L-N^G-nitroarginine using independent samples t-tests. **D** Mean (±s.e.m) capillary dilation (as a percentage of the diameter in the absence of drugs) evoked by 500 µM glutamate in the absence and presence of 100 µM L-N^G-nitroarginine. P values on the bars assess the significance of the glutamate-evoked dilation (compared to no response) using a one-sample t-test. P values above the bars assess the significance of the difference between the glutamate-evoked dilation in the presence and absence of L-N^G-nitroarginine using independent samples t-tests.

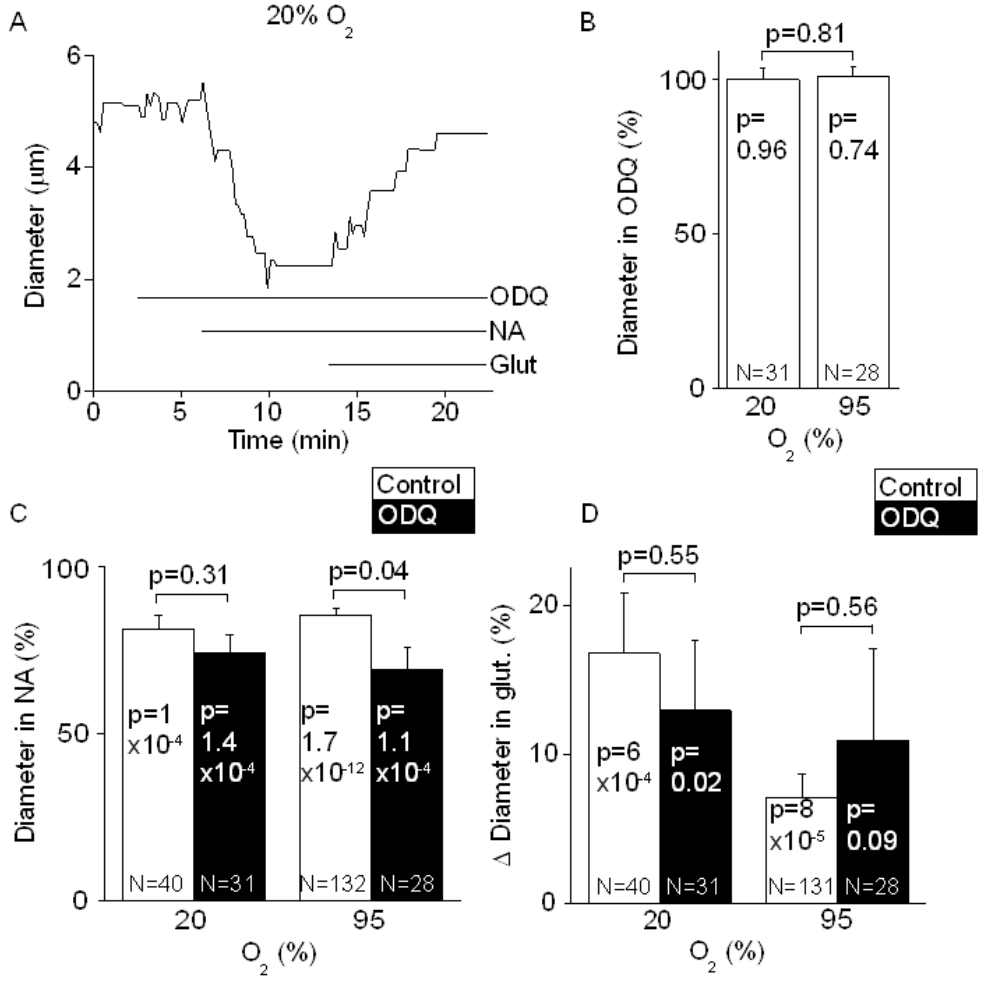

Figure 4.7: Effect of the guanylate cyclase blocker ODQ on cerebellar capillary diameter and on the response to noradrenaline and glutamate. A Plot of the capillary diameter (at a region constricted by a pericyte when noradrenaline was applied) in solution containing 20% O_2. **B** Mean (±s.e.m) capillary diameter (as a percentage of the diameter in the absence of drugs) in the absence and presence of 10 µM ODQ, in solution containing 20% and 95% O_2. P values on the bars assess the significance of ODQ-evoked diameter changes compared to 100% using one-sample t-tests. P value above bars assesses the significance of the difference between O_2 conditions using an independent samples t-test. **C** Mean (±s.e.m) capillary diameter (as a percentage of the diameter in the absence of drugs) in 2 µM noradrenaline in the absence and presence of 10 µM ODQ, at 20% and 95% O_2. P values on the bars assess the significance of the noradrenaline-evoked constriction compared to 100% using a one-sample t-test. P values above bars assess the significance of the difference between noradrenaline-evoked constriction in the presence and absence of ODQ using independent samples t-tests. **D** Mean (±s.e.m) capillary dilation (as a percentage of the diameter in the absence of drugs) evoked by 500 µM glutamate, in the absence and presence of 10 µM ODQ, at 20% and 95% O_2. P values on the bars assess the significance of the glutamate-evoked dilations (compared to no response) using a one-sample t-test. P values above the bars assess the significance of the difference between the glutamate-evoked dilation in the absence and presence of ODQ using independent samples t-tests.

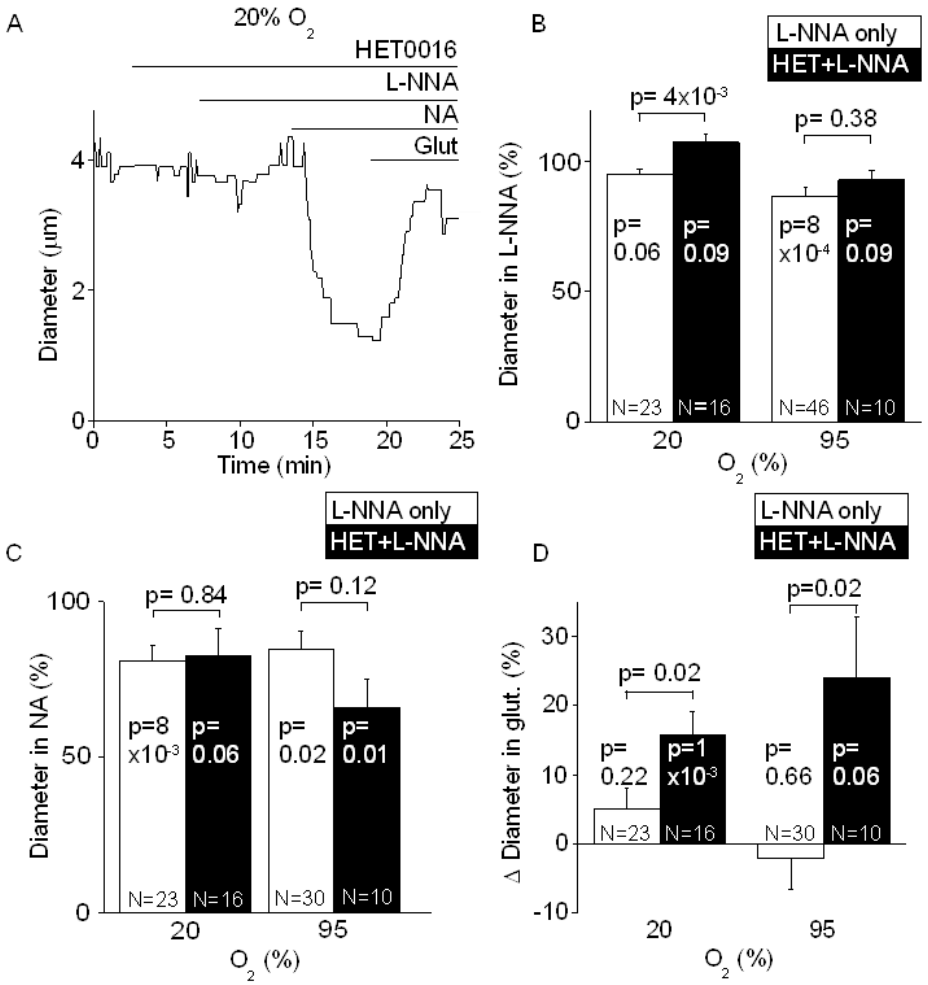

Figure 4.8: In the presence of HET0016, L-NG-nitroarginine does not alter cerebellar capillary diameter or the response to glutamate. A Plot of the capillary diameter (at a region constricted by a pericyte when noradrenaline was applied) in solution containing 20% O_2. **B** Mean (±s.e.m) capillary diameter (as a percentage of diameter in the absence of drugs) in 100 µM L-N^G-nitroarginine with or without 1 µM HET0016, in solution containing 20% and 95% O_2. P values on bars assess the significance of L-N^G-nitroarginine and HET0016-evoked changes in diameter compared to 100% using a one-sample t-test. P values above the bars assess the significance of the difference between oxygen conditions using an independent samples t-test. **C** Mean (±s.e.m) capillary diameter (as a percentage of the diameter in the absence of drugs) in 2 µM noradrenaline, in 100 µM L-N^G-nitroarginine with or without 1 µM HET0016, at 20% and 95% O_2. P values on the bars assess the significance of the noradrenaline-evoked constriction compared to 100% using a one-sample t-test. P values above the bars assess the significance of the difference between noradrenaline-evoked constriction in L-N^G-nitroarginine in the absence or presence of HET0016 using independent samples t-tests. **D** Mean (±s.e.m) capillary dilation (as a percentage of the diameter in the absence of drugs) evoked by 500 µM glutamate in the presence of 100 µM L-N^G-nitroarginine, in the absence or presence of HET0016, at 20% and 95% O_2. P values on the bars assess the significance of the glutamate-evoked dilation (compared to no response) using a one-sample t-test. P values above the bars assess the significance of the difference between the glutamate-evoked dilation in the absence and presence of HET0016 using independent samples t-tests.

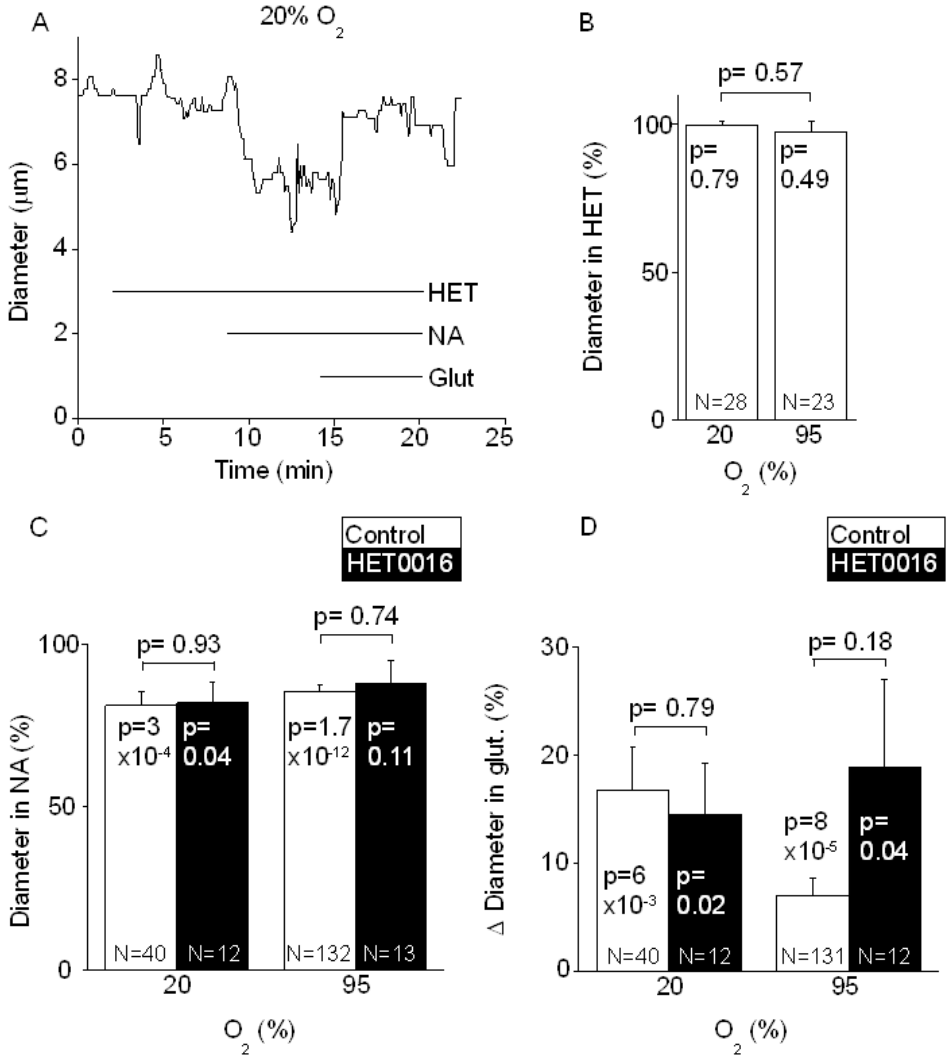

Figure 4.9: Effect of HET0016 alone on capillary diameter and on the response to noradrenaline and glutamate. A Plot of the capillary diameter (at a region constricted by a pericyte when noradrenaline was applied) in solution containing 20% O_2. **B** Mean (±s.e.m) capillary diameter (as a percentage of the diameter in the absence of drugs) in the absence and presence of 1 µM HET0016. P values on the bars assess the significance of any change of diameter evoked by HET0016 compared to 100% using one-sample t-tests. P value above the bars assesses difference between the diameters in solution containing 20% and 95% O_2 using an independent samples t-test. **C** Mean (±s.e.m) capillary diameter in 2 µM noradrenaline (as a percentage of the diameter in the absence of drugs) in the absence and presence of 1 µM HET0016 in solution containing 20% and 95% O_2. P values on the bars assess the significance of the noradrenaline-evoked constriction compared to 100% using one-sample t-tests. P values above the bars assess the significance of the difference between the noradrenaline-evoked constriction in the absence and presence of HET0016 using independent samples t-tests. **D** Mean (±s.e.m) capillary dilation (as a percentage of the diameter in the absence of drugs) evoked by 500 µM glutamate in the absence and presence of 1 µM HET0016 at 20% and 95% O_2. P values on the bars assess the significance of the dilations (compared to no response) using one-sample t-tests. P values above the bars assess the significance of the difference between the glutamate responses in the absence and presence of HET0016 using independent samples t-tests.

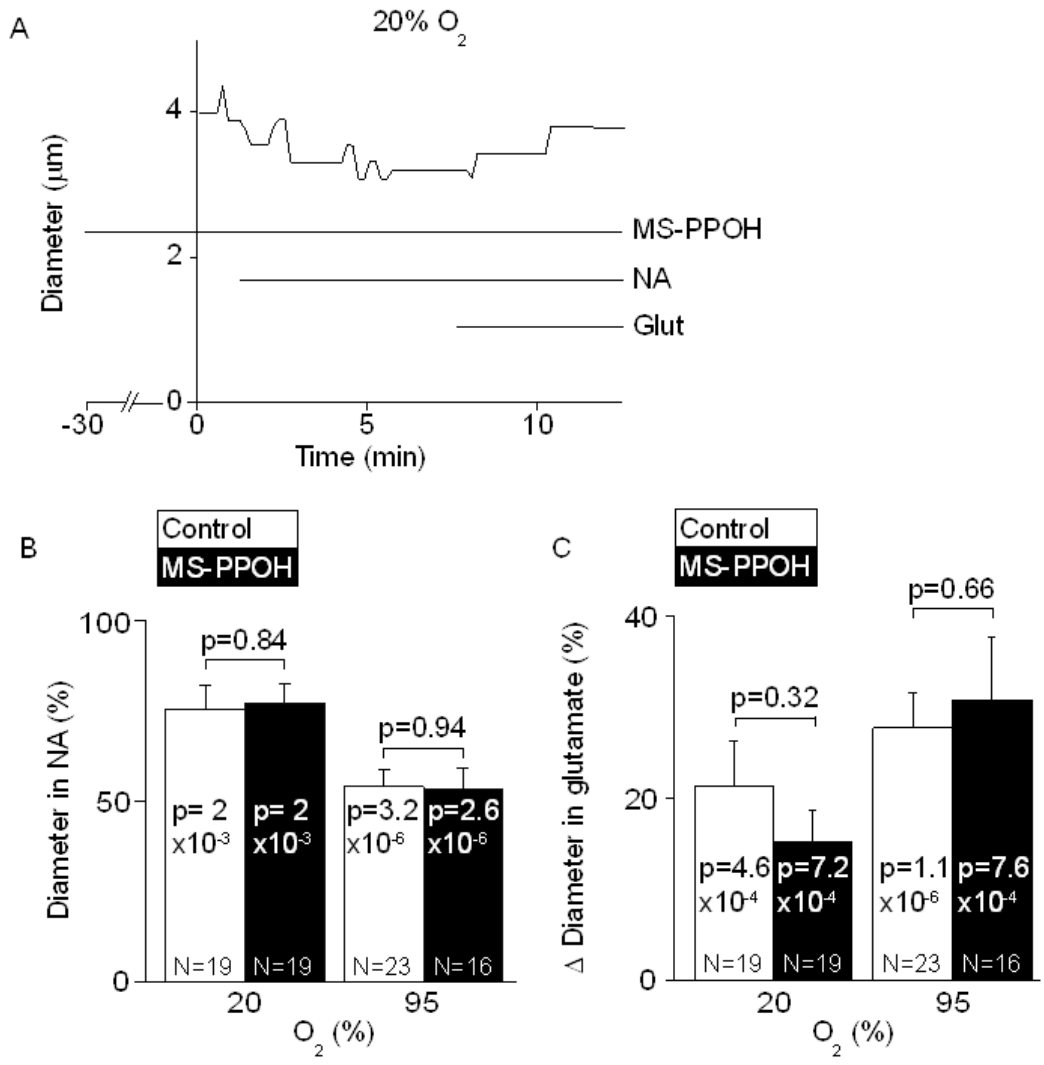

Figure 4.10: Effect of the EET synthesis inhibitor MS-PPOH on capillary diameter and responses to noradrenaline and glutamate. A Plot of the capillary diameter (at a region constricted by a pericyte when noradrenaline was applied) in solution containing 20% O_2. **B** Mean (±s.e.m) capillary diameter in 2 µM noradrenaline (as a percentage of the diameter in the absence of drugs) in the absence and presence of 20 µM MS-PPOH, in solution containing 20% and 95% O_2. P values on the bars assess the significance of the noradrenaline-evoked constriction compared to 100% using one-sample t-tests. P values above the bars assess the significance of the difference between the noradrenaline-evoked constriction in the absence and presence of MS-PPOH using independent samples t-tests. **C** Mean (±s.e.m) capillary dilation (as a percentage of the diameter in the absence of drugs) evoked by 500 µM glutamate in the absence or presence of 20 µM MS-PPOH, at 20% and 95% O_2. P values on the bars assess the significance of the glutamate-evoked dilations (compared to no response) using one-sample t-tests. P values above the bars assess the significance of the difference between the glutamate-evoked dilations in the absence and presence of MS-PPOH, using independent samples t-tests.

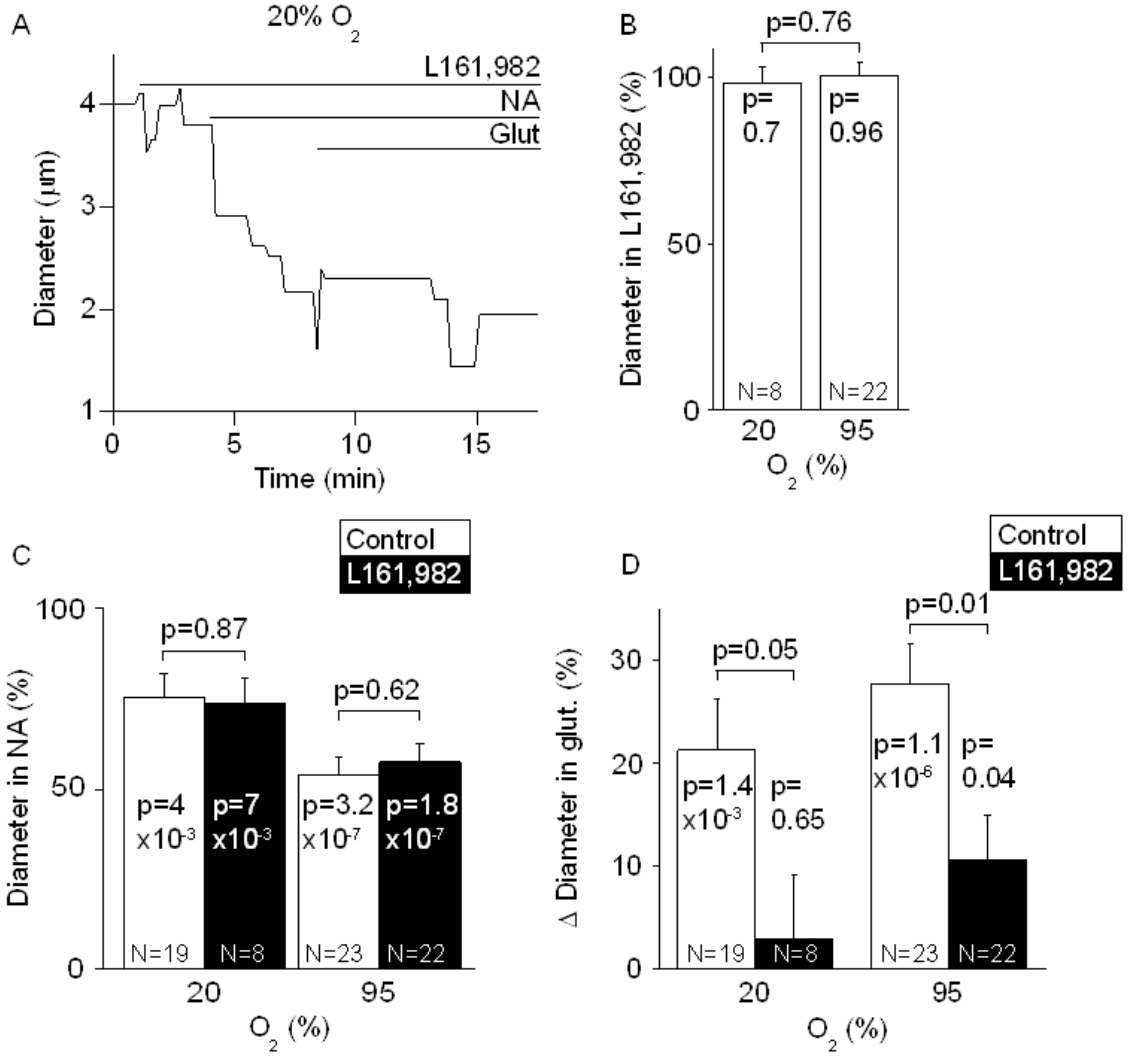

Figure 4.11: Effect of the EP4R blocker, L161,982 on capillary diameter and responses to noradrenaline and glutamate. A Plot of the capillary diameter (at a region constricted by a pericyte when noradrenaline was applied) in solution containing 20% O_2. **B** Mean (±s.e.m) capillary diameter (as a percentage of the diameter in the absence of drugs) in the absence and presence of 1 µM L161,982. P values on the bars assess the significance of any change of diameter evoked by L161,982 compared to 100%, using one-sample t-tests. P value above the bars assesses difference between the diameters, in solution containing 20% and 95% O_2, using an independent samples t-test. **C** Mean (±s.e.m) capillary diameter in 2 µM noradrenaline (as a percentage of the diameter in the absence of drugs) in the absence and presence of 1 µM L161,982, in solution containing 20% and 95% O_2. P values on the bars assess the significance of the noradrenaline-evoked constriction compared to 100% using one-sample t-tests. P values above the bars assess the significance of the difference between the noradrenaline-evoked constriction in the absence and presence of L161,982 using independent samples t-tests. **D** Mean (±s.e.m) capillary dilation (as a percentage of the diameter in the absence of drugs) evoked by 500 µM glutamate in the absence and presence of 10 µM L161,982, at 20% and 95% O_2. P values on the bars assess the significance of the glutamate-evoked dilations (compared to no response) using a one-sample t-test. P values above the bars assess the significance of the difference between the glutamate-evoked dilations in the absence and presence of L161,982, using independent samples t-tests.

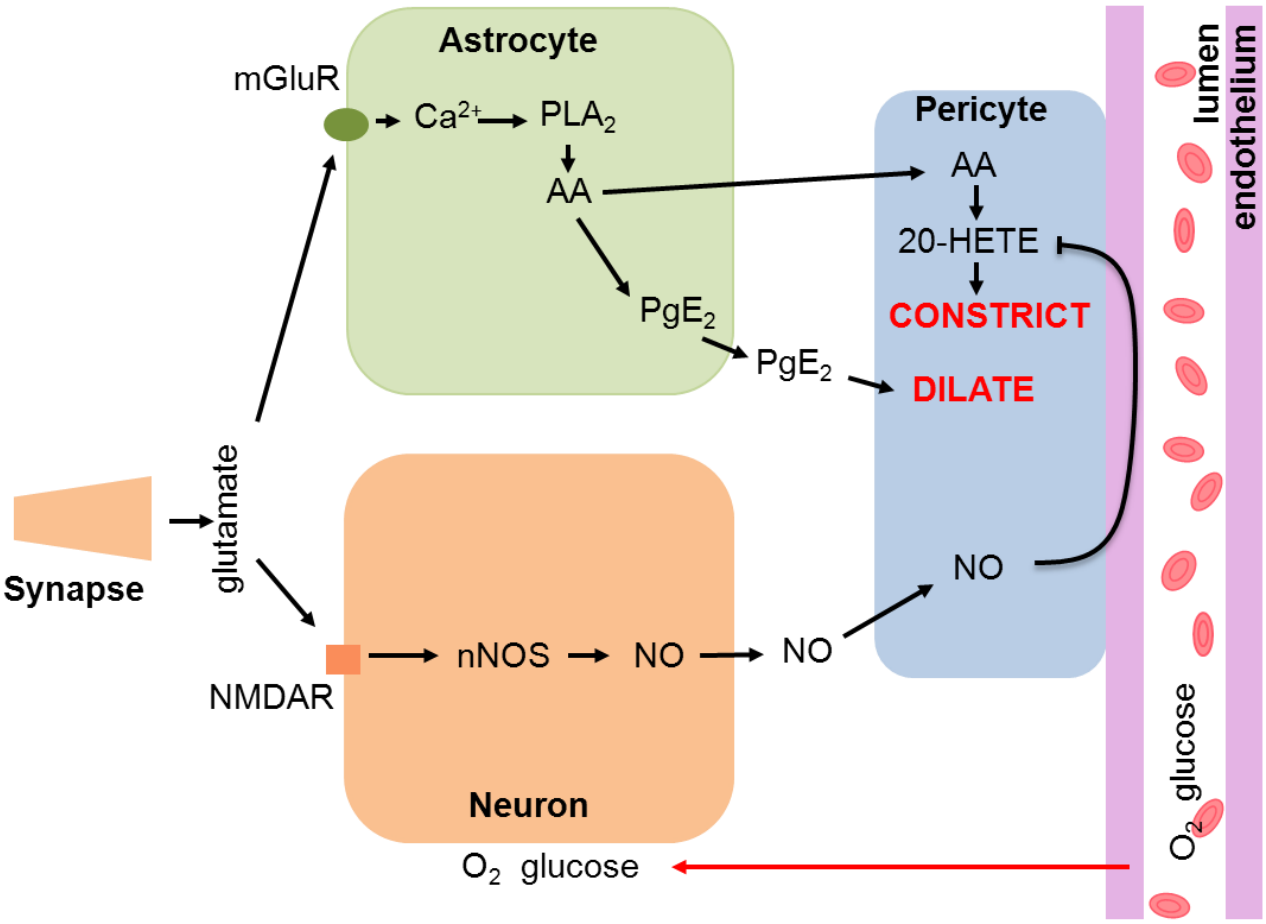

Figure 4.12: Diagram showing mechanisms by which glutamate regulates cerebral blood flow at the capillary level. This diagram updates Figure 4.1 according to the data obtained. Active neurons release glutamate, which acts on both NMDA receptors on neurons and mGluRs on astrocytes. As a result $[Ca^{2+}]_i$ rises in both cell types, releasing NO and derivatives of arachidonic acid. The production of the vasoconstricting arachidonic acid metabolite 20-HETE is suppressed by NO. The vasodilatory arachidonic acid metabolite prostaglandin E_2 acts on EP_4 receptors producing capillary dilation.

Chapter 5: Electrical responses of cerebellar and cortical pericytes

5.1 Introduction

It is likely that a crucial mechanism underlying the constrictions and dilations of pericytes (seen in Chapter 4) lies in the plasma membrane of these cells, where a change in membrane voltage may trigger voltage-gated calcium channels to alter the intracellular calcium concentration and thus alter the contraction of the pericyte myofilaments.

Retinal pericytes express several types of voltage-sensitive potassium channels, including inward-rectifying (K_{ir}) channels (von Beckerath et al., 2000; Cao et al., 2006), voltage-gated potassium channels (von Beckerath et al., 2000) and big and small conductance calcium-activated potassium channels (BK_{Ca} and SK_{Ca}; Wiederholt et al., 1995; Quignard et al., 2003) as well as, voltage-insensitive ATP-sensitive potassium channels (K_{ATP}; Li and Puro, 2001). Activation of these potassium channels causes hyperpolarization, decreasing calcium influx through voltage-gated calcium channels, and producing dilation. Several agonists have been found to cause hyperpolarization and relaxation of pericytes, including nitric oxide (Haefliger et al., 1994; Sakagami et al., 2001) and adrenomedullin (Takata et al., 2009). The capillary dilation evoked by glutamate application (Peppiatt et al., 2006; Chapter 4) may therefore be triggered by a pericyte hyperpolarization.

Pericyte constrictions, on the other hand, appear to be evoked by rises of intracellular calcium concentrations (Sakagami et al., 1999, 2001; Kamouchi et al., 2004; Sugiyama et al., 2005; Peppiatt et al., 2006). Calcium entry may occur through voltage-gated calcium channels (VGCC; Sakagami et al., 1999; Kamouchi et al., 2004), nonspecific cation channels (Sakagami et al., 1999), and calcium activated chloride channels (Cl_{Ca}, which cause depolarization in these cells due to a high intracellular chloride concentration; Kawamura et al., 2002). Activation of any of these channels causes depolarization and calcium concentration increase, leading to pericyte contraction. Pericytes express α-adrenergic receptors (Elfont et al., 1989), and noradrenaline has been found to produce membrane depolarization and contraction of pericytes (Helbig et al., 1992; Peppiatt et al., 2006).

In this chapter, I use NG2-DsRed mice to begin to investigate the electrical properties of cerebellar and cortical pericytes, using the patch-clamp technique to record the currents that underlie the response of pericytes to the vasoconstrictor, noradrenaline, and the vasodilator, glutamate.

5.2 Methods

5.2.1 Preparations

Experiments were performed on 200 µm coronal forebrain and sagittal cerebellar slices from P10-P15 NG2-DsRed C57BL/6J mice. Solutions and tissue preparation are described in Chapter 2, sections 2.1.1, 2.3.1 and 2.3.2.

5.2.2 Patch-clamp recordings

Pericytes were identified as DsRed-expressing cells located on capillaries. Pericytes were whole-cell clamped between -40 and -75 mV with pipettes containing solution as described in Chapter 2 section 2.1.3. Pipettes were pulled from thick-walled borosilicate glass to a resistance of 7-9 MΩ (with a tip of approximately 1 µm). Electrode junction potentials were compensated. Patch-clamped cells were morphologically confirmed to be pericytes by dye filling and checking that the intracellular dye was in the same cell as the DsRed. The series resistance was 21.9 ± 3.8 MΩ. In 11 cells, the mean resting potential was -58.5 ± 8.9 mV, and the mean input resistance at the resting potential was 132.0 ± 20.3 MΩ.

5.3 Results

5.3.1 Electrical properties of pericytes

I used the fluorescent labelling of pericytes in NG2-DsRed mice to target pericytes for patch-clamping and then dye-filled the patched cells with alexa488. Figure 5.1 shows images of a pericyte before patch-clamping, in bright-field during patch-clamping and when dye-filled during patch-clamping (white arrow). The patch pipette is attached to the cell body of the pericyte, obscuring the view in Figure 5.1C. Several processes can be seen lining the vessel (which itself can clearly be seen in the bright-field image; Figure 5.1B). Pericytes have small cell bodies (approximately 10 µm in diameter) and are enclosed by a thick layer of collagenous basement membrane making it very difficult to make whole-cell patch clamp recordings with a good access resistance. For the cell pictured in Figure 5.1, R_m and C_m were 223 MΩ and 29 pF respectively. The resting membrane potential was measured (when the current was 0) as -30 mV, a value comparable with the range of values recorded from cultured retinal pericytes (between -20 and -50 mV; Helbig et al., 1992). Current responses typical of patch-clamped pericytes in response to a series of voltage steps are shown in Figure 5.2A. The average current responses for 11 cells are shown in Figure 5.2B. No time-dependent currents were observed. The steady-state current-voltage responses are approximately ohmic, varying linearly with voltage.

5.3.2 The effect of glutamate receptor activation on pericyte membrane current

Glutamate application produces a capillary dilation, which is attributed to pericyte relaxation (Chapter 4 and see Peppiatt et al., 2006). This might be produced by a hyperpolarization of pericytes. To investigate whether this is the case, I measured pericyte currents in response to bath application of 500 μM glutamate and, the glutamate receptor agonist, NMDA (100 μM).

I found that glutamate application produced a small initial inward current in some pericytes. The average current observed was -12.6 ± 10.5 pA, however only two out of eleven cells showed any measurable inward current. This response was followed by a larger, and more consistent, outward current of 34.2 ± 12.3 pA (with measurable responses seen in 7 out of 11 cells; Figure 5.3A and 5.3B). On a second application of glutamate, the inward current was negligible (-5.5 ± 5.5 pA with only 1 out of 5 cells showing a measurable response) but the outward current was reproduced (30.2 ± 16.0 pA with 3 out of 5 cells showing a measurable response; Figure 5.3B). Similarly, application of NMDA produced an outward current of 28.6 ± 21.7pA with no preceding inward current (2 out of 4 cells showed measurable responses; Figure 5.3A and 5.3C). In the case of one cell there were membrane current oscillations that were abolished on glutamate application (Figure 5.3D).

The finding that glutamate receptor activation leads to an outward current in pericytes provides a possible mechanism underlying glutamate-evoked capillary dilations (Chapter 4; Peppiatt et al., 2006). The hyperpolarization produced by an outward current would be expected to cause a decrease in calcium ion influx and thus relaxation (Webb, 2003). The fact that only a proportion of the pericytes that I patch-clamped showed measurable current responses to glutamate receptor activation supports the finding that not all pericytes dilate capillaries in response to glutamate application (Peppiatt et al., 2006)

Membrane current oscillations have been observed in vasa recta pericytes (Zhang et al., 2008). Anecdotally, I patch-clamped one cortical pericyte that appeared to have similar oscillations in membrane current. These oscillations were inhibited by glutamate application (Figure 5.3D).

5.3.3 The effect of noradrenaline on pericyte membrane current

Noradrenaline causes constriction of arterioles and pericytes (Raichle et al., 1975; Peppiatt et al., 2006), and it has been shown to depolarize cultured retinal pericytes (Helbig et al., 1992). I bath applied 2 μM noradrenaline to brain slices and recorded the current response of pericytes.

Noradrenaline application evoked an inward current in pericytes (-33.0 ±19.7 pA; Figure 5.4A and 5.4B). A measurable response to noradrenaline was recorded in three out of six pericytes patch-clamped.

This inward current in pericytes in brain slices is consistent with findings that noradrenaline depolarizes retinal pericytes (Helbig et al., 1992) and may be responsible for generating the capillary constriction seen in response to noradrenaline application (Chapter 4; Peppiatt et al., 2006). The fact that not all of the pericytes showed a measurable current response to noradrenaline application supports existing evidence that not all pericytes constrict capillaries on application of noradrenaline (Peppiatt et al., 2006).

5.4 Discussion

These preliminary results have found that pericytes can be whole-cell patch-clamped *in situ* in cortical and cerebellar brain slices. Pericytes show little voltage-evoked current but glutamate receptor activation produces an outward current while noradrenaline application produces an inward current. These responses could explain the dilation and constriction of pericytes seen in response to these signalling agents.

5.4.1 Glutamate receptor activation causes an outward current in pericytes

The glutamate evoked outward current in pericytes supports a dilatory role for glutamate at the capillary level. Glutamate is thought to produce smooth muscle relaxation through activation of EP_4 receptors (see Chapter 4). EP_4 receptor activation leads to increased intracellular cAMP concentration, promoting dilation by decreasing the sensitivity of contractile apparatus, inhibiting calcium channels and activating potassium channels (Karaki et al., 1997, Ishikawa et al., 1993, Quayle et al., 1997). Prostaglandins also hyperpolarize arteriolar smooth muscle by activating calcium-dependent potassium channels (Serebryakov et al., 1994), reducing voltage-gated calcium entry into the cells, and thus decreasing contraction. The findings of Chapter 4 suggest that this pathway is also present at the pericyte level, so the outward current that I observe might be expected to be blocked by an EP_4 receptor blocker. Unfortunately, the difficulty of these experiments precluded me testing this during my PhD.

The observation, in one cell, that glutamate prevents current oscillations in the pericyte, sits well with evidence found that depolarizing agents, such as noradrenaline, produce spike-like calcium oscillations in retinal pericytes (Helbig et al., 1992). Similarly, oscillations are seen in pericytes, in the kidney, in response to angiotensin II (Zhang et al., 2008). The oscillations were attributed to repetitive cycles of calcium entry (Zhang et al., 2008) or calcium release and reuptake from intracellular stores (Borysova et al., 2013). Exposing retinal pericytes to calcium free extracellular solution inhibited current oscillations (Helbig et al., 1992), suggesting

that oscillations may be involved in regulating contractile behaviour. Similar oscillations have been observed in smooth muscle cells (Somlyo and Somlyo, 1968; Nelson et al., 1990).

5.4.2 Noradrenaline causes an inward current in pericytes

Noradrenaline produces an inward current in pericytes, consistent with previous findings that noradrenaline application causes membrane depolarization and contraction (Helbig et al., 1992; Peppiatt et al., 2006). Noradrenaline is a vasoconstrictor used to pre-constrict vessels in Chapter 4. Noradrenaline is thought to produce pericyte constriction through α-adrenoceptor activation (Weiss et al., 1977; Chapter 1.3). Helbig et al. (1992) found that prazosin inhibited noradrenaline induced pericyte depolarization, suggesting it acts through the α_1 receptor. A study into the adrenoceptor expression of cortical pericytes, however, found that these cells do not express α_1 receptors but that they do express α_2 and, to a lesser extent, β receptors (Elfont et al., 1989). Activation of α_2 receptors reduces the production of cAMP, promoting contraction (see Chapter 1.4). Another possibility is that noradrenaline acts on the α_1 receptors of astrocytes to increase astrocytic calcium (Duffy and MacVicar, 1995; Bekar et al., 2008) which then leads to an increased production of 20-HETE (Mulligan and MacVicar, 2004), which can then depolarize pericytes in the same way that it acts on smooth muscle cells, increasing calcium entry through voltage-gated calcium channels (see Chapter 1 and 4; Lange et al., 1997; Gebremedhin et al., 1998).

5.4.3 Conclusion

I found that not every cell responded to drug application with a current response. This may be due to heterogeneity of pericytes and agrees with data showing that not all pericytes constrict or dilate in response to signalling agents. Li and Puro (2001) found that, although not every retinal pericyte showed a change in tone on application of the potassium channel activator pinacidil, all cells responded with a hyperpolarization. This suggests a difference between retinal and cerebral pericytes.

Overall, these results provide support for the roles of glutamate and noradrenaline laid out in Chapter 4 and gives insight into the mechanisms by which these transmitters act. Glutamate produces an outward current in pericytes that would explain pericyte relaxation and capillary dilation, whereas noradrenaline produces an inward current that would explain the pericyte contraction and capillary constriction observed in imaging experiments.

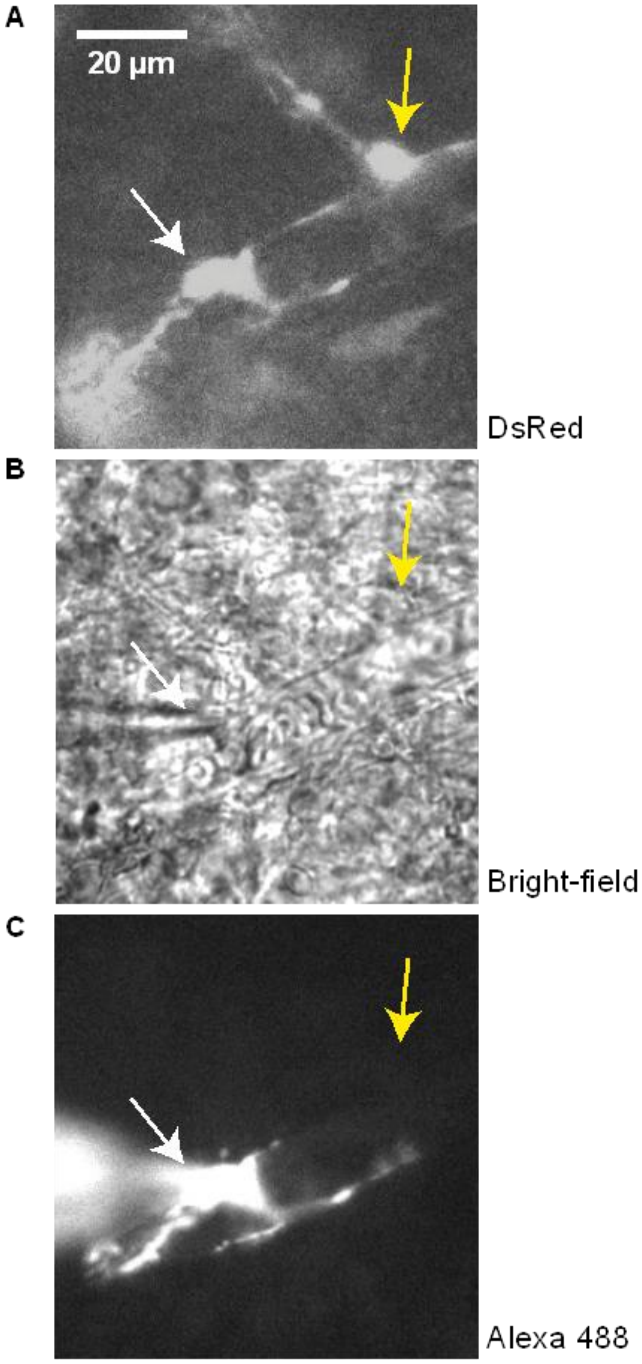

Figure 5.1: Morphology of patch-clamped pericyte. A DsRed positive pericytes in a cortical brain slice are indicated by arrows **B** Bright-field image of the same field of view as in **A**. Pericytes cannot be seen well in the bright-field image but are still indicated by arrows. The pipette can be seen in the left of the image. The pipette is attached to the pericyte indicated by the white arrow. **C** Image showing the pericyte with Alexa 488 introduced from the patch pipette (indicated by white arrow). The cell body is obscured by the patch pipette but the cells processes can be seen enwrapping the vessel. The pericyte indicated by the yellow arrow is not filled with dye.

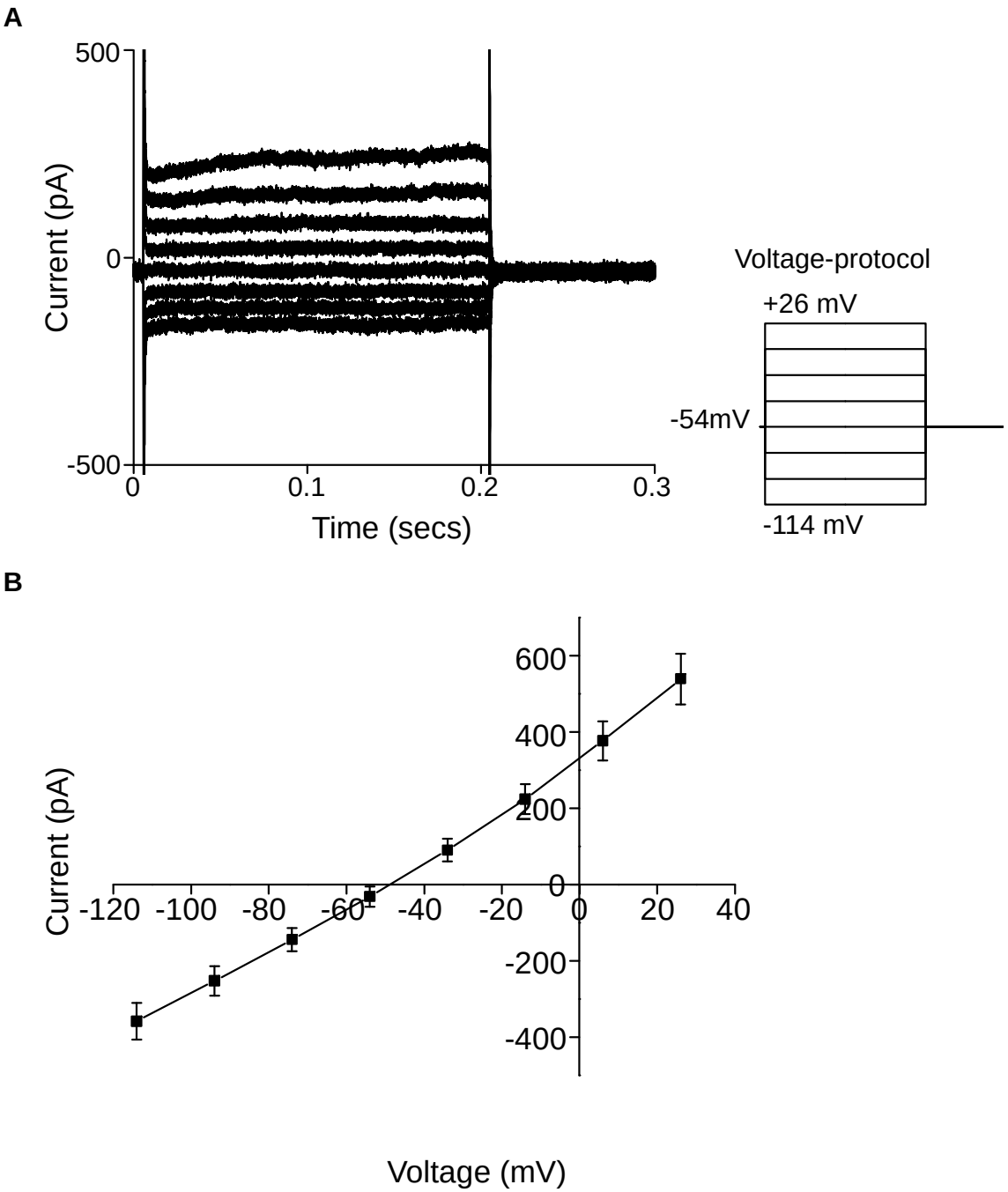

Figure 5.2: Electrical properties of pericytes. A The responses of a pericyte to a series of positive and negative voltage steps from -114 mV to +26 mV. The voltage clamp protocol is shown below the traces. **B** The average current voltage relation for the 11 pericytes patch-clamped.

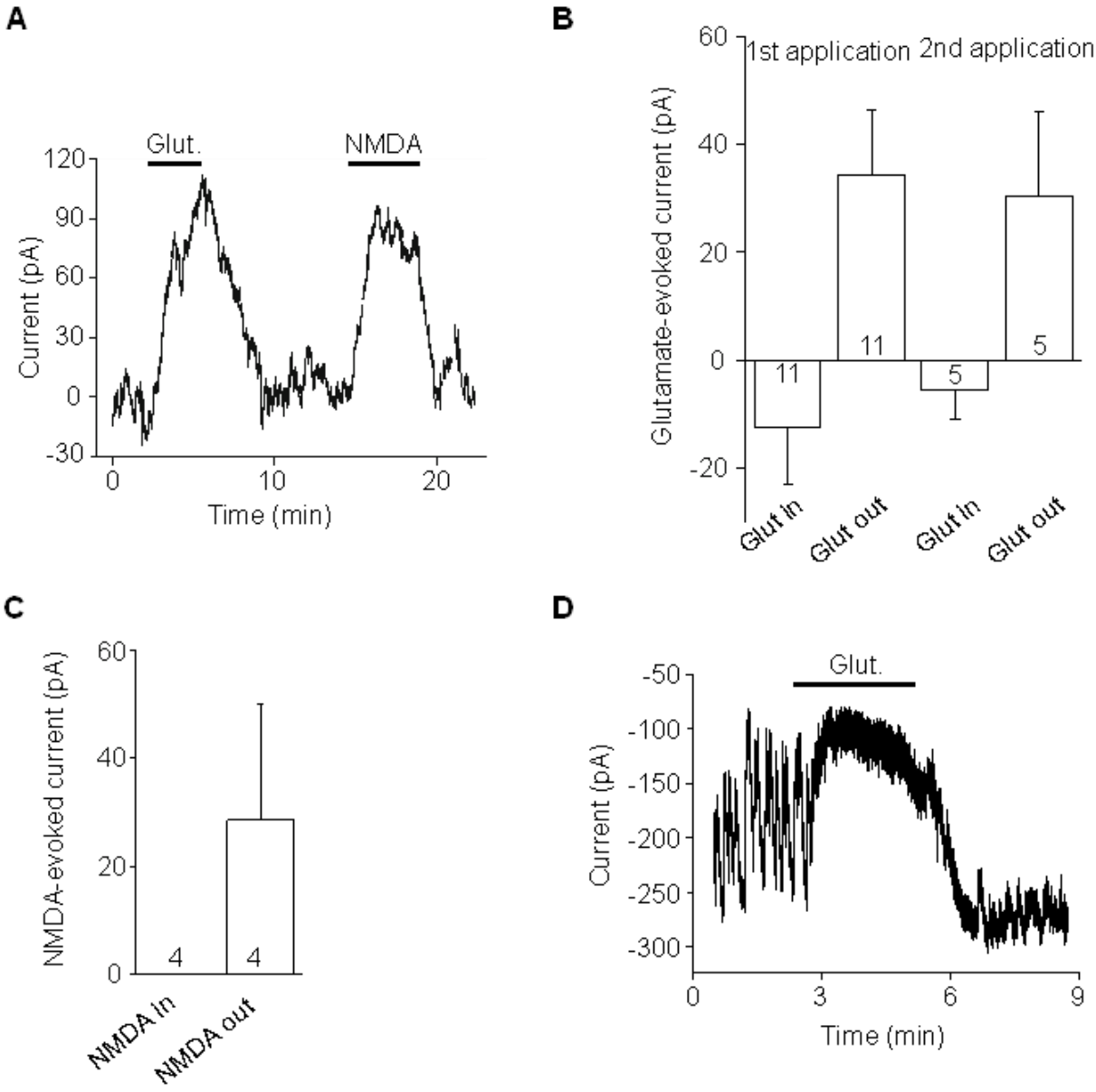

Figure 5.3: The effect of glutamate receptor activation on pericyte currents. A A trace showing that application of glutamate (500 µM) and NMDA (100 µM) leads to an outward current in a patch-clamped pericyte held at -55 mV **B** Mean ± s.e.m inward and outward currents evoked by 1st and 2nd applications of glutamate **C** Mean ± s.e.m inward and outward currents evoked by NMDA **D** A trace showing that application of glutamate inhibits current oscillations in a patch-clamped pericyte.

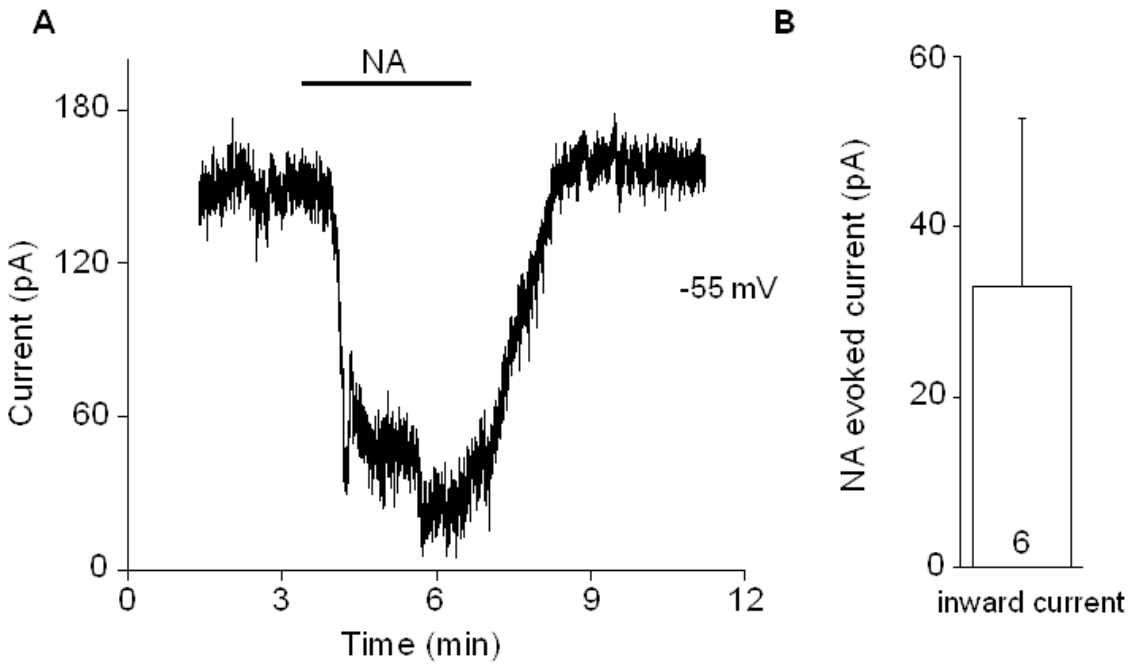

Figure 5.4: The effect of noradrenaline on pericyte currents. A A trace showing application of noradrenaline (2 μM) leads to an inward current in patch-clamped pericyte held at -55 mV **B** Mean ± s.e.m current evoked by application of noradrenaline.

Chapter 6: The pericyte response to ischaemia

6.1 Introduction

Ischaemia is known to constrict pericytes (Peppiatt et al., 2006) and this constriction has been suggested to be long lasting following an ischaemic insult (Yemisci et al., 2009). It has also been found that pericytes are vulnerable to death following exposure to reactive oxygen species and hypoxia in culture (Shojaee et al., 1999; Yu et al., 2012). *In vivo,* following middle cerebral artery occlusion (MCAO) and reperfusion, pericytes are unhealthy, with disrupted membranes that allow a labelling antigen to leak from the cells (Fernández-Klett et al., 2013). Pericyte constriction and death may be at least partly responsible for the long lasting decrease of blood flow that is observed following ischaemia and reperfusion (Ames, 1968; Leffler et al., 1989; Hauck et al., 2004; see Section 1.7.6 for more details). A chronic decrease in blood flow following ischaemia may exacerbate neuronal death by limiting oxygen and glucose delivery to, and removal of CO_2 from, the tissue that is struggling to recover from metabolic disruption.

As reviewed in Chapter 1, ischaemia kills cells by many mechanisms. A reduced energy supply initially causes neuronal depolarization because there is insufficient energy to fuel the pumps that maintain the resting membrane potential. This leads to an excessive release of glutamate, initially through synaptic release of glutamate and then, more importantly, through reversal of glutamate transporters (Szatkowski and Attwell, 1994; Rossi et al., 2000). The released glutamate activates postsynaptic receptors causing a further large influx of positively charged (sodium and calcium) ions culminating in cell death (Sattler and Tymianski., 2001). Intracellular calcium concentration increases can lead to cell death through accumulation in mitochondria (Sciamanna et al., 1992; Schinder et al., 1996). Mitochondrial depolarization, due to calcium entry, promotes opening of the mitochondrial permeability transition pore (MPTP; Dubinsky and Levi, 1998) which in turn impairs oxidative phosphorylation, causes release of apoptogenic proteins and generates reactive oxygen species (ROS; Piantadosi and Zhang, 1996; Dubinsky and Levi, 1998; Starkov et al., 2004). In addition, ischaemic activation of neuronal nitric oxide synthase (NOS) by the rise of $[Ca^{2+}]_i$ occurring increases the production of NO, which can react with superoxide to form the potent oxidant, peroxynitrite (Saran et al., 1990). Peroxynitrite has many damaging effects including cell membrane disruption and enzyme inactivation through lipid peroxidation and protein oxidation (Halliwell, 1992). The rise of $[Ca^{2+}]_i$ produced by ischaemia also activates phospholipases and thus increases the concentration of arachidonic acid and its metabolites, including several types of eicosanoid (Tegtmeier et al., 1990). After ischaemia, when a thrombus is cleared, the re-introduction of oxygen by reperfusion is thought to contribute to delayed secondary brain damage. As

discussed in Chapter 1.7, the mechanisms of damage at this stage include many of the pathways described above (Schaller and Graf, 2004).

In this Chapter I examine pericyte death in response to simulated ischaemia, as well as ischaemia followed by reoxygenation. The approach used was to quantify pericyte death in brain slices following incubation in oxygen and glucose free solution (mimicking an ischaemic insult) and then reintroduction of oxygen and glucose (mimicking reperfusion following an ischaemic insult), while pharmacologically manipulating the pathways potentially involved in pericyte death. The results obtained in slices were then extended to the *in vivo* situation using a MCAO model of stroke (see Chapter 2.7.2).

6.2 Methods

6.2.1 Preparations

Experiments were performed on 200 µm coronal forebrain slices from P21 Sprague Dawley rats, or on anaesthetised adult Wistar rats (weighing 253-312g), all of male sex. Solutions and tissue preparation used are described in Chapter 2, sections 2.1.1, 2.1.2 and 2.3.2.

6.2.2 Oxygen and glucose deprivation

To quantify pericyte death in response to ischaemia, *in vitro* slices were incubated in oxygen and glucose deprived (OGD) solution. This involved incubating slices at 37^0 C in aCSF in which glucose was replaced with 7mM sucrose, and oxygen was removed by equilibrating solutions with 5% CO_2 and 95% N_2 for 1 hour. Control slices were incubated at 37^0 C in aCSF and gassed with 5% CO_2, 95% O_2. All slices were incubated in isolectin B_4-FITC conjugate (IB_4, 10µg/ml) which labels blood vessels, including pericytes, and in propidium iodide (PI, 37µM) which labels dead cells (as shown in Figure 6.1A). PI is a 669 Dalton molecular weight dye that enters cells when membrane integrity has been lost and, once inside, it intercalates into the fragmented DNA and becomes fluorescent. Slices were then fixed for 20 minutes in 4% PFA and mounted for imaging.

In initial experiments, slices were labelled with an NG2 antibody as in Figure 6.1A (for the protocol, see Chapter 2, section 2.4.2). NG2 is a commonly used pericyte marker (see Chapter 3.3.1). However, I found that the NG2 labelling had very poor depth penetration. Because of this I mainly used IB_4 labelling and morphology to identify pericytes, as described in Chapter 3.3.3.

6.2.3 Middle cerebral artery occlusion

To quantify pericyte death in response to ischaemia *in vivo*, I prepared 200 µm brain slices from the brain tissue of rats that had been subjected to middle cerebral artery occlusion (MCAO) for 90 minutes followed by 22.5 hours of recovery. As described in more detail in Chapter 2.7.2, MCAO was produced by inserting a filament into the internal carotid artery and advancing it to block the opening of the middle cerebral artery. As a control, slices were prepared from naïve animals and animals that underwent a sham operation. The sham operation involved insertion of a filament into the internal carotid artery, as in the MCAO protocol, but in these cases the filament was not advanced to occlude the middle cerebral artery. During procedures, cerebral blood flow was continuously monitored by placing a laser Doppler probe over a thinned skull of the MCA territory approximately 4 mm lateral and 1.5 mm caudal to bregma. In MCAO animals, averaged over the period of occlusion, blood flow fell to 34.9±7.1% of baseline (n=6), while in sham animals it dropped significantly less to only 67.9±11.0% (n=3, t-test p = 0.035; a drop still occurs because of occlusion of the common and internal carotid arteries). After 22.5 hours of reperfusion, neurological deficit was assessed by investigating limb symmetry, motor function, activity and sensory stimulation. A maximum score of 15 equates to severe neurological deficit, while a minimum score of 0 implies no neurological deficit. MCAO animals had a mean score of 7.5$\pm$1.7, which was significantly greater than that of sham animals (0.3$\pm$0.3, p = 0.027). In both the MCAO and sham animals the right hemisphere was operated on, and thus is referred to as the lesioned hemisphere. In the naïve animals, neither hemisphere was operated on but the right hemisphere is still referred to as the lesioned hemisphere. My colleague, Brad Sutherland, at Oxford University carried out the surgery.

The slices obtained from these animals were then labelled, as in described in section 6.2.2, with isolectin B_4-FITC conjugate and propidium iodide. Example images from this tissue can be seen in Figure 6.1B.

6.2.4 Imaging

After fixation and labelling, slices from both the *in vitro* and the *in vivo* experiments were imaged with a Zeiss LSM 700 or 710 confocal microscope using a x20 water immersion objective.

6.2.5 Analysis and statistics

Prior to analysis, image identities were recoded using a custom-written Image J macro so that I was blind to the condition that each tissue slice had undergone. PI-positive dead perivascular cells were counted using ImageJ. Dead or alive pericytes were identified by their “bump on a log” morphology on vessels surrounded by IB_4 labelling (see Chapter 3.3.3). Endothelial cells were identified by their elongated cell body. Since only the cell bodies of dead cells were visible, only dead endothelial cells could be counted. The total number of endothelial cells present, and therefore the percentage of dead endothelial cells, was estimated from the total number of pericytes, assuming a 1:3 ratio of pericytes to endothelial cells (Pardridge, 1999)

There were high levels of cell death within the surface 20 μm of the slice (Figure 6.1C), which was thought to be caused by the trauma of slicing. Because of this, the surface 20 μm of each slice were excluded from analysis.

Data are presented as mean ± s.e.m Results in each condition are compared to results in the absence of drugs. All control experiments without drugs were pooled together, although comparing drug data with control data obtained on the same day gave essentially identical results. Statistical methods are given in Chapter 2, section 2.8. All statistical analysis was conducted using IBM SPSS21 statistics software or Microsoft Excel.

6.3 Results

6.3.1 Pericyte death in oxygen-glucose deprivation and reoxygenation, in cortical slices

The model of ischaemia used in these experiments was oxygen and glucose deprivation (OGD). Exposure to 1 hour of OGD significantly increased pericyte death from 7.1±1.6% to 41.9±3.0% of all pericytes counted ($p=8.7x10^{-7}$; Figure 6.1D). Because this model of ischaemia is reversible, I was also able to investigate pericyte death when OGD was followed by a period of oxygen and glucose reintroduction (reoxygenation). Exposure to 1 hour of OGD followed by an hour of reoxygenation increased pericyte death from 12.7±2.2% to 65.8±2.5% of all pericytes counted ($p=5.7x10^{-16}$; Figure 6.1D). Thus, the percentage of pericytes that die in OGD was significantly increased when OGD was followed by an hour of reoxygenation ($p=6.6x10^{-7}$; Figure 6.1D).

These results indicate that pericytes die following OGD, and that this death is increased if OGD is followed by the reintroduction of oxygen and glucose.

6.3.2 The effect of inhibiting glutamate receptors on pericyte death in OGD and reoxygenation, in cortical slices

Cell death in ischaemia may be caused by glutamate excitotoxicity. Exposure of neurons in culture and in slices to glutamate or glutamate receptor agonists leads to cell death (Choi, 1985; Garthwaite & Garthwaite, 1986). In order to investigate whether the pericyte death observed in OGD, and OGD with reoxygenation, was due to activation of glutamate receptors, I used inhibitors of either ionotropic or metabotropic glutamate receptors.

In the presence of ionotropic glutamate receptor blockers (D-AP5, 7-CK and NBQX), pericyte death was still significantly increased after 1 hour of OGD as well as after 1 hour of OGD followed by an hour of reoxygenation ($p=2x10^{-3}$ and $p=1.9x10^{-8}$ respectively; Figure 6.2A). The pericyte death observed after either 1 hour of OGD or 1 hour of OGD followed by 1 hour reoxygenation, all in the presence of the ionotropic glutamate receptor blockers, was, however, reduced by 37.2% and 29.6% respectively i.e. significantly lower than that seen in the absence of drugs ($p=7x10^{-3}$ and $p=1.7x10^{-4}$; Figure 6.2A)

In the presence of the metabotropic glutamate receptor blocker (MCPG), pericyte death was no longer significantly increased after 1 hour of OGD ($p=0.31$; Figure 6.2B) there was, however, no significant difference in the death in the absence and presence of MCPG following 1 hour of OGD ($p=0.3$; Figure 6.2B). When 1 hour of OGD was followed by 1 hour of reoxygenation, all in the presence of MCPG, there was a significant increase in pericyte death ($p=1.4x10^{-4}$; Figure 6.2B), and in fact there was an increase in pericyte death when compared to results in the absence of MCPG ($p=2.7x10^{-3}$; Figure 6.2B).

These results suggest that inhibition of ionotropic glutamate receptors reduces pericyte death in response to OGD, as well as the pericyte death seen with OGD followed by reoxygenation. It appears that inhibition of metabotropic glutamate receptors, however, may increase pericyte death when OGD is followed by reoxygenation. This increase in death seen on reoxygenation in the presence of a metabotropic glutamate receptor antagonist may support the notion of a protective role of metabotropic glutamate receptor activation following ischaemia: it was previously found that application of a metabotropic glutamate receptor blocker following MCAO reduced excitotoxicity (Chiamulera et al., 1992).

6.3.3 The effect of removing calcium or inhibiting mitochondrial calcium uptake on pericyte death in OGD and reoxygenation, in cortical slices

Glutamate-mediated cell death is to a large extent calcium-dependent (Choi, 1985; Garthwaite & Garthwaite, 1986). In order to investigate whether the pericyte death observed in response to OGD, or OGD with reoxygenation, involved a calcium influx, I removed calcium from the extracellular solution.

On removal of extracellular calcium, pericyte death was no longer significantly increased after 1 hour of OGD or 1 hour of OGD followed by an hour of reoxygenation ($p=0.07$ and $p=0.09$ respectively; Figure 6.3A). Pericyte death in calcium free solution was significantly reduced compared to the pericyte death seen when calcium was present in the solution in both conditions, with a reduction in pericyte death of 46.1% and 56.1% respectively ($p=0.01$ and $p=4.1x10^{-6}$; Figure 6.3A).

One of the mechanisms through which calcium is thought to produce cell death is through uptake into the mitochondria. During calcium overload mitochondria act as a sink for calcium. Mitochondrial calcium accumulation triggers the assembly and opening of a high-conductance pore in the inner mitochondrial membrane, causing a collapse of the electrochemical gradient for protons, stopping ATP production and triggering production of reactive oxygen species. Furthermore, during reperfusion, isolated mitochondria show a calcium-concentration dependent morphological damage and swelling, which is thought to be due to the loss of the mitochondrial membrane potential and an increase in reactive oxygen species production (Li et al., 2012).

In the presence of a mitochondrial calcium uptake inhibitor (Ru360), pericyte death was significantly increased after 1 hour of OGD as well as after 1 hour of OGD followed by reoxygenation ($p=8.8x10^{-4}$ and $p=0.03$ respectively; Figure 6.3B). The pericyte death observed after an hour of OGD in the presence of Ru360 was not significantly different to the death seen in the absence of the drug ($p=0.06$), but the pericyte death after 1 hour of OGD and reoxygenation, all in the presence of Ru360, was reduced by 21.1% i.e. significantly lower than that seen in the absence of drugs ($p=0.04$; Figure 6.3B).

These results suggest that calcium influx contributes to the pericyte death seen in response to OGD as well as the pericyte death seen in OGD followed by reoxygenation. Mitochondrial calcium uptake does not appear to contribute to pericyte death in OGD but may contribute to pericyte death during reoxygenation.

6.3.4 The effect of inhibiting 20-HETE production on pericyte death in OGD and reoxygenation, in cortical slices

Ischaemia increases the release of free fatty acids, including arachidonic acid (Tegtmeier et al., 1990). As mentioned in Chapters 1 and 4, there are several vasoactive metabolites of arachidonic acid including 20-HETE. Increased arachidonic acid release may thus lead to increased 20-HETE production. 20-HETE constricts smooth muscle by inhibiting potassium channels, depolarizing the cell and thus increasing voltage-gated Ca^{2+} influx and activating protein kinase C (Lange et al., 1997), as well as by directly activating L-type Ca^{2+} channels (Gebremedhin et al., 1998). These mechanisms may also occur at capillary level pericytes. Increases in intracellular calcium concentration would be expected to lead to a constriction of smooth muscle or pericytes, but may also lead to a calcium concentration high enough to cause cell death. In order to investigate whether the pericyte death observed in or after OGD involved 20-HETE production, I used HET0016, a ω-hydroxylase enzyme inhibitor (for more information on HET0016 see Chapter 4.3.7).

In the presence of HET0016, pericyte death was significantly increased after 1 hour of OGD as well as after 1 hour of OGD followed by an hour of reoxygenation ($p=6.1x10^{-4}$ and $p=2.1x10^{-5}$ respectively; Figure 6.4). Pericyte death in the presence of HET0016 was not significantly different to the pericyte death in the absence of HET0016, for either condition ($p=0.88$ and $p=0.95$ respectively; Figure 6.4).

These results suggest that 20-HETE production does not contribute to the pericyte death seen in response to OGD or the pericyte death seen in OGD followed by reoxygenation. It is nevertheless possible that the increased release of free fatty acids in OGD causes cell death through another mechanism, possibly through free radical production (Lipton, 1999).

6.3.5 The effect of inhibiting oxidative-nitrative stress on pericyte death in OGD and reoxygenation, in cortical slices

It has been suggested that oxidative and nitrative stress lead to constriction of pericytes (Yemisci et al., 2009) and it is known that production of reactive oxidative species, especially peroxynitrite, causes cell death (Halliwell, 1992). As peroxynitrite is formed from nitric oxide and superoxide, I investigated whether the pericyte death observed in OGD, and OGD with reoxygenation, was reduced by incubation with a nitric oxide synthase inhibitor or a superoxide scavenger.

In the presence of the nitric oxide synthase inhibitor L-NNA (L-N^G-nitroarginine), pericyte death was significantly increased after 1 hour of OGD as well as after 1 hour of OGD followed by an hour of reoxygenation ($p=3x10^{-3}$ and $p=4x10^{-6}$ respectively; Figure 6.5A). Pericyte death in the presence of L-NNA

after 1 hour of OGD, or 1 hour of OGD followed by 1 hour reoxygenation, was not significantly different to the pericyte death in the absence of L-NNA (p=0.17 and p=0.24; Figure 6.5A). Similarly, in the presence of the superoxide scavenger MnTBAP (Szabó et al., 1996), pericyte death was significantly increased after 1 hour of OGD as well as after 1 hour of OGD followed by reoxygenation (p=0.04 and $p=4.4x10^{-8}$ respectively; Figure 6.5B), but the pericyte death observed in either condition in the presence of MnTBAP was not significantly different to the death seen in the absence of the drug (p=0.5 and p=0.1 respectively; Figure 6.5B).

In order to confirm the results found with MnTBAP, I carried out experiments with another superoxide scavenger, PBN (Carney and Floyd, 1991). In the presence of PBN, pericyte death was significantly increased after 1 hour of OGD as well as after 1 hour of OGD followed by reoxygenation ($p=1.3x10^{-6}$ and p=0.04 respectively; Figure 6.5B). However, the pericyte death in either condition in the presence of PBN was not significantly different to the death seen in the absence of the drug (p=0.95 and p=0.50 respectively; Figure 6.5B).

These results suggest that neither nitric oxide production nor superoxide production contribute to the pericyte death seen in response to OGD, nor to the pericyte death seen in OGD followed by reoxygenation.

6.3.6: Pericyte death in the striatum following MCAO compared to naïve and sham conditions

In order to test whether pericyte death was also observed in response to ischaemia *in vivo,* I quantified death in the striatum where the core of an ischaemic lesion occurs following MCAO. I compared the pericyte death in these animals with the pericyte death observed in naïve animals and animals that underwent a sham operation.

In naïve animals, that had no surgery, pericyte death in the striatum was not significantly different between the 'lesioned' hemisphere and the control hemisphere (p=0.37; Figure 6.6).

In animals that had a sham operation, pericyte death in the striatum showed a trend towards increased death in the lesioned hemisphere when compared to the control hemisphere, increasing from 17.8±4.0% in the control hemisphere to 43.4±9.4% in the lesioned hemisphere, but this difference was not significant (p=0.09; Figure 6.6). There was also a trend towards increased death in the striatum of the lesioned hemisphere of the sham animal when compared to the 'lesioned' hemisphere of the naïve animal, but this difference also did not reach significance (p=0.07; Figure 6.6). Both of these increases in death may reflect the 32.1% decrease of blood flow that is produced even with the sham operation because the common carotid artery is ligated and the occluding filament is inserted partly into the internal carotid artery.

In animals that had MCAO, which decreased the blood flow measured in the MCA territory decreased by 65.1%, pericyte death was significantly increased in the striatum of the lesioned hemisphere when compared to the control hemisphere, increasing from 28.0±5.7% in the control hemisphere to 70.5±5.1% in the lesioned hemisphere ($p=1.2x10^{-8}$; Figure 6.6). The pericyte death in the lesioned hemisphere was significantly higher than the pericyte death seen in the corresponding hemisphere of both the sham and the naïve animals ($p=0.02$ and $p=3.3x10^{-7}$ respectively; Figure 6.6).

These results demonstrate that pericyte death increases in the striatum in response to MCAO followed by 22.5 hours reperfusion.

6.3.7: Pericyte death in the cortex following MCAO compared to naïve and sham conditions

The striatum, in which I quantified pericyte death for Figure 6.6, is where the core of the ischaemic lesion produced by MCAO occurs. In order to test whether pericyte death in response to ischaemia *in vivo* was also seen in the penumbra of the lesion produced by MCAO, I quantified death in the cortex.

As for the striatum, in naïve animals that had no surgery or in sham operated animals, pericyte death was not significantly different between the lesioned hemisphere and the control hemisphere ($p=0.84$ and $p=0.16$ respectively; Figure 6.7). Similarly, the death in the lesioned hemisphere of the sham animal was not significantly different to that in the 'lesioned' hemisphere of the naïve animal ($p=0.21$; Figure 6.7).

In animals that had MCAO, pericyte death was significantly increased in the lesioned hemisphere when compared to the control hemisphere, increasing from 16.4±6.5% in the control hemisphere to 50.9±12.7% in the lesioned hemisphere ($p=1.3x10^{-3}$; Figure 6.7). The pericyte death in the lesioned hemisphere of the MCAO animal was significantly higher than the pericyte death seen in the lesioned hemisphere of the naïve animals ($p=0.03$; Figure 6.7) but was not significantly higher than the pericyte death seen in the lesioned hemisphere of sham animals ($p=0.18$; Figure 6.7).

Thus, just as in the core of the lesion, in the cortical penumbra pericyte death increases in response to MCAO followed by 22.5 hours reperfusion.

6.3.8: Endothelial cell death in the striatum and cortex following MCAO compared to naïve and sham conditions

Some studies have found that vascular endothelial cells die in response to hypoxia and ischaemia (Gobbel et al., 1994; Zhang et al., 2000; Walford et al., 2004) In order to compare endothelial cell vulnerability to ischaemia *in vivo* with that of pericytes, I quantified endothelial cell death in the striatum and cortex

following MCAO. Endothelial cell death in MCAO animals was compared with the death observed in naïve animals and animals that underwent a sham operation.

In naïve animals, that had no surgery, endothelial cell death was not significantly different between the 'lesioned' hemisphere and the control hemisphere in the striatum or cortex (p=0.55 and p=0.64 respectively; Figure 6.8 and 6.9). In animals that had a sham operation, endothelial cell death was also not significantly different between the lesioned hemisphere and the control hemisphere in the striatum or cortex (p=0.60 and p=0.79 respectively; Figure 6.8 and 6.9), and there was no difference in the level of endothelial cell death in the lesioned hemisphere of the sham animal when compared to the 'lesioned' hemisphere of the naïve animal (p=0.46 and p=0.93 respectively; Figure 6.8 and 6.9). Following MCAO, in the striatum, there was no significant difference in endothelial cell death between hemispheres (p=0.07; Figure 6.8), with no significant difference between the level of endothelial cell death in the lesioned hemisphere of the MCAO animals when compared to the 'lesioned' hemisphere of the naïve animals (p=0.1; Figure 6.8). There was, however, significantly higher endothelial cell death in the lesioned hemisphere of the MCAO animal than was observed in the lesioned hemisphere of the sham animals ($p=1.6x10^{-4}$; Figure 6.8).

In the cortex, endothelial cell death was significantly higher in the lesioned hemisphere than in the control hemisphere following MCAO ($p=6.5x10^{-4}$; Figure 6.9). The endothelial cell death in the lesioned hemisphere of the MCAO animal was also significantly higher than the endothelial cell death seen in the lesioned hemisphere of either the sham or the naïve animals ($p=8x10^{-3}$ and $p=2.6x10^{-4}$ respectively; Figure 6.9).

These results suggest that endothelial cell death increases in both the striatum and the cortex in response to MCAO (although variability in the striatal data from the naive, but not the sham, animals prevented this increase reaching significance). However, the endothelial cell death produced by MCAO is much less dramatic than the pericyte death (2.5±1.6% of endothelial cells died in cortex compared to 50.9±12.7% of pericytes; $p=4.7x10^{-10}$).

6.4 Discussion

I have investigated the mechanisms by which pericytes die in response to ischaemia, by quantifying pericyte death following OGD alone, and after OGD followed by reoxygenation, and blocking various mechanisms that might contribute to the death. The results indicate that, firstly, pericytes die in response to OGD. Secondly, pericyte death in response to OGD is increased when OGD is followed by reoxygenation. Thirdly, pericyte death can be reduced by inhibiting ionotropic, but not metabotropic, glutamate receptors.

Fourthly, pericyte death can be reduced by removing extracellular calcium. Fifthly, pericyte death is not altered in the presence of nitric oxide synthase inhibition or application of superoxide scavengers. Finally, I also found that pericytes die in response to ischaemia *in vivo,* following MCAO, and that this death was far higher than the death of endothelial cells.

6.4.1 Pericyte death in OGD and reoxygenation involves ionotropic glutamate receptor activation

Inhibition of ionotropic glutamate receptors decreases pericyte death in OGD and OGD followed by reoxygenation. It is not known whether pericytes express glutamate receptors themselves but they are known to respond to bath application of glutamate (see Chapters 1 and 4, and Peppiatt et al., 2006). Under physiological conditions glutamate is thought to hyperpolarize pericytes and cause relaxation (see Chapter 5). In ischaemia glutamate release increases, due to neuronal depolarization and reversal of glutamate transporters (Szatkowski and Attwell, 1994; Rossi et al., 2000), and this excessive release of glutamate may produce a pathological response in the pericyte. Pericyte constriction in ischaemia (Peppiatt et al., 2006; Yemisci et al., 2009) suggests that, in these conditions, glutamate causes a depolarization and calcium influx rather than hyperpolarization. It is unclear from this study where glutamate is acting to cause pericyte death after OGD.

6.4.2 Pericyte death in OGD and reoxygenation involves extracellular calcium

Removal of calcium from the extracellular solution decreased pericyte death produced by OGD or OGD followed by reoxygenation. In ischaemia the level of extracellular calcium decreases dramatically as it enters cells (Kristián and Siesjö, 1998). A large influx of calcium into the pericyte in ischaemia may trigger cell death, along with the observed constriction (Peppiatt et al., 2006; Yemisci et al., 2009). One pathway through which calcium is thought to cause cell death is mitochondrial calcium accumulation (Sciamanna et al., 1992; Schinder et al., 1996), though it has also been speculated that calcium uptake into mitochondria is neuroprotective (Nicholls, 1985). Inhibition of calcium uptake into mitochondria had no effect on pericyte death in OGD but slightly reduced pericyte death when OGD was followed by reoxygenation. Thus, pericyte death during reoxygenation may be partly due to calcium accumulation in the mitochondria.

6.4.3 Pericyte death in OGD and reoxygenation does not involve oxidative or nitrative stress

Inhibition of nitric oxide production and application of superoxide scavengers did not reduce pericyte death in OGD, nor in OGD followed by reoxygenation. This suggests that, unlike the pericyte constriction occurring in ischaemia, pericyte death in ischaemia is not caused by oxidative and nitrative stress. Yemisci et al. (2009) found that pericyte constriction, in response to ischaemia and reperfusion, could be prevented by both nitric oxide synthase inhibition or by application of superoxide scavengers. These results imply that the mechanism through which pericyte constriction and death is produced are different. It has, however, previously been found that both nitric oxide synthase inhibition and application of superoxide scavengers can be neuroprotective, decreasing infarct size following ischaemia (Cao and Phillis, 1994; Margaill et al., 1997) or reducing neuronal death following excitotoxicity (Patel, 1996) and PBN application improves recovery of brain energy state following ischaemia (Folbergrová et al., 1995). Thus it is possible that oxidative and nitrative stress is involved in neuronal death following ischaemia. Controversially, however, application of nitric oxide donors have also been found to protect neurons following ischaemia and reperfusion (Jung et al., 2006). Similarly, a protective effect of peroxynitrite has been suggested (Bolanos et al., 2004). These contradictory findings demonstrate that the role of nitric oxide and its free radical products in ischaemia are not fully understood. My results, however, strongly suggest that oxidative and nitrative stress is not involved in pericyte death in ischaemia or reperfusion.

6.4.4 Pericytes are more vulnerable to death than endothelial cells following MCAO and reperfusion *in vivo*

Confirming my results in brain slices, pericytes die following MCAO (and 22.5 hours reperfusion) *in vivo* and the pericyte death occurring was much higher than that seen for endothelial cells. These data support previous observations that pericyte damage precedes endothelial cell damage following ischaemia (Fernández-Klett et al., 2013) as well as the finding that pericytes are more vulnerable to apoptosis, following exposure to ROS, than endothelial cells (Shojaee et al., 1999). The greater vulnerability of pericytes, compared to endothelial cells, suggests that pericytes may be a more important therapeutic target than endothelial cells.

6.4.5 Conclusion

My data suggest that pericytes are vulnerable to death in ischaemia and reperfusion, and that the mechanism of pericyte death involves activation of ionotropic glutamate receptors and calcium influx, but does

not involve oxidative-nitrative stress. I also found that pericytes are more vulnerable to death following ischaemia and reperfusion than endothelial cells.

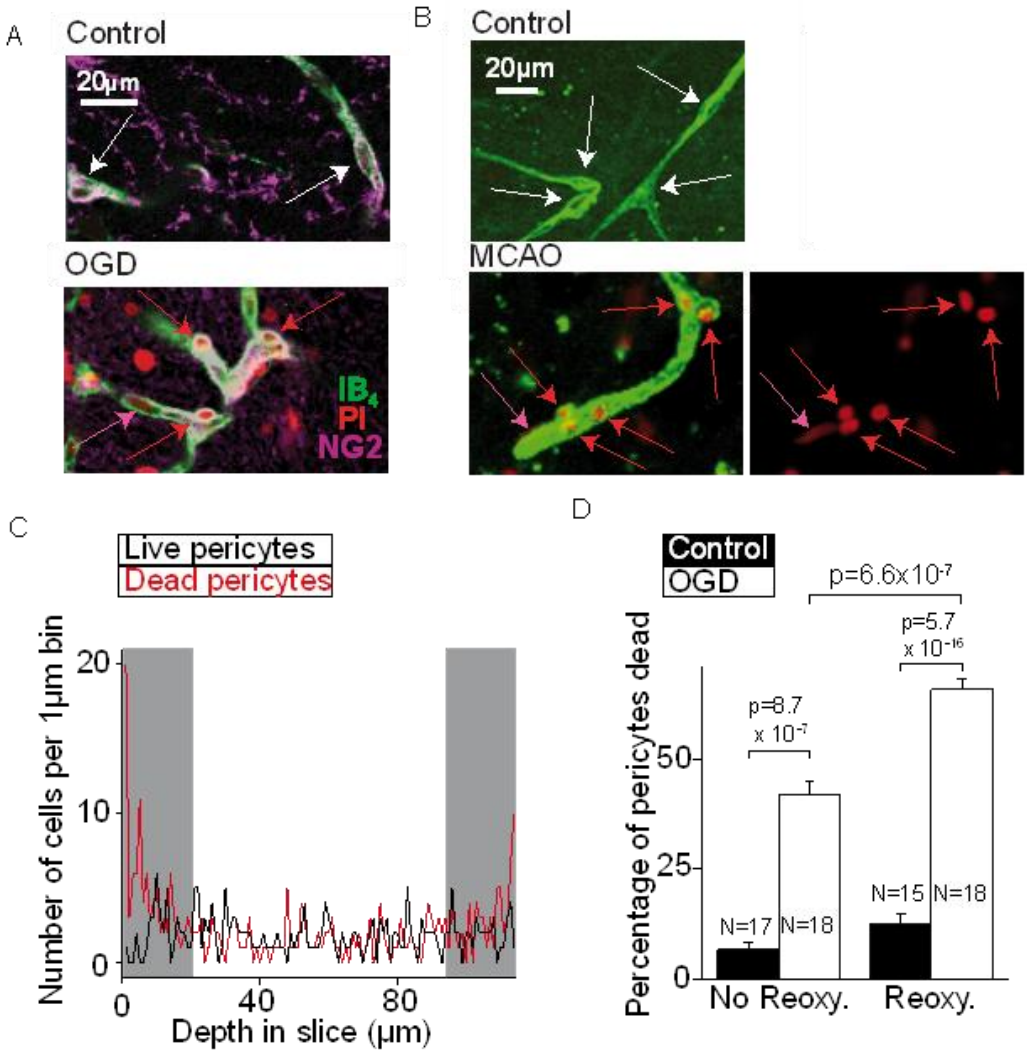

Figure 6.1: Methodology. A Example of cortical tissue from *in vitro* OGD experiment labelled with isolectin B_4-FITC conjugate (IB_4; green), propidium iodide (PI; red) and NG2 (magenta). Live pericytes in control tissue are labelled with IB_4 and NG2 (indicated by white arrows). Dead pericytes in OGD tissue are labelled with IB_4, NG2 and PI (indicated by red arrows). Dead endothelial cells in OGD are labelled with IB_4 and PI (indicated by pink arrows). **B** Example of cortical tissue from *in vivo* MCAO experiment labelled with IB_4 and PI, and PI alone. Live pericytes in control tissue are labelled with IB_4 (indicated by white arrows). Live and dead pericytes in MCAO tissue are labelled with IB_4 and PI (indicated by white and red arrows respectively). Dead endothelial cells in MCAO tissue are labelled with IB_4 and PI (indicated by pink arrows). Image showing PI alone allow identification of a dead endothelial cell, in MCAO condition, that was obscured by IB_4 labelling. **C** Plot of the number of live and dead pericytes per 1 µm depth bin as a function of depth in a cortical slice which was not exposed to OGD. The number of dead pericytes increases at the surface of the slice. The grey bars indicate the surface 20 µm of the slice, these regions were not included in subsequent cell counts. The apparent thickness of the slice (120 µm) is less than the thickness the slices were cut at (200 µm) because of tissue shrinkage during fixation. **D** Mean (± s.e.m) pericyte death after an hour of OGD (No Reoxy.) or an hour of OGD followed by an hour of reoxygenation (Reoxy.). P values assess the significance of the difference in pericyte death between the control and OGD conditions, and the significance of pericyte death between OGD alone and OGD followed by a reoxygenation period.

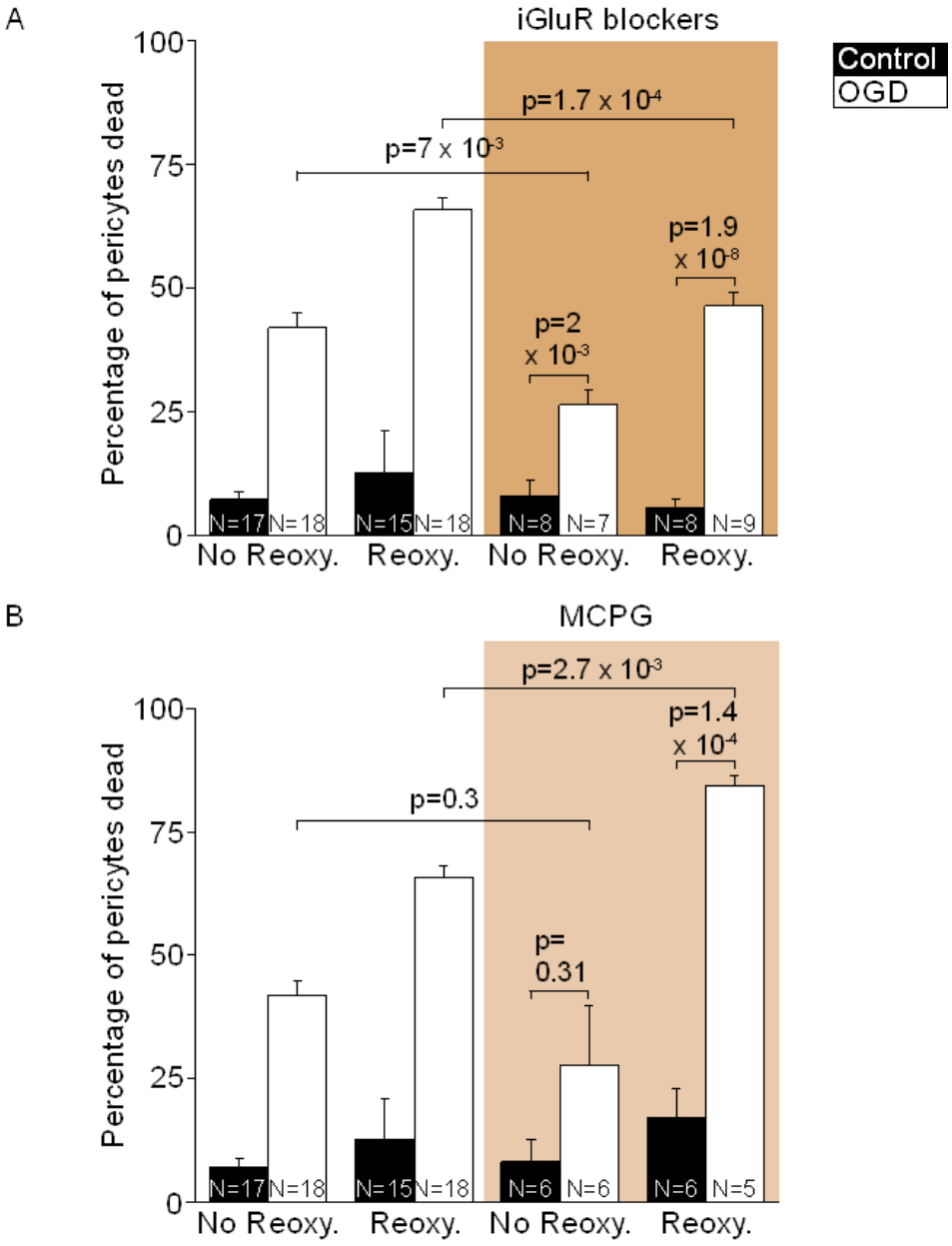

Figure 6.2: Effect of ionotropic and metabotropic glutamate receptor blockers on pericyte death in OGD and reoxygenation in cortical slices. A Mean (± s.e.m) pericyte death after an hour of OGD (No Reoxy.) or an hour of OGD followed by an hour of reoxygenation (Reoxy.) in the absence of drugs (data repeated from Fig 6.1) and in the presence of the ionotropic glutamate receptor blockers, D-AP5 (50 μM), 7-CK (100 μM) and NBQX (25 μM). P values assess the significance of the difference in pericyte death between the control and OGD conditions and the significance of the difference in pericyte death in the absence and presence of D-AP5, 7-CK, and NBQX. **B** Mean (± s.e.m) pericyte death after an hour of OGD (No Reoxy.) or an hour of OGD followed by an hour of reoxygenation (Reoxy.) in the absence of drugs and in the presence of metabotropic glutamate receptor blocker, MCPG (500 μM). P values assess the significance of the difference in pericyte death between the control and OGD conditions and the significance of the difference in pericyte death in the absence and presence of MCPG.

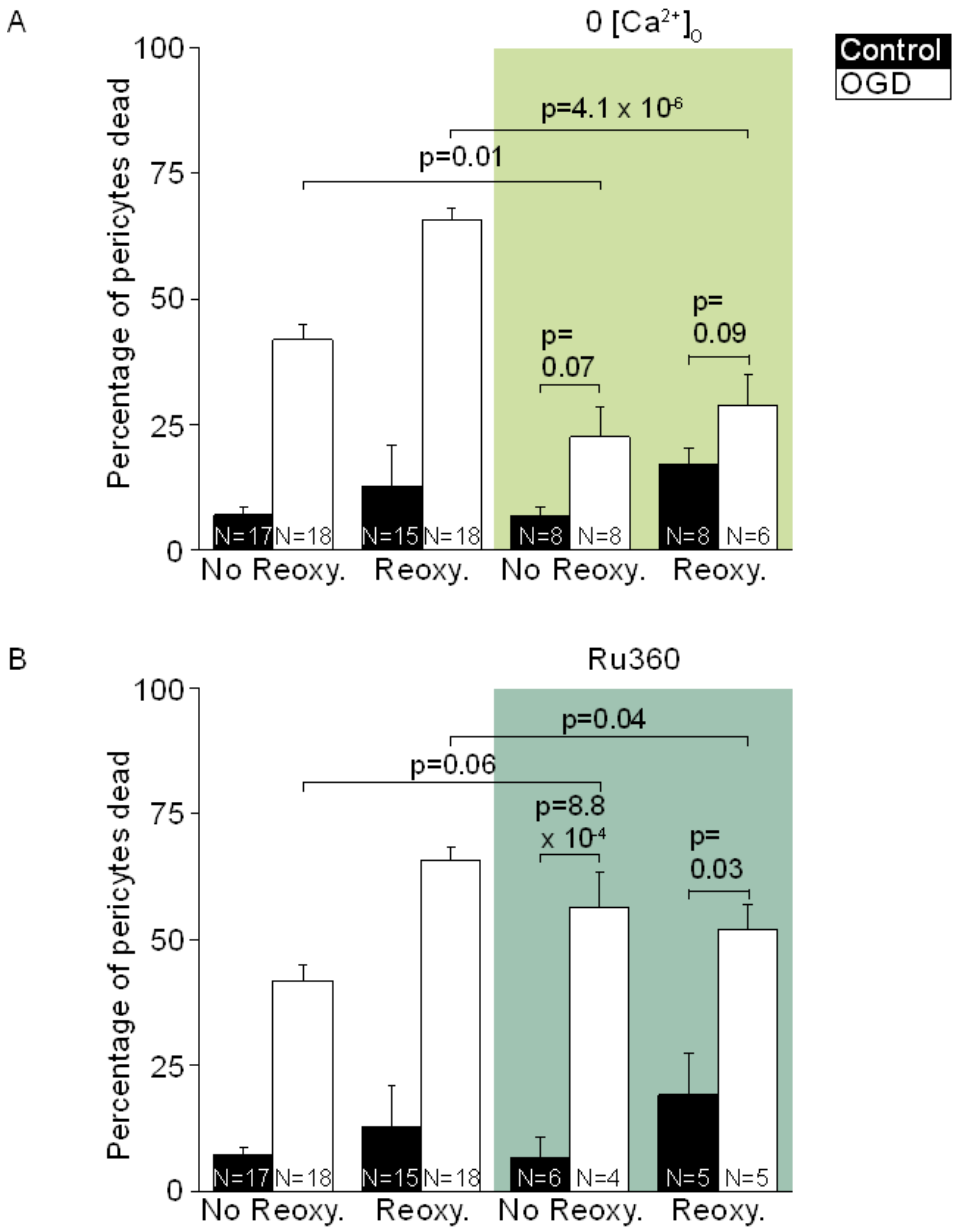

Figure 6.3: Effect of calcium removal and mitochondrial calcium uptake inhibition on pericyte death in OGD and reoxygenation in cortical slices. A Mean (± s.e.m) pericyte death after an hour of OGD (No Reoxy.) or an hour of OGD followed by an hour of reoxygenation (Reoxy.) in control solution (data repeated from Fig 6.1) and solution containing zero calcium (0 $[Ca^{2+}]_O$). P values assess the significance of the difference in pericyte death between the control and OGD conditions and the significance of the difference in pericyte death between OGD in control solution and solution containing zero calcium. **B** Mean (± s.e.m) pericyte death after an hour of OGD (No Reoxy.) or an hour of OGD followed by an hour of reoxygenation (Reoxy.) in the absence of drugs and in the presence of the mitochondrial calcium uptake inhibitor, Ru360 (50 μM). P values assess the significance of the difference in pericyte death between the control and OGD conditions, or the significance of pericyte death between OGD in the absence and presence of Ru360.

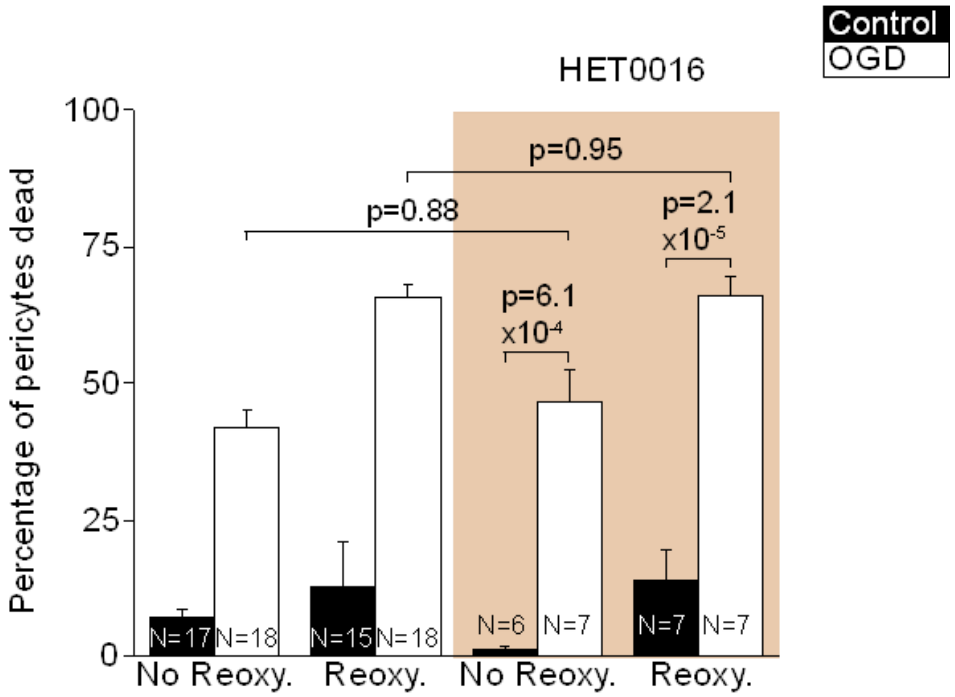

Figure 6.4: Effect of HET0016 on pericyte death in OGD and reoxygenation in cortical slices. Mean (± s.e.m) pericyte death after an hour of OGD (No Reoxy.) or an hour of OGD followed by an hour of reoxygenation (Reoxy.) in the absence of drugs (data repeated from Fig 6.1) and in the presence of HET0016 (1 μM). P values assess the significance of the difference in pericyte death between the control and OGD conditions and the significance of the difference in pericyte death between OGD in the absence and presence of HET0016.

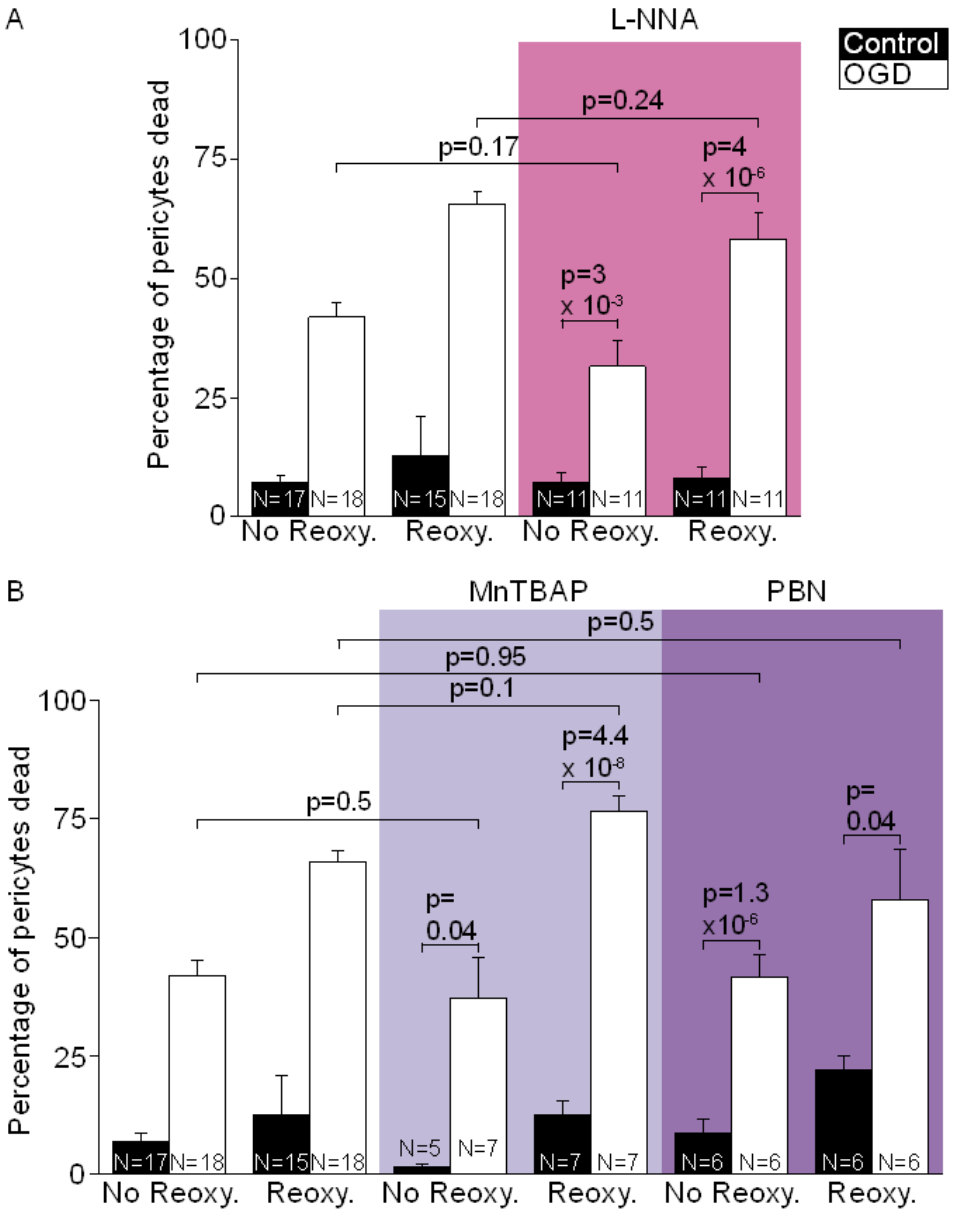

Figure 6.5: **Effect of nitric oxide synthesis inhibition and superoxide scavenging on pericyte death in OGD and reoxygenation in cortical slices. A** Mean (± s.e.m) pericyte death after an hour of OGD (No Reoxy.) or an hour of OGD followed by an hour of reoxygenation (Reoxy.) in the absence of drugs (data repeated from Fig 6.1) and in the presence of nitric oxide synthase inhibitor, L-NNA (100 μM). P values assess the significance of the difference in pericyte death between the control and OGD conditions and the significance of the difference in pericyte death in the absence and presence of L-NNA. **B** Mean (± s.e.m) pericyte death after an hour of OGD (No Reoxy.) or an hour of OGD followed by an hour of reoxygenation (Reoxy.) in the absence of drugs (data repeated from Fig 6.1) and in the presence of superoxide scavengers, MnTBAP (150 μM) or PBN(100 μM). P values assess the significance of the difference in pericyte death between the control and OGD conditions and the significance of the difference in pericyte death in the absence and presence of MnTBAP or PBN.

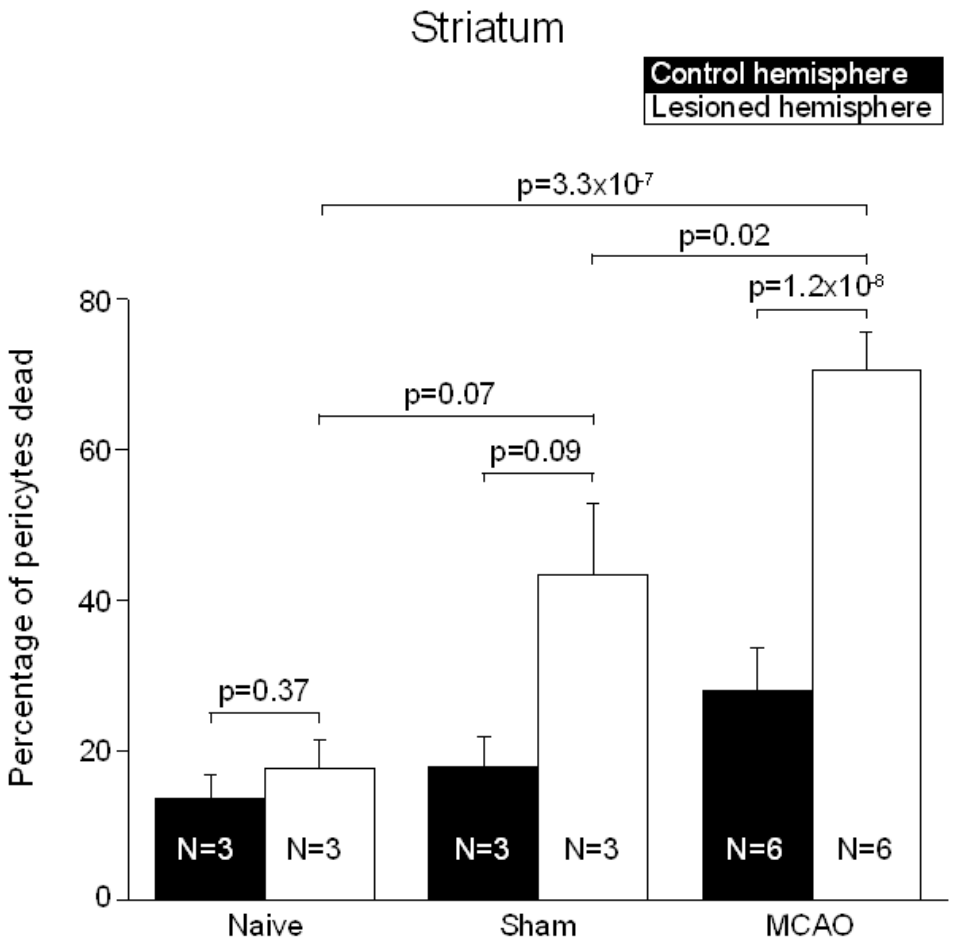

Figure 6.6: Pericyte death in the striatum *in vivo* following MCAO compared to naïve and sham conditions. Mean (± s.e.m) pericyte death in the striatum of control and lesion hemispheres of naïve animals (naïve), animals that underwent sham surgery followed by 22.5 hours recovery (sham), and animals that underwent the MCAO procedure followed by 22.5 hours recovery (MCAO). P values assess the significance of the difference in pericyte death in the striatum between the control hemisphere and the lesioned hemisphere, and the significance of the difference in pericyte death within the lesioned hemisphere between different conditions.

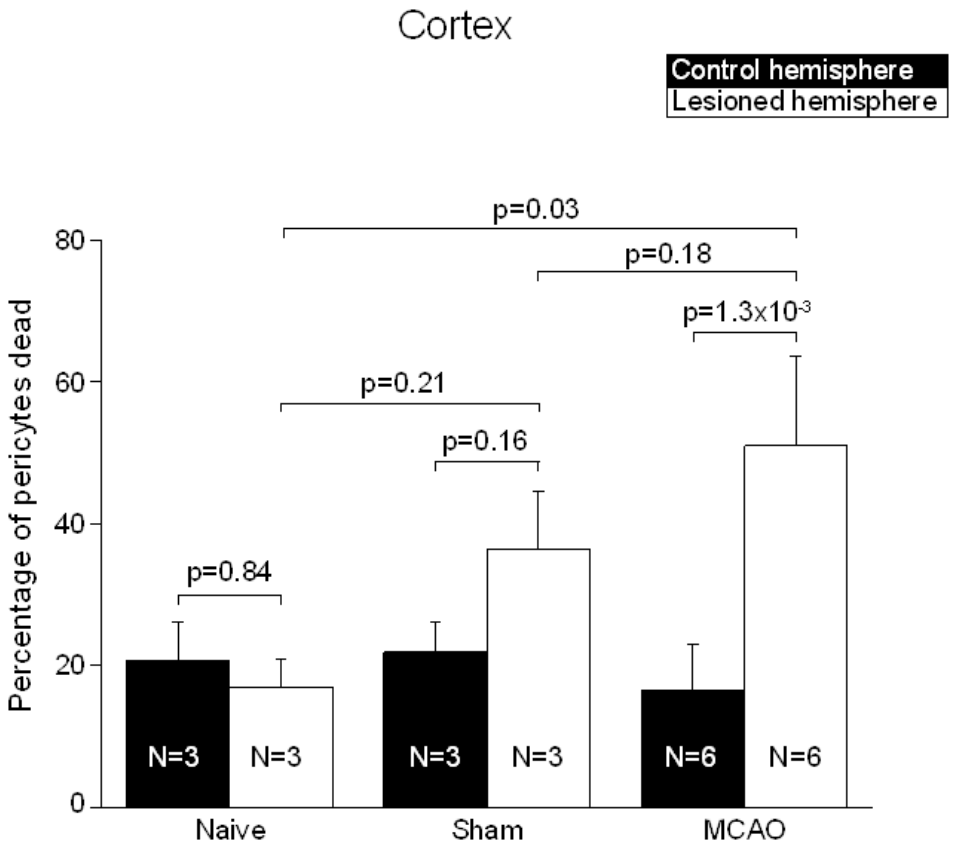

Figure 6.7: Pericyte death in the cortex *in vivo* following MCAO compared to naïve and sham conditions. Mean (± s.e.m) pericyte death in the cortex of control and lesion hemispheres of naïve animals (naïve), animals that underwent sham surgery followed by 22.5 hours recovery (sham), and animals that underwent the MCAO procedure followed by 22.5 hours recovery (MCAO). P values assess the significance of the difference in pericyte death between the cortex of the control hemisphere and the lesioned hemisphere, and the significance of the difference in pericyte death within the lesioned hemisphere between different conditions.

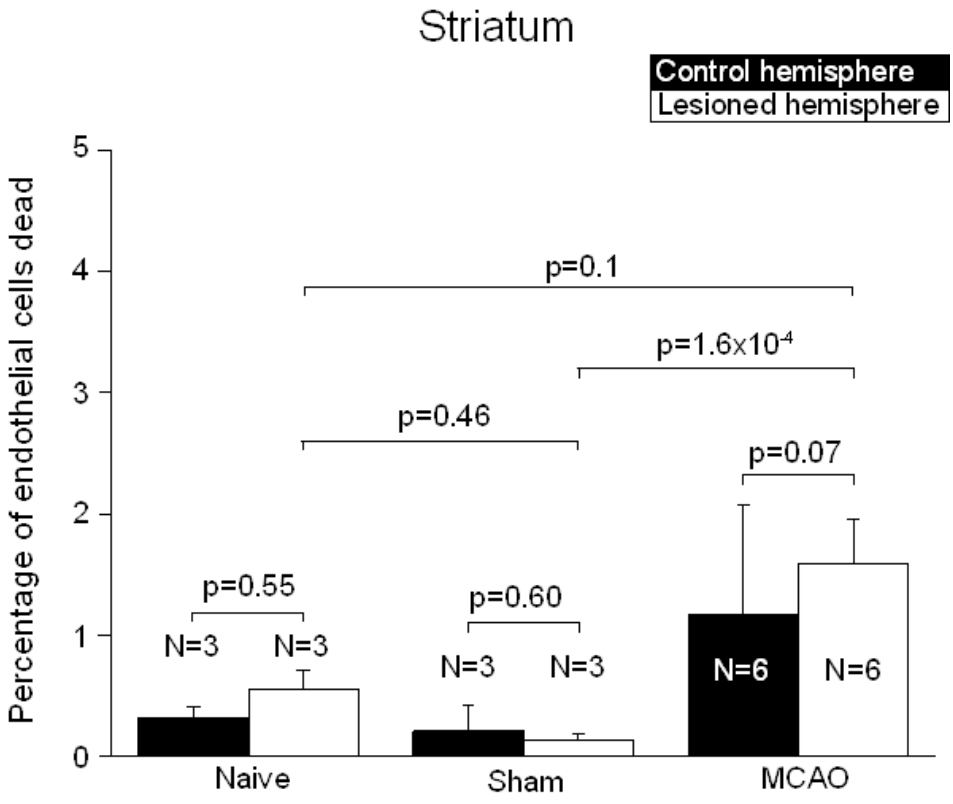

Figure 6.8: Endothelial cell death in the striatum *in vivo* following MCAO compared to naïve and sham conditions. Mean (± s.e.m) endothelial cell death in the striatum of control and lesion hemispheres of naïve animals (naïve), animals that have undergone sham surgery followed by 22.5 hours recovery (sham), and animals that have undergone the MCAO procedure followed by 22.5 hours recovery (MCAO). P values assess the significance of the difference in endothelial cell death between the striatum of the control hemisphere and the lesioned hemisphere, and the significance of the difference in endothelial cell death within the lesioned hemisphere between different conditions.

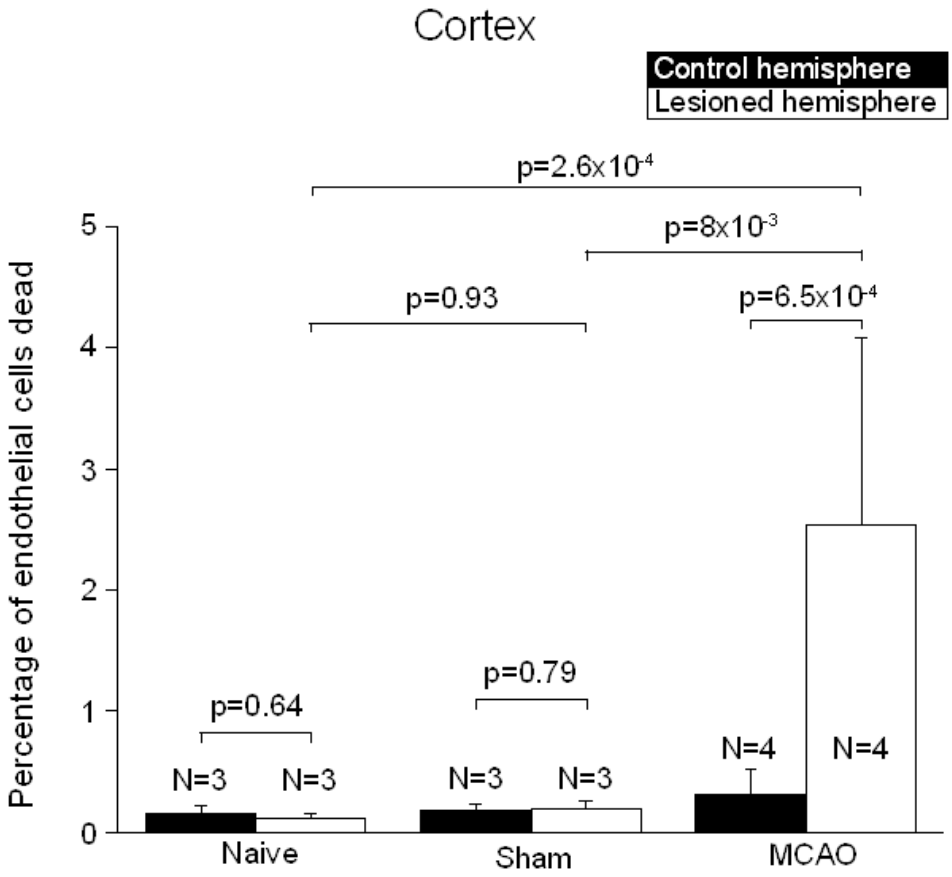

Figure 6. 9: Endothelial cell death in the cortex *in vivo* following MCAO compared to naïve and sham conditions. Mean (± s.e.m) endothelial cell death in the cortex of control and lesion hemispheres of naïve animals (naïve), animals that have undergone sham surgery followed by 22.5 hours recovery (sham), and animals that have undergone MCAO procedure followed by 22.5 hours recovery (MCAO). P values assess the significance of the difference in endothelial cell death between the control hemisphere and the lesioned hemisphere, and the significance of the difference in endothelial cell death within the lesioned hemisphere between different conditions.

Chapter 7: The physiology of developmental changes in BOLD functional imaging signals

7.1 Introduction

Most of my PhD work involved experimental analysis of how neuronal activity evokes local increases of cerebral blood flow. As explained in Chapter 1 section 1.10, these local increases of blood flow are the main generator of the BOLD fMRI (blood oxygenation level dependent, functional magnetic resonance imaging) signal. BOLD fMRI provides a widely used means of measuring brain activity in humans. Critically, the technique is non-invasive and thus safe for use across all age groups, including children. This makes fMRI potentially the most powerful tool available today for studying the neural underpinnings of the vast cognitive and social development that occurs during the first years of life. Over the past twenty years, fMRI has been vital in providing insight into the normal development of the neural strategies involved in human language acquisition, visual recognition, and memory (Baird et al., 1999; Casey et al., 1995; Gaillard et al., 2000; Thomas et al., 1999). fMRI is also well suited to studying abnormal neural development in diseases such as epilepsy and schizophrenia, and in disorders such as dyslexia and ADHD (Gaillard, 2000; Gur and Gur, 2010; Pugh et al., 2000; Vaidya et al., 1998).

It is important to note, however, that the conclusions drawn from developmental fMRI studies often rely on the assumption that the BOLD signal reflects the same set of processes in the developing brain as in the adult brain (despite neuronal signalling changes as dramatic as GABA switching from being an excitatory transmitter in early development to being inhibitory later: see section 7.5.3). This assumption is worth assessing critically because the BOLD signal is not a direct measure of any one component of neural activity, but in fact reflects the behaviour of several different brain processes, which all undergo massive developmental changes in the early years of life. For example, regional blood flow, the levels of neuronal and astrocytic enzymes that regulate blood vessel diameter, astrocyte morphology, and hence neurovascular coupling, may all change alongside neural activity. These changes in neurovascular coupling mechanisms, and in cellular energy use, may compromise the power of BOLD imaging to detect “real” developmental changes in neuronal information processing, possibly producing changes of BOLD signal with development when there is no change in neuronal processing (false positives), or obscuring BOLD signal changes that would otherwise occur as neuronal signalling changes with age (false negatives). An extreme example of such interpretational problems, discussed in detail later (section 7.4), is that sensory stimulation evokes a “normal” positive BOLD signal in neonates and adults, but a negative BOLD signal in infants and young children, implying that there are two transitional ages at which no BOLD signal is produced by neural activity. For

robust interpretation of developmental fMRI data, therefore, it is crucially important to understand in as much detail as possible the developmental changes of brain processes other than neuronal activity which may influence the BOLD signal.

This chapter provides a review, based on the expertise I gained in carrying out the experiments for my PhD, of the physiological changes that occur in neuronal and vascular networks in the developing brain, with a particular focus on those features that may alter the BOLD signal with age. I then discuss which factors are primarily responsible for changes in the BOLD signal during development, and outline the main considerations that should be taken into account when interpreting the results of developmental fMRI studies. This chapter, apart from some updating added for this thesis, has been published as Harris, Reynell & Attwell (2011) to which I made a 50% contribution.

7.2 Changes in neural circuitry with development

As the brain develops, its processing capabilities become increasingly sophisticated through changes in several components of the neural circuitry. These include experience-dependent and -independent changes to synaptic architecture, transmitter signalling, cell numbers, temporal response characteristics and myelination. Here, I will describe several of these changes from birth, through childhood and adolescence, to adulthood.

Inevitably, much of our knowledge of developmental changes in neural circuitry and in the systems mediating neurovascular coupling has come from animals (particularly rodents) rather than humans. In what follows, therefore, it is useful to bear in mind the following approximate correspondence between the stages of rodent and human brain development. The main period of corpus callosum myelination in rats and mice occurs from about P7 to P35 (Hamano et al., 1998), corresponding to human ages from birth to ~18 years (Pujol et al., 1993; Lenroot and Giedd, 2006). Human adolescence has been suggested to map onto rat ages P30-P42 (Spear and Brake, 1983), with the rat brain being regarded as adult by P60. As detailed data for developmental changes were not available for all the species from which data were taken for this review, and developmental comparisons may be complicated by interspecies differences in the order of developmental events, in what follows age classifications are limited to the broad time windows of childhood, adolescence and adulthood.

7.2.1 Cortical thickness and wiring

One of the most remarkable developmental circuitry changes is apparent in the increase in thickness and then slower thinning of human cortical grey matter which occurs over the period from childhood through adolescence into early adulthood (Paus 2005; Shaw et al., 2008; Ostby et al., 2009; Tamnes et al., 2010), which at least partly reflects the excess formation and then selective deletion of synapses (this is after the main period of neurogenesis and programmed cell death that occurs earlier in brain development: Chan et al., 2002). The initial phase of expansion – underpinned by synaptogenesis in parallel with dendritic growth (Rakic et al., 1994) – coincides with rapid changes in the functional properties of neurons and cortical circuitry (Khazipov et al., 2001). The slower thinning phase – underpinned by activity-dependent synaptic pruning (Huttenlocher, 1990; Bourgeois and Rakic, 1993) – allows for the deletion of unnecessary synapses, thereby increasing processing efficiency (Mimura et al., 2003).

While this general pattern is followed across cortical areas, the exact time-course of the expansion and thinning phases differs depending on the region, and appears closely related to the developmental timeline of the behaviour that the region subserves. Synaptogenesis in the human primary visual cortex, for example, begins in the foetus, reaching a maximum at around 8 months postnatally, after which visual experience-dependent pruning decreases synaptic density to the adult level (about 60% of the maximum) by 11 years (Garey and Courten, 1983). This timescale correlates with the period of visual plasticity in infant monkeys, and with the establishment of visual acuity, stereopsis and oculomotor function in humans (Garey and Courten, 1983). In the human prefrontal cortex (PFC), on the other hand, grey matter density increases up until the onset of puberty and then decreases throughout adolescence and into early adulthood (Sowell et al., 2003; Toga et al., 2006). Over the period of grey matter reduction there is a marked behavioural maturation in the social skills that the PFC is considered responsible for, namely, an understanding of other people's intentions, beliefs and desires, and an ability to predict the behaviour of others (Blakemore, 2008).

Over the period of synaptic density changes, specific neuronal connections are developed and maintained. The determinants of which connections become stable are likely to vary depending on the function of the region, but one common principle is the wiring up of similarly tuned cells. This is clearly seen in topographic maps, where the spatial layout of sensory input or motor output varies systematically across a cortical region, and neurons that are tuned to the same spatial field have a higher likelihood of being connected (Alonso and Martinez, 1998; Hubel and Wiesel, 1963). The formation of these maps tends to rely both on an intrinsic organisation mechanism – the retinotectal map, for example, is patterned in the

nasotemporal and dorsoventral planes from the earliest stages of tectal innervation (Holt and Harris, 1983) – and a component of experience-dependent development – proper binocular organisation in the visual cortex map, for example, depends on visual input from both eyes (Blakemore, 1979). In addition to sensory and motor regions, topographic maps have recently been found in human cortical areas associated with high order cognition: visual field topography has been observed in the parietal (Sereno et al., 2001) and frontal (Kastner et al., 2007) cortex, and may be important for spatial attention, working memory and decision making (Silver and Kastner, 2009). It is as yet unclear, however, on what time course these higher-order maps develop and on what processes their development depends.

7.2.2 Inhibition

Another important principle of synaptic connectivity that develops early on is lateral inhibition, where the neighbours of excited neurons are inhibited by GABAergic interneurons, thus sharpening the neural response to a stimulus (Sillito, 1975; Crook et al., 1998; Gabernet et al., 2005). This effect requires inhibitory circuitry to develop alongside excitatory circuitry and, indeed, there is evidence that, within days of sensory experience, inhibitory responses to sensory stimulation become increasingly selective and correlated with excitatory responses (in rat auditory cortex; Dorrn et al., 2010; in mouse visual cortex; Gandhi et al., 2008). In addition to shaping receptive fields, the balance between excitation and inhibition becomes critical for regulating firing rates and information flow in the developing network (Akerman and Chine, 2007). To achieve this balance, in most brain regions different GABAergic interneuron classes appear at different times, which are related to critical periods in network development. In monkey visual cortex, for example, calbindin-containing interneurons appear early in development, correlated with the onset of the thalamocortical innervation, while parvalbumin-containing interneurons appear after birth, correlated with the onset of visually driven activity (Hendrickson et al., 1991). In humans the GABAergic system in visual cortex continues to mature well into adulthood (Pinto et al., 2010), undergoing three distinct developmental changes during childhood (when receptor subunits change), adolescence (when proteins mediating GABA synthesis increase in level while vesicular uptake falls) and adulthood (when GABA synthesis decreases and vesicular uptake increases).

The development of interneuron networks also plays a role in shaping the temporal characteristics of circuit-level activity. While early development is characterized by spontaneous bursts of synchronous activity which are thought to be critical for the activity-dependent wiring of similarly tuned cells (Meister et al., 1991; Garaschuk, et al., 1998), later development is characterized by more oscillatory network-level activity,

particularly in the gamma frequency range (30-100 Hz). Werkle-Bergner et al (2009), for example, used EEG in humans to show that visually-evoked synchronous gamma oscillations developed by 11 years, but were not maximally sensitive to stimulus changes until adulthood. Gamma oscillations are thought to be generated by an interaction between stimulus-driven excitatory and inhibitory activity (Atallah and Scanziani, 2009; Ray & Maunsell, 2010), and therefore the integration of GABAergic interneurons into the excitatory circuitry may be important in the development of several behavioural functions. For example, gamma oscillations have been suggested as a solution to the binding problem (Singer and Gray, 1995; but see Ray and Maunsell, 2010), promoting integration of distributed information for its coherent processing and possibly contributing to the improving executive function seen throughout adolescence (Blakemore and Choudhury, 2006). Gamma oscillations may also have a direct role in learning and memory, as their synchronisation of synaptic inputs has been shown to directly enhance synaptic strength (König et al. 1995; Salinas and Sejinowski, 2001).

7.2.3 Myelination

Synaptic synchrony is also increased throughout development by myelination, which is now known to play a role in fine tuning the timing of spike arrival (Salami et al., 2003; Seidl et al., 2010) and thus increasing connection efficiency (Hagmann et al., 2010). The human corpus callosum, for example, undergoes an intricate myelination process throughout childhood and adolescence, with several thickness changes thought to result from varying the degree of myelination (Luders et al., 2010), possibly in order to fine tune input arrival times in cortical areas. A similar process of myelin maturation, involving changes in axonal diameter and myelin wrap number and density, occurs postnatally across the whole brain in a wave from posterior to anterior regions. The progression is slow, with the frontal lobes being the last to myelinate towards the end of adolescence (Fields, 2008) and the white matter not becoming fully mature until well into adulthood (20-30 years, Benes et al., 1994; Yakovlev and Lecours, 1967). One potential benefit of this slow progression is in maintaining white matter plasticity in regions that can be influenced by experience and learning, through activity-dependent effects on myelination (reviewed in Markham and Greenough, 2004; Ullen, 2009). For example, Bengtsson et al. (2005) used diffusion tensor imaging (DTI) to show that myelination in many regions, including the corticospinal tract (a white matter tract involved in voluntary skilled movements of distal limbs) is positively correlated with the amount of piano practice in children. They also found a positive correlation between myelination and piano practice in adults, but mainly in corticocortical pathways and not in the now mature corticospinal tract.

7.2.4 Amine system development

Another relatively slow process is the maturation of amine neurotransmitter systems, which are thought to play key roles in cognitive development, but also in control of cerebral blood flow (see below). The dopamine, serotonin and noradrenaline networks, which are closely involved in mood and attention, undergo large-scale changes at several developmental stages, from the infant to the ageing brain. Catecholamines and serotonin, for example, show early postnatal surges of development on different timescales (Lambe et al., 2000; Murrin et al., 2007), influencing the functional development of different cortical systems (Levitt et al., 1997). Broadly speaking, noradrenaline synthesis and endogenous concentration increases steadily throughout the brain until adulthood (Goldman-Rakic and Brown, 1982). Serotonergic development occurs more quickly, reaching mature levels of synthesis and concentration by childhood, with the largest percentage increases occurring in the parietal and occipital cortex (Goldman-Rakic and Brown, 1982). Dopamine synthesis and concentration, on the other hand, tend to peak during adolescence, and gradually decrease towards adulthood, remaining the highest in frontal regions (Goldman-Rakic and Brown, 1982). These changes are accompanied by dramatic changes in those behaviours that the dopamine system is thought to subserve, namely, reward-seeking and incentive-driven action, which also peak during adolescence (Wahlstrom et al., 2010).

7.2.5 Plasticity in the mature brain

Finally, even after these large-scale neural features have reached maturity, the brain retains a high level of plasticity. Synapses can alter their strength on the basis of activity, allowing us to learn and remember new things, throughout life. Entire cortical regions retain the capacity to reorganise themselves, and may do so in extreme circumstances, such as the loss of part of a limb (Merzenich and Jenkins, 1993).

7.2.6 Implications

The developmental neural circuitry changes discussed here (and schematized in Figure 7.1), which can be closely linked to behavioural changes, are often the very neurophysiological features that researchers hope to track across ages with fMRI, and their particular effects on the BOLD signal are discussed in Section 7.5. However, less commonly considered are parallel developmental changes in the microvasculature and neurovascular coupling, which may have confounding age-related effects on the BOLD signal. It is therefore important to have a clear picture of how these components of the vascular system develop alongside the neural circuitry.

7.3 Changes in neurovascular coupling with development

The relationship between neuronal activity and blood flow depends critically on the characteristics of the signalling pathways regulating blood flow. It not only varies between brain regions (Sloan et al., 2010), but can depend on which set of afferents to a brain area are activated. For example, even at a fixed developmental stage, Enager et al. (2009) found that the relationship between neural activity and blood flow response differed within the same small cortical area, the barrel field of the primary somatosensory cortex, depending on which set of synaptic inputs was activated. Stimulating at a low frequency evoked a larger blood flow response when stimulation was applied to the thalamocortical afferents than when applied to trans-callosal inputs from the contralateral cortex, whereas at high stimulation frequencies the relative influence of the two pathways was reversed. Thus neurovascular coupling exhibits pathway-specific signalling differences, possibly reflecting differences in the signalling molecules involved (Gotoh et al., 2001) or in the anatomical arrangement of the neurons (and astrocytes) relative to the blood vessels they control. These differences in the dependence of blood flow on neural activity in the same cortical area and at the same developmental stage show that a constant relationship between BOLD signal and neural activity cannot be taken for granted as neurovascular coupling changes during brain development. This is reinforced by the fact that human regional cerebral blood flow at the age of 5-6 years is 50-85% higher than that in an adult or at birth (Chiron et al., 1992). During development the brain undergoes many changes which have the potential to alter neurovascular coupling, ranging from the development of the vasculature to changes of the expression of enzymes responsible for producing vasoactive mediators. This section will give an overview of the changes that occur in neurovascular coupling during development.

7.3.1 Vascular development

At birth vascular development is incomplete, and the vasculature matures as the brain develops. From newborn to adult, the primate cerebral vascular vessel volume increases 2.7-fold and the mean distance between any point in the tissue and the nearest vessel decreases by 32% (Risser et al., 2009). Similarly, in rat, the capillary volume fraction increases 3-fold between postnatal days 7 and 20 (corresponding in humans roughly to the period from birth to adolescence) and then decreases slowly to become approximately 30% less in adulthood (Keep & Jones, 1990). These changes in blood volume fraction will, other things being equal, produce proportional changes in BOLD signal with development (Ogawa et al., 1993; Bandettini & Wong, 1997; Mandeville & Marota, 1999; Buxton et al., 2004). Vessel growth results from a mismatch in microvascular supply and metabolic demand, so areas that use more energy become more highly

vascularised than less active areas (Riddle et al., 1993; Weber et al., 2008). In both the cerebral and the cerebellar cortices of rats, the vascular density increases through early development from the inside to the outside of the tissue (Conradi et al., 1980; Yu et al., 1994), while in cat visual cortex the rich capillary supply to the highly active layer IV is not present at birth but appears at 5 weeks postnatally (Tieman et al., 2004). Similarly, human cerebral cortical studies show a rapid increase in blood vessel density between either 26-35 gestational weeks (Mito et al., 1991) or post 36 gestational weeks (Miyawaki et al., 1998). In a study of foetal and juvenile vasculature, radially orientated vessels were seen at 15 gestational weeks, with lateral branching observed at 20-27 weeks (Norman and O'Kusky, 1986). Branching occurs at an earlier stage in the lower half of the cortex, in keeping with the inside to outside pattern mentioned above. Capillary formation occurs after birth and is most prominent in vascular layer 3/neuronal laminae IV and Va (starting between term and 3 months postnatal: Norman and O'Kusky, 1986). Other post-birth changes in vasculature include a decrease in pial vessel coverage of the brain's surface occurring over the first postnatal years (Norman and O'Kusky, 1986). During the developmental increases of blood vessel density in the brain parenchyma, neural activity presumably is not coupled to blood flow increases as efficiently as when the vasculature is fully developed.

7.3.2 Neuronal NOS development

Interneuron numbers and the vasoactive substances they produce show developmental changes, which will alter the neuronal pathway of neurovascular coupling. In mice the number of nNOS containing interneurons in the cerebral cortex decreases somewhat with age (Eto et al., 2010), with higher expression for the first two postnatal weeks and a decrease from four to eight weeks (i.e. through adolescence and into adulthood). There is disagreement over whether the number of nNOS expressing neurons then increases or decreases as animals become senile (Reuss et al., 2000; Sánchez-Zuriaga et al., 2007). The total level of nNOS (reflecting number of cells expressing NOS and expression level per cell) has also been studied in the first few weeks of rodent postnatal life (Ogilvie et al., 1995; Riobo et al., 2002). Cytoplasmic nNOS is expressed weakly at embryonic stages and increases in early development. The age at which the peak expression is reached varies between brain regions being, for example, P9 in the neocortex and P20 in the cerebellum. Expression then declines to an adult level, with the time taken for this process varying between regions, occurring between P12-15 in the neocortex and P20-60 in the cerebellum (Ogilvie et al., 1995). Studies of nNOS development in human cortex have focussed on foetal and adult expression, and information on juvenile and adolescent expression is lacking. Expression of nNOS in the human cerebral cortex has a similar distribution to that in the foetal brain but at a lower density: the density of nNOS expressing cells

increases from 13 to 32 gestational weeks (GW) and then decreases (Ohyu and Takashima, 1998; Downen et al., 1999). Two types of nNOS positive interneuron are found in developmental studies (Estrada and DeFelipe, 1998; Ohyu and Takashima, 1998). Type 1 cells are large and intensely stained. These cells appear at 15-18 GW (Ohyu and Takashima, 1998; Yan et al., 1996), and reach an adult distribution at 32 GW. Type 2 cells are smaller and more weakly stained, and appear at 26-32 GW (Ohyu and Takashima, 1998; Yan et al., 1996), and increase in expression until term. The pattern of expression follows the inside to outside development mentioned above.

7.3.3 Astrocyte development

Astrocytes also show developmental changes in size and connectivity which may affect the size and spatial extent of blood flow responses caused by neuronal activity. An immunocytochemical study of cat visual cortex found that mature astrocytes only develop in the 3rd postnatal week, reaching adult density at the 4th week and then continuing to mature until 7 weeks after birth (Müller, 1992). Astrocytes increase in number and size during development, reaching their adult number by about P24 in rat hippocampus and P50 in rat cortex (Stichel et al., 1991; Nixdorf-Bergweiler et al., 1994). Changes in density and size are accompanied by changes in morphology, such as branching and orientation. Gap junctional coupling of astrocytes, which may enlarge the area over which neuronal activity can influence blood flow, develops by P11 in rat visual cortex, and remains stable throughout development (Binmöller and Müller, 1992), although before this stage astrocytes appear not to be coupled.

Developmental changes in the expression of the metabotropic glutamate receptors (mGluR5: Romano et al., 1995) which raise astrocyte $[Ca^{2+}]_i$ in response to neuronal activity may alter the astrocytic pathway of neurovascular coupling. Early studies showed that globally, mGluR5 is highly expressed in the brain during early life (rat postnatal day 1) and decreases within the first postnatal weeks to an adult level between P30 and P60 (Catania et al., 1994). The decrease in expression differs between brain regions: mGluR5 expression in the hypothalamus decreases 6 fold, whereas in the cortex expression decreases by only 3 fold (Van den Pol et al., 1995). More recently, astrocyte specific mGluR5 expression has been found to peak at P7 in mice, falling sharply by P14, and eventually showing no expression in adulthood (P70-84; Sun et al., 2013). Similarly, adult human cortical and hippocampal astrocytes showed no mGluR5 expression (Sun et al., 2013). These findings suggest that the astrocytic mGluR5-mediated contribution to neurovascular coupling may only be relevant early in development.

Prostaglandin signalling from astrocytes to blood vessels is probably altered during development.

Prostaglandin synthesis in rat brain homogenates or induced by convulsions in the *in vivo* brain is low at postnatal day 1 and increases strongly to adult levels in three weeks (Seregi et al., 1987), suggesting that prostaglandin induced dilations will increase with development. Similarly, expression of prostaglandin receptors is lower in newborn pigs than in adults (Li et al., 1995). However, the signalling consequences of upregulation of prostaglandin synthesis and receptor density with development are opposed, over the first postnatal month in mice, by an increase in expression of the transporter (PGT) which terminates prostaglandin signalling (Scafidi et al., 2007).

Astrocyte-mediated increases in blood flow may also be altered by developmental changes in the expression or properties of potassium channels, including the calcium-activated large conductance (BK_{Ca}) K^+ channels expressed on astrocyte endfeet, as well as inward rectifying potassium channels on vascular smooth muscle (Filosa et al., 2006). For example, in rabbit Müller cells (astrocyte-like cells found in the retina), the open probability of BK_{Ca} channels strongly decreases within the early postnatal period, possibly due to the resting potential becoming more negative (Bringmann et al., 1999). As a result, to activate the channel in older cells requires both a strong depolarization and an increase in intracellular calcium, whereas in early postnatal cells only a small change in membrane potential is needed to activate the channels, suggesting that neurovascular coupling mediated by these channels might become less efficient with age.

7.3.4 Vasoconstricting pathways

All of these developmental changes in vasodilating pathways may be potentiated or opposed by corresponding effects on constricting pathways, including either the aminergic pathways that help to set the basal tone of the arterioles (Blanco et al., 2008) or the 20-HETE pathway which can constrict vessels in response to astrocyte $[Ca^{2+}]_i$ increases (Mulligan and MacVicar, 2004).

7.3.5 Implications

The complex developmental changes in components of the signalling systems mediating neurovascular coupling that I have outlined above do not provide a simple prediction for how neuronal activity evoked blood flow changes, and hence the BOLD response, will alter, suggesting that far more research is needed to understand this. However, they highlight the importance of considering how developmental changes in the BOLD signal may in some cases reflect factors other than neuronal activity.

7.4 Changes in neural energy use with development

In both Chapter 1 and Section 7.1 I explained that the magnitude of the BOLD signal is affected by the O_2 use of the area of brain being studied - the larger is the increase of O_2 use evoked by neural activity (relative to the increase of blood flow) the smaller is the positive BOLD response. Although many factors affect the O_2 use, most brain energy in primates is predicted to be used on synaptic transmission (Attwell and Laughlin, 2001), and this conclusion has been reinforced by the fact that action potentials are now thought to use 3-fold less energy than was originally believed (Alle et al., 2009). Thus, the neural activity evoked increase of O_2 consumption is expected to increase with the increase of synaptic density that occurs over the first ~10 years of life, and to decrease as synaptic pruning occurs later on. Indeed, O_2 usage has been reported to rapidly increase with synapse development in children (Muramoto et al., 2002) and later to decrease by ~0.5% per year with ageing in the adult (Pantano et al., 1984; Leenders et al., 1990; Takada et al., 1992).

A greater fractional increase of neural activity-evoked energy (O_2) use than of blood flow has been postulated to occur in infants and young children to explain why (in contrast to the situation in neonates and adults for whom the blood flow increase exceeds the increase of O_2 use) infants and young children over a few years of early development show negative BOLD signals in response to sensory stimulation, i.e. a decrease of MRI signal rather than the usual increase (Yamada et al., 1997; Born et al., 1998; Anderson et al., 2001; Muramoto et al., 2002). Of concern for the interpretation of developmental changes in BOLD signals, the transition from a negative BOLD signal (in infants, when the task-evoked increase in O_2 use outweighs the increase in blood flow) to a positive BOLD signal (when, as is usual in adults, the increase of blood flow outweighs the increase in O_2 consumption) implies that at some intermediate developmental stage it is possible for an active area to show no BOLD response. This would occur if the increase of O_2 use and the increase of blood flow cancel out each other's effects on the deoxyhaemoglobin level (see Chapter 1.10). For a study starting from this (young) age, the developmental increase in task-evoked blood flow increase (relative to that of O_2 use) would result in the appearance of activation in an area that previously did not show it, even if that area was equally involved in processing the information at all ages.

7.5 How do developmental changes of neural circuitry and of neurovascular coupling combine to produce developmental changes in BOLD signals?

Many of the neural changes that underpin behavioural changes during development are expected to have clear effects on the BOLD signal, making their detection possible with fMRI. It would be ideal if this notion could be reversed, so that changes in BOLD signals could be assumed to reflect a change in the underlying neuronal processing of information. Conclusions based on BOLD data, however, depend critically on the usually unstated assumption that there are no confounding changes in the neurovascular coupling that generates the BOLD signal. Given the vast array of developmental changes in the mechanisms mediating neurovascular coupling, which I have described above, it would be extremely surprising if they did not contribute significantly to at least some of the developmental changes in BOLD signals that have been observed experimentally.

Developmental changes reported in BOLD signals include those showing the appearance at one developmental stage of a BOLD response in an anatomical region where it does not occur at another developmental stage (e.g. Monk et al., 2003; Passarotti et al., 2003; Blakemore et al., 2007), a change in the amplitude of the BOLD signal at one anatomical location (e.g. Casey et al., 1995; Kwon et al., 2002; Monk et al., 2003; Durston et al., 2006; Wang et al., 2006; Turkeltaub et al., 2008; Maril et al., 2010; Keulers et al., 2011), or an expansion or contraction of the spatial area activated within one anatomical region (e.g. Casey et al., 2002; Durston et al., 2006; Gaillard et al., 2000, 2003; Golarai et al., 2007; Kwon et al., 2002; Passarotti et al., 2003). I will now consider the possible problems of interpreting each of these kinds of change.

7.5.1 Alterations of activation locus

In general, a movement of the locus of BOLD activation is interpreted as the involvement of a new area for processing of information to perform a task, as the neural wiring progresses and regional specialisation develops. For example, tasks taxing social cognition start to activate the right superior temporal sulcus more (and the prefrontal cortex less) as development proceeds (Blakemore et al., 2007), suggesting a change in the neural strategies underpinning social cognition. Similarly, Monk et al. (2003) found a loss of the amygdala response to viewing fearful faces ongoing from adolescence to adulthood, and Holland et al. (2001) found increased left hemispheric lateralization of responses with age during a verb generation task. Alteration of the anatomical location of an activated area is the developmental change in BOLD response that is most likely to unequivocally reflect changes occurring in the underlying neuronal information processing (but see Section 7.4 for a scenario where activity could evoke no BOLD response at a young age and a positive BOLD

response in the adult, as a result of a decrease with development of the ratio of O_2 use evoked by activity to blood flow increase evoked by activity).

7.5.2 Alterations of BOLD amplitude at one anatomical location

Increases or decreases in BOLD signal amplitude with development are usually interpreted as indicating more or less involvement of neuronal activity in the activated area in the task being performed. For this conclusion to be secure, however, it is necessary to be sure that the altered amplitude does not simply reflect a change in blood volume fraction (see Section 7.3.1) or in the strength of neurovascular coupling, for example producing a larger increase of blood flow for the same amount of neural activity and energy use, and thus producing a larger BOLD signal.

In rats, BOLD signals increase in amplitude and decrease in latency with development (Colonnese et al., 2008) and some human studies also report a shorter latency for BOLD signals in adults than in children (Brauer et al., 2008; but see Richter and Richter, 2003). This might be expected from many of the developmental changes in the neural circuitry summarised in Section 7.2, e.g. the development and refinement of synaptic connections leading to more effective excitation in adults (indeed Colonnese et al. (2008) found that neural excitation occurred with a decreased latency at older ages), increased myelination leading to more synchrony of incoming synaptic activation (Olesen et al., 2003; Fornari et al., 2007), and perhaps a greater influence of attention mediated by amine transmitter systems. However, the many developmental changes in neurovascular coupling noted in Section 7.3 are also likely to contribute to developmental alterations of BOLD signal amplitude and latency.

First, as noted in Section 7.4, a developmental increase in the amplitude of the positive BOLD signal can result from the activity-evoked blood flow increasing more with age than the activity-evoked O_2 use, for example as a result of the developmental maturation of the systems mediating neurovascular coupling. To complicate this, however, the extra blood flow and O_2 use evoked by neural activity may have different dependencies depending on the amount of neural activity occurring, as seen in visual cortex where increasing the number of active neurons apparently increases O_2 use more than it increases blood flow, resulting in an unchanged or even a smaller BOLD signal (Goodyear and Menon, 1998; Marcar et al., 2004a,b). This implies that the age-related changes of BOLD signal may depend critically on the amount of neural activity produced by the task.

Second, the increase of vascular volume fraction that develops with age (Keep & Jones, 1990; Risser et al., 2009) is expected to increase the BOLD signal (Ogawa et al., 1993; Bandettini & Wong, 1997;

Mandeville & Marota, 1999; Buxton et al., 2004), all other factors being equal. On the other hand, the increase in vascular density may lead to a decrease in the fall of deoxyhaemoglobin level occurring during activity and thus decrease the BOLD signal, as suggested by Marcar et al. (2004b) when comparing the more highly vascularized visual cortical area V1 with V2 (although differences in the information processing occurring in V1 and V2 could also contribute to the differences observed). An increased vascular density, perhaps decreasing the distance that neurovascular messengers must diffuse to increase blood flow, may also explain the decrease of BOLD latency with development (which is too large to be accounted for by alterations of the onset of neural activity: Colonnese et al., 2008).

Third, developmental alterations of the basal tone provided by amine transmitter systems may alter the blood flow response to neural activity, and thus alter the BOLD response, even in the absence of changes of neuronal information processing. However, it is currently unclear exactly how an increased baseline vasoconstriction might alter the BOLD signal. One possibility is that an overall greater restriction of blood flow would simply reduce the BOLD signal. On the other hand, tighter vasoconstriction might increase the amount by which a vessel can dilate in response to glutamatergic transmission, thereby increasing activity-related blood flow responses and BOLD signals (Blanco et al., 2008). Consistent with this, dilation of blood vessels with CO_2 to increase basal blood flow has been shown to decrease the BOLD response (Cohen et al., 2002) and also alters the apparent area of activation by altering the signal to noise ratio (Thomason et al., 2005). Of course developmental changes in amine systems will also produce developmental changes in neuronal function, for example dopamine system development between childhood and adulthood can directly modulate the excitability of interneurons in the prefrontal cortex (Tseng and O'Donnell, 2007). The challenge, as with "pharmacological fMRI" of adults in which amine systems are manipulated with drugs (Attwell and Iadecola, 2002) is to separate amine effects on neuronal function from effects on neurovascular coupling.

7.5.3 Expansion or contraction of the spatial area activated within one anatomical region

Changes in the area showing BOLD activation within an anatomical region are often used to infer changes in the underlying neuronal processing. An expansion of the activated area of V1 after trace (but not after delay) eyeblink conditioning of rabbits (Miller et al., 2008) was interpreted as showing that more neurons were activated after learning to carry out the more cognitively complex task. In humans, expansion of activated somatosensory and motor areas over a three week period of motor skill acquisition was considered to reflect the cortical plasticity that underpinned performance improvement (Karni et al., 1998; Hluštík et al., 2004). Importantly, while Miller et al's work studied relatively rapid changes in synaptic strength, allowing

unequivocal conclusions to be reached, for longer-term learning and developmental studies over greater time durations changes in neurovascular coupling need to be ruled out as a cause of the activated area altering in size. In addition, because changes of the amplitude of the BOLD signal also commonly occur during development, it is essential to consider the possibility that the activated area merely appears to change in size because of an altered signal to noise ratio.

Changes in the spatial scale of neurovascular coupling may come about as a consequence of the developmental changes described in Section 7.3. Alterations of enzyme levels (see Section 7.3) will change the spatial area over which levels of neurovascular messengers are produced at a high enough concentration to affect blood vessels, and the development of the astrocyte network (Binmöller and Müller, 1992) may allow neurons to influence more distant vessels. Furthermore, the development of the vascular network itself may either provide more spatially localised control of blood flow (due to local control of individual vessels developing within a network which has increased in vessel density) or allow activity in one area to influence blood flow over a larger area (if vascular dilatory responses propagate back to larger vessels which feed a larger volume of brain: Iadecola et al., 1997). However, whereas the expansion of the activated area reported by Miller et al. (2008) occurred on a millimetre scale, neurovascular coupling changes seem more likely to alter blood flow on a scale of a few hundred microns.

Frequently, brain development is associated with a decrease in the area activated in BOLD studies, correlating with the refinement of cortical wiring being accompanied by a shift from spatially diffuse task-specific brain activity to more focal brain activity, as regional specialisation emerges. For example, Casey et al. (2002) in the striatum and hippocampus, and Gaillard et al. (2000) and Passarotti et al. (2003) in the cortex, using stimulus-response compatibility, verbal fluency, and face matching tasks, respectively, found that progression from childhood to adulthood was accompanied by a shift from diffuse to more focal activation. This supports the idea that, before precise pruning, the less efficient connections that exist result in more widespread activity in response to tasks that later activate only highly specialised brain areas.

Part of the increasing spatial localization of BOLD signals that occurs may reflect the development of inhibitory circuits. GABAergic signalling is thought to decrease the BOLD signal by inhibiting excitatory cells, thus reducing glutamate release and decreasing the local CBF response (Lauritzen, 2005; Lauritzen and Gold, 2003; Muthukumaraswamy et al., 2009; Donahue et al., 2010). This may enhance the spatial localization of positive BOLD responses by generating an area of decreased neuronal firing and decreased blood flow around a central area of increased cell firing (Devor et al., 2007). This development of inhibitory

responses may also contribute to sparser stimulus-evoked activation. In adult monkeys, for example, visual object learning is associated with more selective object representation in the inferior temporal cortex (Baker et al., 2002; Sigala and Logothetis, 2002), and in humans, the fusiform face area (FFA) has been shown to respond to faces with increasing selectivity across development from childhood to adulthood (Peelen et al., 2009). Similarly, the spatial receptive field organisation in topographically mapped regions becomes increasingly refined, and blocking inhibition removes this specificity (Sillito, 1975; Crook et al., 1998). As noted in Section 7.3.2, some inhibitory interneurons release nitric oxide. Thus, in addition to indirectly reducing the BOLD signal by inhibiting glutamatergic neurons, interneuron activity can influence the BOLD signal through the release of NO and other vasoactive agents that directly regulate the local blood flow.

In early development, GABA is not inhibitory but produces depolarizing potentials, perhaps providing an excitatory drive for synapse formation before glutamate takes over (Ben-Ari et al., 1989; Ben-Ari, 2002; Cherubini et al., 1991; Tyzio et al., 2011; but see Rheims et al., 2009). This occurs because at young ages the Nernst potential for the Cl^- ions that pass through $GABA_A$ receptors is more positive than the resting potential. The reduction and spatial sharpening of the BOLD signal by inhibitory activity may, therefore, not be in effect until glutamate and GABA are well established in their mature roles as excitatory and inhibitory neurotransmitters. Once GABA is inhibitory, increases in the strength of GABAergic inhibition may decrease the size of the BOLD signal (Muthukumaraswamy et al., 2009; Donahue et al., 2010), thus decreasing the signal to noise ratio and possibly decreasing the area apparently activated, or even induce negative BOLD signals (Northoff et al., 2007).

7.6 Can neurovascular coupling changes ever be ruled out as a cause of developmental BOLD changes?

The main message of this chapter is that developmental changes in neurovascular coupling are likely to contribute to observed developmental changes in BOLD signals. How, then, can the BOLD researcher reliably attribute changes in BOLD signals to a change in neural information processing rather than a change of blood flow control? While there is no simple answer to this question, I believe there are three approaches to the problem.

First, being aware (for example from animal work) of the changes of neurovascular coupling and blood volume fraction that are occurring in the region of interest over the period under consideration, it may be possible to rule them out as a cause of the changes seen. For example, changes in the spatial scale of BOLD responses may be larger than is plausible to be explained by changes in astrocyte morphology or blood

vessel branching patterns, as outlined above. Similarly, changes that occur rapidly as a result of learning, at a time after the enzyme systems controlling blood flow have matured, are unlikely to reflect alterations of neurovascular coupling or blood volume fraction. However, it is always possible that studies which document a change during development in the amplitude of the BOLD signal in a particular area may be confounded by developmental changes of neurovascular signalling mechanisms (or neuronal energy use) that have yet to be discovered by researchers working at the cellular level. Measuring how development alters some parameter of the stimulus that evokes a BOLD response may suggest an explanation in terms of changes of neural information processing (e.g. an increase in a parameter describing the specificity of a stimulus may be interpreted in terms of increasing lateral inhibition between cortical columns or between different cortical areas), but it is still necessary to consider whether non-linear changes in the relationship between neuronal activity and blood flow could account for the data. It is not obvious how any kind of subtractive protocol design can get around the need to consider possible confounding by changes of neurovascular coupling.

Second, detailed information on the changes of neurovascular coupling and of neural energy use occurring over the period of a study will often not be available, particularly for humans. In this case a functional approach needs to be taken. Church et al. (2010) have put forward the notion that neurovascular coupling changes cannot be the cause of changes of BOLD signal during development if different tasks produce opposing changes with development in the same area (i.e. one task produces an increase in response with development, while the other task produces a decrease with development). This is a promising approach, but one needs to be sure that the same input connections to the area studied are activated for both tasks. As noted in Section 7.3, the relationship between blood flow and neuronal activity is different for different inputs to cortical regions (Enager et al., 2009), and so may undergo different developmental changes.

Thirdly, it may be advantageous to document, and try to understand, developmental BOLD changes in simpler “low level” neural circuits, such as the visual, somatosensory and auditory cortices, the wiring and function of which are reasonably well known, in order to have a better framework for interpreting changes of BOLD signals in “higher” areas where the neural basis of the information processing is far more poorly understood. I therefore advocate the construction of a publicly accessible database as a repository in which to deposit atlases of BOLD responses to standard stimuli, recorded in a standardised imaging setting at key developmental stages. The stimuli used could include stationary and drifting gratings or random moving dots for the visual system, vibration to the skin for the somatosensory system, and tone sequences for the auditory system (some stimuli for which BOLD signals in sensory cortices are reasonably well understood in terms of

the responses of neurons are collected by Schölvinck et al. (2008).

Ultimately, a full understanding of developmental changes in BOLD responses is likely to require much work characterising how neurovascular coupling alters, in order to isolate changes produced by the maturation of neural information processing. Being aware of this issue is crucial for the rigorous interpretation of developmental fMRI studies.

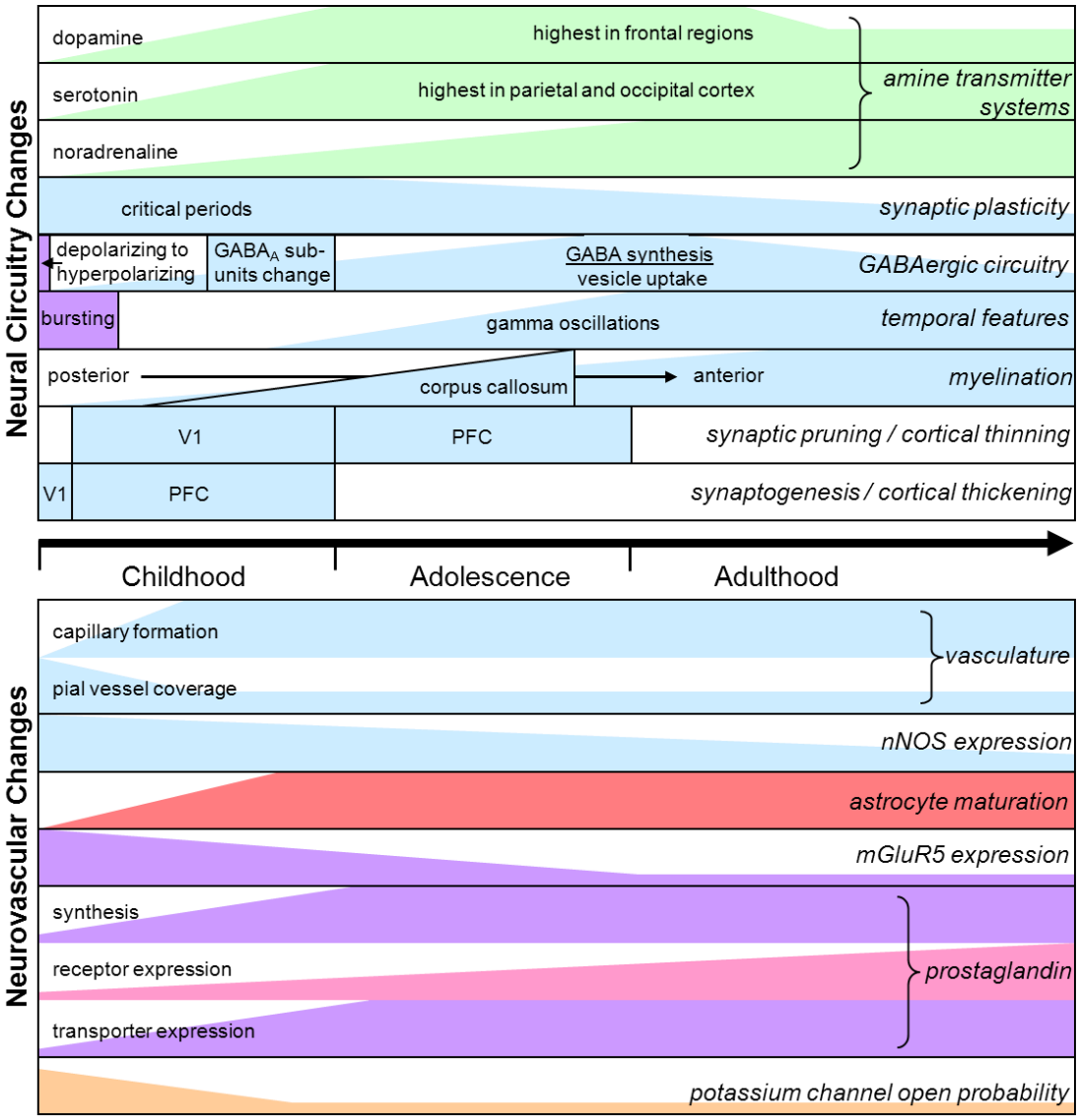

Figure 7.1: Summary of the developmental time courses of changes in neural information processing mechanisms (top) and of components of the signalling pathways regulating blood flow and thus controlling the BOLD response (bottom). Changes shown in blue are from human data; green is from macaque; lilac from rat or mouse; red from cat; pink from pig; light orange from rabbit.

Chapter 8: Discussion

8.1 Introduction

In this Chapter I will summarize and evaluate the findings presented within this thesis. I have discussed my findings at the end of each preceding results chapter, so here I will briefly review these results and describe possible future experiments that could further the work.

8.2 Distinguishing pericytes from other perivascular cell classes

8.2.1 Discussion

As there is no specific marker for pericytes and different pericytes may have different developmental origins (Díaz-Flores et al., 2009) suggesting that there may be several distinct populations of these cells, it is of use to have multiple markers that label the same population to increase confidence in cell identification. Although I mainly used NG2 as the marker for pericytes in this thesis, because I was able to use the NG2-DsRed transgenic mice, I confirmed in Chapter 3 that other markers could also be used to identify the same population of cells that I was studying, specifically PDGFRβ or isolectin-B_4. I also showed that some pericytes appear to express the contractile proteins desmin and αSMA, however these results were not conclusive. Lastly, I found that pericytes defined by NG2 expression do not overlap with endothelial cells (defined by vWF expression) or perivascular immune cells (defined by Iba-1 expression).

It is possible that not all perivascular immune cells were labelled by Iba1. There is a marker, ED2, that is thought to be specific for perivascular immune cells (part of the scavenger receptor CD163; Graeber et al., 1989). I tried to label brain tissue from the NG2-DsRed mice with an antibody for ED2 but in my hands this antibody showed only nonspecific labelling.

Due to their suggested role in blood flow control it was of great interest to investigate the contractile protein expression of these cells. My findings supported previous work showing that pericytes on larger capillaries express contractile protein but pericytes on smaller, true, capillaries did not. However, to be able to make any statements about the proportion or subpopulation of pericytes that are contractile, further work will be needed to study the expression profile throughout the arterio-venous axis. My study only focused on a small population of capillaries.

8.2.2 Future work

Although there was no overlap between the endothelial cell population, or immune cells labelled with Iba1, and pericytes, it is possible that there are other, less well characterized perivascular cells that could be mistaken for pericytes, such as stem cell progenitors (Zimmerlin et al., 2011; Crisan et al., 2008; Corselli et al., 2010). Using the same technique as I did in Chapter 3, labelling of NG2-DsRed tissue using an antibody that targets mesenchymal stem cells (such as CD44, CD73, CD90, and CD105; Corselli et al., 2010), I could investigate whether the cells that I identify as pericytes express mesenchymal stem cell markers.

The majority of the experiments in this chapter were carried out on juvenile animals between postnatal days 10 and 15. As I discussed in Chapter 1 (section 1.5.2), pericytes are thought to have different functions at different developmental stages, and thus it may be expected that the proteins they express change with development. In order to explore whether the pericyte markers that I investigated in this thesis (NG2, PDGFRβ and isolectin-B_4) change with maturation, I could carry out labelling experiments in adult brain tissue. This would enable me to compare any possible overlap in expression of these markers at different developmental stages. If I were to see the occurrence of cells that share expression of these markers that may lead to further questions about changes in pericyte function at different developmental stages.

The labelling studies I carried out using antibodies for contractile proteins markers (αSMA and desmin) did not enable me to quantify the proportion of pericytes that express contractile proteins. In order to get more solid data for this, I think that work needs to go into the rigorous classification of vessels. It has been said that 'true' capillary pericytes do not express contractile proteins and my work supports the finding that expression is more likely on larger capillaries. What is not clear, however, is when we should define a vessel as an arteriole rather than a capillary. Pericytes are present on both of these classes of vessel. There are morphological differences in these cells throughout the microvasculature, and apparently changes in protein expression, but they are still currently classed as the same cell type. The definition of capillaries that I used in this thesis was that capillaries are vessels of less than 10 μm in diameter (although the average diameter of the vessels studied in Chapter 4 was in fact 4.88±0.97 μm) that do not have a continuous lining of smooth muscle. Many vessels that would be classed by others as pre-capillary arterioles have a diameter similar to the vessels that I studied and may not have a smooth muscle layer as seen using bright field imaging. The few imaging studies that I have carried out trying to investigate neurovascular coupling at the level of arterioles led to ambiguity in distinguishing them from capillaries and venules. Using brain tissue from the NG2-DsRed mouse I could carry out a study looking at the morphology of vascular smooth muscle cells and pericytes

starting from large pial vessels, following the same vessel into the tissue and investigating the changes that occur as the vessel branches, such as the change in the distance between the nuclei of smooth muscle cell/pericytes, the change in the morphology of these cells and the change in expression within them of contractile proteins (such as αSMA). This may help to prevent misclassification of vessels, or even to allow a further sub-classification of vessel types.

8.3 Signalling pathways underlying pericyte dilation of CNS capillaries in response to glutamate

8.3.1 Discussion

It was found by Peppiatt et al. (2006) that glutamate produces capillary dilation in cerebellar slices. I replicated these experiments and investigated the mechanisms by which glutamate evokes this response. I found that nitric oxide is needed for glutamate-evoked dilation, but that it is not acting through generating cGMP but rather by inhibiting 20-HETE production. In addition, activation of EP_4 receptors, presumably by PGE_2, produces dilation.

These results show similarities to studies looking at the signalling pathways involved in neurovascular coupling at the arteriole level, which suggests that capillaries are also actively involved in neurovascular coupling. However, most evidence (including mine) supporting an active role of pericytes in controlling blood flow has come from *in vitro* studies, either in culture, in retinal whole mounts or in brain slices.

8.3.2 Future work

For the experiments in Chapter 4 I used bath application of glutamate to mimic neuronal activity. Synaptic glutamate release, during neuronal activity, has a very different time frame from bath application of a drug (milliseconds compared to minutes). In order to look at more physiologically realistic responses it would be interesting to use electrical stimulation of neurons whilst imaging nearby capillaries. In the cerebellum it would be possible to stimulate the parallel fibres whilst imaging the vessels that span the molecular layer. These experiments would provide a more physiologically relevant model of neuronal activity. Based on the work in this thesis, Anusha Mishra and Fergus O'Farrell in the lab have found that parallel fibre stimulation does indeed give a dilation of cerebellar capillaries which is blocked by an EP_4 receptor antagonist.

I carried out the imaging experiments in this Chapter using bright-field imaging. Because of this I could not always visualise pericytes on the capillaries that I imaged. Carrying out the same experiments using the NG2-DsRed mice and fluorescence imaging would allow me to identify pericytes as well as pericyte

processes on the vessels that I image. Using only fluorescence imaging, it is possible to measure the diameter of the vessel by measuring the light intensity profile of the vessel (using the DsRed). This however does not measure the vessel lumen well but measures the inner or outer diameter of pericytes on the outside of the endothelial cells. In the few experiments I have carried out using this technique, diameter changes measured using the DsRed fluorescence were very small. This may be because the change in diameter assessed from the pericyte being imaged does not reflect the change in diameter of the underlying vessel lumen. In order to confirm the presence of pericytes but also measure capillary lumen diameter, I could combine fluorescence and bright-field imaging.

The pharmacological work described in Chapter 4 took about 1.5 years to perform, but still leaves some uncertainties. In order to rule out the involvement of (constitutive) endothelial nitric oxide production I could use a specific inhibitor of endothelial nitric oxide synthase. Similarly, to confirm that the agonist activating EP_4 receptors is PGE_2, I could pharmacologically block PGE_2 production with cyclooxygenase inhibitors (SC-560 to block COX-1 and NS-398 to block COX-2). There is still a slight glutamate-evoked dilation in the presence of L-161,982 (Chapter 4.3.10). While this may just reflect incomplete block, it would be of interest to carry out experiments with a combination of L-NNA and L-161,982 (or a cyclooxygenase inhibitor) to confirm that the glutamate-evoked dilation is completely abolished with both the nitric oxide and prostaglandin pathways blocked. There are many other vasoactive mediators that may also be involved (e.g. adenosine, potassium, PGI_2; see Attwell et al., 2010) so it is possible that there may be another pathway contributing to the glutamate-evoked capillary dilation.

The pharmacological agents I used in this thesis were mostly antagonists. It has been suggested that different results can be found when using agonists rather than antagonists. PGE_2, specifically, has been shown to cause arteriole constriction (Dabertrand et al., 2013), which contradicts research using blockers that suggest PGE_2 is a vasodilator (Zonta et al., 2003). Dabetrand and colleagues (2013) suggest that blocking prostaglandin production alters synaptic signalling and thus indirectly alters neurovascular coupling. I could carry out experiments to investigate whether application of PGE_2 would evoke a cerebellar capillary dilation similar to the dilation observed on application of glutamate.

The magnitude of the response to stimulation has been found to depend on the tone of vessel (Fergus et al., 1995; Blanco et al., 2008). In order to achieve a more physiological vessel tone, and thus allow more physiological responses to glutamate (or electrical stimulation), it may be possible to penetrate an upstream arteriole and perfuse with solution (Lovick et al., 2004). This would most likely cause damage to the arteriole,

but would hopefully not have an effect at the site of the downstream capillary that is being imaged. This technique may produce more reliable pre-constriction than application of noradrenaline, which only constricts approximately 50% of vessels (Peppiatt et al., 2006). However Lovick reports that this technique is extremely difficult (personal communication to David Attwell).

It would be interesting to see whether similar pathways are involved in the glutamate-evoked capillary dilation in all other brain regions, since there is evidence that neurovascular coupling varies over different brain regions (Devonshire et al., 2012). Based on my work, Anusha Mishra in the lab has shown that EP_4 receptor block also inhibits glutamate-evoked capillary dilation in cortical capillaries.

8.4 Electrical responses of cerebellar and cortical pericytes

8.4.1 Discussion

In Chapter 5, I reported that pericytes can be patch-clamped in slices and that glutamate application produces an outward current in pericytes while noradrenaline application produces an inward current, which are expected to produce dilation and constriction respectively.

8.4.2 Future work

In order to study further the link between pericyte membrane currents and tone, I would like to look at the effect of the pharmacological agents that I used in Chapter 4 on pericyte membrane currents. If pericyte hyperpolarization does underlie capillary dilation then I would expect the glutamate-induced outward current to be suppressed by L-NNA and L161,982.

As I stated above, glutamate application is not the most physiologically relevant model of neuronal activity and I would like to carry out further experiments using electrical stimulation to mimic neuronal activity and release of endogenous glutamate. It would be of interest to see if electrical stimulation produces a hyperpolarization of pericytes.

My success rate in patch-clamping pericytes was not very high. These cells are covered in basement membrane and I found that the pipette resistance increased by very little, even when the pipette was clearly touching the cell. Previous studies have incubated tissue in a collagenase enzyme before carrying out experiments to break down the basement membrane and increase accessibility to the cell (Peppiatt et al., 2006). I would like to try this, but if I am still unable to successfully patch-clamp enough cells I could use calcium imaging (with AM-ester dye-loading) to monitor pericyte intracellular signalling. This technique could

be used alongside measurement of vessel diameter, to allow investigation of the extent to which [Ca^{2+}] changes are solely responsible for controlling pericyte tone.

8.5 The pericyte response to ischaemia

8.5.1 Discussion

In Chapter 6 I demonstrated that pericytes were vulnerable to death when exposed to oxygen and glucose deprivation as well as OGD followed by reperfusion. Pericyte death was reduced when slices were incubated with ionotropic glutamate receptor blockers or in calcium free extracellular solution. I also found that pericyte death following MCAO was much more pronounced that endothelial cell death.

These results suggest that pericytes may be a useful therapeutic target for reducing damage following stroke. Preventing pericyte death following ischaemia may improve cerebral blood flow recovery. The resulting increased energy supply to the brain may reduce further neuronal death.

8.5.2 Future work

Although I was able to target some pathways that were able to reduce pericyte death in OGD and reperfusion, I was not able to identify a drug that could be translated to the *in vivo* setting. Ideally, carrying out the same experiments using other drugs that are thought to be involved in excitotoxic death might identify a drug that could be taken thorough to *in vivo* experiments, and potentially clinical trials.

There is a possibility that the mitochondrial calcium uptake inhibitor that I tested in Chapter 6, Ru360, may fail to penetrate cells sufficiently to produce a response (personal communication with Martin Lauritzen). There is also evidence that Ru360 undergoes oxidation, and thus inactivation, in room air (Abramov and Duchen, 2008). Because of these issues it may be worth repeating these experiments with an alternative calcium uptake inhibitor.

In order to investigate the mechanisms of pericyte death during OGD and reoxygenation I could carry out experiments similar to those carried out in Chapter 6 but only expose the brain slices to the ‘drug’ (or calcium free solution) for either the OGD period or the reoxygenation period. I would be interested in identifying a mechanism of pericyte death, and hopefully recovery, that was specific to the reoxygenation period because this is the more realistic therapeutic window for treatment.

Although previous work has supported a role for oxidative stress in pericyte constriction in ischaemia (Yemisi et al., 2010), I found little effect of PBN and L-NNA on pericyte death in OGD with or without reoxygenation. These findings do not disagree with each other, because they measure different things, but

they do suggest that there are separate signalling pathways controlling pericyte constriction and pericyte death. I could carry out further studies to measure the diameter of capillaries that have been exposed to OGD and reoxygenation in the presence of blockers, especially PBN and L-NNA, in order to confirm the finding of Yemisci et al. (2010).

8.6 The physiology of developmental changes in BOLD functional imaging signals

8.6.1 Discussion

In Chapter 7, I discussed the information processing and cognitive changes that occur over development that many psychology researchers are interested in investigating using BOLD fMRI. I then speculated how these changes may be obscured in fMRI experiments by corresponding changes in neurovascular coupling and energy use over the same time period. I described example case studies in which changes in BOLD responses were observed over development and discussed the possible ways that information processing changes could be clearly distinguished from changes in energy use and neurovascular coupling.

8.6.2 Future work

As discussed in Chapter 7 section 7.6, several potential ways of ruling out potential differences in neurovascular coupling and energy use between participants experimentally have been proposed. The most promising way of increasing our understanding of the relationship between neuronal activity and the BOLD signal is by using a combination of imaging and physiological research in animals (Devonshire et al., 2012; Schulz et al., 2012). In human studies, researchers can use a combination of BOLD and measurement of electrical activity through EEG.

Along with experimental techniques, researchers can make sure they are aware of the possible changes in neurovascular coupling that are occurring over the period of study and take this in to account when interpreting their results. I believe that the field will benefit greatly from being aware of the confounds that measuring neuronal activity with BOLD fMRI indirectly introduces. I have co-written another review with Julia Harris discussing similar problems that may arise when comparing the BOLD responses between participants with autism and control participants (Reynell and Harris, 2013). Much like in development, neurovascular coupling pathways may be altered in autism. Similar literature reviews would be beneficial for other participant differences, such as gender and medication state. Although these literature reviews are highly speculative, it is of use for researchers to make themselves aware of the issues that may be influencing their results.

8.7 Conclusions

In summary, the work presented in this thesis has investigated the characteristics of CNS pericytes and the role they play in neurovascular coupling in physiological and pathological conditions. The experiments undertaken provide information which will further the understanding of the regulation of brain blood supply in health and disease. They also provide insight into the cellular mechanisms which underlie functional brain imaging, and will aid our understanding and interpretation of these signals.

Bibliography

Aarts M, Iihara K, Wei WL, Xiong ZG, Arundine M, Cerwinski W, MacDonald JF, Tymianski M.2003. A key role for TRPM7 channels in anoxic neuronal death. Cell 115(7):863-877.

Abramov AY, Duchen MP. 2008. Mechanisms underlying the loss of mitochondrial membrane potential in glutamate excitotoxicity. Biochim Biophys Acta. 1777:953-964.

Aiello EA, Walsh MP, Cole WC. 1995. Phosphorylation by protein kinase A enhances delayed rectifier K+ current in rabbit vascular smooth muscle cells. Am J Physiol. 268(2):H926-934.

Akerman CJ, Cline HT. 2007. Refining the roles of GABAergic signalling during neural circuit formation. Trends Neurosci. 30:382-389.

Akgören N, Dalgaard P, Lauritzen M. 1996. Cerebral blood flow increases evoked by electrical stimulation of rat cerebellar cortex: relation to excitatory synaptic activity and nitric oxide synthesis. Brain Res 710:204-214.

Akima M, Nonaka H, Kagesawa M, Tanaka K. 1987. A study on the microvasculature of the cerebellar cortex. Acta Neuropathol. 75:69-76.

Alkayed NJ, Narayanan J, Gebremedhin D, Medhora M, Roman RJ, Harder DR. 1996. Molecular characterization of an arachidonic acid epoxygenase in rat brain astrocytes. Stroke 27:971-979.

Alle H, Roth A, Geiger JR. 2009. Energy-efficient action potentials in hippocampal mossy fibers. Science 325:1405-1408.

Allt G, Lawrenson JG. 2001. Pericytes: cell biology and pathology. Cells Tissues Organs 169(1):1-11.

Alonso JM, Martinez LM. 1998. Functional connectivity between simple cells and complex cells in cat striate cortex. Nat Neurosci 1:395-403.

Ames A, Wright RL, Kowada M, Thurston JM, Majno G. 1968. Cerebral ischemia. II. The no-reflow phenomenon. Am J Pathol. 52(2):437-453.

Amruthesh SC, Boerschel MF, McKinney JS, Willoughby KA, Ellis EF. 1993. Metabolism of arachidonic acid to epoxyeicosatrienoic acids, hydroxyeicosatetraenoic acids, and prostaglandins in cultured rat hippocampal astrocytes. J Neurochem 61:150-159.

Anderson AW, Marois R, Colson ER, Peterson BS, Duncan CC, Ehrenkranz RA, Schneider KC, Gore JC, Ment LR. 2001. Neonatal auditory activation detected by functional magnetic resonance imaging. Magn Reson Imaging 19:1-5.

Arima T, Kitamura Y, Nishiya T, Kiriyama Y, Taniguchi T, Nomura Y. 1997. NG-nitro-L-[3H]arginine binding properties of neuronal nitric oxide synthase in rat brain. Neurochem Int. 30(3):239-245.

Armulik A, Genové G, Betsholtz C. 2011. Pericytes: developmental, physiological, and pathological perspectives, problems, and promises. Dev Cell 21(2):193-215.

Armulik A, Genové G, Mäe M, Nisancioglu MH, Wallgard E, Niaudet C, He L, Norlin J, Lindblom P, Strittmatter K, Johansson BR, Betsholtz C. 2010. Pericytes regulate the blood-brain barrier. Nature. 468(7323):557-561.

Arnerić SP, Honig MA, Milner TA, Greco S, Iadecola C, Reis DJ. 1988. Neuronal and endothelial sites of acetylcholine synthesis and release associated with microvessels in rat cerebral cortex: ultrastructural and neurochemical studies. Brain Res. 454(1-2):11-30.

Atallah BV, Scanziani M. 2009. Instantaneous modulation of gamma oscillation frequency by balancing excitation with inhibition. Neuron 62:566-577.

Attwell D, Buchan AM, Charpak S, Lauritzen M, Macvicar BA, Newman EA. 2010. Glial and neuronal control of brain blood flow. Nature 468:232-243.

Attwell D, Iadecola C. 2002. The neural basis of functional brain imaging signals. Trends Neurosci 25:621-625.

Attwell D, Laughlin SB. 2001. An energy budget for signaling in the grey matter of the brain. J Cereb Blood Flow Metab 21:1133-1145.

Baird AA, Gruber SA, Fein DA, Maas LC, Steingard RJ, Renshaw PF, Cohen BM, Yurgelun-Todd DA. 1999. Functional magnetic resonance imaging of facial affect recognition in children and adolescents. J Am Acad Child Adolesc Psychiatry 38:195-199.

Baker CI, Behrmann M, Olson CR. 2002. Impact of learning on representation of parts and wholes in monkey inferotemporal cortex. Nat Neurosci 5:1210-1216.

Balabanov R, Dore-Duffy P. 1998. Role of the CNS microvascular pericyte in the blood-brain barrier. J Neurosci Res 53:637-644.

Balabanov R, Washington R, Wagnerova J, Dore-Duffy P. 1996. CNS microvascular pericytes express macrophage-like function, cell surface integrin alpha M, and macrophage marker ED-2. Microvasc Res 52:127-142.

Ballabh P, Braun A, Nedergaard M. 2004. The blood-brain barrier: an overview: structure, regulation, and clinical implications. Neurobiol Dis. 16(1):1-13.

Bandettini PA, Wong EC. 1997. A hypercapnia-based normalization method for improved spatial localization of human brain activation with fMRI. NMR Biomed 10:197–203.

Bano D, Nicotera P. 2007. Glutamate-independent calcium toxicity: introduction. Ca2+ signals and neuornal death in brain ischemia. Stroke 38:674-676.

Bandopadhyay R, Orte C, Lawrenson JG, Reid AR, De Silva S, Allt G. 2001. Contractile proteins in pericytes at the blood-brain barriers. J. Neurocytology 30:35-44.

Barón M, Gallego A. 1972. The relation of the microglia with the pericytes in the cat cerebral cortex. Z Zellforsch Mikrosk Anat. 128(1):42-57.

Bauer HC, Bauer H, Lametschwandtner A, Amberger A, Ruiz P, Steiner M. 1993. Neovascularization and the appearane of morphological charachteristics of the blood-brain barrier in the embryonic mouse central nervous system. Brain Res Dev Brain Res. 75(2):269-278.

Bautch VL. 2011. Stem cells and the vasculature. Nat Med. 17(11):1437-1443.

Beazley MA, Tong A, Wei WL, Van Tol H, Sidhu B, MacDonald JF. 2006. D2-class dopamine receptor inhibition of NMDA currents in prefrontal cortical neurons is platelet-derived growth factor receptor-dependent. J Neurochem. 98(5):1657-1663.

Bechmann I, Priller J, Kovac A, Böntert M, Wehner T, Klett FF, Bohsung J, Stuschke M, Dirnagl U, Nitsch R. 2001. Immune surveillance of mouse brain perivascular spaces by blood-borne macrophages. Eur J Neurosci. 14(10):1651-1658.

Behm DJ, Ogbonna A, Wu C, Burns-Kurtis CL, Douglas SA. 2009. Epoxyeicosatrienoic acids function as selective, endogenous antagonists of native thromboxane receptors: identification of a novel mechanism of vasodilation. J Pharmacol Exp Ther 328:231-239.

Bekar LK, He W, Nedergaard M. 2008. Locus coeruleus alpha-adrenergic-mediated activation of cortical astrocytes *in vivo*. Cereb Cortex 18:2789-2795.

Bell RD, Winkler EA, Sagare AP, Singh I, LaRue B, Deane R, Zlokovic BV. 2010. Pericytes control key neurovascular functions and neuronal phenotype in the adult brain and during brain aging. Neuron 68(3):409-427.

Bellamy TC, Garthwaite J. 2002. Pharmacology of the nitric oxide receptor, soluble guanylyl cyclase, in cerebellar cells. Br J Pharmacol. 136(1):95-103.

Ben-Ari Y. 2002. Excitatory actions of gaba during development: the nature of the nurture. Nat Rev Neurosci 3:728-739.

Ben-Ari Y, Cherubini E, Corradetti R, Gaiarsa JL. 1989. Giant synaptic potentials in immature rat CA3 hippocampal neurones. J Physiol 416:303-325.

Benagiano V, Virgintino D, Maiorano E, Rizzi A, Palombo S, Roncali L, Ambrosi G. 1996. VIP-like immunoreactivity within neurons and perivascular neuronal processes of the human cerebral cortex. Eur J Histochem. 40(1):53-56.

Benes FM, Turtle M, Khan Y, Farol P. 1994. Myelination of a key relay zone in the hippocampal formation occurs in the human brain during childhood, adolescence, and adulthood. Arch Gen Psychiatry 51:477-484.

Bengtsson SL, Nagy Z, Skare S, Forsman L, Forssberg H, Ullen F. 2005. Extensive piano practicing has regionally specific effects on white matter development. Nat Neurosci 8:1148-1150.

Berg BR, Cohen KD, Sarelius IH. 1997. Direct coupling between blood flow and metabolism at the capillary level in striated muscle. Am J Physiol. 272:H2693-2700.

Bergers G, Song S. 2005. The role of pericytes in blood-vessel formation and maintenance. Neuro Oncol. 7(4):452-464.

Bernstrom K, Kayganich K, Murphy RC, Fitzpatrick FA. 1992. Incorporation and distribution of epoxyeicosatrienoic acids into cellular phospholipids. J Biol Chem 267:3686-3690.

Betsholtz C. 2004. Insight into the physiological functions of PDGF through genetic studies in mice. Cytokine Growth Factor Rev. 15(4):215-228.

Betz AL, Goldstein GW. 1986. Specialized properties and solute transport in brain capillaries. Annu Rev Physiol. 48:241-250.

Bhardwaj A, Northington FJ, Carhuapoma JR, Falck JR, Harder DR, Traystman RJ, Koehler RC. 2000. P-450 epoxygenase and NO synthase inhibitors reduce cerebral blood flow response to N-methyl-D-aspartate. Am J Physiol Heart Circ Physiol. 279(4):H1616-1624.

Binmöller FJ, Müller CM. 1992. Postnatal development of dye-coupling among astrocytes in rat visual cortex. Glia 6:127-137.

Blakemore C. 1979. The development of stereoscopic mechanisms in the visual cortex of the cat. Proc R Soc Lond B Biol Sci 204:477-484.

Blakemore SJ. 2008. The social brain in adolescence. Nat Rev Neurosci 9:267-277.

Blakemore SJ, Choudhury S. 2006. Development of the adolescent brain: implications for executive function and social cognition. J Child Psychol Psychiatry 47:296-312.

Blakemore SJ, den Ouden H, Choudhury S, Frith C. 2007. Adolescent development of the neural circuitry for thinking about intentions. Soc Cogn Affect Neurosci 2:130-139.

Blanco VM, Stern JE, Filosa JA. 2008. Tone-dependent vascular responses to astrocyte-derived signals. Am J Physiol Heart Circ Physiol 294:H2855-2863.

Boado RJ, Pardridge WM. 1994. Differential expression of alpha-actin mRNA and immunoreactive protein in brain microvascular pericytes and smooth muscle cells. J Neurosci Res. 39(4):430-435.

Bolanos JP, Garcia-Nogales P, Almeida A. 2004. Provoking neuroprotection by peroxynitrite. Curr Pharm Des. 10(8):867-877.

Bolotina VM, Najibi S, Palacino JJ, Pagano PJ, Cohen RA. 1994. Nitric oxide directly activates calcium-dependent potassium channels in vascular smooth muscle. Nature 368:850-853.

Bondjers C, He L, Takemoto M, Norlin J, Asker N, Hellström M, Lindahl P, Betsholtz C. 2006. Microarray analysis of blood microvessels from PDGF-B and PDGF-Rbeta mutant mice identifies novel markers for brain pericytes. FASEB J 20(10):1703-1705.

Bondjers C, Kalém M, Hellström M, Scheidl SJ, Abramsson A, Renner O, Lindahl P, Cho H, Kehrl J, Betsholtz C. 2003. Transcription profiling of platelet-derived growth factor-B-deficient mouse embryos identifies RGS5 as a novel marker for pericytes and vascular smooth muscle cells. Am J Pathol. 162(3):721-729.

Born P, Leth H, Miranda MJ, Rostrup E, Stensgaard A, Peitersen B, Larsson HB, Lou HC. 1998. Visual activation in infants and young children studied by functional magnetic resonance imaging. Pediatr Res 44:578-583.

Borysova L, Wray S, Eisner DA, Burdyga T. 2013. How calcium signals in myocytes and pericytes are integrated across *in situ* microvascular networks and control microvascular tone. Cell Calcium 54(3):163-174.

Bourgeois JP, Rakic P. 1993. Changes of synaptic density in the primary visual cortex of the macaque monkey from fetal to adult stage. J Neurosci 13:2801-2820.

Brauer J, Neumann J, Friederici AD. 2008. Temporal dynamics of perisylvian activation during language processing in children and adults. Neuroimage 41:1484-1492.

Bringmann A, Biedermann B, Reichenbach A. 1999. Expression of potassium channels during postnatal differentiation of rabbit Muller glial cells. Eur J Neurosci 11:2883-2896.

Burette A, Zabel U, Weinberg RJ, Schmidt HH, Valtschanoff JG. 2002. Synaptic localization of nitric oxide synthase and soluble guanylyl cyclase in the hippocampus. J Neurosci 22:8961-8970.

Burnette JO, White RE. 2006. PGI2 opens potassium channels in retinal pericytes by cyclic AMP-srimulated, cross-activated of PKG. Exp Eye Res. 83(6):11359-1365.

Busija DW, Bari F, Domoki F, Louis T. 2007. Mechanisms involved in the cerebrovascular dilator effects of N-methyl-d-aspartate in cerebral cortex. Brain Res Rev 56:89-100.

Buxton RB, Uludağ K, Dubowitz DJ, Liu TT. 2004. Modeling the hemodynamic response to brain activation. NeuroImage 23 Suppl 1:S220-233.

Campbell WB, Gebremedhin D, Pratt PF, Harder DR. 1996. Identification of epoxyeicosatrienoic acids as endothelium-derived hyperpolarizing factors. Circ Res 78:415-423.

Cancilla PA, Baker RN, Pollock PS, Frommes SP. 1972. The reaction of pericytes of the central nervous system to exogenous protein. Lab Invest. 26(4):376-383.

Cao C, Goo JH, Lee-Kwon W, Pallone TL. 2006. Vasa recta pericytes express a strong inward rectifier K^+ conductance. Am J Physiol Regul Integr Comp Physiol. 290(6):R1601-1607.

Cao X, Phillis JW. 1994. alpha-Phenyl-tert-butyl-nitrone reduces cortical infarct and edema in rats subjected to focal ischemia. Brain Res. 644(2):267-272.

Carney JM, Floyd RA. 1991. Protection against oxidative damage to CNS by alpha-phenyl-tert-butyl nitrone (PBN) and other spin-trapping agents: a novel series of nonlipid free radical scavengers. J Mol Neurosci. 3(1):47-57.

Casey BJ, Cohen JD, Jezzard P, Turner R, Noll DC, Trainor RJ, Giedd J, Kaysen D, Hertz-Pannier L, Rapoport JL. 1995. Activation of prefrontal cortex in children during a nonspatial working memory task with functional MRI. Neuroimage 2:221-229.

Casey BJ, Thomas KM, Davidson MC, Kunz K, Franzen PL. 2002. Dissociating striatal and hippocampal function developmentally with a stimulus-response compatibility task. J. Neurosci. 22:8647-8652.

Catania MV, Landwehrmeyer GB, Testa CM, Standaert DG, Penney JB, Jr., Young AB. 1994. Metabotropic glutamate receptors are differentially regulated during development. Neuroscience 61:481-495.

Cauli B, Tong XK, Rancillac A, Serluca N, Lambolez B, Rossier J, Hamel E. 2004. Cortical GABA interneurons in neurovascular coupling: relays for subcortical vasoactive pathways. J Neurosci 24:8940-8949.

Chaigneau E, Oheim M, Audinat E, Charpak S. 2003. Two-photon imaging of capillary blood flow in olfactory bulb glomeruli. Proc Natl Acad Sci U S A 100:13081-13086.

Chan LS, Li WY, Khatami M, Rockey JH. 1986. Actin in cultured bovine retinal capillary pericytes: morphological and functional correlation. Exp Eye Res. 43(1):41-54.

Chan WY, Lorke DE, Tiu SC, Yew DT. 2002. Proliferation and apoptosis in the developing human neocortex. Anat Rec 267:261-276.

Cherubini E, Gaiarsa JL, Ben-Ari Y. 1991. GABA: an excitatory transmitter in early postnatal life. Trends Neurosci. 14:515-519.

Chiamulera C, Albertini P, Valerio E, Reggiani A. 1992. Activation of metabotropic receptors has a neuroprotective effect in a rodent model of focal ischaemia. Eur J Pharmacol. 216(2):335-336.

Chiron C, Raynaud C, Maziere B, Zilbovicius M, Laflamme L, Masure MC, Dulac O, Bourguignon M, Syrota A. 1992. Changes in regional cerebral blood flow during brain maturation in children and adolescents. J Nucl Med 33:696-703.

Cho H, Kozasa T, Bondjers C, Betsholtz C, Kehrl JH. 2003. Pericyte-specific expression of Rgs5: implications for PDGF and EDG receptor signaling during vascular maturation. FASEB J. 17(3):440-442.

Choi DW. 1985. Glutamate neurotoxicity in cortical cell culture is calcium dependent. Neurosci Lett. 58(3):293-297.

Christian S, Winkler R, Helfrich I, Boos AM, Besemfelder E, Schadendorf D, Augustin HG. 2008. Endosialin (Tem1) is a marker of tumor-assocaited myofibroblasts and tumor vessel-associateed mural cells. Am J Pathol. 172(2):486-494.

Church JA, Petersen SE, Schlaggar BL. 2010. The "Task B problem" and other considerations in developmental functional neuroimaging. Hum Brain Mapp 31:852-862.

Cinti S, Cigolini M, Bosello O, Björntorp P. 1984. A morphological study of the adipocyte precursor. J Submicrosc Cytol. 16(2):243-251.

Clark D, Sokoloff L. 1999. Circulation and energy metabolism of the brain. Basic Neurochemistry: Molecular, Cellular and medical aspects. Ed. GJ Siegel, BW Agranoff, RW Albers, SK, Fisher, MD Uhler pp 637-670 Philadelphia Lippincott-Raven.

Cohen Z, Bonvento G, Lacombe P, Hamel E. 1996. Serotonin in the regulation of brain microcirculation. Prog Neurobiol 50:335-362.

Cohen Z, Molinatti G, Hamel E. 1997. Astroglial and vascular interactions of noradrenaline terminals in the rat cerebral cortex. J Cereb Blood Flow Metab 17:894-904.

Cohen ER, Ugurbil K, Kim SG. 2002. Effect of basal conditions on the magnitude and dynamics of the blood oxygenation level-dependent fMRI response. J Cereb Blood Flow Metab 22:1042-1053.

Colonnese MT, Phillips MA, Constantine-Paton M, Kaila K, Jasanoff A. 2008. Development of hemodynamic responses and functional connectivity in rat somatosensory cortex. Nat Neurosci 11:72-79.

Conradi NG, Engvall J, Wolff JR. 1980. Angioarchitectonics of rat cerebellar cortex during pre- and postnatal development. Acta Neuropathol 50:131-138.

Conti MA, Adelstein RS. 1981. The relationship between calmodulin binding and phosphorylation of smooth muscle myosin kinase by the catalytic subunit of 3':5' cAMP-dependent protein kinase. J Biol Chem. 256(7):3178-3181.

Cornwell TL, Pryzwansky KB, Wyatt TA, Lincoln TM. 1991. Regulation of sarcoplasmic reticulum protein phosphorylation by localized cyclic GMP-dependent protein kinase in vascular smooth muscle cells. Mol Pharmacol. 40(6):923-931.

Corselli M, Chen CW, Crisan M, Lazzari L, Péault B. 2010. Perivascular ancestors of adult multipotent stem cells. Arterioscler Thromb Vasc Biol. 30(6):1104-1109.

Courtoy PJ, Boyles J. 1983. Fibronectin in the microvasculature: localization in the pericyte-endothelial interstitium. J Ultrastruct Res. 83(3):258-273.

Crisan M, Yap S, Casteilla L, Chen CW, Corselli M, Park TS, Andriolo G, Sun B, Zheng B, Zhang L, Norotte C, Teng PN, Traas J, Schugar R, Deasy BM, Badylak S, Buhring HJ, Giacobino JP, Lazzari L, Huard J, Péault

B. 2008. A perivascular origin for mesenchymal stem cells in multiple human organs. Cell Stem Cell 3(3):301-313.

Crook JM, Kisvárday ZF, Eysel UT. 1998. Evidence for a contribution of lateral inhibition to orientation tuning and direction selectivity in cat visual cortex: reversible inactivation of functionally characterized sites combined with neuroanatomical tracing techniques. Eur. J. Neurosci. 10:2056-2075.

Dabertrand R, Hannah RM, Pearson JM, Hill-Eubanks DC, Brayden JE, Nelson MT. 2013. Prostaglandin E2, a postulated astrocyte-derived neurovascular coupling agent, constricts rather than dilates parenchymal arterioles. J Cereb Blood Flow Metab. 33(4):479-482.

Daneman R, Zhou L, Kebede AA, Bares BA. 2010. Pericytes are required for blood-brain barrier integrity during embryogenesis. Nature 468(7323):562-566.

Darland DC, D'Amore PA. 2001. Cell-cell interactions in vascular development. Curr Top Dev Biol. 52:107-149.

Darland DC, Massingham LJ, Smith SR, Piek E, Saint-Geniez M, D'Amore PA. 2003. Pericyte production of cell-associated VEGF is differentiation-dependent and is associated with endothelial survival. Dev Biol 264(1):275-288.

Das A, Frank RN, Weber ML, Kennedy A, Reidy CA, Mancini MA. 1988. ATP causes retinal pericytes to contract *in vitro*. Exp Eye Res 46:349-62.

Davis RJ, Murdoch CE, Ali M, Purbrick S, Ravid R, Baxter GS, Tilford N, Sheldrick RL, Clark KL, Coleman RA. 2004. EP4 prostanoid receptor-mediated vasodilatation of human middle cerebral arteries. Br J Pharmacol 141:580-585.

de Oliveira F. 1966. Pericytes in diabetic retinopathy. Br J Ophthalmol. 50(3):134-143.

del Zoppo GJ. 2008. Virchow's triad: the vascular basis of cerebral injury. Rev Neurol Dis. 5(1):S12-21.

del Zoppo GJ, Schmid-Schönbein GW, Mori E, Copeland BR, Chang CM. 1991. Polymorphonuclear leukocytes occlude capillaries following middle cerebral artery occlusion and reperfusion in baboons. Stroke 22(10):1276-1283.

Dermietzel R, Krause D. 1991. Molecular anatomy of the blood-brain barrier as defined by immunocytochemistry. Int Rev Cytol. 127:57-109.

Devor A, Tian P, Nishimura N, Teng IC, Hillman EM, Narayanan SN, Ulbert I, Boas DA, Kleinfeld D, Dale AM. 2007. Suppressed neuronal activity and concurrent arteriolar vasoconstriction may explain negative blood oxygenation level-dependent signal. J Neurosci 27:4452-4459.

Díaz-Flores L, Gutiérrez R, Madrid JF, Varela H, Valladares F, Acosta E, Martín-Vasallo P, Díaz-Flores L Jr. 2009. Pericytes. Morphofunction, interactions and pathology in a quiescent and activated mesenchymal cell niche. Histol Histopathol. 24(7):909-969.

Díaz-Flores L, Gutiérrez R, Varela H,Rancel N, Valladares F. 1991. Microvascular pericytes: a review of their morphological and functional characteristics. Histol Histopathol. 6(2):269-286.

Dings J, Meixensberger J, Jäger A, Roosen K. 1998. Clinical experience with 118 brain tissue oxygen partial pressure catheter probes. Neurosurgery 43:1082-1095.

Dirnagl U, Lindauer U, Villringer A. 1993. Role of nitric oxide in the coupling of cerebral blood flow to neuronal activation in rats. Neurosci Lett 149:43-46.

Dodge AB, Hechtman HB, Shepro D. 1991. Microvascular endothelial-derived autocoids regulate pericyte contractility. Cell Motil Cytoskeleton 18(3):180-188.

Domercq M, Sánchez-Gómez MV, Sherwin C, Etxebarria E, Fern R, Matute C. 2007. System xc- and glutamate transporter inhibition mediates microglial toxicity to oligodendrocytes. J Immunol. 178(10):6549-6556.

Donahue MJ, Near J, Blicher JU, Jezzard P. 2010. Baseline GABA concentration and fMRI response. Neuroimage 53:392-398.

Dore-Duffy P, Katychex A, Wang X, Van Buren E. 2006. CNS microvascular pericytes exhibit multipotential stem cell activity. J Cereb Blood Flow Metab. 26(5):613-624.

Dore-Duffy P. 2008. Pericytes: plurpotent cells of the blood brain barrier. Curr Pharm Des. 14(16):1581-1593.

Dorrn AL, Yuan K, Barker AJ, Schreiner CE, Froemke RC. 2010. Developmental sensory experience balances cortical excitation and inhibition. Nature 465:932-936.

Downen M, Zhao ML, Lee P, Weidenheim KM, Dickson DW, Lee SC. 1999. Neuronal nitric oxide synthase expression in developing and adult human CNS. J Neuropathol Exp Neurol 58:12-21.

Drew GM, Whiting SB. 1979. Evidence for two distinct types of postsynaptic alpha-adrenoceptor in vascular smooth muscle *in vivo*. Br J Pharmacol 67:207-215.

Dubinsky JM, Levi Y. 1998. Calcium-induced activation of the mitochondrial permeablity transition in hippocampal neurons. J Neurosci Res. 53(6):728-741.

Duffy S, MacVicar BA. 1995. Adrenergic calcium signaling in astrocyte networks within the hippocampal slice. J Neurosci 15:5535-5550.

Durston S, Davidson MC, Tottenham N, Galvan A, Spicer J, Fossella JA, Casey BJ. 2006. A shift from diffuse to focal cortical activity with development. Dev. Sci. 9:1-8.

Duvernoy H, Delon S, Vannson JL. 1981. Cortical blood vessels of the human brain. Brain Res Bull. 7(5):519-579.

Duvernoy H, Delon S, Vannson JL. 1983. The vascularisation of the human cerebellar cortex. Brain Res Bull. 11(4):419-480.

Earley S, Heppner TJ, Nelson MT, Brayden JE. 2005. TRPV4 forms a novel Ca2+ signaling complex with ryanodine receptors and BKCa channels. Circ Res 97:1270-1279.

East SJ, Garthwaite J. 1990. Nanomolar N(G)-nitroarginine inhibits NMDA-induced cyclic GMP formation in rat cerebellum. Eur J Pharmacol184:311-313.

Elfont RM, Sundaresan PR, Sladek CD. 1989. Adrenergic receptors on cerebral microvessels: pericyte contribution. Am J Physiol. 256:R224-230.

Ellis EF, Police RJ, Yancey L, McKinney JS, Amruthesh SC. 1990. Dilation of cerebral arterioles by cytochrome P-450 metabolites of arachidonic acid. Am J Physiol 259:H1171-1177.

Enager P, Piilgaard H, Offenhauser N, Kocharyan A, Fernandes P, Hamel E, Lauritzen M. 2009. Pathway-specific variations in neurovascular and neurometabolic coupling in rat primary somatosensory cortex. J Cereb Blood Flow Metab 29:976-986.

Esiri MM, McGee J. 1986. Monoclonal antibody to macrophages (EBM/11) labels macrophages and microglial cells in human brain. J. Clin. Pathol 39:615–621.

Estrada C, DeFelipe J. 1998. Nitric oxide-producing neurons in the neocortex: morphological and functional relationship with intraparenchymal microvasculature. Cereb Cortex 8:193-203.

Eto R, Abe M, Kimoto H, Imaoka E, Kato H, Kasahara J, Araki T. 2010. Alterations of interneurons in the striatum and frontal cortex of mice during postnatal development. Int J Dev Neurosci 28:359-370.

Fang X, Kaduce TL, Weintraub NL, Harmon S, Teesch LM, Morisseau C, Thompson DA, Hammock BD, Spector AA. 2001. Pathways of epoxyeicosatrienoic acid metabolism in endothelial cells. Implications for the vascular effects of soluble epoxide hydrolase inhibition. J Biol Chem 276:14867-14874.

Faraci FM, Breese KR. 1993. Nitric oxide mediates vasodilation in response to activation of N-methyl-D-aspartate receptors in brain. Circ Res. 72(2):476-480.

Favard C, Simon A, Vigny A, Nguyen-Legros J. 1990. Ultrastructural evidence for a close relationship between dopamine cell processes and blood capillary walls in Macaca monkey and rat retina. Brain Res. 523(1):127-133.

Feekes JA, Hsu SW, Chaloupka JC, Cassell MD. 2005. Tertiary microvascular territories define lacunar infarcts in the basal ganglia. Ann Neurol. 58(1):18-30.

Feng Y, vom Hagen F, Pfister F, Djokic S, Hoffmann S, Back W, Wagner P, Lin J, Deutsch U, Hammes HP. 2007. Impaired pericyte recruitment and abnormal retinal angiogenesis as a result of angiopoietin-2 overexpression. Thromb Haemost. 97(1):99-108.

Fenwick EM, Marty A, Neher E. 1982. A patch-clamp study of bovine chromaffin cells and of their sensitivity to acetylcholine. J Physiol 331:577-597.

Fernández-Klett F, Offenhauser N, Dirnagl U, Priller J, Lindauer U. 2010. Pericytes in capillaries are contractile *in vivo*, but arterioles mediate functional hyperemia in the mouse brain. Proc Natl Acad Sci U S A 107:22290-22295.

Fernández-Klett F, Potas JR, Hilpert D, Blazej K, Radke J, Huck J, Engel O, Stenzel W, Genové G, Priller J. 2013. Early loss of pericytes and pervascular stromal cell-induced scar formation after stroke. J Cereb Blood Flow Metab. 33(3):428-439.

Fields RD. 2008. White matter matters. Sci Am 298:42-49.

Filosa JA, Bonev AD, Straub SV, Meredith AL, Wilkerson MK, Aldrich RW, Nelson MT. 2006. Local potassium signaling couples neuronal activity to vasodilation in the brain. Nat Neurosci 9:1397-1403.

Folbergrová J, Zhao Q, Katsura K, Siesjö BK. 1995. N-tert-butyl-alpha-phenylnitrone improves recovery of brain energy state in rats following transient focal ischemia. Proc Natl Acad Sci U S A 92(11):5057-5061.

Foo SS, Turner CJ, Adams S, Compagni A, Aubyn D, Kogata N, Lindblom P, Shani M, Zicha D, Adams RH. 2006. Ephrin-B2 controls cell motility and adhesion during blood-vessel-wall assembly. Cell 124(1):161-173.

Forbes MS, Rennels ML, Nelson E. 1977. Ultrastructure of pericytes in mouse heart. Am J Anat. 149(1):47-70.

Fornari E, Knyazeva MG, Meuli R, Maeder P. 2007. Myelination shapes functional activity in the developing brain. Neuroimage 38:511-518.

Fox PT, Raichle ME. 1986. Focal physiological uncoupling of cerebral blood flow and oxidative metabolism during somatosensory stimulation in human subjects. Proc Natl Acad Sci U S A 83(4):1140-1144.

Frank RN, Dutta S, Mancini MA. 1987. Pericyte coverage is greater in the retinal than in the cerebral capillaries of the rat. Invest Ophthalmol Vis Sci. 28(7):1086-1091.

Frid MG, Shekhonin BV, Koteliansky VE, Glukhova MA. 1992. Phenotypic changs of human smooth muscle cells during development: late expression of heavy caldesmon and calponin. Dev Biol. 153(2):185-193.

Fritsch RM, Saur D, Kurjak M, Oesterle D, Schlossmann J, Geiselhöringer A, Hofmann F, Allescher HD. 2004. InsP3R-associated cGMP kinase substrate (IRAG) is essential for nitric oxide-induced inhibition of calcium signaling in human colonic smooth muscle. J Biol Chem. 279(13):12551-12559.

Fujimoto T, Singer SJ. 1987. Immunocytochemical studies of desmin and vimentin in pericapillary cells of chicken. J Histochem Cytochem 35:1105-15.

Fukushi J, Makagiansar IT, Stallcup WB. 2004. NG2 proteoglycan promotes endothelial cell motility and angiogenesis via engagement of galectin-3 and alpha3beta1 integrin. Mol Biol Cell 15(8):3580-3590.

Gabernet L, Jadhav SP, Feldman DE, Carandini M, Scanziani M. 2005. Somatosensory intergration controlled by dynamic thalamocortical feed-forward inhibition. 48:315-327.

Gaillard WD. 2000. Cortical function in epilepsy. Curr Opin Neurol 13:193-200.

Gaillard WD, Hertz-Pannier L, Mott SH, Barnett AS, LeBihan D, Theodore WH. 2000. Functional anatomy of cognitive development: fMRI of verbal fluency in children and adults. Neurology 54:180-185.

Gaillard WD, Sachs BC, Whitnah JR, Ahmad Z, Balsamo LM, Petrella JR, Braniecki SH, McKinney CM, Hunter K, Xu B, Grandin CB. 2003. Developmental aspects of language processing: fMRI of verbal fluency in children and adults. Hum Brain Mapp 18:176-185.

Gandhi SP, Yanagawa Y, Stryker MP. 2008. Delayed plasticity of inhibitory neurons in developing visual cortex. Proc Natl Acad Sci U S A 105:16797-16802.

Garaschuk O, Hanse E, Konnerth A. 1998. Developmental profile and synaptic origin of early network oscillations in the CA1 region of rat neonatal hippocampus. J Physiol 507 (Pt 1):219-236.

Garey LJ, de Courten C. 1983. Structural development of the lateral geniculate nucleus and visual cortex in monkey and man. Behav Brain Res 10:3-13.

Garthwaite J, Charles SL, Chess-Williams R. 1988. Endothelium-derived relaxing factor release on activation of NMDA receptors suggests role as intercellular messenger in the brain. Nature 336:385-388.

Garthwaite G, Garthwaite J. 1986. Neurotoxicity of excitatory amino acid receptor agonists in rat cerebellar slices: dependence on calcium concentration. Neurosci Lett. 66(2):193-198.

Garthwaite J, Southam E, Boulton CL, Nielsen EB, Schmidt K, Mayer B. 1995. Potent and selective inhibition of nitric oxide-sensitive guanylyl cyclase by 1H-[1,2,4]oxadiazolo[4,3-a]quinoxalin-1-one. Mol Pharmacol 48:184-188.

Gebremedhin D, Lange AR, Narayanan J, Aebly MR, Jacobs ER, Harder DR. 1998. Cat cerebral arterial smooth muscle cells express cytochrome P450 4A2 enzyme and produce the vasoconstrictor 20-HETE which enhances L-type Ca2+ current. J Physiol 507 (Pt 3):771-781.

Globus MY, Busto R, Martinez E, Valdés I, Dietrich WD, Ginsberg MD. 1991. Comparative effect of transient global ischemia on extracellular levels of glutamate, glycine, and gamma-aminobutyric acid in vulnerable and nonvulnerable brain regions in the rat. J Neurochem. 57(2):470-478.

Gobbel GT, Chan TY, Gregory GA, Chan PH. 1994. Response of cerebral endothelial cells to hypoxia:modification by fructose-1,6-bisphosphate but not glutamate receptor antagonists. Brain Res. 653(1-2):23-30.

Golarai G, Ghahremani DG, Whitfield-Gabrieli S, Reiss A, Eberhardt JL, Gabrieli JD, Grill-Spector K. 2007. Differential development of high-level visual cortex correlates with category-specific recognition memory. Nat Neurosci 10:512-522.

Goldman-Rakic PS, Brown RM. 1982. Postnatal development of monoamine content and synthesis in the cerebral cortex of rhesus monkeys. Dev Brain Res 4:339-349.

Goodyear BG, Menon RS. 1998. Effect of luminance contrast on BOLD fMRI response in human primary visual areas. J Neurophysiol 79:2204-2207.

Gordon GR, Choi HB, Rungta RL, Ellis-Davies GC, MacVicar BA. 2008. Brain metabolism dictates the polarity of astrocyte control over arterioles. Nature 456:745-749.

Göritz C, Dias DO, Tomilin N, Barbacid M, Shupliakov O, Frisén J. 2011. A pericyte origin of spinal cord scar tissue. Science 333(6039):238-242

Gotoh J, Kuang TY, Nakao Y, Cohen DM, Melzer P, Itoh Y, Pak H, Pettigrew K, Sokoloff L. 2001. Regional differences in mechanisms of cerebral circulatory response to neuronal activation. Am J Physiol Heart Circ Physiol 280:H821-829.

Graeber MB, Banati RB, Streit WJ, Kreutzberg GW. 1989. Immunophenotypic characterization of rat brain macrophages in culture. Neurosci Lett. 103(3):241-246.

Gragera RR, Muñiz E, Martínez-Rodriguez R. 1993. Electron microscopic immunolocalization of GABA and glutamic acid decarboxylase (GAD) in cerebellar capillaries and their microenvironment. Cell Mol Biol. 39(8):809-817.

Grako KA, Ochiya T, Barritt D, Nishiyama A, Stallcup WB. 1999. PDGF alpha-receptor is unresponsive to PDGF-AA in aortic smooth muscle cells from the NG2 knockout mouse. J Cell Sci. 112(6):905-915.

Grako KA, Stallcup WB. 1995. participation of the NG2 proteoglycan in rat aortic smooth muscle cell responses to platelet-derived growth factor. Exp Cell Res. 221(1):231-240.

Gur RE, Gur RC. 2010. Functional magnetic resonance imaging in schizophrenia. Dialogues Clin Neurosci 12:333-343.

Haak LL, Heller HC, van den Pol AN. 1997. Metabotropic glutamate receptor activation modulates kainate and serotonin calcium response in astrocytes. J Neurosci. 17(5):1825-1837.

Haefliger IO, Zschauer A, Anderson DR. 1994. Relaxation of reinal pericyte contractile tone through the nitric oxide-cyclic guanosine monophosphate pathway. Invest Ophthalmol Vis Sci. 35:991-997.

Hager H. 1975. EM findings in the source of reactive microglia on the mammalian brain. Acta Neuropathol Suppl. 6:279-283.

Hagmann P, Sporns O, Madan N, Cammoun L, Pienaar R, Wedeen VJ, Meuli R, Thiran JP, Grant PE. 2010. White matter maturation reshapes structural connectivity in the late developing human brain. Proc Natl Acad Sci U S A 107:19067-19072.

Halestrap AP. 2006. Calcium, mitochondria and reperfusion injury: a pore way to die. Biochem Soc Trans. 34(2): 232-237.

Hall CN, Klein-Flügge MC, Howarth C, Attwell D. 2012. Oxidative phosphorylation, not glycolysis, powers presynaptic and postsynaptic mechanisms underlying brain information processing. J Neurosci. 32(26):8940-8951.

Halliwell B. 1992. Reactive oxygen species and the central nervous system. J Neurochem. 59(5):1609-1623.

Hamann M, Rossi DJ, Mohr C, Andrade AL, Attwell D. 2005. The electrical response of cerebellar purkinje neurons to simulated ischaemia. Brain 128(10):2408-2420.

Hamano K, Takeya T, Iwasaki N, Nakayama J, Ohto T, Okada Y. 1998. A quantitative study of the progress of myelination in the rat central nervous system, using the immunohistochemical method for proteolipid protein. Brain Res Dev Brain Res 108:287-293.

Hamel E. 2006. Perivascular nerves and the regulation of cerebrovascular tone. J Appl Physiol 100:1059-1064.

Hamilton NB, Attwell D, Hall CN. 2010. Pericyte-mediated regulation of capillary diameter: a component of neurovascular coupling in health and disease. Front Neuroenergetics 21:2.

Hansen AJ. 1985. Effect of anoxia on ion distribution in the brain. Physiol Rev. 65(1):101-148.

Harris JJ, Reynell C, Attwell D. 2011. The physiology of developmental changes in BOLD functional imaging signals. Dev Cogn Neurosci. 1(3):199-216.

Hartmann C, Zozulya A, Wegener J, Galla HJ. 2007. The impact of glia-derived extracellular matrices on the barrier function of cerebral endothelial cells: as *in vitro* study. Exp Cell Res. 313(7):1318-1325.

Hathaway DR, March KL, Lash JA, Adam LP, Wilensky RL. 1991. Vascular smooth muscle. A review of the molecular basis of contractility. Circulation 83(2):382-390.

Hauck EF, Apostel S, Hoffmann JF, Heimann A, Kempski O. 2004. Capillary flow and diameter changes during reperfusion after global cerebral ischaemia studied by intravital video microscopy. J Cereb Blood Flow Metab. 24(4):383-391.

Helbig H, Kornacker S, Berweck S, Stahl F, Lepple-Wienhues A, Wiederholt M. 1992. Membrane potentials in retinal capillary pericytes: excitability and effect of vasoactive substances. Invest Ophthalmol Mol Vis Sci. 33(7):2105-2112.

Hellström M, Kalén M, Lindahl P, Abramsson A, Betsholtz C. 1999. Role of PDGF-B and PDGFR-beta in recruitment of vascular smooth muscle cells and pericytes during embryonic blood vessel formation in the mouse. Development 126(14):3047-3055.

Hendrickson AE, Van Brederode JF, Mulligan KA, Celio MR. 1991. Development of the calcium-binding protein parvalbumin and calbindin in monkey striate cortex. J Comp Neurol 307:626-646.

Herman IM, D'Amore PA. 1985. Microvascular pericytes contain muscle and nonmuscle actins. J Cell Biol 101:43-52.

Hertz L. 2008. Bioenergentics of cerebral ischemia: a cellular perspective. Neuropharmacol. 55(3):289-309.

Hirschi KK, Rohovsky SA, Beck LH, Smith SR, D'Amore PA. 1999. Endothelial cells modulate the proliferation of mural cell precursors via platelet-derived growth factor-BB and heterotypic cell contact. Circ Res. 84(3):298-305.

Hluštík P, Solodkin A, Noll DC, Small SL. 2004. Cortical plasticity during three-week motor skill learning. J Clin Neurophysiol 21:180-191.

Ho KL. 1985. Ultrastructure of cerebellar capillary hemangioblastoma. IV. Pericytes and their relationship to endothelial cells. Acta Neuropathol. 67(3-4):254-264.

Hoddle KC, Sercombe R. 1996. The anatomy of the brain vasculature. Neurophysiological basis of cerebral blood flow control. London, Libbey 111-144.

Hoksbergen AW, Legemate DA, Ubbink DT, Jacobs MJ. 2000. Collateral variations in circle of willis in atherosclerotic population assessed by means of transcranial color-coded duplex ultrasonography. Stroke 31(7):1656-1660.

Holland SK, Plante E, Weber Byars A, Strawsberg RH, Schmithorst VJ, Ball Jr WS. 2001. Normal fMRI brain activation patterns in children performing a verb generation task. Neuroimage. 14:837-843.

Holt CE, Harris WA. 1983. Order in the initial retinotectal map in Xenopus: a new technique for labelling growing nerve fibres. Nature 301:150-152.

Hori S, Ohtsuki S, Hosoya K, Nakashima E, Terasaki T. 2004. A pericyte-derived angiopoietin-1 multimeric complex induces occludin gene expression in brain capillary endothelial cells through tie-2 activation *in vitro*. J Neurochem. 89(2):503-513.

Huang FJ, You WK, Bonaldo P, Seyfried TN, Pasquale EB, Stallcup WB. 2010. Pericyte deficiencies lead to aberrant tumor vascularization in the brain of the NG2 null mouse. Dev Biol. 344(2):1035-1046.

Hubel DH, Wiesel TN. 1963. Shape and arrangement of columns in cat's striate cortex. J Physiol 165:559-568.

Hughes S, Chan-Ling T. 2004. Characterization of smooth muscle cell and pericyte differentiation in the rat retina *in vivo*. Invest Ophthalmol Vis Sci. 45(8):2795-2806.

Humphreys BD, Lin SL, Kobayashi A, Hudson TE, Nowlin BT, Bonventre JV, Valerius MT, McMahon AP, Duffield JS. 2010. Fate tracing reveals the pericyte and not epithelial origin of myofibroblasts in kidney fibrosis. Am J Pathol. 176(1):85-97.

Hutchinson EB, Stefanovic B, Koretsky AP, Silva AC. 2006. Spatial flow-volume dissociation of the cerebral microcirculatory response to mild hypercapnia. Neuroimage 32:520-530.

Huttenlocher PR. 1990. Morphometric study of human cerebral cortex development. Neuropsychologia 28:517-527.

Iadecola C. 2004. Neurovascular regulation in the normal brain and in Alzheimer's disease. Nat Rev Neurosci 5:347-360.

Iadecola C, Yang G, Ebner TJ, Chen G. 1997. Local and propagated vascular responses evoked by focal synaptic activity in cerebellar cortex. J Neurophysiol 78:651-659.

Iliff JJ, Jia J, Nelson J, Goyagi T, Klaus J, Alkayed NJ. 2010. Epoxyeicosanoid signaling in CNS function and disease. Prostaglandins Other Lipid Mediat 91:68-84.

Ishikawa T, Hume JR, Keef KD. 1993. Regulation of Ca^{2+} channels by cAMP and cGMP in vascular smooth muscle cells. Circ Res. 73(6):1128-1137.

Ito U, Hakamata Y, Kawakami E, Oyanagi K. 2011. Temporary cerebral ischemia results in swollen astrocytic end-feet that compress microvessels and lead to delayed focal cortical infarction. J Cereb Blood Flow Metab. 31(1):328-338.

Ito D, Imai Y, Ohsawa K, Nakajima K, Fukuuchi Y, Kohsaka S. 1998. Microglia-specific localisation of a novel calcium binding protein, Iba1. Brain Res Mol Brain Res. 57(1):1-9.

Janzer RC, Raff MC. 1987. Astrocytes induce blood-brain barrier properties in endothelial cells. Nature 325(6101):253-257.

Javazon EH, Beggs KJ, Flake AW. 2004. Mesenchymal stem cells: paradoxes of passaging. Exp Hematol. 32(5):414-425.

Jespersen SN, Østergaard L. 2012. The roles of cerebral blood flow, capillary transit time heterogeneity, and oxygen tension in brain oxygenation and metabolism. J Cereb Blood Flow Metab. 32(2):264-277.

Jones N, Iljin K, Dumont DJ, Alitalo K. 2001. Tie receptors: new modulators of angiogenic and lymphangiogenic responses. Nat Rev Mol Cell Biol. 2(4):257-267.

Joyce NC, De Camilli P, Boyles J. 1984. Pericytes, like smooth muscle cells, are immunocytochemically positive for cGMP-dependent protein kinase. Microvasc. Res 28:206-219.

Joyce NC, Haire MF, Palade GE. 1985. Contractile proteins in pericytes. I. Immunoperoxidase localization of tropomyosin. J Cell Biol100:1379-1386.

Joyce NC, Haire MF, Palade GE. 1985. Contractile proteins in pericytes. II. Immunocytochemical evidence for the presence of two isomyosins in graded concentrations. J Cell Biol. 100:1387-1395.

Judas M, Sestan N, Kostovic I. 1999. Nitrinergic neurons in the developing and adult human telencephalon: transient and permanent patterns of expression in comparison to other mammals. Microsc Res Tech 45:401-419.

Jung KH, Chu K, Ko SY, Lee ST, Sinn DI, Park DK, Kim JM, Song EC, Kim M, Roh JK. 2006. Early intravenous infusion of sodium nitrite protects brain against *in vivo* ischemia-reperfusion injury. Stroke 37(11):2744-2750.

Juttler E, Kohrmann M, Schellinger PD. 2006. Therapy for early reperfusion after stroke. Nat Clin Pract Cardiovasc Med. 3(12):656-663.

Kamouchi M, Kitazono T, Ago T, Wakisaka M, Kuroda J, Nakamura K, Hagiwara N, Ooboshi H, Ibayashi S, Lida M. 2007. Hydrogen peroxide-induced Ca2+ responses in CNS pericytes. Neurosci Lett. 416(1):12-16.

Kamouchi M, Kitazono T, Ago T, Wakisaka M, Ooboshi H, Ibayashi S, Lida M. 2004. Calcium influx pathways in rat CNS pericytes. Brain Res Mol Brain Res. 126(2):114-120.

Kandel ER, Schwartz JH, Jessell TM. 2000. Principles of neural science. *4th ed.* McGraw-Hill, New York.

Karaki H, Ozaki H, Hori M, Mitsui-Saito M, Amano K, Harada K, Miyamoto S, Nakazawa H, Won KJ, Sato K. 1997. Calcium movements, distribution, and functions in smooth muscle. Pharmacol Rev. 49(2):157-230.

Kargacin GJ, Cooke PH, Abramson SB, Fay FS. 1989. Periodic organization of the contractile apparatus in smooth muscle revealed by the motion of dense bodies in single cells. J Cell Biol. 108(4):1465-1475.

Karni A, Meyer G, Rey-Hipolito C, Jezzard P, Adams MM, Turner R, Ungerleider LG. 1998. The acquisition of skilled motor performance: fast and slow experience-driven changes in primary motor cortex. 95:861-868.

Kasischke KA, Lambert EM, Panepento B, Sun A, Gelbard HA, Burgess RW, Foster TH, Nedergaard M. 2011. Two-photon NADH imaging exposes boundaries of oxygen diffusion in cortical vascular supply regions. J Cereb Blood Flow Metab. 31(1):68-81.

Kastner S, DeSimone K, Konen CS, Szczepanski SM, Weiner KS, Schneider KA. 2007. Topographic maps in human frontal cortex revealed in memory-guided saccade and spatial working-memory tasks. J Neurophysiol 97:3494-3507.

Katchman AN, Hershkowitz N. 1993. Early anoxia-induced vesicular glutamate release results from mobilization of calcium from intracellular stores. J Neurophysiol. 70(1):1-7.

Kawamura H, Oku H, Li Q, Sakagami K, Puro DG. 2002. Endothelin-induced changes in the physiology of retinal pericytes. Invest Ophthalmol Vis Sci. 43:882-888.

Keep RF, Jones HC. 1990. Cortical microvessels during brain development: a morphometric study in the rat. Microvasc Res. 40:412-426.

Kelley C, D'Amore P, Hechtman HB, Shepro D. 1987. Microvascular pericyte contractility in vitro: comparison with other cells of the vascular wall. J Cell Biol 104:483-90.

Kelley C, D'Amore P, Hechtman HB, Shepro D. 1988. Vasoactive hormones and cAMP affect pericyte contraction and stress fibres in vitro. J Muscle Res Cell Motil 9:184-94.

Keulers EH, Stiers P, Jolles J. 2011. Developmental changes between ages 13 and 21 years in the extent and magnitude of the BOLD response during decision making. Neuroimage 54:1442-1454.

Khazipov R, Esclapez M, Caillard O, Bernard C, Khalilov I, Tyzio R, Hirsch J, Dzhala V, Berger B, Ben-Ari Y. 2001. Early development of neuronal activity in the primate hippocampus in utero. J Neurosci 21:9770-9781.

Kida S, Steart PV, Zhang ET, Weller RO. 1993. Perivascular cells act as scavengers in the cerebral perivascular spaces and remain distinct from pericytes, microglia and macrophages. Acta Neuropathol. 85(6):646-652.

Kniesel U, Risau W, Wolburg H. 1996. Development of blood-brain barrier tight junctions in the rat cortex. Brain Res Dev Brain Res. 96(1-2):229-240.

Ko KR, Ngai AC, Winn HR. 1990. Role of adenosine in regulation of regional cerebral blood flow in sensory cortex. Am J Physiol 259:H1703-1708.

Koehler RC, Roman RJ, Harder DR. 2009. Astrocytes and the regulation of cerebral blood flow. Trends Neurosci 32:160-169.

König P, Engel AK, Singer W. 1995. Relation between oscillatory activity and long-range synchronization in cat visual cortex. Proc Natl Acad Sci U S A 92:290-294.

Krimer LS, Muly EC, 3rd, Williams GV, Goldman-Rakic PS. 1998. Dopaminergic regulation of cerebral cortical microcirculation. Nat Neurosci 1:286-289.

Kristián T, Siesjö BK. 1998. Calcium in ischemic cell death. Stroke 29(3):705-718.

Krueger M, Bechmann I. 2010. CNS Pericytes: Concepts, misconceptions, and a way out. Glia 58(1):1-10.

Kunz J, Krause D, Kremer M, Dermietzel R. 1994. The 140-kDa protein of blood-brain barrier-associated pericytes is identical to aminopeptidase N. J Neurochem. 62(6):2375-2386.

Kuwabara T, Cogan DG. 1960. Studies of retinal vascular patterns. I. Normal architecture. Arch. Ophthalmol 64:904:911.

Kwon H, Reiss AL, Menon V. 2002. Neural basis of protracted developmental changes in visuo-spatial working memory. Proc Natl Acad Sci U S A 99:13336-13341.

Lambe EK, Krimer LS, Goldman-Rakic PS. 2000. Differential postnatal development of catecholamine and serotonin inputs to identified neurons in prefrontal cortex of rhesus monkey. J Neurosci 20:8780-8787.

Lange A, Gebremedhin D, Narayanan J, Harder D. 1997. 20-Hydroxyeicosatetraenoic acid-induced vasoconstriction and inhibition of potassium current in cerebral vascular smooth muscle is dependent on activation of protein kinase C. J Biol Chem 272:27345-27352.

Larson DM, Carson MP, Haudenschild CC. 1987. Junctional transfer of small molecules in cultured bovine brain microvascular endothelial cells and pericytes. Microvasc Res. 34(2):184-199.

Lauritzen M. 2005. Reading vascular changes in brain imaging: is dendritic calcium the key? Nat Rev Neurosci 6:77-85.

Lauritzen M, Gold L. 2003. Brain function and neurophysiological correlates of signals used in functional neuroimaging. J Neurosci 23:3972-3980.

Le Beux YJ, Willemot J. 1978. Actin- and myosin-like filaments in rat brain pericytes. Anat Rec. 190(4):811-826.

Leenders KL, Perani D, Lammertsma AA, Heather JD, Buckingham P, Healy MJ, Gibbs JM, Wise RJ, Hatazawa J, Herold S, et al. 1990. Cerebral blood flow, blood volume and oxygen utilization. Normal values and effect of age. Brain 113:27-47.

Leffler CW, Busija DW, Mirro R, Armstead WM, Beasley DG. 1989. Effects of ischaemia on brain blood flow and oxygen consumption of newborn pigs. Am J Physiol. 257:H1917-1926.

Leithner C, Royl G, Offenhauser N, Fuchtemeier M, Kohl-Bareis M, Villringer A, Dirnagl U, Lindauer U. 2010. Pharmacological uncoupling of activation induced increases in CBF and CMRO2. J Cereb Blood Flow Metab 30:311-322.

Lenroot RK, Giedd JN. 2006. Brain development in children and adolescents: insights from anatomical magnetic resonance imaging. Neurosci Biobehav Rev 30:718-729.

Levine JM, Reynolds R, Fawcett JW. 2001. The oligodendrocyte precursor cell in health and disease. Trends Neurosci 24(1):39-47.

Levitt P, Harvey JA, Friedman E, Simansky K, Murphy EH. 1997. New evidence for neurotransmitter influences on brain development. Trends Neurosci 20:269-274.

Li J, Iadecola C. 1994. Nitric oxide and adenosine mediate vasodilation during functional activation in cerebellar cortex. Neuropharmacology 33(11):1453-1461.

Li J, Ma X, Yu W, Lou Z, Mu D, Wang Y, Shen B, Qi S. 2012. Reperfusion promotes mitochondrial dysfunction following focal cerebral ischemia in rats. PLoS One 7(9):e46498.

Li Q, Puro DG. 2001. Adenosine activates ATP-sensitive K^+ currents in pericytes of rat retinal microvessels: role of A1 and A2a receptors. Brain Res. 907:93-99.

Li DY, Varma DR, Chemtob S. 1995. Up-regulation of brain PGE2 and PGF2 alpha receptors and receptor-coupled second messengers by cyclooxygenase inhibition in newborn pigs. J Pharmacol Exp Ther 272:15-19.

Lindahl P, Johansson BR, Levéen P, Betsholtz C. 1997. Pericyte loss and microaneurysm formation in PDGF-B-deficient mice. Science 277(5323):242-245.

Lindauer U, Megow D, Matsuda H, Dirnagl U. 1999. Nitric oxide: a modulator, but not a mediator, of neurovascular coupling in rat somatosensory cortex. Am J Physiol 277:H799-811.

Lindblom P, Gerhardt H, Liebner S, Abramsson A, Enge M, Hellstrom M, Backstrom G, Fredriksson S, Landegren U, Nystrom HC, Bergstrom G, Dejana E, Ostman A, Lindahl P, Betsholtz C. 2003. Endothelial PDGF-B retention is required for proper investment of pericytes in the microvessel wall. Genes Dev. 17(15):1835-1840.

Lipski J, Park TI, Li D, Lee SC, Trevarton AJ, Chung KK, Freestone PS, Bai JZ. 2006. Involvement of TRP-like channels in the acute ischemic response of hippocampal CA1 neurons in brain slices. Brain Res. 1077(1): 187-199.

Lipton P. 1999. Ischemic cell death in brain neurons. Physiol Rev. 79(4):1431-1568.

Liu X, Li C, Falck JR, Roman RJ, Harder DR, Koehler RC. 2008. Interaction of nitric oxide, 20-HETE, and EETs during functional hyperemia in whisker barrel cortex. Am J Physiol Heart Circ Physiol 295:H619-631.

Logothetis NK. 2008. What we can do and what we cannot do with fMRI. Nature 453(7197):869-878.

Lovick TA, Brown LA< Key BJ. 1999. Neurovascular relationships in hippocampal slices: physiological and anatomical studies of mechanisms underlying flow-metabolism coupling in intraparenchymal microvessels. Neuroscience 92(1):47-60.

Lowe RF, Gilboe DD. 1971. Demonstration of alpha and beta adrenergic receptors in canine cerebral vasculature. Stroke 2(2):193-200.

Luders E, Thompson PM, Toga AW. 2010. The development of the corpus callosum in the healthy human brain. J Neurosci 30:10985-10990.

Machwate M, Harada S, Leu CT, Seedor G, Labelle M, Gallant M, Hutchins S, Lachance N, Sawyer N, Slipetz D, Metters KM, Rodan SB, Young R, Rodan GA. 2001. Prostaglandin receptor EP(4) mediates the bone anabolic effects of PGE(2). Mol Pharmacol. 60(1):36-41.

Malonek D, Dirnagl U, Lindauer U, Yamada K, Kanno I, Grinvald A. 1997. Vascular imprints of neuronal activity: relationships between the dynamics of cortical blood flow, oxygenation, and volume changes following sensory stimulation. Proc Natl cad Sci U S A 94(26):14826-14831.

Mandeville JB, Marota JJA. (1999) Vascular filters of functional MRI: spatial localization using BOLD and CBV Contrast. Mag Reson Med 42:591-598.

Marcar VL, Loenneker T, Straessle A, Girard F, Martin E. 2004a. How much luxury is there in 'luxury perfusion'? An analysis of the BOLD response in the visual areas V1 and V2. Magn Reson Imaging 22:921-928.

Marcar VL, Straessle A, Girard F, Loenneker T, Martin E. 2004b. When more means less: a paradox BOLD response in human visual cortex. Magn Reson Imaging 22:441-450.

Margaill I, Allix M, Boulu RG, Plotkine M. 1997. Dose- and time-dependence of L-NAME neuroprotection in transient focal cerebral ischaemia in rats. Br J Pharmacol. 120(1):160-163.

Maril A, Davis PE, Koo JJ, Reggev N, Zuckerman M, Ehrenfeld L, Mulkern RV, Waber DP, Rivkin MJ. 2010. Developmental fMRI study of episodic verbal memory encoding in children. Neurology 75:2110-2116.

Markham JA, Greenough WT. 2004. Experience-driven brain plasticity: beyond the synapse. Neuron Glia Biol 1:351-363.

Markhotina N, Liu GJ, Martin DK. 2007. Contractility of retinal pericytes grown on silicone elastomer substrates is through a protein kinase A- mediated intracellular pathway in response to vasoactive peptides. IET Nanobiotechnol. 1(3):44-51.

Martin JH. 2012. Neuroanatomy text and atlas fourth edition. McGraw-Hill Companies, Inc.

Mathiisen TM, Lehre KP, Danbolt NC, Ottersen OP. 2010. The perivascular astroglial sheath provides a complete covering of the brain microvessels: an electron microscopic 3D reconstruction. Glia 58(9):1094-1103.

Matsugi T, Chen Q, Anderson DR. 1997a. Contractile responses of cultured bovine retinal pericytes to angiotensin II. Arch Ophthalmol. 115(10):1281-1285.

Matsugi T, Chen Q, Anderson DR. 1997b. Adenosine-induced relaxation of cultured bovine retinal pericytes. Invest Ophthalmol Vis Sci. 38(13):2695-2701.

Matsumoto H, Kumon Y, Watanabe H, Ohnishi T, Shudou M, Chuai M, Imai Y, Takahashi H, Tanaka J. 2008. Accumulation of macrophage-like cells expressing NG2 proteoglycan and Iba1 in ischemic core of rat brain after transient middle cerebral artery occlusion. J Cereb Blood Flow Metab. 28(1):149-163.

Matsuzawa A, Ichijo H. 2005. Stress-responsive protein kinases in redox-regulated apoptosis signalling. Antioxid Redox Signal 7:472-481.

Maxwell LC, Herlihy JT, Riedel GL. 1983. Effects of ascorbic acid and EDTA on vascular concentration-response to catecholamines. Microvasc. Res 26(1):81-88.

maxwell DS, Kruger L. 1965. Small blood vessels and the origin of phagocytes in the rat cerebral cortex following heavy particle irradiation. Exp Neurol. 12:33-54.

McGrath JC. 1983. The variety of vascular alpha-adrenoceptors. Trends Pharmacol Sci. 4:14-18.

McGrath JC, Wilson V. 1988. Alpha-adrenoceptor subclassification by classical by classical and response-related methods:same question, different answers. Trends Pharmacol Sci. 9:162-165.

Meister M, Wong RO, Baylor DA, Shatz CJ. 1991. Synchronous bursts of action potentials in ganglion cells of the developing mammalian retina. Science 252:939-943.

Merzenich MM, Jenkins WM. 1993. Reorganization of cortical representations of the hand following alterations of skin inputs induced by nerve injury, skin island transfers, and experience. J Hand Ther 6:89-104.

Metea MR, Newman EA. 2006. Glial cells dilate and constrict blood vessels: a mechanism of neurovascular coupling. J Neurosci 26:2862-2870.

Meyrick B, Reid L. 1978. The effect of continued hypoxia on rat pulmonary arterial circulation. An ultrastructural study. Lab Invest. 38(2):188-200.

Miller B, Sheppard AM, Bicknese AR, pearlman AL. 1995. Chondroitin sulfate proteoglycans in the developing cerebral cortex: the distribution of neurocan distinguishes forming afferent and efferent axonal pathways. J Comp Neurol. 355(4):615-628.

Miller MJ, Weiss C, Song X, Iordanescu G, Disterhoft JF, Wyrwicz AM. 2008. Functional magnetic resonance imaging of delay and trace eyeblink conditioning in the primary visual cortex of the rabbit. J Neurosci 28:4974-4981.

Mimura K, Kimoto T, Okada M. 2003. Synapse efficiency diverges due to synaptic pruning following overgrowth. Phys Rev E Stat Nonlin Soft Matter Phys 68:031910.

Mito T, Konomi H, Houdou S, Takashima S. 1991. Immunohistochemical study of the vasculature in the developing brain. Pediatr Neurol 7:18-22.

Miyata N, Taniguchi K, Seki T, Ishimoto T, Sato-Watanabe M, Yasuda Y, Doi M, Kametani S, Tomishima Y, Ueki T, Sato M, Kameo K. 2001. HET0016, a potent and selective inhibitor of 20-HETE synthesizing enzyme. Br J Pharmacol 133:325-329.

Miyawaki T, Matsui K, Takashima S. 1998. Developmental characteristics of vessel density in the human fetal and infant brains. Early Hum Dev 53:65-72.

Molinoff PB. 1984. Alpha- and beta-adrenergic receptor subtypes properties, distribution and regulation. Drugs 2:1-15.

Monk CS, McClure EB, Nelson EE, Zarahn E, Bilder RM, Leibenluft E, Charney DS, Ernst M, Pine DS. 2003. Adolescent immaturity in attention-related brain engagement to emotional facial expressions. Neuroimage 20:420-428.

Mori E, del Zoppo GJ, Chambers JD, Copeland BR, Arfors KE. 1992. Inhibition of polymorphonuclear leukocyte adherence suppresses no-reflow after focal cerebral ischemia in baboons. Stroke 23(5):712-718.

Müller CM. 1992. Astrocytes in cat visual cortex studied by GFAP and S-100 immunocytochemistry during postnatal development. J Comp Neurol 317:309-323.

Mulligan SJ, MacVicar BA. 2004. Calcium transients in astrocyte endfeet cause cerebrovascular constrictions. Nature 431:195-199.

Muramoto S, Yamada H, Sadato N, Kimura H, Konishi Y, Kimura K, Tanaka M, Kochiyama T, Yonekura Y, Ito H. 2002. Age-dependent change in metabolic response to photic stimulation of the primary visual cortex in infants: functional magnetic resonance imaging study. J Comput Assist Tomogr 26:894-901.

Murrant CL, Duza T, Kim MB, Cohen KD, Sarelius IH. 2004. Arteriolar dilations induced by contraction of hamster cremaster muscle are dependent on changes in endothelial cell calcium. Acta Physiol Scand. 180(3):231-238.

Murrin LC, Sanders JD, Bylund DB. 2007. Comparison of the maturation of the adrenergic and serotonergic neurotransmitter systems in the brain: implications for differential drug effects on juveniles and adults. Biochem Pharmacol 73:1225-1236.

Muthukumaraswamy SD, Edden RA, Jones DK, Swettenham JB, Singh KD. 2009. Resting GABA concentration predicts peak gamma frequency and fMRI amplitude in response to visual stimulation in humans. Proc Natl Acad Sci USA. 106:8356-8361.

Nakamura K, Koga Y, Sakai H, Homma K, Ikebe M. 2007. cGMP-dependent relaxation of smooth muscle is coupled with the change in the phoshphorylation of myosin phosphatase. Cric Res. 101(7):712-722.

Natarajan A, Han G, Chen SY, Yu P, White R, Jose P. 2010. The D5 dopamine receptor mediates large-conductance, calcium- and voltage-activated potassium channel activation in human coronary artery smooth muscle cells. J Pharmacol Exp Ther. 332(2):640-649.

Nehls V, Denzer K, Drenckhahn D. 1992. Pericyte involvement in capillary sprouting during angiogenesis in situ. Cell Tissue Res. 270(3):469-474.

Nehls V, Drenckhahn D. 1991. Heterogeneity of microvascular pericytes for smooth muscle type alpha-actin. J. Cell. Biol 113:147-154.

Nehls V, Drenckhahn D. 1993. The versatility of microvascular pericytes: from mesenchyme to smooth muscle? Histochemistry 99(1):1-12.

Nelson MT, Huang Y, Brayden JE, Hescheler J, Standen NB. 1990. Arterial dilations in response to calcitonin gene-related peptide involve activation of K^+ channels. Nature. 344:770-773.

Nestler EJ, Hyman SE, Malenka RC. 2008. Molecular pharmacology: A foundation for clinical neuroscience 2nd ed. McGraw-Hill Companies, Inc.

Newman EA. 2001. Propagation of intracellular calcium waves in retinal astrocytes and Müller cells. J Neurosci. 21(7):2215-2223.

Nicholls DG. 1985. A role for the mitochondrion in the protection of cells against calcium overload? Prog Brain Res. 63:97-106.

Nishiyama A, Dahlin KJ, Stallcup WB. 1991. The expression of NG2 proteoglycan in the developing rat limb. Development 111(4):933-944.

Nishiyama A, Lin XH, Giese N, Heldin CH, Stallcup WB. 1996. Co-localization of NG2 proteoglycan and PDGF alpha-receptor on O2A progenitor cells in the developing rat brain. J Neurosci Res. 43(3):299-314.

Niwa K, Araki E, Morham SG, Ross ME, Iadecola C. 2000. Cyclooxygenase-2 contributes to functional hyperemia in whisker-barrel cortex. J Neurosci 20:763-770.

Nixdorf-Bergweiler BE, Albrecht D, Heinemann U. 1994. Developmental changes in the number, size, and orientation of GFAP-positive cells in the CA1 region of rat hippocampus. Glia 12:180-195.

Norman MG, O'Kusky JR. 1986. The growth and development of microvasculature in human cerebral cortex. J Neuropathol Exp Neurol 45:222-232.

Northoff G, Walter M, Schulte RF, Beck J, Dydak U, Henning A, Boeker H, Grimm S, Boesiger P. 2007. GABA concentrations in the human anterior cingulate cortex predict negative BOLD responses in fMRI. Nat Neurosci 10:1515-1517.

Oberheim NA, Wang X, Goldman S, Nedergaard M. 2006. Astrocytic complexity distinguishes the human brain. Trends Neurosci 29:547-553.

Offenhauser N, Thomsen K, Caesar K, Lauritzen M. 2005. Activity-induced tissue oxygenation changes in rat cerebellar cortex: interplay of postsynaptic activation and blood flow. J Physiol 565:279-294.

Ogawa S, Lee TM, Barrere B. 1993. The sensitivity of magnetic resonance image signals of a rat brain to changes in the cerebral venous blood oxygenation. Magn Reson Med 29:205–210.

Ogawa S, Lee TM, Kay AR, Tank DW. 1990. Brain magnetic resonance imaging with contrast dependent on blood oxygenation. Proc Natl Acad Sci U S A 87(24):9868-9872.

Ogilvie P, Schilling K, Billingsley ML, Schmidt HH. 1995. Induction and variants of neuronal nitric oxide synthase type I during synaptogenesis. FASEB J 9:799-806.

Ohyu J, Takashima S. 1998. Developmental characteristics of neuronal nitric oxide synthase (nNOS) immunoreactive neurons in fetal to adolescent human brains. Brain Res Dev Brain Res 110:193-202.

Olesen PJ, Nagy Z, Westerberg H, Klingberg T. 2003. Combined analysis of DTI and fMRI data reveals a joint maturation of white and grey matter in a fronto-parietal network. Brain Res Cogn Brain Res 18:48-57.

Orlidge A, D'Amore PA. 1987. Inhibition of capillary endothelial cell growth by pericytes and smooth muscle cells. J Cell Biol. 105(3):1455-1462.

Ostby Y, Tamnes CK, Fjell AM, Westlye LT, Due-Tønnessen P, Walhovd KB. 2009. Heterogeneity in subcortical brain development: A structural magnetic resonance imaging study of brain maturation from 8 to 30 years. J Neurosci 29:11772-11782.

Ozerdem U, Grako KA, Dahlin-Huppe K, Monosov E, Stallcup WB. 2001. NG2 proteoglycan is expressed in expressed exclusively by mural cells during vascular morphogenesis. Dev. Dyn 222:218-227.

Pantano P, Baron JC, Lebrun-Grandié P, Duquesnoy N, Bousser MG, Comar D. 1984. Regional cerebral blood flow and oxygen consumption in human aging. Stroke15:635-641.

Pardridge WM. 1999. Blood-brain barrier biology and methodology. J Neurovirol. 5(6):556-569.

Paspalas CD, Papadopoulos GC. 1996. Ultrastructural relationships between noradrenergic nerve fibers and non-neuronal elements in the rat cerebral cortex. Glia 17:133-146.

Passarotti AM, Paul BM, Bussiere JR, Buxton RB, Wong AC, Stiles J. 2003. The development of face and location processing: an fMRI study. 6:100-117.

Patan S. 1998. TIE1 and TIE2 receptor tyrosine kinases inversely regulate embryonic angiogenesis by the mechanism of intussesceptive microvascular growth. Microvasc Res. 56(1):1-21.

Patel M. 1996. Superoxide involvement in excitotoxicity: a SOD-mimetic holds promise as a novel neuroprotective agent. Mol Psychiatry 1(5):362-363.

Pauling L, Coryell CD. 1936. The magnetic properties and structure of hemoglobin, oxyhemoglobin and carbonmonoxyhemoglobin. Proc Natl Acad Sci U S A 22(4):210-216.

Paus T. 2005. Mapping brain maturation and cognitive development during adolescence, Trends Cogn Sci 9:60–68.

Peelen MV, Glaser B, Vuilleumier P, Eliez S. 2009. Differential development of selectivity for faces and bodies in the fusiform gyrus. Dev Sci 12:F16-25.

Peng X, Carhuapoma JR, Bhardwaj A, Alkayed NJ, Falck JR, Harder DR, Traystman RJ, Koehler RC. 2002. Suppression of cortical functional hyperemia to vibrissal stimulation in the rat by epoxygenase inhibitors. Am J Physiol Heart Circ Physiol. 283(5):H2029-2037.

Peppiatt CM, Howarth C, Mobbs P, Attwell D. 2006. Bidirectional control of CNS capillary diameter by pericytes. Nature 443:700-704.

Peters MW, Canham PB, Finlay HM. 1983. Circumferential alignment of muscle cells in the tunica media of the human brain artery. Blood vessels 20(5):221-233.

Peters BP, Goldstein IJ. 1979. The use of fluorescein-conjugated Bandeiraea simplicifolia B4-isolectin as a histochemical reagent for the detection of alpha-D-galactopyranosyl groups. Their occurrence in basement membranes. Exp Cell Res. 120(2):321-334.

Phillis JW, Smith-Barbour M, O'Regan MH. 1996. Changes in extracellular amino acid neurotransmitters and purines during and following ischemias of different durations in the rat cerebral cortex. Neurochem Int. 29(2):115-120.

Piantadosi CA, Zhang J. 1996. Mitochondrial generation of reactive oxygen species after brain ischemia in the rat. Stroke 27(2):327-331.

Pinto JG, Hornby KR, Jones DG, Murphy KM. 2010. Developmental changes in GABAergic mechanisms in human visual cortex across the lifespan. Front Cell Neurosci 4:16.

Porter JT, McCarthy KD. 1996. Hippocampal astrocytes in situ respond to glutamate released from synaptic terminals. J Neurosci 16:5073-5081.

Pouly S, Becher B, Blain M, Antel JP. 1999. Expression of a homologue of rat NG2 on human microglia. Glia 27(3):259-268.

Pouly S, Prat A, Blain M, Olivier A, Antel J. 2001. NG2 immunoreactivity on human brain endothelial cells. Acta. Neuropathol 102:313-320.

Pugh KR, Mencl WE, Jenner AR, Katz L, Frost SJ, Lee JR, Shaywitz SE, Shaywitz BA. 2000. Functional neuroimaging studies of reading and reading disability (developmental dyslexia). Ment Retard Dev Disabil Res Rev 6:207-213.

Pujol J, Vendrell P, Junque C, Marti-Vilalta JL, Capdevila A. 1993. When does human brain development end? Evidence of corpus callosum growth up to adulthood. Ann Neurol 34:71-75.

Quayle JM, Nelson MT, Standen NB. 1997. ATP-sensitive and inwardly rectifying potassium channels in smooth muscle. Physiol Rev. 77(4):1165-1232.

Quignard JF, Harley EA, Duhault J, Vanhoutte PM, Feletou M. 2003. K^+ channels in cultured bovine retinal pericytes: effects of beta-adrenergic stimulation. J Cardiovasc. Pharmacol. 42:379-388.

Raichle ME. 1983. The pathophysiology of brain ischemia. Ann Neurol. 13(1):2-10.

Raichle ME, Hartman BK, Eichling JO, Sharpe LG. 1975. Central noradrenergic regulation of cerebral blood flow and vascular permeability. Proc Natl Acad Sci USA. 72(9):3726-3730.

Rakic P, Bourgeois JP, Goldman-Rakic PS. 1994. Synaptic development of the cerebral cortex: implications for learning, memory, and mental illness. Prog Brain Res 102:227-243.

Rapoport RM. 1986. Cyclic guanosine monophosphate inhibition of contraction may be mediated through inhibition of phosphatidylinositol hydrolysis in rat aorta. Circ Res. 58(3):407-410.

Rashatwar SS, Cornwell TL, Lincoln TM. 1987. Effects of 8-bromo-cGMP on Ca2+ levels in vascular smooth muscle cells: possible regualtion of Ca2+-ATPase by cGMP-dependent protein kinase. Proc Natl Acad Sci U S A 84(16):5685-5689.

Ray S, Maunsell JH. 2010. Differences in gamma frequencies across visual cortex restrict their possible use in computation. Neuron 67:885-896.

Reilly Tm, Seldes R, Luchetti W, Brighton CT. 1998. Similarities in the phenotypic expression of pericytes and bone cells. Clin Orthop Relat Res. (346):95-103.

Reuss S, Schaeffer DF, Laages MH, Riemann R. 2000. Evidence for increased nitric oxide production in the auditory brain stem of the aged dwarf hamster (Phodopus sungorus): an NADPH-diaphorase histochemical study. Mech Ageing Dev 112:125-134.

Reynell C, Harris JJ. 2013, The BOLD signal and neurovascular coupling in autism. Dev Cogn Neurosci. 12:72-79.

Rheims S, Holmgren CD, Chazal G, Mulder J, Harkany T, Zilberter T, Zilberter Y. 2009. GABA action in immature neocortical neurons directly depends on the availability of ketone bodies. J Neurochem 110:1330-1338.

Rhodin JA. 1968. Ultrastructure of mammalian venous capillaries, venules, and small collecting veins. J Ultrastruct Res. 25(5):452-500.

Rhodin JA, Fujita H. 1989. Capillary growth in the mesentery of normal young rats. Intravital video and electron microscope analyses. J Submicrosc Cytol Pathol. 21(1):1-34.

Richter W, Richter M. 2003. The shape of the fMRI BOLD response in children and adults changes systematically with age. Neuroimage 20:1122-1131.

Riddle DR, Gutierrez G, Zheng D, White LE, Richards A, Purves D. 1993. Differential metabolic and electrical activity in the somatic sensory cortex of juvenile and adult rats. J Neurosci 13:4193-4213.

Riobo NA, Melani M, Sanjuan N, Fiszman ML, Gravielle MC, Carreras MC, Cadenas E, Poderoso JJ. 2002. The modulation of mitochondrial nitric-oxide synthase activity in rat brain development. J Biol Chem 277:42447-42455.

Risser L, Plouraboue F, Cloetens P, Fonta C. 2009. A 3D-investigation shows that angiogenesis in primate cerebral cortex mainly occurs at capillary level. Int J Dev Neurosci 27:185-196.

Robinson R, Stokes R. 1965. Electrolyte Solutions, 2nd Edition. London:Butterworth.

Roman RJ. 2002. P-450 metabolites of arachidonic acid in the control of cardiovascular function. Physiol Rev 82:131-185.

Romano C, Sesma MA, McDonald CT, O'Malley K, Van den Pol AN, Olney JW. 1995. Distribution of metabotropic glutamate receptor mGluR5 immunoreactivity in rat brain. J Comp Neurol 355:455-469.

Rossi DJ, Oshima T, Attwell D. 2000. Glutamate release in severe brain ischaemia is mainly by reversed uptake. Nature 403(6767):316-321.

Roufail E, Stringer M, Rees S. 1995. Nitric oxide synthase immunoreactivity and NADPH diaphorase staining are co-localised in neurons closely associated with the vasculature in rat and human retina. Brain Res. 684(1):36-46.

Rouget C. 1874. Note sur le developpement de la tunique contractile des vaisseaux. Compt Rend Acad Sci. 59:559-562.

Roy CS, Sherrington CS. 1890. On the Regulation of the Blood-supply of the Brain. J Physiol 11:85-158 117.

Ruiter DJ, Schlingemann RO, Westphal JR, Denijn M, Rietveld FJ, DeWaal RM. 1993. Angiogenesis in wound healing and tumor metastasis. Behring Inst Mitt. 92:258-272.

Sakagami K, Kawamura H, Wu DM, Puro DG. 2001. Nitric osixde/cGMP-induced inhibition of calcium and chloride currents in retinal pericytes. Microvasc Res. 62:196-203.

Sakagami K, Wu D, Puro DG. 1999. Physiology of rat retinalpericytes: modulation of ion channel activity by serum-derived molecules. J Physiol. 521:637-650.

Salami M, Itami C, Tsumoto T, Kimura F. 2003. Change of conduction velocity by regional myelination yields constant latency irrespective of distance between thalamus and cortex. Proc Natl Acad Sci U S A 100:6174-6179.

Salinas E, Sejnowski TJ. 2001. Correlated neuronal activity and the flow of neural information. Nat Rev Neurosci 2:539-550.

Salvucci O, Maric D, Economopoulou M, Sakakibara S, Merlin S, Follenzi A, Tosato G. 2009. EphrinB reverse signaling contributes to endothelial and mural cell assembly into vascular structures. Blood 114(8):1707-1716.

Sánchez-Zuriaga D, Marti-Gutierrez N, De La Cruz MA, Peris-Sanchis MR. 2007. Age-related changes of NADPH-diaphorase-positive neurons in the rat inferior colliculus and auditory cortex. Microsc Res Tech 70:1051-1059.

Sanders KM. 2008. Regulation of smooth muscle excitation and contraction. Neurogastroenterol Motil. 1:39-53.

Saran M, Michel C, Bors W. 1990. Reaction of NO with O2-. implications for the action of endothelium-derived relaxing factor (EDRF). Free Radic Res Commun. 10(4-5):221-226.

Sarelius IH, Cohen KD, Murrant CL. 2000. Role for capillaries in coupling blood flow with metabolism. Clin Exp Pharmacol Physiol. 27(10):826-829.

Sato Y, Rifkin DB. 1989. Inhibition of endothelial cell movement by pericytes and smooth muscle cells: activation of a latent transforming growth factor-beta 1-like molecule by plasmin during co-culture. J Cell Biol. 109(1):309-315.

Sattler R, Tymianski M. 2001. Molecular mechanisms of glutamate receptor-mediated excitotoxic neuronal cell death. Mol Neurobiol. 24:107-129.

Scafidi S, Douglas RM, Farahani R, Banasiak KJ, Haddad GG. 2007. Prostaglandin transporter expression in mouse brain during development and in response to hypoxia. Neuroscience 146:1150-1157.

Schaller B, Graf R. 2004. Cerebral ischemia and reperfusion: the pathophysiologic concept as a basis for clinical therapy. J Cereb Blood Flow Metab. 24(4):351-371.

Schinder AF, Olson EC, Spitzer NC, Montal M. 1996. Mitochondrial dysfunction is a primary event in glutamate neurotoxicity. J Neurosci. 16(19):6125-6133.

Schlingemann RO, Rietveld FJ, de Waal RM, Ferrone S, Ruiter DJ. 1990. Expression of the high molecular weight melanoma-assocaited antigen by pericytes during angiogenesis in tumors and in healing wounds. Am J Pathol. 136(6):1393-1405.

Schölvinck ML, Howarth C, Attwell D. 2008. The cortical energy needed for conscious perception. Neuroimage. 40:1460-1468.

Schönfelder U, Hofer A, Paul M, Funk RH. 1998. In situ observation of living pericytes in rat retinal capillaries. Microvasc Res 56:22-29.

Schor AM, Schor SL. 1986. The isolation and culture of endothelial cells and pericytes from the bovine retinal microvasculature: a comparative study with large vessel vascular cells. Microvasc Res. 32(1):21-38.

Schrappe M, Klier FG, Spiro RC, Waltz TA, Reisfeld RA, Gladson CL. 1991. Correlation of chondroitin sulfate proteoglycan expression on proliferating brain capillary enfothelial cells with the malignant phenotype of astroglial cells. Cancer Res. 51(18):4986-4993.

Schulz K, Sydekum E, Krueppel R, Engelbrecht CJ, Schlegel F, Schröter A, Rudin M, Helmchen F. 2012. Simultaneous BOLD fMRI and fiber-optic calcium recording in rat neocortex. Nat Methods 9(6):597-602.

Sciamanna MA, Zinkel J, Fabi AY, Lee CP. 1992. Ischemic injury to rat forebrain mitochondria and callular calcium homeostasis. Biochem Biophys Acta. 1134(3):223-232.

Seidl AH, Rubel EW, Harris DM. 2010. Mechanisms for adjusting interaural time differences to achieve binaural coincidence detection. J Neurosci 30:70-80.

Siesjö BK. 1988. Mechanisms of ischemic brain damage. Crit Care Med. 16(10):954-963.

Serebryakov V, Zakharenko S, Snetkov V, Takeda K. 1994. Effects of prostaglandins E1 and E2 on cultured smooth muscle cells and strips of rat aorta. Prostaglandins 47:353-365.

Seregi A, Keller M, Hertting G. 1987. Are cerebral prostanoids of astroglial origin? Studies on the prostanoid forming system in developing rat brain and primary cultures of rat astrocytes. Brain Res 404:113-120.

Sereno MI, Pitzalis S, Martinez A. 2001. Mapping of contralateral space in retinotopic coordinates by a parietal cortical area in humans. Science 294:1350-1354.

Shaw P, Kabani NJ, Lerch JP, Eckstrand K, Lenroot R, Gogtay N, Greenstein D, Clasen L, Evans A, Rapoport JL, Giedd JN, Wise SP. 2008. Neurodevelopmental trajectories of the human cerebral cortex. J Neurosci 28:3586-3594.

Shepro D, Morel NM. 1993. Pericyte physiology. FASEB J 7(11):1031-1038.

Shojaee N, Patton WF, Hechtman HB, Shepro D. 1999. Myosin translocation in retinal pericytes during free-radical induced apoptosis. J Cell Biochem. 75(1):118-129.

Siekmann AF, Lawson ND. 2007. Notch signalling and the regulation of angiogenesis. Cell Adh Migr. 1(2):104-106.

Sigala N, Logothetis NK. 2002. Visual categorization shapes feature selectivity in the primate temporal cortex. Nature 415:318-320.

Sillito AM. 1975. The contribution of inhibitory mechanisms to the receptive field properties of neurones in the striate cortex of the cat. J Physiol 250:305-329.

Silver MA, Kastner S. 2009. Topographic maps in human frontal and parietal cortex. Trends Cogn Sci 13:488-495.

Simard M, Arcuino G, Takano T, Liu QS, Nedergaard M. 2003. Signaling at the gliovascular interface. J Neurosci 23:9254-9262.

Sims DE. 1986. The pericyte--a review. Tissue Cell 18(2):153-174.

Sims DE. 1991. Recent advances in pericyte biology--implications for health and disease. Can J Cardiol. 7(10):431-443.

Sims DE. 2000. Diversity within pericytes. Clin Exp Pharmacol Physiol. 27(10):842-846.

Singer W, Gray CM. 1995. Visual feature integration and the temporal correlation hypothesis. Annu Rev Neurosci 18:555-586.

Skalli O, Pelte MF, Peclet MC, Gabbiani G, Gugliotta P, Bussolati G, Ravazzola M, Orci L. 1989. Alpha-smooth muscle actin, a differentiation marker of smooth muscle cells, is present in microfilamentous bundles of pericytes. J Histochem Cytochem. 37(3):315-321.

Skalli O, Ropraz P, Trzeciak A, Benzonana G, Gillessen D, Gabbiani G. 1986. A monoclonal antibody against alpha-smooth muscle actin: a new probe for smooth muscle differentiation. J Cell Biol 103:2787-2796.

Sloan HL, Austin VC, Blamire AM, Schnupp JW, Lowe AS, Allers KA, Matthews PM, Sibson NR. 2010. Regional differences in neurovascular coupling in rat brain as determined by fMRI and electrophysiology. Neuroimage 53:399-411.

Smits A, Kato M, Westermark B, Nistér M, Heldin CH, Funa K. 1991. Neurotrophic activity of platelet-derived growth factor (PDGF):Rat neuronal cells possess functional PDGF beta-type receptors and respond to PDGF. Proc Natl Acad Sci U S A 88(18):8159-8163.

Sobey CG, Faraci FM. 1997. Effects of a novel inhibitor of guanylyl cyclase on dilator responses of mouse cerebral arterioles. Stroke. 28: 837-842.

Sobue K, Yamamoto N, Yoneda K, Hodgson ME, Yamashiro K, Tsuruoka N, Tsuda T, Katsuya H, Miura Y, Asai K, Kato T. 1999. Induction of blood-brain barrier properties in immortalized bovine brain endothelial cells by astrocytic factors. Neurosci Res. 35(2):155-164.

Sofroniew MV. 2009. Molecular dissection of reactive astrogliosis and glial scar formation. Trends Neurosci. 32(12):638-647.

Somlyo AP, Somlyo AV. 1968. Vascular smooth muscle. I. Normal structure, pathology, biochemistry, and biophysics. Pharmacol. Rev. 20(4):197-272.

Sowell ER, Peterson BS, Thompson PM, Welcome SE, Henkenius AL, Toga AW. 2003. Mapping cortical change across the human life span. Nat Neurosci 6:309-315.

Spear LP, Brake SC. 1983. Periadolescence: age-dependent behavior and psychopharmacological responsivity in rats. Dev Psychobiol 16:83-109.

Spector AA, Fang X, Snyder GD, Weintraub NL. 2004. Epoxyeicosatrienoic acids (EETs): metabolism and biochemical function. Prog Lipid Res 43:55-90.

St Lawrence KS, Ye FQ, Lewis BK, Frank JA, McLaughlin AC. 2003. Measuring the effects of indomethacin on changes in cerebral oxidative metabolism and cerebral blood flow during sensorimotor activation. Magn Reson Med 50:99-106.

Stallcup WB. 2002. The NG2 proteoglycan: past insights and future prospects. J Neurocytol. 31(6-7):423-435.

Standen NB, Quayle JM. 1998. K+ channel modulation in arterial smooth muscle. Acta Physiol Scand. 164(4):549-557.

Starkov AA, Chinopoulos C, Fiskum G. 2004. Mitochondrial calcium and oxidative stress as mediators of ischemic brain injury. Cell Calcium 36(3-4):257-264.

Stefanovic B, Hutchinson E, Yakovleva V, Schram V, Russell JT, Belluscio L, Koretsky AP, Silva AC. 2008. Functional reactivity of cerebral capillaries. J Cereb Blood Flow Metab 28:961-972.

Stenman JM, Rajagopal J, Carroll TJ, Ishibashi M, McMahon J, McMahon AP. 2008. Canonical Wnt signalling regulates organ-specfic assembly and differentiation of CNS vasculature. Sceince 322(5905):1247-1250.

Stichel CC, Muller CM, Zilles K. 1991. Distribution of glial fibrillary acidic protein and vimentin immunoreactivity during rat visual cortex development. J Neurocytol 20:97-108.

Streit WJ, Kreutzberg GW. 1987. Lectin binding by resting and reactive microglia. J Neurocytol. 16(2):249-260.

Stephens RB, Stilwell DL. 1969. Arteries and veins of the human brain. Thomas (Springfield, III).

Sugawara T, Chan PH. 2003. Reactive oxygen radicals and pathogenesis of neuronal death after cerebral ischemia. Antioxid Redox Signal 5(5):597-607.

Sugawara T, Fujimura M, Noshita N, Kim GW, Saito A, Hayashi T, Narasimhan P. 2004. Neuronal death/survival signaling pathways in cerebral ischemia. NeuroRx 1(1):17-25.

Sugiyama T, Kawamura H, Yamanishi S, Kobayashi M, Katsumura L, Puro DG. 2005. Regulation of P2X7-induced pore formation and cell death in pericyte-containing retinal microvessels. Am J Physiol Cell Physiol. 288: C568-C576.

Sun CW, Falck JR, Okamoto H, Harder DR, Roman RJ. 2000. Role of cGMP versus 20-HETE in the vasodilator response to nitric oxide in rat cerebral arteries 279:H339-350.

Sun W, McConnell E, Pare JF, Xu Q, Chen M, Peng W, Lovatt D, Han X, Smith Y, Nedergaard M. 2013. Glutamate-dependent meuroglial calcium signalling differs between young and adult brain. 339(6116):197-200.

Sundberg C, Ivarsson M, Gerdin B, Rubin K. 1996. Pericytes as collagen-producing cells in excessive dermal scarring. Lab Invest. 74(2):452-466.

Szabó C, Day BJ, Salzman AL. 1996. Evaluation of the relative contribution of nitric oxide and peroxynitrite to the suppression of mitochondrial respiration in immunostimulated macrophages using a manganese mesoporphyrin superoxide dismutase mimetic and peroxynitrite scavenger. FEBS Lett. 381(1-2):82-86.

Szatkowski M, Attwell D. 1994. Triggering and execution of neuronal death in brain ischaemia: two phases of glutamate release by different mechanisms. Trends Neurosci. 17(9):359-365.

Takada H, Nagata K, Hirata Y, Satoh Y, Watahiki Y, Sugawara J, Yokoyama E, Kondoh Y, Shishido F, Inugami A, et al. 1992. Age-related decline of cerebral oxygen metabolism in normal population detected with positron emission tomography. Neurol Res 14:128-131.

Takano T, Tian GF, Peng W, Lou N, Libionka W, Han X, Nedergaard M. 2006. Astrocyte-mediated control of cerebral blood flow. Nat Neurosci 9:260-267.

Takata F, Dohgu S, Nishioku T, Takahashi H, Harada E, Makino I, Nakashima M, Yamauchi A, Kataoka. 2009. Adrenomedullin-induced relaxation of rat brain pericytes is related to the rduced phosphorylation of myosin light chain through the cAMP/PKA signalling pathway. Neurosci Lett. 449:71-75.

Tamnes CK, Ostby Y, Fjell AM, Westlye LT, Due-Tønnessen P, Walhovd KB. 2010. Brain maturation in adolescence and young adulthood: regional age-related changes in cortical thickness and white matter volume and microstructure. Cerebral Cortex 20:534-548.

Tauskela JS. 2007. MitoQ a mitochondria-targeted antioxidant. IDrugs. 10(6):399-412.

Tegtmeier F, Weber C, Heister U, Haker I, Scheller D, Nikolov R, Höller M. 1990. Eicosanoids in rat brain during ischemia and reperfusion--correlation to DC depolarization. J Cereb Blood Flow Metab. 10(3):358-364.

Tessier-Lavigne M, Attwell D, Mobbs P, Wilson M. 1988. Membrane currents in retinal bipolar cells of the axolotl. J Gen Physiol 91:42-72.

Thomas WE. 1999. Brain macrophages: on the role of pericytes and perivascular cells. Brain research reviews 31:42-57.

Thomas KM, King SW, Franzen PL, Welsh TF, Berkowitz AL, Noll DC, Birmaher V, Casey BJ. 1999. A developmental functional MRI study of spatial working memory. Neuroimage 10:327-338.

Thomason ME, Burrows BE, Gabrieli JD, Glover GH. 2005. Breath holding reveals differences in fMRI BOLD signal in children and adults. Neuroimage 25:824-837.

Thurston G. 2003. Role of angiopoietins and tie receptor tyrosine kinases in angiogenesis and lymphangiogenesis. Cell Tissue Res. 314(1):61-68.

Tieman SB, Mollers S, Tieman DG, White J. 2004. The blood supply of the cat's visual cortex and its postnatal development. Brain Res 998:100-112.

Tilton RG, Kilo C, Williamson JR. 1979. Pericyte-endothelial relationships in cardiac and skeletal muscle capillaries. Microvasc Res. 18(3):325-335.

Toga AW, Thompson PM, Sowell ER. 2006. Mapping brain maturation. Trends Neurosci 29:148-159.

Toribatake Y, Tomita K, Kawahara N, Baba H, Ohnari H, Tanaka S. 1997. Regulation of vasomotion of arterioles and capillaries in the cat spinal cord: role of alpha actin and endothelin-1. Spinal Cord 35(1):26-32.

Tseng KY, O'Donnell P. 2007. Dopamine modulation of prefrontal cortical interneurons changes during adolescence. Cereb Cortex 17:1235-1240.

Turkeltaub PE, Flowers DL, Lyon LG, Eden GF. 2008. Development of ventral stream representations for single letters. Ann N Y Acad Sci 1145:13-29.

Tyzio R, Allene C, Nardou R, Picardo MA, Yamamoto S, Sivakumaran S, Caiati MD, Rheims S, Minlebaev M, Milh M, Ferre P, Khazipov R, Romette JL, Lorquin J, Cossart R, Khalilov I, Nehlig A, Cherubini E, Ben-Ari Y.

2011. Depolarizing actions of GABA in immature neurons depend neither on ketone bodies nor on pyruvate. J Neurosci 31:34-45.

Uemura A, Ogawa M, Hirashima M, Fujiwara T, Koyama S, Takagi H, Honda Y, Wiegand SJ, Yancopoulos GD, Nishikawa S. 2002. Recombinant angiopoietin-1 restores higher-order architecture of growing blood vessels in mice in the absence of mural cells. J Clin Invest. 110(11):1619-1628.

Ullen F. 2009. Is activity regulation of late myelination a plastic mechanism in the human nervous system? Neuron Glia Biol 5:29-34.

Ushiwata I, Ushiki T. 1990. Cytoarchitecture of the smooth muscles and pericytes of rat cerebral blood vessels. A scanning electron microscopic study. J Neurosurg. 73(1):82-90.

Vaidya CJ, Austin G, Kirkorian G, Ridlehuber HW, Desmond JE, Glover GH, Gabrieli JD. 1998. Selective effects of methylphenidate in attention deficit hyperactivity disorder: a functional magnetic resonance study. Proc Natl Acad Sci U S A 95:14494-14499.

van den Pol AN, Romano C, Ghosh P. 1995. Metabotropic glutamate receptor mGluR5 subcellular distribution and developmental expression in hypothalamus. J Comp Neurol 362:134-150.

Vanhoutte PM, Rimele TJ. 1982. Calcium and alpha-adrenoceptors in activation of vascular smooth muscle. J Cardiovasc Pharmacol 4 Suppl 3:S280-286.

Verbeek MM, Otte-Höller I, Wesseling P, Ruiter DJ, de Waal RM. 1994. Induction of alpha-smooth muscle actin expression in cultured human brain pericytes by transforming growth factor-beta 1. Am J Pathol. 144(2):372-382.

Vimtrup BS. 1922. Beitrage zur anatomie der kapillaren: uber kontractile elemente in der gefasswand der blutkapillaren. Z. Anat. Entwick-lungsgesch 65:150-182.

von Beckerath N, Nees S, Neumann FJ, Krebs B, Juchem B, Schömig A. 2000. An inward rectifier and a voltage-dependent K^+ current in single, cultured pericytes from bovine heart. Cardiovasc. Res. 46(3):569-578.

Wahlstrom D, White T, Luciana M. 2010. Neurobehavioral evidence for changes in dopamine system activity during adolescence. Neurosci Biobehav Rev 34:631-648.

Walford GA, Moussignac RL, Scribner AW, Loscalzo J, Leopold JA. 2004. Hypoxia potentiates nitric oxide-mediated apoptosis in endothelial cells via peroxynitrite-induced activation of mitochondria-dependent and -independent pathways. J Biol Chem. 279(6):4425-4432.

Wallace MN, Brown IE, Cox AT, Harper MS. 1995. Pyramidal neurones in human precentral gyrus contain nitric oxide synthase. Neuroreport 6:2532-2536.

Walmsley JG, Canham PB. 1979. Orientation of nuclei as indicators of smooth muscle cell alignment in the cerebral artery. Blood Vessels 16(1):43-51.

Wang T, Baron M, Trump D. 2008. An overview of notch3 function in vascular smooth muscle cells. Prog Biophys Mol Biol. 96(1-3):499-509.

Wang AT, Lee SS, Sigman M, Dapretto M. 2006. Developmental changes in the neural basis of interpreting communicative intent. Soc Cogn Affect Neurosci 1:107-121.

Webb RC. 2003. Smooth muscle contraction and relaxation. Adv Physiol Educ. 27, 201-206.

Weber B, Keller AL, Reichold J, Logothetis NK. 2008. The microvascular system of the striate and extrastriate visual cortex of the macaque. Cereb Cortex 18:2318-2330.

Werkle-Bergner M, Shing YL, Muller V, Li SC, Lindenberger U. 2009. EEG gamma-band synchronization in visual coding from childhood to old age: evidence from evoked power and inter-trial phase locking. Clin Neurophysiol 120:1291-1302.

Wiederholt M, Berweck S, Helbig H. 1995. Electrophysiological properties of cultured retinal capillary pericytes. Prog. Retin. Eye Res. 14:437-451.

Williamson JR, Tilton RG, Kilo C, Yu S. 1980. Immunofluorescent imaging of capillaries and pericytes in human skeletal muscle and retina. Microvasc Res. 20(2):233-241.

Winkler EA, Bell RD, Zlokovic BV. 2010. Pericyte-specific expression of PDGF beta receptor in mouse models with normal and deficient PDGF beta receptor signalling. Mol Neurodegener 5:32

Wirz W, Antoine M, Tag CG, Gressner AM, Korgg T, Hellerbrand C, Kiefer P. 2008. Hepatic stellate cells display a functional vascular smooth muslce cell phenotype in a three-dimensional co-culture model with endothelial cells. Differentiation. 76(7):784-794.

Woodrum DA, Brophy CM, Wingard CJ, Beall A, Rasmussen H. 1999. Phosphorylation events associated with cyclic nucleotide-dependent inhibition of smooth muscle contraction. Am J Physiol. 277:H931-939.

Woolsey TA, Rovainen CM, Cox SB, Henegar MH, Liang GE, Liu D, Moskalenko YE, Sui J Wei L. 1996. Neuronal units linked to microvascular modules in cerebral cortex: response elements for imaging the brain. Cereb Cortex 6(5):647-660.

Xiong Z, Sperelakis N. 1995. Regulation of L-type calcium channels of vascular smooth muscle cells. J Mol Cell Cardiol. 27(1):75-91.

Xiong ZG, Zhu XM, Chu XP, Minami M, Hey J, Wei WL, MacDonald JF, Wemmie JA, Price MP, Welsh MJ, Simon RP. 2004. Neuroprotection in ischemia: blocking calcium-permeable acid-sensing ion channels. Cell 118(6):687-698.

Yakovlev PI, Lecours AR. 1967. Regional Development of the Brain in Early Life: Blackwell Scientific Publications: Boston.

Yamada H, Sadato N, Konishi Y, Kimura K, Tanaka M, Yonekura Y, Ishii Y. 1997. A rapid brain metabolic change in infants detected by fMRI. Neuroreport 8:3775-3778.

Yamagishi S, Yonekura H, Yamamoto Y, Fujimori H, Sakurai S, Tanaka N, Yamamoto H. 1999. Vascular endothelial growth factor acts as a pericyte mitogen under hypoxic conditions. Lab Invest. 79(4):501-509.

Yan XX, Garey LJ, Jen LS. 1996. Prenatal development of NADPH-diaphorase-reactive neurons in human frontal cortex. Cereb Cortex 6:737-745.

Yaseen MA, Srinivasan VJ, Sakadžić S, Radhakrishnan H, Gorczynska I, Wu W, Fujimoto JG, Boas DA. 2011. Microvascular oxygen tension and flow measurements in rodent cerebral cortex during baseline conditions and functional activation. J Cereb Blood Flow Metab. 31(4):1051-1063.

Yemisci M, Gursoy-Ozdemir Y, Vural A, Can A, Topalkara K, Dalkara T. 2009. Pericyte contraction induced by oxidative-nitrative stress impairs capillary reflow despite successful opening of an occluded cerebral artery. Nat Med. 15(9):1031-1037.

Yokoyama A, Sakamoto A, Kameda K, Imai Y, Tanaka J. 2006. NG2 proteoglycan-expressing microglia as multipotent neural progenitors in normal and pathologic brains. Glia 53(7):754-768.

You WK, Yotsumoto F, Sakimura K, Adams RH, Stallcup WB. 2013. NG2 proteoglycan promotes tumour vascularization via integrin-dependent effects on pericyte function. Angiogenesis. Epub ahead of print.

Yu X, Radulescu A, Chen CL, James IO, Besner GE. 2012. Heparin-binding EGF-like growth factor protects pericytes from injury. j Surg Res. 172(1):165-176.

Yu M, Sun CW, Maier KG, Harder DR, Roman RJ. 2002. Mechanism of cGMP contribution to the vasodilator response to NO in rat middle cerebral arteries. Am J Physiol Heart Circ Physiol 282:H1724-1731.

Yu BP, Yu CC, Robertson RT. 1994. Patterns of capillaries in developing cerebral and cerebellar cortices of rats. Acta Anat (Basel) 149:128-133.

Zeng W, Mak DO, LiQ, Shin DM, Foskett JK, Muallem S. 2003. A new mode of Ca2+ signaling by G protein-coupled receptors: gating of IP3 receptor Ca2+ release channels by Gbetagamma. Curr Biol. 13(10):872-876.

Zhang Q, Cao C, Zhang Z, Wier WG, Edwards A, Pallone TL. 2008. Membrane current oscillations in descending vasa recta pericytes. Am J Physiol Renal Physiol. 294(3):F656-666.

Zhang J, Tan Z, Tran ND. 2000. Chemical hypoxia-ischemia induces apoptosis in cerebromicrovascular endothelial cells. Brain Res. 877(2):134-140.

Zhu X, Bergles D, Nishiyama A. 2008. NG2 generates both oligodendrocytes and grey matter astrocytes. Development 135(1):145-157.

Zimmerlin L, Donnenberg VS, Donnenberg AD. 2011. Rare event detection and analysis in flow cytometry: bone marrow mesenchymal stem cells, breast cancer stem/progenitor cells in malignant effusions, and pericytes in disaggregated adipose tissue. Methods Mol Biol. 669:251-273.

Zimmermann KW. 1923. Der feinere bau der blutkapillaren. Z Anat Entwicklungsgesch. 68:29-109.

Zlokovic BV. 2008. The blood-brain barrier in health and chronic neurodegenerative disorders. Neuron. 57(2):178-201.

Zonta M, Angulo MC, Gobbo S, Rosengarten B, Hossmann KA, Pozzan T, Carmignoto G. 2003. Neuron-to-astrocyte signaling is central to the dynamic control of brain microcirculation. Nat Neurosci 6:43-50.

Zuo XL, Wu P, Ji AM. 2012. Nylon filament coated with paraffin for intraluminal permanent middle cerebral artery occlusion in rats. Neurosci Lett. 519(1):42-46.